Smart biocompatible conductive beads and nanoparticles for energy conversion

Monica Brachi

THÈSE

Pour obtenir le grade de

DOCTEUR DE L'UNIVERSITÉ GRENOBLE ALPES

École doctorale : CSV- Chimie et Sciences du Vivant
Spécialité : Chimie Physique Moléculaire et Structurale
Unité de recherche : Département de Chimie Moléculaire

Billes et nanoparticules biocompatibles et intelligentes pour la conversion dénergie

Smart biocompatible conductive beads and nanoparticles for energy conversion

Présentée par :

MONICA BRACHI

Direction de thèse :

Serge COSNIER DIRECTEUR DE RECHERCHE, Université Grenoble Alpes	Directeur de thèse
Alan LE GOFF DIRECTEUR DE RECHERCHE, Université Grenoble Alpes	Co-directeur de thèse

Rapporteurs :

Carole CHAIX
DIRECTRICE DE RECHERCHE, CNRS délégation Rhône Auvergne
Christophe INNOCENT
CHARGE DE RECHERCHE HDR, CNRS délégation Occitanie Est

Thèse soutenue publiquement le **16 décembre 2022**, devant le jury composé de :

Serge COSNIER DIRECTEUR DE RECHERCHE, CNRS délégation Alpes	Directeur de thèse
Alan LE GOFF DIRECTEUR DE RECHERCHE, CNRS délégation Alpes	Co-directeur de thèse
Carole CHAIX DIRECTRICE DE RECHERCHE, CNRS délégation Rhône Auvergne	Rapporteure
Christophe INNOCENT CHARGE DE RECHERCHE HDR, CNRS délégation Occitanie Est	Rapporteur
Carole BAFFERT MAITRE DE CONFERENCES HDR, Aix-Marseille Université	Examinatrice
Fabrice THOMAS PROFESSEUR DES UNIVERSITES, Université Grenoble Alpes	Président

Table of contents

Résumé:

Les nanomatériaux peuvent améliorer remarquablement les performances des bioélectrodes, à la fois dans les biopiles enzymatiques et les biocapteurs, en raison de leurs caractéristiques intéressantes telles qu'une grande surface, des propriétés électrocatalytiques et une morphologie contrôlée. Cette thèse vise à explorer la post-fonctionnalisation de deux types de nano-objets : les nanotubes de carbone multiparois (MWCNT) et les glyconanoparticules dérivées de glucides (GNP) et leur application dans la construction de bioélectrodes pour la biodétection et la conversion d'énergie. Dans la première partie de la thèse, une réaction thiol-yne photoinduite a été étudiée par électrochimie sur des MWCNT modifiés par un alcyne à l'aide de sondes rédox thiolées. Cette réaction représente une alternative aux autres réactions de «click-chemistry» et possède l'avantage d'être exempte de catalyseur métallique et de pouvoir être contrôlée de manière spatiale et temporelle. L'immobilisation de médiateurs redox, dérivés de ferrocène et de quinone, sur des électrodes à base de MWCNT par cette réaction a conduit à une amélioration considérable de l'électrocatalyse médiée par des enzymes de type FAD-déshydrogénases oxydant le glucose. La deuxième partie est centrée sur la fonctionnalisation de GNPs assemblés à partir d'un copolymère bloc polystyrène-β-cyclodextrine via la formation de complexes d'inclusion entre les β-cyclodextrines exposées à la surface des GNPS et les groupements adamantane d'un dérivé fluorescent de l'heptazine. Les nanoparticules résultantes ont été caractérisées par spectroscopie en solution et en surface après leur immobilisation sur des films de poly(pyrrole) électropolymérisés de manière spatialement contrôlée surélectrodes interdigitées. Dans la dernière partie, les GNPs ont été utilisés comme matériau d'électrode pour l'immobilisation d'une enzyme glucose oxydase modifiée avec des groupements adamantane pour la détection du glucose. Les performances analytiques des bioélectrodes avec ou sans GNPs ancrées sur différents films fonctionnels de poly-pyrrole sont comparées et discutées.

Abstract:

Nanomaterials can remarkably improve the performances of bioelectrodes, both in enzymatic biofuel cells and biosensors, due to their attractive characteristics such as large surface area, electrocatalytic properties and controlled morphology. This thesis aims at exploring the post-functionalization of two types of nano-objects: multiwalled carbon nanotubes (MWCNTs)

and carbohydrate-derived glyconanoparticles (GNPs) and their application in the construction of bioelectrodes for biosensing and energy conversion. In the first part of the thesis, a photoinduced thiol-yne reaction has been investigated by electrochemistry on alkyne-modified MWCNTs using thiol-modified redox probes. The reaction is a compelling alternative to other "click-chemistry" reactions since is it is metal-catalyst-free and it can be controlled in a spatial and temporal way. The immobilization of redox mediators, ferrocene and quinone derivatives, on MWCNT-based electrodes by this reaction led to a considerable improvement in the mediated electrocatalysis by glucose oxidizing enzymes, FAD-dehydrogenases.. The second part is centered on the functionalization of GNPs assembled from a polystyrene-β-cyclodextrin block copolymer via formation of inclusion complexes between the β-cyclodextrins exposed at the surface of the GNPs and the adamantane groups of a fluorescent heptazine derivative. The resulting nanoparticles have been spectroscopically characterized in solution and on surface after their immobilization on electropolymerized poly(pyrrole) films at interdigitated electrodes in a spatially controlled way. In the last part, the GNPs have been used as electrode material for the immobilization of a glucose oxidase enzyme modified with adamantane groups for the detection of glucose. The analytical performances of the bioelectrodes with or without GNPs anchored on different functional poly-pyrrole films are compared and discussed.

Chapter I

General Introduction

Summary

1. Biofuel cells: overview

1.1. Principles of fuel cells

Up today, the majority of the world energy comes from fossil fuels such as oil, coal, natural gas, and their derivatives that provide around 85% of global energy demands [1]. The stocks of fossil fuels are limited and such resources have been extensively utilized as a consequence of the growth of the human population and technological advancements. Furthermore, the use of fossil fuels pones serious environmental issues, since their extraction requires large infrastructures and leads to contamination of the area [1]. The combustion of fossil fuels produces greenhouse gases such as CO_2 that leads to air pollution and contributes to global warming. Altough, nuclear energy can be an alternative, no viable solution has yet been found for the management of toxic waste produced by this method. The dangerous humanitarian and ecological effects of these systems have been highlighted recently after the Fukushima nuclear accident. For this reason, the press in using alternative sources of power and energy, environmentally friendly and renewable, is increasing all over the world. One of the most promising alternative energy conversion technology is represented by fuel cells.

The concept of fuel cell was introduced by Grove and Schoenbein in 1839 [2,3]. Fuel cells are devices that are able to directly convert chemical energy into electrical energy. A fuel cell consists of two electrodes, an anode (negative electrode) and a cathode (positive electrode) connected by an electrolyte medium. An oxidation reaction occurs at the anode and a reduction reaction at the cathode. The oxidation releases electrons, which travel to the cathode via the external circuit doing electrical work. This flow of electrons is compensated by a flux of charges, usually protons, through the permeable membrane that separates the anodic and cathodic compartments.

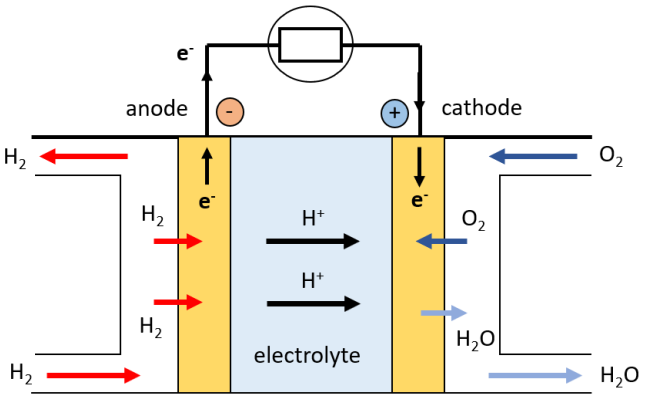

Fig. 1: scheme of a H_2/O_2 fuel cell, exploiting H_2 as fuel and O_2 as oxidant. The overall chemical reaction is: $H_{2(g)} + 1/2\,O_{2(g)} \rightarrow H_2O_{(l)}$

An example of a fuel cell, in which the oxidation of dihydrogen is coupled with the reduction of oxygen at the cathode, one of the most studied system, is reported in *Fig. 1*.

Theorically, as long as the fuels are supplied to the electrodes and the electrode material is stable, fuel cells can operate indefinitely (in reality, the degradation and primarily the corrosion, limit the fuel cell operability). The fuels and products are generally non-pollutants species (like water) and thus the environmental impact is limited.

Conventional fuel cells are classified in five main cathegories based on the nature of the electrolytes and fuels used: proton exchange membrane or polymer electrolyte membrane fuel cell (PEMFC), alkaline fuel cells (AFC), phosphoric acid fuel cells (PAFC), molten carbonate fuel cells (MCFC), solide oxide fuel cells (SOFC) [4]. PEMFCs have been developed by several companies (Toyota, Honda and Hyundai) for powering vehicles while AFCs were used by NASA for powering spacecrafts during the Apollo missions [5]. The advantages of these fuel cells, especially the high operational efficiency, are partially offset by the necessity of expensive and non-renewable catalysts, high operational temperatures and corrosive electrolytes [6]. The performances of fuel cells can decrease over time due to the passivation of the electrode with species such as CO, CO_2, Cl_2. The overall characteristics of the different cathegories of fuel cells are summarized in *Table 1*.

	PEMFC	**AFC**	**PAFC**	**MCFC**	**SOFC**
Electrolyte	Ion exchange membrane	Potassium hydroxide	Liquid phosphoric acid	Liquid molten carbonate	Ceramic
Operating temperature	80 °C	65-220 °C	205 °C	650 °C	600-1000 °C
Charge carrier	H^+	OH^-	H^+	CO_3^-	O^-
Catalyst	Platinum	Platinum	Platinum	Nickel	Perovskites
Applications	Transportation, portable electronics	Space, stationary power, military,	Stationary power, transportation	Distributed power generation	Distributed power generation

Table 1

1.2. Biofuel cells

Biofuel cells (BFCs) are a subcathegory of fuel cells that rely on biological entities like proteins, enzymes or whole organisms as catalysts [7]. The generation of electrical energy from a half cell containing a biological system was first observed by Potter M. in 1911 [8]. In 1960 the interest of NASA in power generation from waste disposal on the space shuttles inspired a

lot of research in this field and ever since, intensive efforts have been conducted focusing in the development and improvement of fuel cells. Many efforts have been made in particular in improving means of enzyme immobilization, electrical communication with the electrodes and ways to limit the use of diffusive redox mediators that are costly and toxic [9]. A critical factor remains the generation of limited power densities, (the upper limit is currently 3.6 W m^{-2} of power using a mixed microbial culture), that falls below those of conventional fuel cells [10]. Despite this, BFCs can operate at mild conditions, lower temperatures (20-40 °C) and at near-neutral pH [7]. Biological catalysts offer compelling advantages: they are renewable and less expensive compared to metallic inorganic catalysts, depending on the scale of production. Another great advantage of BFCs is that they can be scaled down. Thus, BFCs are ideal candidates to replace commercial lithium batteries and conventional fuel cells for low power and portable gadgets. In particular, they can be suitable for providing localized power generation in remote places, for the removal of organic pollutants from wastewater and for powering implantable or non-invasive medical devices and self-powered sensors [9]. BFCs can be classified based on the type of catalyst: microbial fuel cells [11], mitochondrial fuel cells [12], enzymatic fuel cells [13].

1.2.1. Microbial fuel cells

In microbial fuel cells (MFCs), the electrochemical reactions from oxidation of organic substrates at the anode are carried out by electrogenic micro-organisms via an extracellular electron transport (EET) mechanism [13]. Electrogenic microbes include bacteria like *Shewanella putrefaciens* as well as fungal microorganisms like *Aspergillus awamori* [1]. Several mechanisms are responsible for the EET according to the microorganism and the environmental conditions:

- indirect electron transfer which is promoted by artificial or self-secreted mediators that can shuffle electrons from the biological electron transport chain of the microorganisms to the electrode,
- the presence of specific proteins, like c-type cytochrome, that are able to transport electrons through the micro-organism out-membrane extablishing a direct connection with the electrode surface,
- the formation of bacteria nanowires (electrically conductive pili) that connect these electrogenic membrane-proteins to the electrode [14]. Some studies have reported that biofilms and their components can also play a role in the EET process [15].

The use of whole organisms as catalysts is convenient for the presence of multiple enzymes that allow the oxidation of multiple substrates (or mixed substrates) and the elimination of the necessity of enzyme purification which in turns reduces the costs. The micro-organism acts as a micro-reactor that provides appropriate conditions for each enzyme. Furthermore, since enzymes and co-factors can be regenerated by the living organism, the life time of these fuel cells can be of several years [16]. However, the power density is limited by the internal resistance, slow mass transport and poor electron transfer caused by the presence of membranes and biofilms and this constitute the main challenge to overcome for their commercialization [17]. Another drawback is the time required for biofilm formation, the unutilized space of the cytoplasm of microorganism not involved in the redox reactions that reduces the volumetric catalytic activity and the necessity to separate the anode and cathode compartments to prevent bacterial growth [17]. One of the promising applications of MFCs is the possibility of harvesting electricity from 'dirty' fuels, such as organic waste and organic matter in solids and sediments for wastewater treatment [17, 18]. They are also used for hydrogen production from biomass [19] and for sensing applications [17].

1.2.2. Enzymatic fuel cells

Enzymatic fuel cells (EFCs) exploit purified enzymes for the fuel oxidation and oxidant reduction for the generation of electricity. The first EFC was reported in 1964 using glucose oxidase (GOx) at the anode [20]. Compared to MFCs, the nanometer size of the enzymes and the absence of a membrane facilitate mass and electron transfer and the volumetric catalytic activity is also considerably higher [17]. The high selectivity of the enzymes towards their substrate eliminates the necessity of compartmentalization. Thus, in absence of cross-over reactions such as the interaction of the oxidants with the enzyme cofactor, the electrodes can be immersed in one chamber without using a membrane to separate the anode and cathode compartments, which in turn favours the design of simple and miniaturized BFCs. Moreover, enzymes typically do not get passivated by impurities in the fuel. Overall, the key obstacles of EFCs for their practical applications are their poor operational stability (ranging from days to weeks due to the fragile nature of the enzymes often deactivated by solvents or by immobilization to the electrode and problems associated with the stability of mediators), limited voltage output and low power density [21]. Compared to MFCs, enzymes just undergo one-oxidation reaction of the fuel and thus, a cascade of enzymes would be necessary to complete the oxidation of the fuel and increase the energy efficiency.

1.2.3. Mitochondrial fuel cells

In recent years, mitochondrial fuel cells have been exploited as an alternative to MFCs and EFCs with characteristics that are a compromise between the aforementioned two. Mitochondria, also known as the powerhouses of the cell, are organelles present in eukaryotic cells. They contain multiple enzymes that can completely oxidize different organic substrates (pyruvate, fatty acids and amino acids). The total number of electrons that can be collected by the complete oxidation of glucose by glycolysis and Kreb's cycle is 24, while only two to four electrons can be collected by purified glucose oxidizing enzymes in EFCs. Thus, mitochondrial fuel cells can provide similar energy efficiency than MFCs. The mass transport and electron transfer, which arer determined by the presence of c-cythochrome on the mitochondrial membrane, are facilitated compared to MFCs and thus the power densities are generally higher. Compared to EFCs, they have higher lifetimes due to the presence of membranes, altough they lack the regeneration properties of microorganisms. The first mitochondrial-based bioanode coupled with a Pt cathode was designed in 2008 by Minteer S. and Arechederra R. for the complete oxidation of pyruvate into carbon dioxide with a power density of 203 $\mu W\ cm^{-2}$ and a lifetime of 60 days [22].

1.3. Characterization of biofuel cells

In general, a reaction at a catalyst-modified electrode can be separated into three phases: 1) mass transfer between the bulk electrolyte and the catalyst active site, 2) the biological catalyzed reaction and 3) the electron transfer between the active site and the electrode. BFCs are characterized by electrical current density, I, voltage cell, E_{cell}, and power which is defined as the product of the latter (*Equation 1.*) [23]:

$$P(W) = E_{cell}(V)\, I(A) \qquad \textit{Equation 1.}$$

The electrical current intensity, I, is the charge flux entering the anode or leaving the cathode. It is often expressed as current density, j, which is the ratio of the current intensity by the surface area. The power is generally expressed as power density as well. The open circuit potential (OCP) is the potential adopted by the electrode when j = 0. The difference between the OCP of the biocathode and the bioanode determines the electrochemical driving force of the reactions or open circuit voltage (OCV, also called E_{cell}) which is the maximum voltage of the fuel cell. The OCV also correponds to the cell voltage at the thermodynamic equilibrium,

E_{eq}. This value can be calculated by *Equation 2.*, where ΔG_{eq} is the change in Gibbs free energy of the reaction, n is the number of electrons, and F is the Faradaic constant:

$$E_{eq} = -\Delta G_{eq} / nF \qquad \textit{Equation 2.}$$

The overvoltage (η) is the difference between the OCP and the apparent standard redox potential and it is an expression of the efficiency of a catalyst and its deviation from ideality.

The performances of EFCs are evaluated by determination of the OCV, polarization curve and power curve [23]. Potential sweep, amperometry and potentiometry techniques can all be used for the characterization of the electrochemical behaviour of a fuel cell. For the study of the bioelectrochemical reactions that take place in a fuel cell, generally cathode and anode are firstly characterized separately as working electrodes in a three-electrode configuration. In *Fig. 2* the polarization curves of a cathode and anode are reported, that allow the calculation of the OCV, the anodic and cathodic overpotentials and the determination of the limiting electrode which is the one displaying the lowest current value.

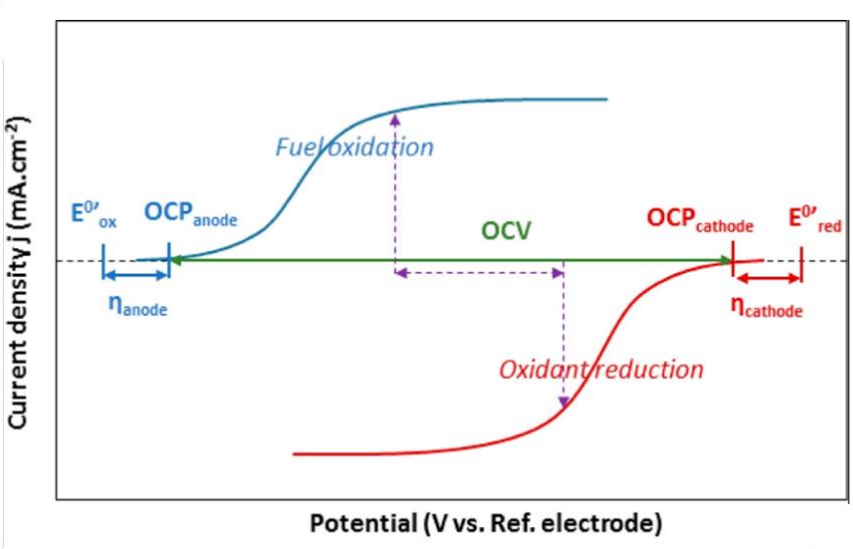

Fig. 2: Linear sweep voltammograms of a bioanode (blue curve) and a biocathode (red curve). At the current density and the cell voltage indicated by the purple arrows, the maximum power density is reached. Ref. [23].

Then, the whole cell behaviour is characterized in a two-electrode configuration in which the cathode is used as the working electrode and the anode as the combination of reference and counter electrodes providing a redout of the OCV. The polarization curve and power curve express the simultaneous evolution of the cell voltage and power density with the current density. When a current starts to flow in the cell, the measured cell potential diverges from its

equilibrium value. Three regions can be distinguished in the polarization curve, in the first region a steady decrease of the cell voltage is observed due to the slow rate of electron transfer kinetics. In the second region, the cell voltage decreases slightly and more linearly following the ohmic voltage drop caused by the intrinsic resistance of the system. The additional lost in the cell voltage until zero observed in the third segment (concentration polarization) is related to mass transport limitations. At this point, the current density reaches its maximum value (j_{max}).

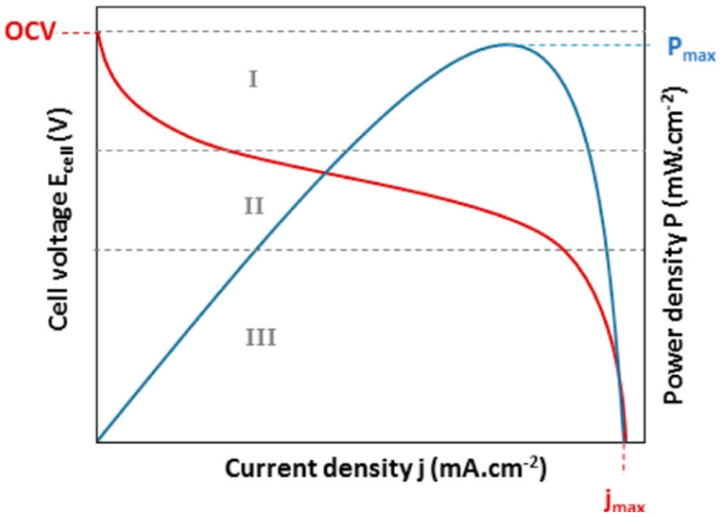

Fig. 3: polarization curve (red) and power curve (blue) of a BFC. Ref. [23].

The potential losses observed in the polarization curve can be mathematically expressed by *Equation 3.* [23] where the cell voltage is the result of the subtraction of the theoretical (thermodynamic) voltage for the total overpotential. This latter includes three different factors: η_{act}, linked with the activation energy required to overcome the energy barrier at the electrolyte-electrode interface, η_{diff} related to mass transport limitations and finally the ohmic overpotential determined by the product of the current that flows through the cell and the sum of the resistances of the system. By optimization of the electrode material and cell design, as well as type and immobilization of catalysts and mediators, each of the above potential losses can be minimized [23]. For instance, ohmic overpotential can be reduced by the choice of high conductive materials, while η_{diff} by the use of porous electrode materials that favour substrates diffusion.

$$E_{cell} = E_{eq} - \eta_{act} - \eta_{diff} - I\Sigma R \qquad \textit{Equation 3.}$$

The power-voltage curve reveals the maximum power delivered by the fuel cell and the optimum operation voltage for maximizing power density.

The current-time curve, determined by chronoamperometry, can be used to examine the operational stability of the electrodes. Galvanostatic charge-discharge measurements are used instead to characterize the capacitance of the device. In particular, the capacitance can be calculated by *Equation 4.*, where I is the constant current applied to charge and discharge the BFCs and ΔU is the voltage drop during the interval Δt.

$$C = I\,\Delta t / \Delta U \qquad \textit{Equation 4.}$$

1.4. Enzymatic biofuel cells

1.4.1. Enzyme wiring

Many enzymes exhibit high catalytic activity, high turnover rates and lower overpotential than the precious metal platinum, although the reached power density is not comparable to that of the conventional fuel cells [17]. The great diversity of enzymes allows the design of different possible EFCs for the oxidation of various substrates and fuels. Furthermore as already mentioned, their high specificity towards their substrates can bypass the necessity of the compartimentalization of the fuel cell. The enzymes used for EFCs are oxydoreductases capable to catalyze a chemical reaction, either an oxidation or reduction.

Three types of enzymes can be distinguished based on the location of the redox active center [24]. One include enzymes in which the cofactor, usually nicotinamide adenine dinucleotide ($NADH/NAD^+$) or nicotinamide adenine dinucleotide phosphate ($NADPH/NADP^+$), is weakly bound to the protein. Examples are glucose dehydrogenase and alcohol dehydrogenase [24]. The regeneration of the cofactor requires organic catalysts such as quinones [25], azines [26], osmium and ruthenium complexes [27], or a biocatalyst such as the enzyme diaphorase [28] or flavin reductase [29]. Another class of enzymes contains the redox center, generally a metallocenter (iron-sulfur cluster, copper center, heme), located at or near the periphery of the protein shell. Multi copper enzymes such as laccases, hydrogenases and peroxidases belong to this group [24]. Finally, some enzymes, like glucose oxidase, contain a strongly bound redox center which is deeply buried in a thick and nonconductive protein or glycoprotein shell. The first two classes of enzymes are able to perform direct electron

transfer (DET). In this case electrons tunnel directly from the enzyme to the electrode without the need of any mediating system. Only a maximum of one monolayer of enzyme molecules can be formed on a planar electrode for DET and the orientation of the enzyme is crucial to maximize the number of enzymes that are favourably connected to the electrode. The reactions start at the standard potential of the redox protein and the cell voltage is thus maximized. According to Marcus's theory, the electron transfer rate decreases exponentially with increasing distance between the electron donor and acceptor [30]. When the tunnelling distance between the redox center and the electrode is too high (> 20 Å), as in the case of enzymes with a buried co-factor, the electrical contact with the electrode needs to be established by using artificial electron donors or acceptors (for reductive or oxidative enzymes, respectively) called mediators [31]. In mediated electron transfer (MET), the redox mediators directly participate in the catalytic reaction. After oxidation of the fuel by the enzyme at the anode, the mediator re-oxidizes the enzyme cofactor while the reduced mediator is re-oxidized by exchanging electrons with the electrode. Thus, mediators repeatedly cycle between the oxidized and reduced forms.

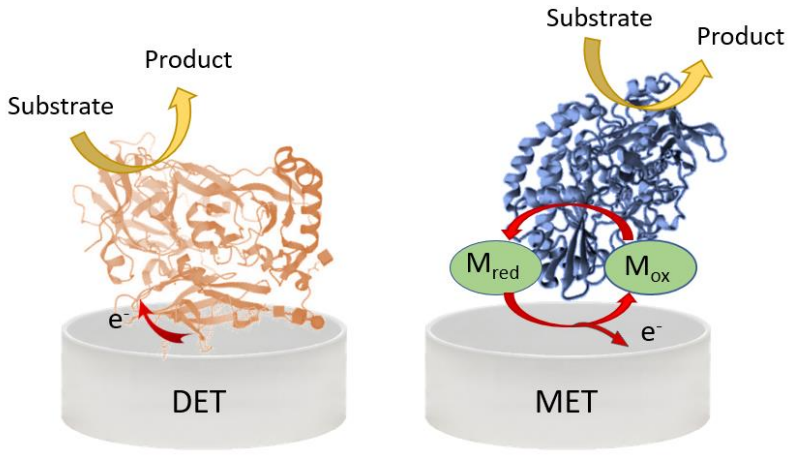

Fig. 4: scheme of the different electron transfer mechanisms.

Mediators should satisfy some criteria:

- their redox potential should be close to the redox potential of the enzyme active center and lower than the oxidation potentials of interfering substances
- reversible electrochemical behaviour
- chemical stability and solubility of both oxidized and reduced forms
- fast electron exchange rate with both the enzyme and the electrode
- absence of direct reaction with the enzyme substrates

The mediators have a large range of possible structures and redox potentials, they can be molecules with low molecular weight such as ferrocene, quinone derivatives and ABTS, transition metal complexes, proteins like cytochrome c, redox polymers such as osmium-based redox polymers. They can be polymerized before enzyme immobilization, co-immobilized with the enzyme or used free in solution [17]. Although MET can increase the number of enzymes electrically wired to the electrode, its usage pones also issues linked with stability and toxicity of mediators, especially for implantable devices. The immobilization of redox mediators at the electrode is thus important, as mediator losses can decrease the current densities. Also, the usage of a mediator inevitably reduces the cell voltage because the reaction takes place at the oxidation or reduction potentials of the redox mediator.

1.4.2. Enzymes used in EFCs

The fuels that can be used at the anodes of EFCs are various, essentially sugars (glucose, lactose, fructose), some alcohols (ethanol, methanol) and dihydrogen.
Significant research has been focused on the use of glucose as the fuel source, since it is ubiquitous and abundant. Glucose is one of the most important energy sources of many living organisms and it is present in human fluids, thus is the ideal candidate as a power source for implantable devices.

Fuels	Enzymes	Cofactor/ metal	Half-reactions
Glucose	Glucose oxidase (GOx) Glucose dehydrogenase (GDH)	FAD NAD^+/PPQ	Glucose → Gluconic acid
Fructose	Fructose dehydrogenase (FDH)	FAD/heme	Fructose → 5-Keto-D-fructose
Cellobiose	Cellobiose dehydrogenase (CDH)	FAD/heme	Cellobiose → Cellobionolactone
Aldehyde	Aldehyde dehydrogenase (AIDH)	NAD^+	Aldehyde → Acid
Lactate	Lactate dehydrogenase (LDH) Lactate oxidase (LOx)	NAD^+ FMN	Lactate → Piruvate
Ethanol Methanol	Alcohol dehydrogenase (ADH)	NAD^+	Alcohol → Aldehyde
Formic acid	Formate dehydrogenase	NAD^+	$HCOOH \rightarrow CO_2$
Hydrogen	Hydrogenase (H_2ase)	[NiFe] [FeFe]	$H_2 \rightarrow 2H^+ + 2e^-$

Table 2.: list of the most common fuels and enzymes for the anodic reactions in EFCs.

Generally, glucose oxidase (GOx) [32] or glucose dehydrogenase (GDH) [33] have high selectivity for β-glucose and they are used for its partial oxidation to gluconolactone at the bioanode. Both GOx and GDH are enzymes with high molecular weight and high stability and a FAD cofactor buried within the protein shell. Thus, mediated bioelectrocatalysis is necessary to promote the electrical communication between the cofactor and the electrode. Other enzymes that are commonly used for the oxidation of glucose are glucose dehydrogenases (GDH) with pyrroloquinoline quinone (PQQ) or nicotinamide adenine dinucleotide (NAD) co-factors [34]. Fructose dehydrogenase (FDH) with a FAD cofactor can be used for the oxidation of fructose instead. Both GDH and FDH have the advantage compared to GOx not to reduce oxygen. The reduction of oxygen at the anode subtracts electrons to the cathode limiting the voltage of the EFCs [35]. The NAD-containing GDH present some disadvantages, primarily the necessity of the addition of NAD to the electrolyte solution thus increasing the cost. The regeneration of the cofactor is also problematic since it generally requires high overpotential [36]. Other examples of enzymes that can be employed at the anode are cellobiose [37], lactate [38], aldehyde [39] and alcohol dehydrogenases [40] that can oxidize cellobiose, lactate, aldehydes or certain alcohols respectively. Hydrogen is a clean fuel with high energy density. Hydrogenases are metalloenzymes containing Ni-Fe or Fe-Fe active sites, able to oxidize dihydrogen. The power output generated by a H_2/O_2 is similar to those of the abiotic conventional fuel cells [41], but the main drawback is that these enzymes are strongly inhibited by the presence of O_2 [42]. In recent years, much research has been directed to the isolation and characterization of O_2-tolerant hydrogenases or in developing strategies to protect the enzyme from the surroundings, for instance by using a viologen-based redox polymer [43].

Fuels	Enzymes	Cofactor/ metal	Half-reactions
O_2	Laccase (Lac) Bilirubine Oxidase (BOx) CueO Polyphenol Oxidase (PPO) Cytochrome Oxidase (Cyt Ox)	Cu	$O_2 + 4H^+ + 4e^- \rightarrow + 2H_2O$
H_2O_2	Horseradish peroxidase (HRP)	Fe/heme	$H_2O_2 + 2H^+ + 2e^- \rightarrow 2H_2O$

Table 3.: list of the most common fuels and enzymes found in EFCs cathodes.

Oxygen is the most widely used oxidizer at the cathode, while only a few devices use hydrogen peroxyde. The four-electron electro-enzymatic reduction of O_2 to water was

described for the first time in 1999 [44]. Enzymes that catalyze the oxygen reduction reaction (ORR) belong to the family of the multicopper oxidases. The family includes laccase [45] and bilirubin oxidase (BOD) [46], which are by far the two most widely used enzymes at the biocathode. Multicopper oxidases possess a group of at least 4 copper centers: T1, where the oxidation of substrates takes place, T2/T3 which is a triatomic copper cluster that facilitates dioxygen reduction and finally the mononuclear copper center allows the transmission of electrons from the substrate to the electrode surface. The main challenge of their use is their appropriate orientation on the electrode surface to favour DET. Other examples of enzymes that can carry out the ORR reaction are polyphenol oxidase (PPO) [47] and cytochrome oxidase (Cyt Ox) [48], but they are rarely used because of the required high overpotential [49]. Peroxidases instead is a class of enzymes that catalyze the two-electron reduction of H_2O_2 to H_2O, they contain a heme group which is responsible of the catalytic activity [50].

The glucose/O_2 EFC, with a glucose oxidizing anode and a O_2 reducing cathode, is particularly interesting since it could become the in vivo source of electricity to power integrated medicals devices [50] (*Fig. 5*).

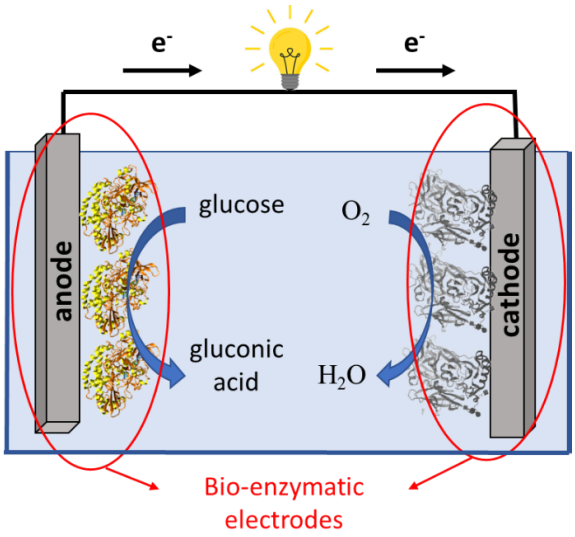

Fig. 5: scheme of an enzymatic glucose/O_2 BFC, with a glucose oxidizing anode and a O_2 reducing cathode.

1.4.3. Applications of EFCs

In the last years, the development of EFCs has been focused mainly on harvesting energy via oxidation of glucose or other fuels with the concomitant reduction of oxygen, constantly available in body fluids of living organisms or in air, via fabrication of portable and

implantable electronic devices. In 2007 Sony showed that a stack of EFCs could power a music player and later on, a glucose-fueled EFC was able to power a toy-car [51]. The implantable devices have the potentiality to replace lithium batteries that pose concerns for human health and that require complex surgical procedures for their substitution [52]. Their power performance is however limited by the concentration of glucose in blood (5 mmol L^{-1}) [53] and oxygen in plasma (~ 90 µmol L^{-1}) [54]. The first implantation was carried out in a grape by Mano and Heller [55]. The partial implantation of EFCs in cyborg lobsters was able to power an electrical watch and a pacemaker [56]. In 2010, the collaboration between Cosnier S. and Cinquin P. led to the first implantation in a mammal. The EFCs composed by a GOx bioanode and a PPO biocathode was placed in the retroperitoneal space of a rat [57]. Various successive studies on implanted devices have been then reported. In one of those, the stability of a biocathode modified with chitosan and implanted in a rat reached 167 days [58]. A MWCNT-based glucose biofuel cell was developed by Cosnier S. et al. was capable to operate stably for 1 year producing 30 mW h [59]. The development of wearable devices, that can be operated using either external fuels or fuels in body fluids, is another potential application of EFCs. They are interesting power sources for health and fitness monitoring. Epidermal lactate/O_2 wearable devices have been fabricated to exploit lactate from sweat as a fuel [60] and lactate based biofuel cells have been integrated onto contact lens to exploit lactate in tears [61].

Considerable challenges still remain and efforts should be addressed in improving the operational stability and voltage output for future practical applications. The power densities of EFCs are in the range 1-1000 µW cm^{-2}, rarely above 1 mW cm^{-2}, still much lower than metal-catalyzed fuel cells or lithium-ion batteries. The lifetime of current commercial lithium batteries is 7-8 years [62], so efforts should be addressed in future also in improving the device lifetime. The implantation in animals can cause inflammation responses and facing sterility and biocompatibility issues is thus fundamental. Both implantable and wearable devices need robust and flexible electrical components to bear body movements. Layer-by-layer, buckypaper or screen printed EFCs are ideal for this purpose since they have the necessary flexibility to withstand frequent bending or folding and low fabrication costs [63]. In addition, the availability of the oxydant may become a limiting factor in power generation, especially in implantable devices [64]. Moreover, current wearable devices based on LOx are not able to provide stable power output due to the fluctuations in the level of lactate in body fluids. To overcome all these limitations, a combination of different strategies of enzyme immobilization, engineering and design of electrode materials are thus necessary.

Fig. 6: scheme of the principal applications of EFCs. Adapted from Ref. [63].

2. Biosensors: overview

2.1. Principles of biosensor

Biosensors are defined as analytical devices that convert a biological response into a quantificable and processable electrical signal [65]. Different parts can be distinguished (*Fig. 4.*):

- an interface where a biological event occurs as a consequence of the binding of a bioreceptor or biorecognition element to an analyte producing a signal.
- the transducer element converts the signal produced by the biorecognition event (current, light, pH, heat, etc.) into another form (generally an optical or electronic signal).
- the electronic components amplify and process the signal, and they convert it in a digital form.
- a computer software with a display generates the result (in the form of graph, figure, number, etc.) that is readable and understandable by human operators.

Various criteria are involved in the classification of biosensors, depending on the type of bioreceptor, transducer, detection system and technology [66]. The major areas of application are in medical diagnosis and environmental monitoring.

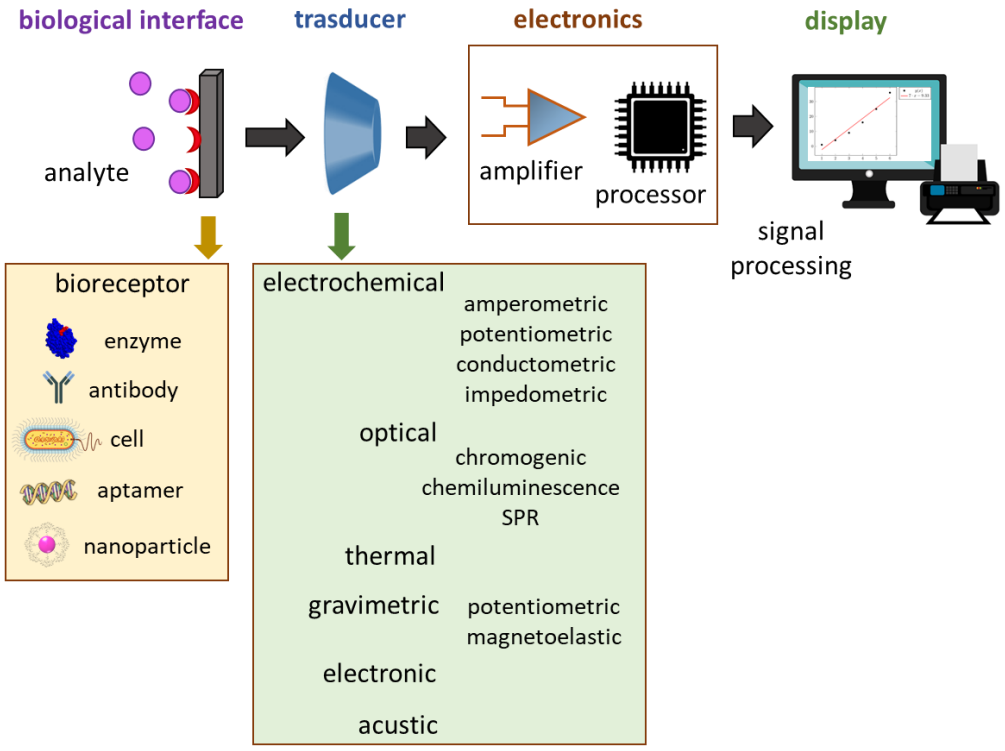

Fig. 7: schematic diagram of a typical biosensor with various types of bioreceptors and transducers.

The biosensor must meet some requirements to be effective:

- the bioreceptor should be highly specific for the analyte and stable at the storing conditions. This means that it should be able to detect a target analyte in a complex sample containing interference species. Any non-specific interaction with the surface of the sensor should be suppressed.
- the reproducibility should be high, both in terms of precision (showing little variation between successive measurements) and accuracy (providing a mean value closer to the actual value every time the sample is measured).
- the response should be fast and linear over the concentration range of interest. The noise arising from electronic components or the transducer noise should be also negligible.

Depending on the type of application, other requirements need to be taken into consideration. For instance, the ones developed for invasive monitoring for clinical purposes should be small and biocompatible and they should provide real-time analyses [65].

2.2. Types of bioreceptors and transducers

The biocatalysts can be enzymes, nucleic acids, antibodies, receptors or living biological systems like whole cells and microrganisms [65]. Analytical devices that rely on antibody-antigen interactions are called immunosensors and they are probably the most widely used, especially in diagnostic due to the high specificity and biocompatibility of the systems. Antibodies or antibody fragments are excellent candidates for sensing applications. The antibody (Ab) structure is made of four polypeptide chains with a Y shape, the arms contain constant and variable domains forming a unique three-dimensional recognition pattern for a determinate antigen. Antigen-based tests become successful for enzyme linked immunosorbent assay (ELISA) but since they are costly and the response time takes hours, antigen-tests based on the recognition of multiple bacteria, viral antigens [67] and cancer markers [68] via electrochemical sensing gained a lot of popularity [69]. Abs can be used directly using fluorescent conjugates or the detection is realized by using a sandwich assay. In this case, a secondary labelled Ab binds the first bioreceptor Ab or an Ab coupled with an enzyme allowing the quantification of the analyte via an enzymatic reaction [70]. Monoclonal Ab produced by specific cell clones as well as recombinant Ab consisting of genetically manipulated fused antigen binding domains have been extensively used for sensing purposes for their augmented stability and smaller sizes [71]. Biosensors based on aptamers or nucleic acids are also very common, in this case the recognition elements are single stranded DNA or RNA oligonucleotide sequences with the capacity to recognize various target molecules [65]. Nucleic acids are isolated from libraries of oligonucleotides by a selection process in vitro called systematic evolution of ligands by exponential enrichment (SELEX) [72]. They achieve sensitivity due to complementary base-pairing that can detect even a single mismatch. While aptamers are unfold in solution, they fold upon association with the analyte forming specific thridimensional structures due to their self-annealing properties. Thus, they are able to recognize their target (small molecules, proteins and even whole cells) based on their shape with high affinity and specificity [73]. Cells, bacteriophages and tissues can be used for detection of analytes and to monitor cell physiology, usually via protein-protein interactions. Enzymes recognize their substrates by a lock-and-key or induced fit model with high specificity. A more detailed description of enzymatic biosensors will be addressed further.

The detection of the target molecules can be achieved by using different transducer elements. Piezoelectric biosensors measure the alterations in the resonance frequencies caused by the

adsorption of molecules on the crystal surface [74]. Thermometric biosensors measure the absorption or the release of heat in the reaction medium [75]. Several optical transducer formats can be adopted for the optical detection of the analyte, they can be based on differences in the refractive index, on the production of chemiluminescent molecules, on absorbance, fluorescence emission or fluorescence quenching [76]. In general these types of sensors are very rapid being only limited by the diffusion of the biomolecule-recognition event but the analysis of turbid sample is not possible and the equipments are expensive. Other detection methods include surface plasmon resonance, that detects changes in the local refractive index originating from the binding of an analyte which in turn causes changes in the optical angle required for the excitation of the surface plasmon [77], and electrochemical biosensors.

2.2.1. Electrochemical biosensors

The detection via electrochemical methods is the most popular and commonly described, especially with enzyme-based biosensors [78]. The advantages include the operational simplicity, the possibility to analyze turbid and complex media and matrices in real-time, the fast response and the cost-effective components. Furthermore, the biosensor components can be easily miniaturized and even easily integrated for parallel analyses. The signal produced by the reaction between the biological element and the analyte under investigation influences measurable electrical properties causing a change in: current (amperometric), potential (potentiometric), conductivity (conductometric) or resistance (impedometric) of the medium [79]. Electrochemical sensing generally requires a reference electrode, a counter or auxiliary electrode and a working electrode, which is the transduction element [65]. The amperometric biosensors continuously measure the current resulting from oxidation or reduction of an electroactive species in a biochemical reaction. The current is measured at a constant potential (amperometry) or during controlled variations of the potential (voltammetry). In the linear range, the magnitude of the measured current is directly proportional to the bulk concentration of the analyte in the sample, and thus to its production or consumption rate as well as its mass transport rate within the adiacent biological layer. Glucose biosensors based on the amperometric detection of hydrogen peroxide are examples of this type. The sensitivity of the amperometric devices is generally higher to potentiometric devices [65].

Potentiometric devices measure the potential at the working electrode versus the reference electrode when no significant current flows between them. They provide information about ion activities inside the electrochemical cell, usually triggered by the activity of an enzyme [65].

The relationship between the concentration of the analyte and the potential is governed by the Nernst equation (*Equation 5.*), where E_{cell} is the observed cell potential at zero current, E^0_{cell} is the constant potential of the cell, R the universal gas constant, T the absolute temperature in degrees Kelvin, n is the number of the electrodes involved in the reaction, F is the Faraday constant and Q is the ratio of ion concentrations between oxidized and reduced forms.

$$E_{cell} = E^0_{cell} - \frac{RT}{nF} lnQ \qquad Equation\ 5.$$

An example of this type of biosensor is offered by Shishkanova T. V. et al. [80], in which the hybridization process of complementary single-stranded (ss) oligonucleotides attached to a PVC membrane, determines a redistribution of the ions within intermolecular regions producing a measurable change in ion concentration.

Conductometric devices can detect changes in the electrical conductivity of a sample solution containing an analyte. Finally, the electrical impedance across the working and counter electrode concerning the reference electrode is measured by impedimetric biosensors. Many immunosensors and aptasensors are impedimetric biosensors [81]. They can be used either to study enzymatic reactions that produce changes in the ionic strenght of the solution or to monitor changes caused by the direct binding of the analyte [65]. For instance, the binding of the analytes can decrease the electron transfer from the solution to the electrode determining an increase of the impedance of the system.

2.2.2. Enzymatic biosensors

Enzymatic biosensors are the most representative class of biosensor [66]. Enzymes are very attractive for biosensor applications because they display high specificity for their substrates. Moreover, the enzymatic reaction can release a pletora of measurable products such as protons, electrons, light, heat. The detection relies typically on two mechanisms, one is the conversion of an analyte to a detectable product and the other is a change of the enzymatic activity upon binding of the analyte both in a positive or negative way (inhibitors) [65].

Enzyme-based electrochemical biosensors have been historically classified into three generations based on the integration of the bio-receptor to the transducer (*Fig. 8*) [66]. In the first generation biosensors, also called mediator-less biosensors, the diffusion of the analyte to the transducer surface is able to produce a measurable signal. The first biosensor produced by the pioneer work of Clark in the 1956, who is considered the 'father' of biosensors [82], that

was able to measure the oxygen concentration in blood, belongs to this group. The enzymatic biosensor fabricated later on, in 1969, by Guilbault G. G. and Montalvo J. G. [83] for the detection of urea, the heat-sensitive enzyme sensor, also known as "thermistor", developed by Mosbach K. [84] and the optical biosensor for alcohol developed by Lübbers D.W. and Opitz N. [85] are other examples. In the second generation biosensors, also called mediator amperometric biosensors, other components such as auxiliary enzymes, mediators, are integrated with the bioreceptor for improving the analytical efficiency. For instance, the lactate analyzer LA 640 developed by Rocher in 1979 [86] exploited a soluble mediator, hexacyanoferrate, to shuffle electrons from lactate dehydrogenase to the electrode. In the third type, the enzymes and eventual mediators are intimately connected to the electrode or into an adjacent matrix. Third generation biosensors offer generally low cost, faster response and feasibility of performing repeated measurements. The biosensor reported by Liedberg B. et al. in 1983 based on surface plasmon resonance [87], is one example of this type.

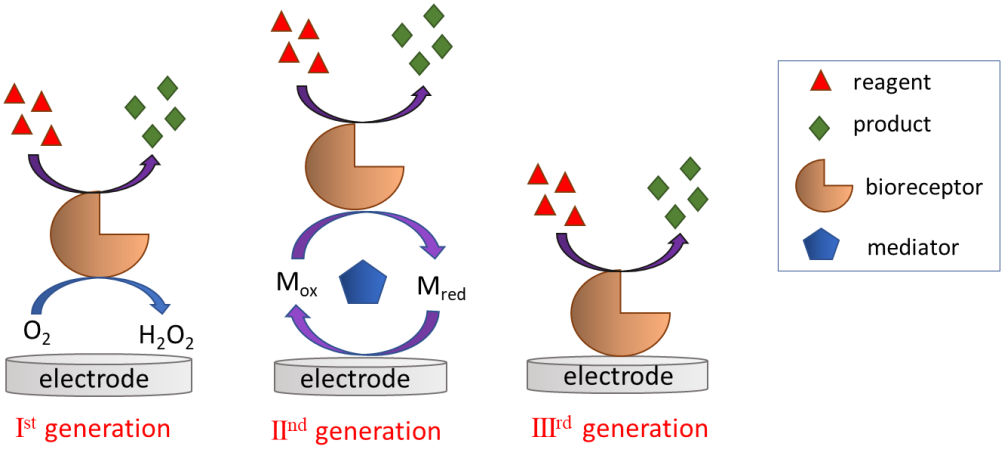

Fig. 8: three generations of the biosensor (M_{OX}: oxidized mediator, M_{red}: reduced mediator).

The most common used enzymes in biosensing are GOx [88], HRP [89] and PPO [90].

GOx is the standard enzyme used for biosensors, it is quite stable and easy to obtain [91]. It has high molecular weight (130-180 kDa), and contain a non-covalently tightly bound FAD co-enzyme in the active site. During the enzymatic reaction, FAD is reduced to $FADH_2$ while glucose is oxidized to gluconolactone. $FADH_2$ is re-oxidized by the dissolved molecular oxygen or by a mediator with the concomintant production of hydrogen peroxide (H_2O_2) [92] (*Equation 6.*). The dominant detection approach is electrochemical and the produced H_2O_2 is

oxidized (+0.7 V vs SCE) leading to a current increase directly proportional to glucose concentration [93].

$$GOx\,(FAD) + glucose \rightarrow GOx\,(FADH_2) + gluconolactone$$
$$GOx\,(FADH_2) + O_2 \rightarrow GOx\,(FAD) + H_2O_2 \qquad \textit{Equations 6.}$$

HRP is a small glycoprotein found in the roots of the horseradish plant. The enzyme catalyzes the two-electron reduction of H_2O_2 to water. The ferriheme prosthetic group of HRP ($HRPFe^{3+}$) is oxidized to compound I (that contains a oxyferryl iron and porphyrin cation radical). This intermediate can be directly electroreduced (via formation of another intermediate compound II) to its native state at the electrode. The enzyme catalyses the oxidation of substrates (phenols, aromatic amines) during the concomitant reduction of H_2O_2. Quinone products can be electroreduced at the electrode (-0.1 V vs SCE) [94]. The catalytic reaction is reported in *Equation 7*.

$$H_2O_2 + substrate \rightarrow 2H_2O + product \qquad \textit{Equation 7.}$$

Apart from electrochemical detection, this enzyme is also commonly used in ELISA assays and immunohistochemistry because the formed products are often coloured [94].

PPO is a high molecular enzyme (130 kDa) that can be naturally found in many vegetables (potatoes, mushrooms), it contains two Cu^{2+} ions coordinated with three histidine amino acids in the active site [95]. It catalyzes the oxidation of phenols into quinones. In literature, many amperometric biosensors based on the oxidation of the enzymatically produced quinones have been reported, many of these are able to sense phenolic compounds which are harmful for human and animal health and which are toxic for the environment [90].

$$1/2\,O_2 + substrate \rightarrow H_2O + product \qquad \textit{Equation 8.}$$

2.2.3. Glucose biosensors

Among the different types of biosensors, glucose biosensor is certainly the most widely studied and the one with an acclaimed success story [86]. Nowadays more than 75% of the global biosensor market is dominated by glucose biosensors with previsions to reach a 38 $ BN market until 2027 [96]. Its importance and success arises from the clinical relevance in diabetic patients. Diabetes affect over 17 million people only in the US with a huge society

cost since it is a life-lasting deasease [97]. The concept of glucose biosensor was developed by Clark in 1962. The biosensor used glucose oxidase (GOx) entrapped at a Clark oxygen electrode by a dialysis membrane and was based on the measurement of oxygen consumption in response to glucose [98]. At present, the preferred alternative is to measure hydrogen peroxide [99]. In 1975, Yellow Spring Instrument Company launched the first successful commercial glucose biosensor based on amperometric detection of the enzymatically produced hydrogen peroxide [100]. In 1976, Clemens A. H. et al. [101] incorporated an electrochemical glucose biosensor in a bedside artificial pancreas. Many improvements have been added since then. Biosensors constituted by disposable electrodes containing an enzyme plus a mediator have been then developed so that the electrons are delivered to the electrode by the mediator and not oxygen to circumvent the limitations linked with the fluctuations in the oxygen levels [102]. Mediators are regenerated at lower applied voltages reducing the background signal of interference species. A mediator-based screen-printed enzyme electrode was launched in 1987 by MediSense (now Abbott) with a pen-sized meter for home blood glucose monitoring [103].

Nowadays, GOx is still the most widely used enzyme in glucose biosensors, followed by glucose dehydrogenase. Despite the enormous amount of publications done in these past years, only few biosensors were commercially viable and successful. The causes can be conducted to the instabilities of the biocomponents and biofueling. Glucose biosensors need to face additional challenges for market introduction such as regulatory apects for medical safety and a reliable long-term calibration. Currently, the most employed are the handheld glucose biosensors that analyze single drops of blood using a lancet. The devices require frequent measurements that are uncomfortable especially for young patients. A major advance for the in vivo applications was reported by Shichiri M. et al. with the first needle-type enzyme electrode for subcutaneous implantation in 1982 [104]. Currently implanted and non-invasive glucose sensors are under development.

Future efforts in biosensor research should be focused in improving stability and biocompatibility of the biological components, for instance with addition of layers of hydrogels, with the combination of nanoparticles or carbon nanotubes in an antibiofouling coating [105, 106], or by using biomimetic approaches. Some of these bioinspired approaches include the use of nanoenzymes [107], which are essentially nanoparticles that mimic the three-dimensional structure of enzymes, the use of molecularly imprinted polymers (MIP) with

synthetic recognition sites as alternatives to natural receptor sites and fabricated by molecular imprinting processes [108].

2.3. Characterization of biosensors

The performance of a biosensor is evaluated generally based on a set of parameters [109]. Enzyme-biosensors are characterized by their apparent K_M and V_{max}. K_M is equal to the substrate concentration at the half-maximum rate. It is a measure of how efficiently an enzyme converts the substrate into a product. V_{max} is the response at the maximal substrate concentration. When the appartent K_M value is significantly greater than its value for the soluble enzyme, the enzymatic reaction is limited by the presence of a significant barrier for substrate diffusion or a co-substrate is reacting with the enzyme with increased rate. K_M and V_{max} are generally determined by the Lineweaver-Burk plot or double reciprocal plot, which is also useful for determining the mechanism of enzyme inhibitors [110], as indicated by *Fig. 9*.

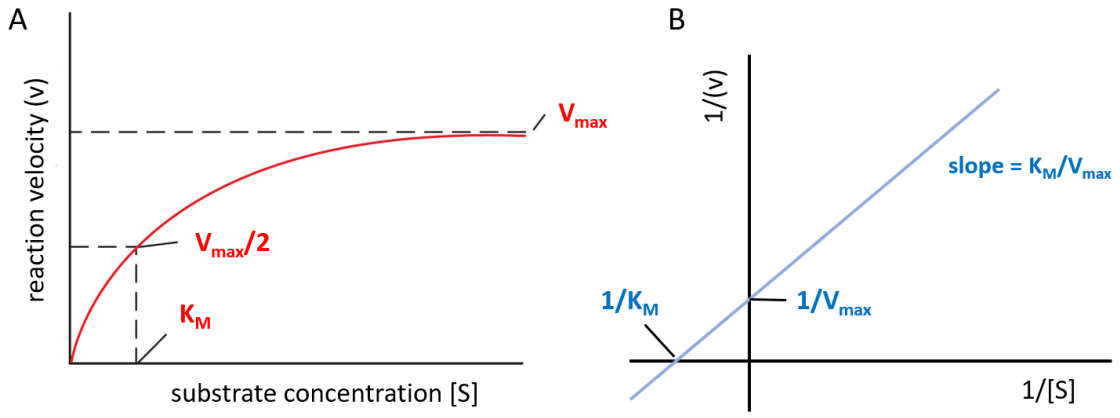

Fig. 9: typical A) Michaelis-Menten saturation curve and B) Lineweaver-Burk reciprocal plot of an enzyme reaction.

Upon analysis of the measurements obtained by a biosensor, a plot is thus produced in which the signal output is correlated to the concentration of the analyte. For instance, in an amperometric glucose biosensor the current density is plotted versus glucose concentration. The sensitivity is defined by the slope of the change in signal output versus the change in concentration (as indicated by *Equation 9.* where X_1 and X_2 are two analyte concentrations in the calibration plot, and Y_1 and Y_2 are their corresponding signals) [109]. The calculation of the sensitivity is applicable only in the linear range, the range in which the signal output is proportional to the fluctuations in analyte concentration. The biosensors characterized by a

steeper slope are more sensible and more able to distinguish a small change in the analyte concentration. The sensitivity is a measure of the ability of a biosensor to detect the lower concentration above zero [109].

$$Sensitivity = \frac{Y_1 - Y_2}{X_1 - X_2} \qquad Equation\ 9.$$

The limit of detection (LOD) is defined as the minimum amount of analyte that can give a distinguishable signal, it is also a measure of the ability of the biosensor to disclose the minimum difference between two measurements at any concentration. It is expressed by *Equations 10.* [111]. In the first, k is the signal-to-noise ratio and $STD_{background}$ is the standard deviation of the background signal. k can be arbitrarily chosen depending on the desired accuracy, typically is around 3. The LOD can also be expressed as the value of three standard deviations divided by the sensitivity of the biosensor [110].

$$LOD = k * STD_{background}$$

$$LOD = \frac{3STD_{background}}{sensitivity} \qquad Equations\ 10.$$

The selectivity is the ability of the biosensor to distinguish a closely related group of molecules, with a structure similar to the analyte, to other molecules in a complex solution [112]. Specificity is the ideal condition, where only a single target analyte is sensed by the biosensor. The response time is another important parameter, described as the time required to generate a signal [110]. In case of an amperometric glucose biosensor for instance, the response time is the time necessary for the generated current to reach its maximum value following the addition of glucose in the solution. It is impacted by mass transport of both analyte and product, the presence of layers or membranes at the electrode interface and their physico-chemical characteristic such as thickness and permeability [110].

3. Enzyme immobilization methods

For both biofuel cells and biosensors, the immobilization of the biologic components in a suitable matrix or support is essential [113, 114]. The performance of the bioelectrodes is related to the amount of enzyme immobilized. A poor immobilization would led to a kinetic losses [114]. The immobilization of enzymes and redox mediators can extend the lifetime of the system because their stability is usually increased compared to those in solution [113]. Moreover, the

enzyme can be used repeatedly after immobilization [115]. In biotechnological applications, the immobilization of enzymes can also be useful to separate the enzyme from the reaction solution and the products. The establishment of an efficient electrical connection to the electrode is essential, and for enzymes capable of performing DET, an immobilization strategy that favours a specific orientation on the electrode becomes a key factor to have a performant bioelectrode. For bioelectronic applications, the miniaturization of the devices requires enzyme immobilization as well. There is a range of approaches for the immobilization of enzymes, including physical adsorption, covalent binding, cross-linking, entrapment, affinity binding (*Figure 10.*) [115]. Each immobilization method presents advantages and drawbacks, the choice of the most suitable depends on the nature of the molecule and the desired application. In all cases, it is important that the catalytic activity of the enzyme is retained as much as possible.

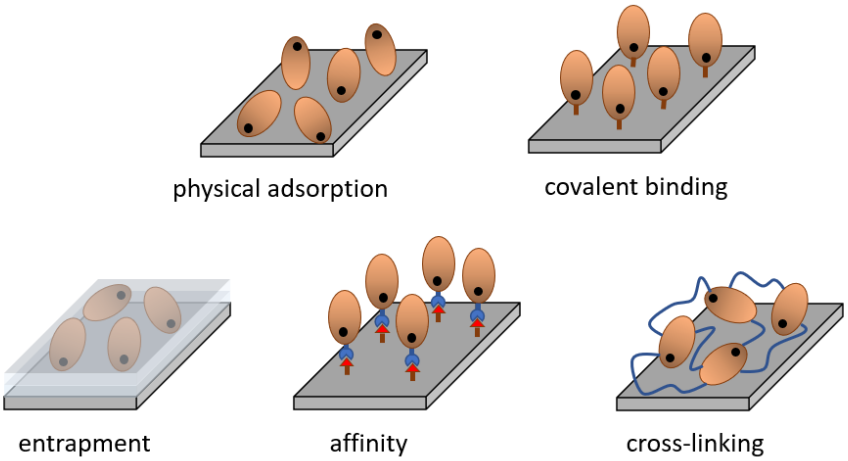

Fig. 10: scheme of the principal enzyme immobilization methods.

3.1. Adsorption

Adsorption is based on non-specific weak bonds: hydrophobic interactions, Van der Waal's forces, hydrogen bonds, electrostatic interactions [116]. This method is practically simple, the enzyme dissolved in solution is placed in contact with the support for a certain amount of time followed by washing steps with buffer to remove the unadsorbed molecules. Alternatively, the enzyme solution is drop-casted on the surface of a support and once dried, it is successively washed [117]. It is low-cost and reagent-free and generally is non-destructive towards enzyme structure. Another advantage is the possibility to regenerate the surface. The main drawback is that the enzyme is loosely bound to the support and it can be easily desorbed from changes

in pH, temperature, ionic strenght or polarity of the solvent. This method is not particularly suitable for enzymatic-biosensors because non-specific adsorption of other proteins or molecules on the transducer can cause interference and contamination. Furthermore, the interaction of the enzyme with a metallic surface can force a change in the native structure with exposure of its inner regions, that could ultimately results in protein denaturation. For this reason self-assembly monolayers of thiols, surfactants, polyelectrolytes, molecular linkers are often used to minimize the direct interaction between enzyme and a metal electrode. Nanomaterials with their three-dimensional configurations can also help preventing enzyme denaturation. Adsorption of the enzyme at the electrode results in casual orientation and thus, the substrate binding sites of the electrode or the redox active sites can be hindered and positioned distant from the surface of the electrode.

It is possible to distinguish some subcategories of adsorption: physical adsorption and electrostatic binding [116]. Physical adsorption involves hydrophobic interactions and Van der Waal's forces mostly. In electrostatic binding, charged surface areas of the enzyme (resulting from the difference between the isoelectric point and the pH of the solution) interact with areas of the support or the matrix with opposite charge, via ionic and strong polar interactions. A common electrostatic binding technique is the layer-by-layer deposition [116]. This method is done by immersing a support coated with a charged polyelectrolyte in a solution of enzyme that bears positive or negative charges at the surface. Polyelectrolytes are water soluble polymers containing ionic charges along the polymer chain. The process of deposition is repeated to obtain a multilayer of opposite-charged layers. The advantages are the simplicity, biocompatibility, low-cost while the activity of the enzyme is not affected significantly. Tough, the presence of a charged matrix can lead to distorsions in the kinetics of substrates and products and affect their diffusion and the pH stability of the enzyme can be altered.

3.2. Covalent binding

This method forms covalent stable bondings between functional groups of the enzyme and a support. Generally, the functional groups involved in the binding are not essential for the enzymatic activity, such as amino groups in lysines, thiol groups of cysteines, carboxylic groups of aspartic and glutamic acids, hydroxyl groups of serine and threonine of the side chains [118]. The procedure followed for the covalent binding can be essentially divided in two steps: the activation of the support using linker molecules with specific functional groups followed by the covalent binding of the enzyme to those groups. Linker molecules are

typically carbodiimide, glutaraldehyde, maleimide. Carbodiimide allows the binding between the carboxyl groups of a support and the amino groups of an enzyme, N-hydroxysuccinimide (NHS) is often associated to carbodiimide to improve the efficiency of the covalent coupling. Glutaraldehyde instead forms a Schiff-base with amino groups of the support followed by reaction with amine groups of the enzyme. Cysteine residues can form stable thioether bonds with the unsaturated carbonyls of maleimide. Click-chemistries can be employed as well for protein immobilization. These reactions, first introduced by Sharpless et al. in 2001 [119] that has been very recently awarded with a Nobel Prize in Chemistry (2022), have rapidly developed in recent years in various research areas. They constitute powerful ligation tools for biomolecule immobilization due to their fascinating features, such as high efficiency, simple operation and mild reaction conditions.

The main advantage of this method is the high stability of the bonding that prevents enzyme detachment from the surface. Substrate accessibility to the active site is generally not hampered and is possible to control the site of immobilization favouring a specific orientation at the electrode to reach an efficient electron transfer. Protein engineering using site-specific mutagenesis can be useful to introduce or remove functional groups at the protein surface to control the site of immobilization, for instance by removal of excess of cysteines or insertion of a unique cysteine residue at a desired site. Reproducibility is often higher with this method than adsorption or entrapment [116]. Despite this, some essential functional groups may get inactivated due to the irreversible bonding to the support that reduces the freedom degree of the enzyme. These phenomena can lead to unfavorable configurational changes with potential loss of the catalytic activity [120].

3.3. Entrapment

An enzyme is physically confined in a three-dimensional polymeric network or inorganic frameworks via this method. The network allows substrate and product diffusion but retains the enzyme molecules preventing leaching [113]. Polymeric composites, in which at least one component is a polymer, are commonly used for enzyme entrapment. Since the enzyme does not react directly with the polymer, enzyme activity is usually conserved and leaching is minimized [113]. Via this method, is possible to recreate a suitable microenvironment for the enzyme by tuning the matrix properties such as polarity and pH. It is also more easy to entrap multiple enzymes. Control over the thickness and pore size of the matrix is necessary since

substrate diffusion and the conductivity can be impaired. At the same time, if the pore size is too large, enzyme leaching can occur.

The immobilization is conducted generally by a polymerization reaction that is triggerred by a change in the experimental conditions or by a chemical reaction (for instance chemical or electrochemical oxidation). In electrochemical polymerization, the monomer is oxidized or reduced at the electrode upon application of a potential forming radical species that react with each other to generate oligomers and finally a polymer that deposits at the surface of the electrode. Conducting polymers such as polyaniline, polypyrrole or polythiophene are often used for this purpose (*Fig. 11A*) [121]. During this process, if an enzyme is dissolved in the monomer solution, it can be encapsulated into the growing polymer without chemically reacting with it. Electrochemical polymerization allows to control the thickness of the film by varying the applied potential, polymerization charge, nature of electrolyte and reaction time [121]. This method thus enables the modulation of the amount of enzyme and redox mediators immobilized [121].

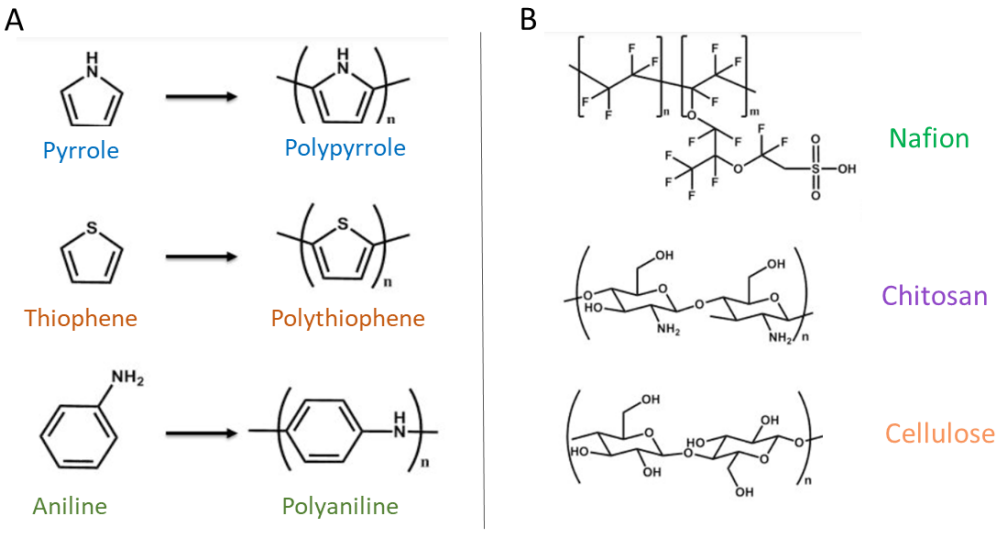

Fig. 11: examples of A) conductive and B) non-conductive polymers for enzyme immobilization.

In photopolymerization, an insoluble matrix is created by a chain-growth polymerization reaction triggered by light exposition in the ultreviolet or visible region. Poly(vinyl alcohol)-bearing styrylpyridinium groups has been used for enzyme entrapment in biosensors [122]. Another alternative method of enzyme immobilization is microencapsulation, the enzyme is enclosed in a lipoidal or polymeric micelles [123]. Polysaccharide-based gels and non-conductive polymers such as Nafion, chitosan, cellulose or alginate are very popular [124, 125, 126]

(*Fig. 11B*). These matrices provide biocompatible, non toxic microenvironments and offer long term stability. Entrapment in a carbon paste, made from a mixture of carbon powder and a binder such as paraffin, is another popular method for the preparation of electrodes with incorporated biological components and mediators [127]. Cosnier S. et coworkers have entrapped enzymes (GOx and laccase) into a CNT matrix by mechanical compression in a mediator-less glucose biofuel cell [128]. The entrapment in metal-organic frameworks (MOFs) is a recent trend due to their high surface area, functionalizable pore and cage walls [129].

3.4. Cross-linking

Protein aggregates are formed on the electrode with the assistance of bifunctional or multifunctional cross-linkers. The cross-linking agents form intramolecular and intermolecular covalent bonds with enzyme molecules. Sometimes enzymes are cross-linked in presence of a functionally inert protein such as bovin serum albumine (BSA). This method creates a stable surrounding microenvironment. Glutaraldehyde [130], poly(ethylene glycol) diglycidyl ether (PEGDGE) [131] and activated ester [132] are examples of cross-linkers that can react with the amine groups of enzymes. The enzyme is initially deposited on the support and then cross-linked with the aid of the cross-linking agent ensuring an high enzyme loading at the surface. The stability of the system can be regulated by changing the concentration of the cross-linker. The advantages and drawbacks are similar to the ones described about the covalent binding.

3.5. Affinity

Affinity interaction is achieved by using specific groups on a matrix support that can selectively interact with enzyme tags via supramolecular interactions. These interactions are formed by the sum of weak and reversible electrostatic interactions, hydrogen bonding, van der Waals' forces, π-π stacking interactions, coordination with metal ions. Avidin-biotin [133], lectin-carbohydrate [134], cyclodextin-adamantane [135], metal ion-chelator [136] are common affinity partners. Cysteine, histidine, mannose-binding protein, adamantane, biotin and glutathione S-transferase are examples of affinity tags [137]. The introduction of these tags requires often complex procedures, but the enzyme activity is generally retained because it involves a single point of attachment and the non-covalent nature of the interaction reduce the risk of conformational changes. Depending on the procedure, affinity-based immobilization allow the control over the orientation of the enzyme. In other cases, such as enzyme

biotinylation, multiple affinity sites can be introduced on a single protein and the process is less controllable.

Biotin and histine can interact with cyclodextrins by inclusion complexes or with nitrilotriacetic acid (NTA) forming a coordination complex with copper or nickel ions [136, 138]. Finally, the affinity of an enzyme for a substrate can also be exploited for the controlled orientation of the enzyme to the electrode. An example is the affinity of the hydrophobic cavity of laccase from *Trametes versicolor* for polycyclic aromatic compounds, such as anthraquinone, that was exploited for enzyme immobilization on multiwalled carbon nanotubes [139].

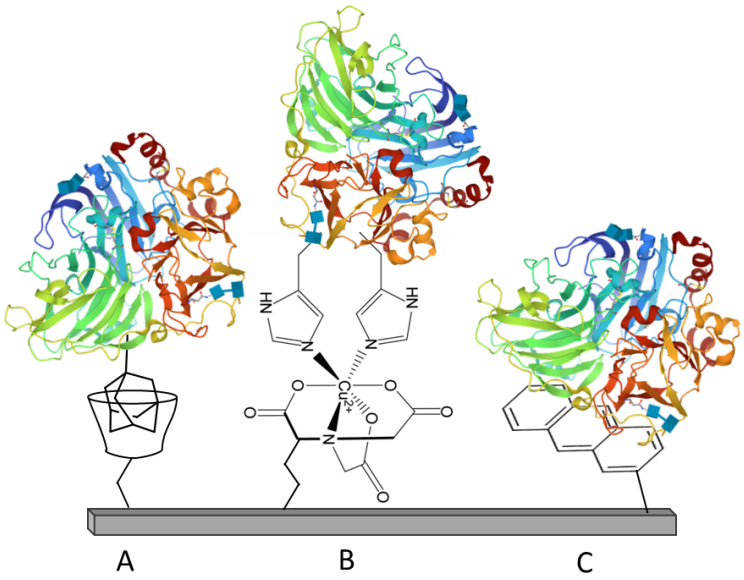

Fig. 12: examples of enzyme immobilization strategies via affinity binding: A) β-cyclodextrin-adamantane host-guest complexes, B) Cu^{2+}-nitriloacetic acid-polyhistidine complex, C) substrate-enzyme affinity complex.

4. Nanomaterials-based bioelectrodes

By definition, nanomaterials are materials with a size smaller than 100 nm, they can exhibit novel and unique properties different from the bulk behaviour [140]. In the last decades, nanomaterials have become essential in numerous applications: cosmetics, electronics, food, drug development [140]. They are mainly employed as biomolecule tracers or for the modification of electrodes [115]. In particular, they confer the capability to control the architecture of the electrodes at a nanometer level. In general, nanostructured electrodes possess an elevated active surface area that can maximize the interaction and immobilization of the biomolecules enabling significant loading of enzymes and mediators in comparison to

planar electrodes. Their use can minimize the enzymatic conformational changes, maintain and improve the catalytic activity of enzymes [141]. Nanomaterials are also important for achieving better DET for enzymes ensuring a preferential orientation of the enzymes [142]. In literature, the EFCs with maximum power densities have been obtained from electrodes altered with nanomaterials [63]. Furthermore, nanomaterials can contribute to the improvement of electrical, chemical, optical and magnetic properties of the sensing devices, improving their sensitivity and stability [143, 144]. Nanoengineered porous materials and nano-objects such as carbon nanotubes, inorganic and organic nanoparticles, are all examples of electrode materials contributing to the improvement of the enzyme-electrode interface.

4.1. Carbon based nanomaterials

Carbon-based materials are versatile, they come in various shapes and forms: zero-dimensional structures such as fullerenes, diamond clusters, one-dimensional structures like carbon nanotubes (CNTs) and nanofibers, two dimensional structures like graphene and three-dimensional structures such as nanocrystalline diamond, fullerites, nanorings, carbon nanodots (CNDs) (*Fig. 8*) [145]. Carbon-based nanomaterials also offer the possibility to form nanocomposites. In these materials, the properties of different nanomaterials are merged in a single novel material, nanoparticles-modified CNT, ceramic-CNT, teflon-CNT are some examples [146].

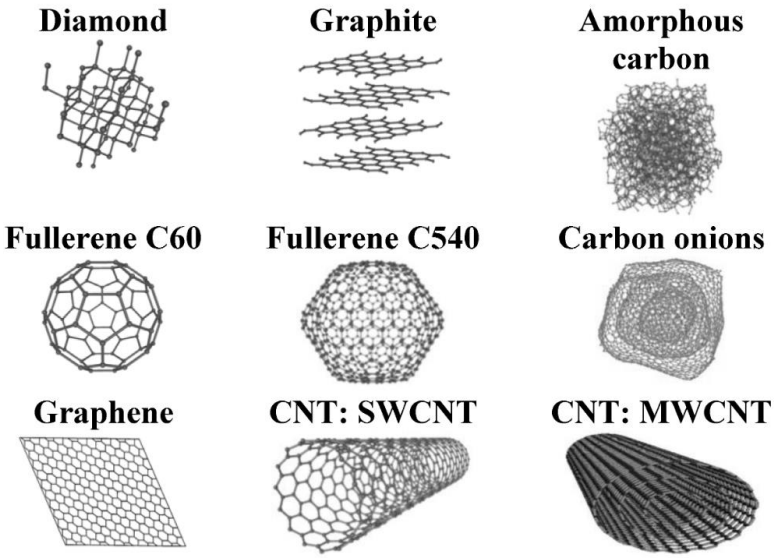

Fig. 13: different types of carbon nanomaterials. Ref. [145].

Among these, carbon nanotubes and graphene are the most widely used. The basic structure of graphene, nanotubes and fullerenes consists of a layer of sp^2-bonded carbon atoms. This configuration is responsible for their good electrical conductivity and ability to form charge-transfer complexes with electron donor groups [147]. The atomic bonds are very strong and stable and they can tolerate extreme conditions of high temperature and pressure. sp^2 hybridized carbon atoms confer them elastic modulus and tensile strength compared to sp^3 hybridized carbon atoms. The implementation of different carbon nanomaterials in the fabrication of biosensors and biofuel cells has received in the course of last years great attention worldwide.

Graphene consists of a one-atom-thick sheet of sp^2 hybridized carbon atoms forming six-member rings. The description of the remarkable characteristics of graphene was reported by Geim and Novoselov in 2004 that won the Nobel Prize in Physics and Chemistry in 2010 for their contribution [148]. A large variety of techniques are available for graphene fabrication, the most common is the mechanical exfoliation (repeated peeling) of highly ordered pyrolytic graphite [149]. The chemical oxidation of graphene leads to graphene oxide, a graphite derivative with hydroxyl, carboxyl and epoxy groups covalently attached to its layers, with an improved dispersion in aqueous solvents [150]. It has been employed as a component of solar cells, aeroplanes, satellites, cars as well as biosensors, bio-batteries and transistors [151].

4.2. Carbon nanotubes

CNTs are are allotropes of carbon in the form of rolled-up graphene sheets with a cylindrical shaped structure. The formation of worm-like carbon deposits were firstly described by Radushkevich L. V. and Lukyanovich V. M. in 1952 [153], while the discovery of MWCNTs is attributed to the Japanese physicist Iijima S. in 1991 [154]. The electronic properties of SWCNTs were described by Mintmire J. W. and al. that brought the attention to this class of materials paving the way to their future application in scientific research [155]. CNTs are divided into two types: single-walled carbon nanotubes (SWCNTs) and multi-walled carbon nanotubes (MWCNTs). SWCNTs with diameters in the range 0.4-3 nm are composed of a single-layer graphite, while MWCNTs are formed by multiple single-wall nanotubes sharing a common axis with diameters in the range 1.4-100 nm, depending on the number of graphene tubes. The interplanar distance between each of the concentric cylinders is 0.32-0.35 nm, similar to that between the graphene layers in graphite [155]. Both have micrometer lengths, although is possible to grow SWCNTs up to centimeters long.

4.2.1. Synthesis

CNTs are synthesized by different methods: physical methods that convert carbon into nanotubes via high-temperature processes, electric arc discharge and laser ablation, or by chemical vapour deposition (CVD), which instead is performed at atmospheric pressure or in vacuum and lower temperature [157, 158].

The electric arc discharge is the most common and probably the easiest method [159]. The reaction chamber is filled with an inert gas (argon, helium) at controlled pressure, while a potential difference is applied between two graphite electrodes separated by approximately 1 mm. When the graphite roads are brought closer, a plasma is formed by high temperature discharge between the electrodes. Carbon atoms are ejected from the anode and they accumulate on the cathode forming a deposit. The deposit contains a mixture of nanotubes, amorphous carbon, nanoparticles, fullerene-structures. Sometimes a metal catalyst is used along with graphite at the anode and in this case, the nanotubes are deposited on the arc chamber walls. In both cases, a further purification step is necessary to separate the nanotubes from other forms of carbon and from metal particles. Different parameters can affect the yield of CNTs formation, for instance the pressure of the gas or the applied potential [159].

In the laser ablation technique, a laser pulse is used to vaporize a carbon target, containing also some traces of a mixture of Ni and Co metals, placed in a reaction tube at 1200 °C. As a result of the ablation, the formed nanotubes are carried by a inert gas flow and finally collected in the cooler end of the tube in the form of ropes [160]. This method was used for the first time by Kroto H. W. to synthesize fullerene in 1985 [161] and successively by Guo T. et al. in 1995 [162] for the formation of nanotubes. After the subsequent heat treatment, which is done to remove the fullerenes structures, each rope is composed by a bundle of aligned SWCNTs. Also in this case, it is possible to control the average diameter of the tubes by varying some parameters. The procedure is quite expensive and metal particles will also residue in the CNTs.

Chemical vapor deposition (CVD) is based on the pyrolysis of a gaseous hydrocarbon such as methane, carbon monoxide or acetylene, as carbon sources, mixed with a metal catalyst at temperatures around 700°C – 900°C and atmospheric pressure [163]. This technique has been used to form various carbon-based materials, including SWCNTs and MWCNTs. The mechanism of CNTs growth is still object of studies. In a first mechanism, called ‘tip growth

mode', the catalyst particles stay at the tips of the growing nanotube during the growth process while in the 'base growth mode' the catalyst particles remain at the nanotube base [164]. This technique offers more control over the type and structure of the obtained nanotubes and the possibility to scale up the process compared to the previous methods.

4.2.2. Properties

CNTs are considered the stiffest materials in nature (approximately ten times higher than steel), especially in the axial direction, while they are quite soft in the radial one [165]. The mechanical strenght increases with the diameter of MWCNTs. At the same time, they bear large bending or compressive strains due to their elastic modulus. CNTs are very good thermal conductors along the tube and good insulators laterally to the tube axis. Due to the one-dimensional structure, they are good electric conductors (a thousand times higher than copper wires) [115]. In CNTs, each carbon atom is covalently bonded to three neighbour carbons via sp^2 molecular orbitals, while the fourth valence electron is delocalized over all atoms contributing to the electrical nature of CNTs. CNTs have either metallic or semiconducting behavior, depending on their diameter and structure [167].

The mechanical, electrical properties of CNTs are also affected by the presence of defects. Different defects, such as inclusion of five- or seven-membered rings, sp^3 hybridized sites and open ends, are produced along the hexagonal graphene framework during the synthesis and the purification of CNTs [177]. For instance, acid treatments with H_2SO_4 and HCl are effective in removing amorphous carbon impurities and metal catalytic particles, but they cause secondary effects such as opening of CNTs ends and oxidative damage of the CNTs sidewalls [168]. Defects are also created intentionally by chemical functionalization of CNTs. The presence of residual metallic impurities is however responsible for some of the electrical and catalytic properties of CNTs [169].

4.2.3. Structure

The structure and helicity of CNTs is described by the roll-up chiral vector (C_h) that can be expressed by *Equation 11.*, in terms of unit vectors a_1 and a_2 of the graphene sheet by means of integers (n, m) [166]. The C_h vector connects crystallographically equivalent sites on a graphene sheet. The translation vector r is orthogonal to C_h, parallel to the tube axis and it represents the length of the unit cell of an (n, m) tube (*Fig. 9*).

There are three possible chiralities for SWCNTs: armchair, zigzag and chiral depending on the (n,m) indices and thus how the hexagons are orientated along the axis of the tube [166]. The electrical properties of the CNTs depend on those configurations and the consequent electronic energy band gaps. In the armchair ((n, n), m = n), the hexagon rings are lined up parallel to the axis of the nanotube and the electrical properties are similar to metals. In CNTs with a zigzag configuration ((n, 0), m = 0), the hexagons are oriented in a circle around the nanotube diameter. Finally, the ones with a chiral configuration ((n, m), n ≠ m), have hexagones that do not form any specific line. In the latter two, CNTs share electrical properties similar to semiconductors. In a random sample of SWNTs, around two thirds of SWCNTs are semiconductor-type and one-third are metallic type. In the case of MWNTs, each layer of graphene can have a different chirality and MWCNTs are generally considered as metallic if at least one graphene layer composing their structure is metallic [169].

$$C_h = n\,a_1 + m\,a_2 \qquad \textit{Equation 11.}$$

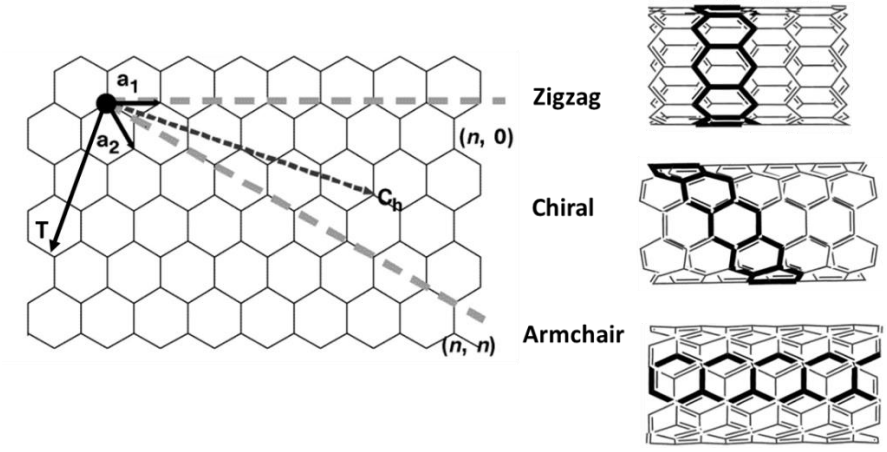

Fig. 9: graphene sheet diagram with the chiral vector and different structures of nanotubes. Adapted from Ref. [167].

4.2.4. Applications

Because of their remarkable electrical, chemical, mechanical properties, CNTs have found a wide range of applications in nanoelectronics, solar cell technology, optics and material science [170]. Over the last decades the number of patents and publications on CNTs has increased exponentially. CNTs have been used as nanofillers for polymer composites, as additives in the costitution of anodes in lithium ion batteries [171] or in proton exchange

membrane fuel cells with the aim of reducing platinum loading while maintaining the fuel cell efficiency [172]. Moreover, they have been used in supercapacitors since their high surface area result in high electrostatic double-layer capacitance [173]. They are extensively used for the construction of bioelectrodes because of their electrical conductivity, large surface area, good biocompatibility and functionalizable sidewalls. The three-dimensional network with high porosity is very advantageous for the immobilization of enzymes. At the same time, the thin diameter of CNTs can approach the active site of enzymes promoting direct electron transfer [144]. The sensitivity of biosensors is improved because of the enhanced adsorption of target molecules promoted by their large specific surface area [174]. CNTs have been used in field effect transistor (FET) biosensors where the bio-recognition event led to changes in the CNTs conductivity. FET based sensors have been developed for enzymatic, immunosensors and even DNA sensors [175].

4.3. Functionalization of carbon nanotubes

Organic solvents or surfactants are required to produce stable dispersion of CNTs for practical applications [176]. To improve the solubility and processibility of CNTs, mechanical methods can be used to increase the number of open ends and defects, ultrasonic treatment is one of those. Alternatively, chemical modification can be used to introduce polar groups: oxygen, hydroxyl, phenyl on the surface of CNTs for the same scope [176]. The functionalization is associated with a change of hybridization of the carbon atoms from sp^2 to sp^3 and the simultaneous loss of p-conjugation system. This results in a variation of the mechanical and electrical properties of the CNTs. The introduction of specific functional groups enables the subsequent chemical reactivity of CNTs and it may be used for several applications [177]. For instance, the presence of oxygenated functional groups introduced by chemical treatment have enhanced the performance of an alcohol dehydrogenase (ADH)-based bioelectrode, promoting the electrooxidation of the NADH generated during the catalytic cycle of ethanol oxidation [178]. Furthermore, the functionalization of CNTs can provide a chance for favourable enzyme orientation.

Various methods have been developed over the years, they can mainly be divided in two types: covalent and non-covalent. These two types are essentially exohedral derivatizations, since they involve the external modification of the sidewalls of the CNTs, while in the endohedral functionalization, the hollow inner cavity of the CNTs is used as a capillary for the storage and incorporation of fullerenes structures or nanoparticles. CNTs can be also

decorated externally with inorganic nanomaterials, mainly metal nanoparticles and metal oxide nanostructures such as ZnO, CuO, SnO_2 to form hybrid nanocomposites [177] (*Fig. 14*).

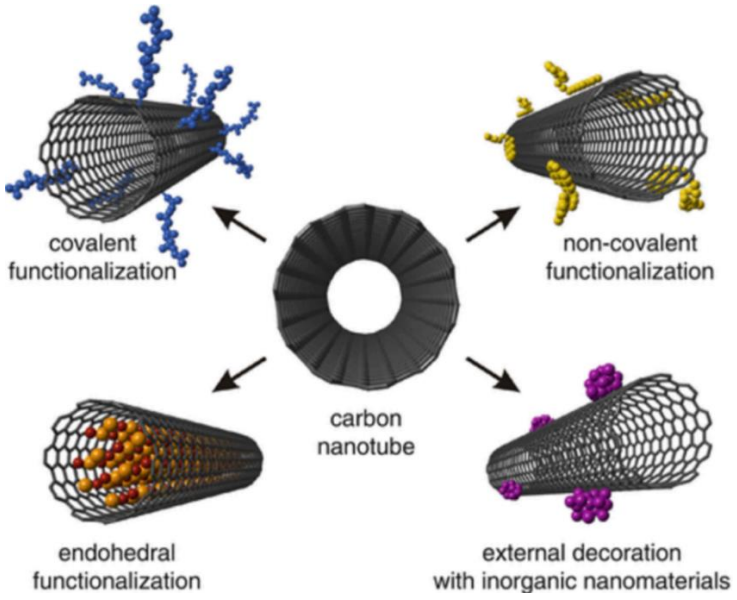

Fig. 14: most common methods of functionalization of CNT. Adapted from Ref. [179].

4.3.1. Covalent functionalization

Covalent functionalization is based on the introduction of functional groups on CNTs by creating stable covalent bonds. The treatment of CNTs with oxidative agents, either strong acids such as sulfuric acid and nitric acid, or basic agents such as ammonium hydroxide or hydrogen peroxide, results in the formation of oxygen-containing groups (carboxylic, carbonyl or hydroxyl groups) on the sidewalls of intact region of the CNTs skeleton or in pre-existing defects or open-ends of the CNTs. The extent of functionalization can be controlled by duration and hardness of the oxidation treatment.

Those groups can then serve as reagents for further coupling reactions with other molecules, mainly through esterification or amidation reactions [180]. Other reactions that form covalent bonds include cycloaddition reactions, addition of carbenes [176] and nitrenes [176, 181] and radical additions [176]. The radical addition of diazonium compounds is one of the most popular method for the covalent modification of CNTs [182].

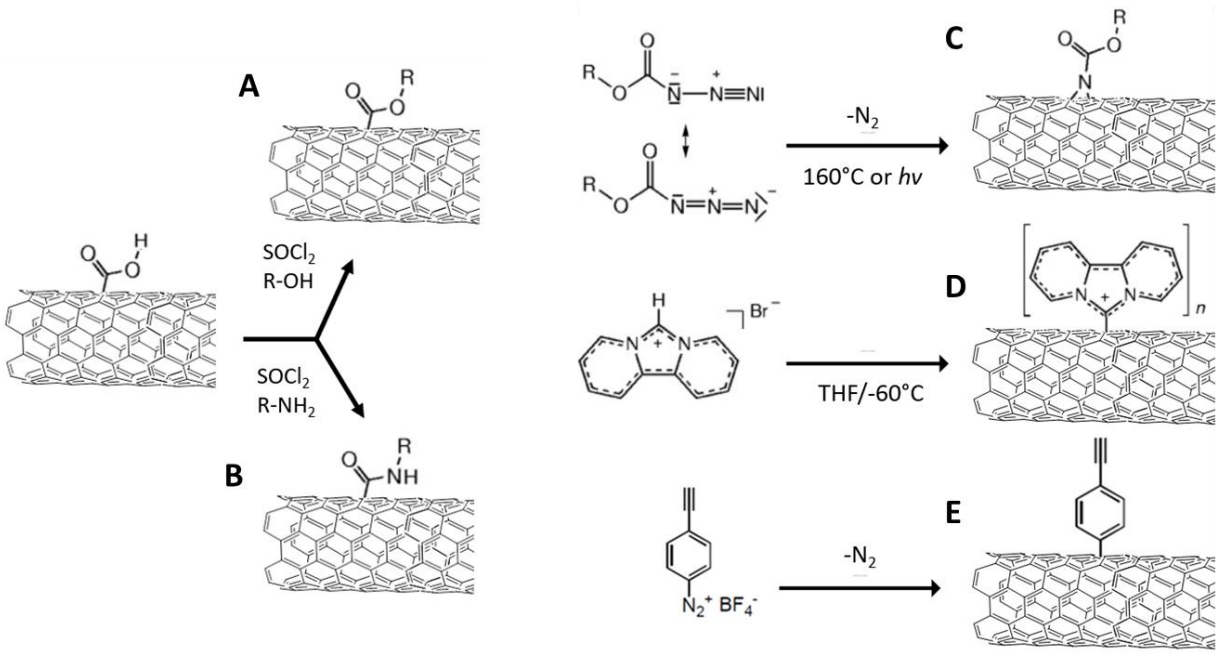

Fig. 15: some of the principal covelent modification strategies of carbon nanotubes: A) esterification, B) amidation, C) addition of nitrenes, D) addition of carbenes, E) addition of a aryl diazonium.

4.3.2. Non-covalent functionalization

These methods exploit the presence of sp^2 carbon atoms on the sidewalls of CNTs and is based on the formation of strong interactions, π-π stacking and hydrophobic interactions, between CNTs and delocalized electron rich-systems such as aromatic compounds [183]. The structure integrity and the intrinsic properties of CNTs are preserved, differently from covalent methods that often have the effect of decreasing the electrical conductivity. The formation of effective π-π stacking interactions using pyrene, anthracene, porphyrins has been used for the immobilization of both redox mediators and enzymes [184, 185].

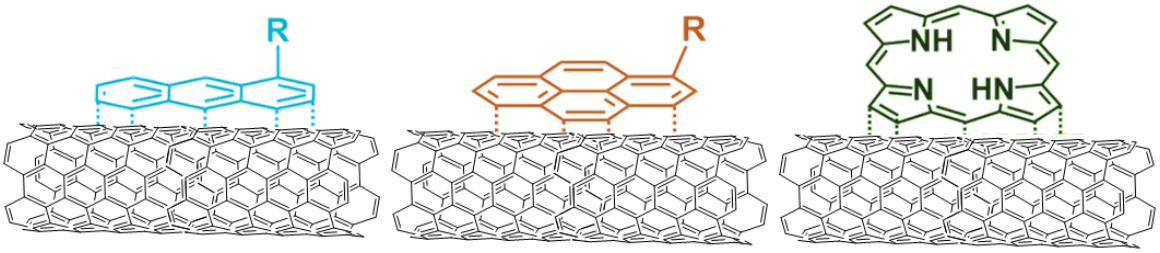

Fig. 16: π-π stacking interactions between aromatic compounds and carbon nanotubes.

Conjugated polymers with polar side chains, like polyvinylpyrrolidone (PVP) or polystyrenesulfonate (PSS), are also used to wrap around nanotubes to improve their solubility [186]. The physical adsorption of surfactants on the CNTs surface has been employed to prevent the aggregation of CNTs [187].

4.4. Nanoparticles: overview

Nanoparticles (NPs) are a type of nanomaterials with different shape and size (1-1000 nm), solid or hollow, with various surface chemistry and chemical composition [188]. They can be classified essentially into two groups: inorganic and organic NPs (*Fig. 17*). More in detail, inorganic NPs are made up of inorganic materials such as carbon, silica and metals such as gold, silver and iron oxide. They can be divided in metal NPs (Ag, Au, Pd), magnetic NPs (that possess a metal oxide core), semiconductor/QDs (based on CdS, CdSe).
Organic NPs are costituted by lipids and polymers of natural or synthetic origin and they can be classified in polymeric NPs, micelles, liposomes, nanogels, dendrimers. Hybrid NPs can also be formed by conjugation of organic and inorganic parts [189].

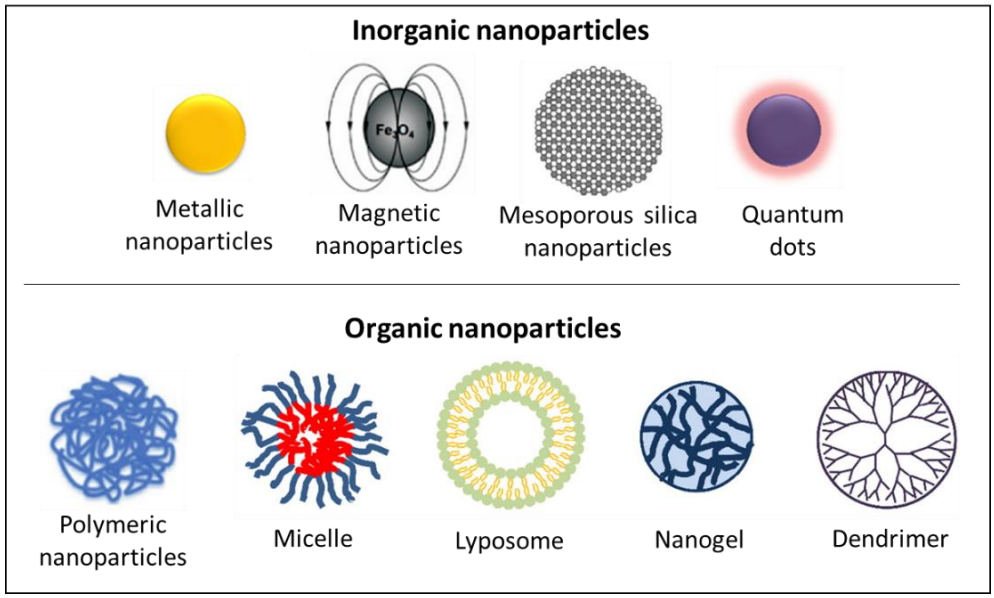

Fig. 17: representative structures of various nanoparticles. Adapted from Ref. [190].

Generally, NPs can be generated by bottom-up strategies or top-down strategies [191]. In the first case, the NPs are assembled from the atomic level in case of inorganic NPs or from the monomeric constituents for the organic ones. For instance, the reduction of Au^{3+} to Au^{0} in presence of stabilizing agents such as citrate or phosphanes that prevent NPs aggregation and

uncontrolled growth, is the bottom-up approach for the synthesis of metallic AuNPs [192]. Nanoprecipitation and procedures based on emulsification are instead the most representative bottom-up methods for the synthesis of organic NPs. The bottom-up methods are very useful for the encapsulation of active molecules into organic NPs. In top-down strategies instead, bulk solids are cracked and down-sized into NPs by procedures such as milling, laser ablation, ion sputtering, high pressure homogenization. These strategies are less common employed because of their high cost [191].

NPs have attractive electronic, catalytic properties, size-dependent optical and magnetic properties, different from those of the bulk materials [144]. Sometimes the properties can be predicted with high precision from the particles size. They have found several applications especially in the biomedical field as therapeutic and diagnostic agents. In biosensing applications, they can be used for the modification of electrode surfaces or for the conjugation with bioreceptors (antibodies, oligonucleotides, enzymes, etc) [193]. They can be effective to improve the biosensor sensitivity, reduce the detection limit and contribute to the signal amplification. NPs are also used as labels in immunosensors, genosensors and cell sensors [197]. NP catalysts exhibit much higher mass activity than film-based catalysts. While the adsorption of enzymes on bulk electrodes leads often to their denaturation, their absorption on nanoparticles is generally less destructive towards enzyme activity. Since the size of the NPs and enzymes are comparable, the enzyme usually maintains its natural conformation. Similarly to CNTs, the electron transfer distance can be decreased by employing NPs and many reports can be found in the literature of the direct electrochemistry of enzymes at NP-modified electrodes [144, 195, 196]. Also, they are becoming increasingly popular in bioenergy conversion and NPs are often introduced as additives to boost microorganism metabolism in biofuel production systems in MFCs applications [197].

4.4.1. Inorganic nanoparticles

Metallic NPs have excellent conductivity, high stability and biocompatibility, high surface area, that make them good candidates in their use in combination with redox enzymes at the electrode surface [197]. Moreover, the synthetic procedure is relatively simple. Due to their intrinsic metallic characteristics, they act as electron carriers between the enzyme and the solid electrode improving the bioelectrocatalytic reaction [198, 199].

Gold nanomaterials have unusual optical and electronic properties and high affinity with thiol groups. They are the most commonly used metal NPs in electrochemical biosensors due to their biocompatibility, vaste electrochemical potentail, and easy protein conjugation [200]. They are often deposited and incorporated on CNTs generating a composite with improved electrocatalytic activity. The combination of aptamers and gold nanomaterials is often used in sensing platforms [201]. In some cases, AuNPs have been not only used as immobilized at the electrode surface but dispersed in the electrolyte to allow the regeneration of the electrode surface [202]. In some potentiometric biosensors, the target molecules after being captured by the primary receptors immobilized on the transducer, are bond to secondary receptors linked with AuNPs that act as labelling agents [203]. In biofuel cells, they are equally often used, like in the mediatorless sugar/oxygen biofuel cell developed by Wang et al. [204] (current density of 40 $\mu A\ cm^{-2}$, with a 20% decreased power density observed after 12 hours). Sometimes core-shell structures composed of AuNPs with a different metal for the shell are used because the lattice strain effect that is created between two different metals can further enhance the catalytic activity. Gold palladium core-shell NPs have been used as cathode catalysts in a MFC for wastewater treatment [205]. Furthermore, AuNPs show excellent electroactive properties towards hydrogen evolution reaction (HER) [206]. Platinum (Pt) nanostructures have been extensively used for the direct electrocatalytic oxidation of small organic molecules such as formic acid and methanol [207]. Palladium (Pd) and copper (Cu) are much more abundant and less espensive than Au and Pt metals and they also show high electro-catalytic and sensing characteristics [208, 209].

Magnetic nanoparticles (MNPs) consist of a magnetic core surrounded by a non-magnetic shell. The most studied core is composed by iron oxides such as magnetite (Fe_3O_4) or maghemite (γ-Fe_2O_3) [210], while the shell is often, for biological applications, composed by silica [211] or an organic polymer [212]. MNPs have been applied mostly for biomedical applications, cell separation, drug delivery. If the size is sufficiently small, they show superparamagnetic behaviour at room temperature, so they become magnetized only in presence of an external magnetic force. Furthermore, they can convert the magnetic energy into heat [213]. This opens the possibility to manipulate the NPs at a distance for therapeutic approaches in vivo such as photothermal tumour ablation [214]. They have also found utility in environmental applications for the removal of heavy metals and organic pollutants [215], in energy storage devices [216], biosensors and detection systems [217]. They can be easily trapped by magnets and be retained efficiently close to the electrode surface. In particular, they have

been used in the so-called ‘dispersible electrodes’ in which biorecognition-functionalized MNPs are dispersed in the sample solution to maximize the interaction with the analytes and subsequently collected by a magnet to a macroscopic electrode for the quantification [218]. MNPs are suitable for biosensing applications since biological receptors do not show any magnetic behaviour and thus, the biorecognition event is not affected by interference or noise. Catalytic active MNPs have been developed as nanoenzymes to provide catalysis for biochemical reactions on biosensors and biofuel cells [66].

Mesoporous silica NPs also offers several benefits such as tunable pore structure, huge surface area and chemical-functionalizable surface [219]. These NPs have been mainly developed as imaging contrast agents, ablative therapy sensitizers [220], and drug delivery vehicles [221]. The loading and release of cargo molecules can be controlled by specific external stimuli. By tailoring the pore sizes, the transport of electrons can be significantly improved. Mesoporous silica NPs with cleavable linkage have been used for the design of an electrochemical sensor for the quantitative measurement of prostate-specific antigens [222].

Quantum dots (QDs), are composed of semiconductor materials from III-V or II-VI groups of the periodic table, such as ZnS, ZnSe, CdS, CdSe, with particle diameters typically ranging from 1 to12 nm [140]. They have also tunable size and they are suitable for imaging applications due to their broad absorption bands, narrow emission, elevated brightness and extremely large Stokes shift. They are resistant to photobleaching and chemical degradation, which make them advantageous compared to common organic dyes and fluorescent proteins [223]. They also have generally high fluorescence quantum yields. Thus, they are suitable for biosensors with optical redout [224]. Some optical DNA or oligonucleotide sensors are based on the Förster (Fluorescence) Resonance Energy Transfer (FRET) quenching, the recognition event between fluorophore-labeled ssDNA oligonucleotides attached on a donor (QDs) and a complementary sequence positioned on a quencher (acceptor) is revealed by the appearance of a fluorescent signal [225, 226]. In other cases, the production of an optical signal is caused by the interaction of QDs with surface plasmons on gold materials or viceversa [227]. QDs have been also used for other type of biosensor transducers, for instance in the measurement of the electrochemical impedance spectroscopy signal by Xu Y. et al. [228].

4.4.2. Organic nanoparticles

Organic NPs have received less attention and investment compared to inorganic materials although research is rising over recent years especially in the pharmaceutical field [228]. They are generally more soluble in aqueous environment and they are more environmentally friendly compared to inorganic NPs [229].

The progress in polymer chemistry, as well as advances in orthogonal chemistry reactions, has pavented the way for the creation of polymeric NPs with precise control over the architecture of the individual monomeric constituents and their properties [230]. Polymeric NPs (nanospheres, nanocapsules and polymersomes) have shown great potential in biotechnological applications due to their biocompatibility, biodegradability, versatile chemistry. A lot of research in pharmaceutical and food industry has been focused on poly (lactic acid), poly (glycolic acid) and recently poly-ε-caprolactone. They are commonly exploited as drug carriers since they show high drug loading efficiency and rate of endocytosis [230].

Micelles are polymeric enclosed structures formed by self-assembly of amphiphilic compounds in aqueous medium. Usually, amphiphilic block copolymers form core/shell-like nanostructures with a size usually in the range from 5 to 100 nm, a hydrophobic core and a hydrophilic shell [229]. Micellar structures with different shapes can be formed by varying the length and number of blocks. These micelles have the ability to solubilize and load hydrophobic therapeutic drugs or imaging agents by encapsulation in the hydrophobic core. Some amphiphilic copolymers are responsive to external stimuli such as temperature, pH.

Liposomes are spherical particles with a size of > 100 nm, formed from one or more lipidic or phospholipidic constituents delimiting an enclosed aqueous compartment. They are thus higly biocompatible and biodegradable. Liposomes are uptaken by cells via endocytosis after a process of adhesion and fusion with the cell membrane bilayers. A few liposome formulations have been approved by US FDA for clinical use. Examples of liposome applications in food industry are the entrapment of proteolytic enzymes for cheese production [231], nutraceuticals, flavours or antimicrobials for enhancing the quality of food [232].

Nanogels are nanosized polymeric networks with high porous structure constituted by cross-linked polymer chains, formed via either aggregation/self-assembly or covalent linkage. They combine the properties of hydrogels (biocompatibility, flexibility and high water content) with those of nanocarriers [233]. The loading capacity available for the incorporation of drugs is

much higher than that of micelles and liposomes due to their highly porous structure. Experimental conditions such as pH, ionic strenght, temperature influence the swelling properties and the drug release [234].

Dentritic NPs are highly branches molecules with a tree-like structure with 1-4 nm size. They do not possess a core but they are formed by multiple shells, each one formed by the repetition of monomeric units [229]. The presence of multiple terminal groups allows a high degree of functionalization. In this case, the drugs can be retained into the void space between the branches via physical interactions with the functional groups or covalently tied to the outer shell. Dendritic molecules used for therapeutic applications have been made from polyamidoamine (PAMAM), poly(propylene imine), polylysine, polyester, polyaryl ethers, polyglycerol.

4.5. Functionalization of nanoparticles

The physical-chemical properties of the NPs, such as surface charges, hydrophilicity and size, can be controlled by functionalization. In other cases, functional polymers are attached as external coatings without affecting the NPs properties. The functionalization can sometimes be achieved before the NPs synthesis or afterwards via post-functionalization strategies. Different conjugation strategies for the immobilization of bioreceptor units (DNA/RNA, oligonucleotides, antibodies, fluorescent dyes, polymers, drugs, tumor markers and enzymes) on NPs have been used for the development of reliable immunosensors, genosensors, enzymatic biosensors [115].

In biomedical applications, the functionalization of NPs is helpful to increase their stability, protect them against hydrolytic and enzymatic degradation, reduce the phagocitic capture, prolonge their circulation in vivo, reduce the toxicity for cells and enhance intracellular bioavailability [235, 236]. Carbohydrate interactions regulate many processes in nature: signaling transduction, cell adhesion, tissue growth and repair, viral/bacterial infection, so glyconanoparticles are very promising in glycobiology, diagnostics and therapy. Nanocarriers are often functionalized with a carbohydrate coating to improve their water solubility, biocompatibility. For instance, thiolated carbohydrate derivatives, such as lactose, glucose and mannose derivatives, are readily assembled on metallic and magnetic NPs or QDs. poly(ethylene glycol) (PEG) is often attached as external layer to metallic NPs, mycelles and lyposomes to prolong their circulation time in the body and regulate the cell uptake [237, 238].

Furthermore, the functionalization allows the attachment of specific ligands that improve the efficiency of targeting via affinity binding with receptors and cells. For instance, the hydrophilic corona of PEG on the NPs has been conjugated with peptides able to target specifically the $\alpha_v\beta_3$ integrin on cancer cells [239]. Other biocompatible materials, such as polydopamine (PDA) [240] or lipoproteins [241] have been used for the decoration of NPs as well.
The attachment of enzymes to NPs can be of great benefit for biosensors. In the glucose biosensor fabricated by Zhang S. X. et al. [242], the aldehyde groups of a GOx are bind with a cysteamine monolayer chemisorbed on AuNPs. The presence of the NPs facilitated the electron transfer without affecting enzyme activity and improved the biosensor sensitivity as a result of the increased surface/bulk atom ratio. In some cases, enzymes immobilized on NPs revealed more stable than their free counterparts [243, 244].

The functionalization can be achieved using multiple strategies, covalent and non-covalent. The most adequate strategy depends on the chemical composition and type of reactive groups on both NPs and molecules to attach and it should be chosen to satisfy specific functional requirements. Overall, in biosensors the conjugation of the bioreceptors should be stable enough to generate a reproducible signal upon analyte binding under various environmental conditions or ensure a proper orientation of the biomolecules while conserving their optimal function and activity.

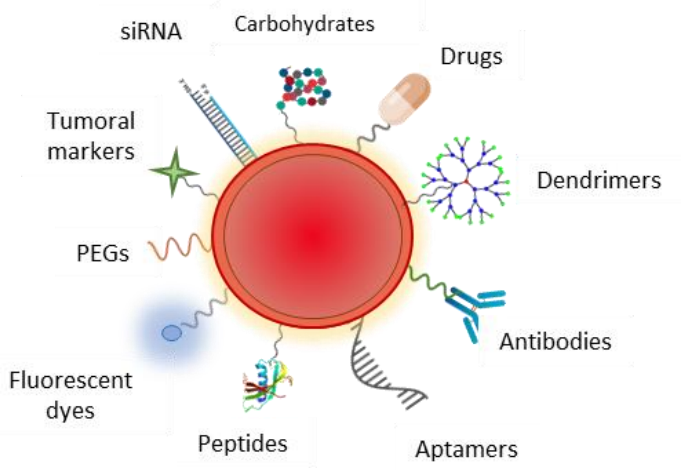

Fig. 18: possibilities of functionalization of nanoparticles with various biomolecules.

4.5.1. Covalent functionalization

As already pointed out, covalent bonding has the advantage of being stable and reproducible. A schematic representation of the main covalent bonding strategies are reported in *Fig. 19*.

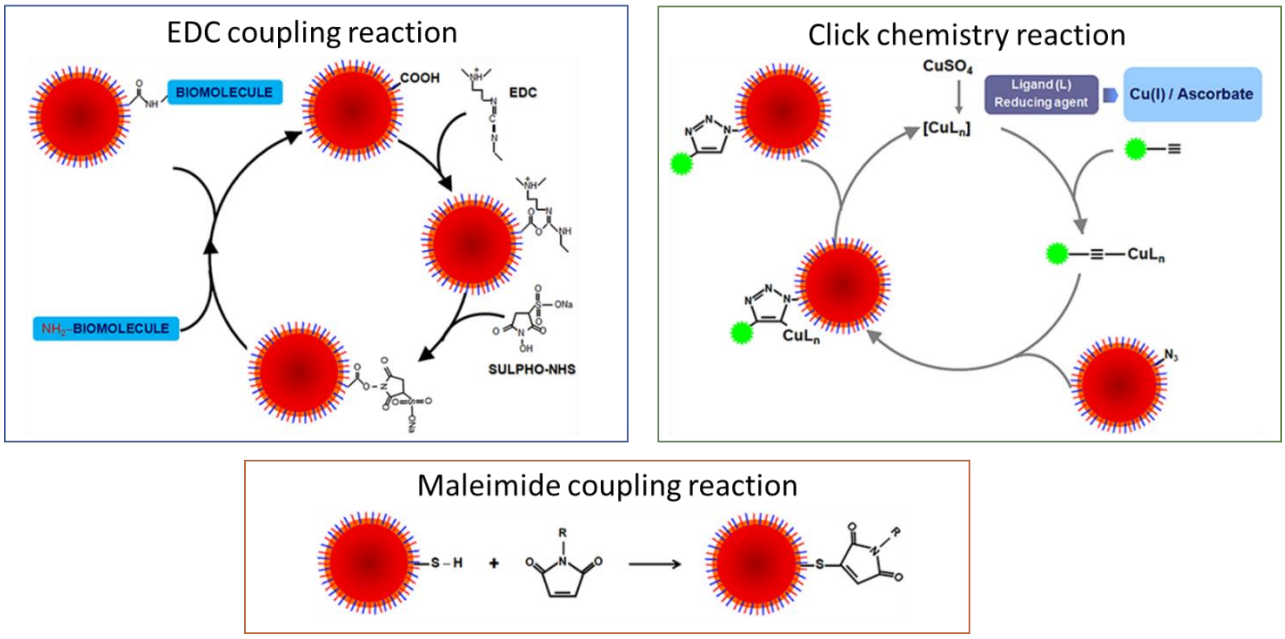

Fig. 19: main covalent strategies used for nanoparticle functionalization. Adapted from Ref. [244].

NPs containing aldehyde, epoxide or anhydride groups can be reacted with amine groups of proteins or viceversa. For instance, a lipase was attached to Fe_2O_3 MNPs via covalent bonds between the amino groups of enzyme and acetyl groups of the NPs [244]. Antibodies, peptides, carbohydrates or oligonucleotides often require a prior modification step for the introduction of specific functional groups to promote the immobilization.

Covalent modification is often pursued using an intermediate linker. EDC-NHS coupling reaction is used to couple carboxyl or phosphate groups to primary amines. One disadvantage of this type of chemistry is that peptides containing both carboxylates and amines can auto-polymerize. Also, it does not guarantee an oriented immobilization in the case of biomolecules with great structural complexity, such as proteins or antibodies that have multiple carboxylic and aminic groups [245].

The use of maleimide to conjugate primary amines to thiols with the formation of a stable ether linkage or two thiols to form a disulfide linkage, is extensively described in the literature and has a lot of potential for a great number of biomolecules that possess thiol or amino species [246]. For instance, thiol–oligonucleotides attached on maleimido-QDs were exploiteded for DNA direct electrochemical detection [247]. Overall, these coupling strategies have the risk of causing the crosslinking between different functionalized NPs.

AuNPs are often directly modified with thiol groups by formation of strong gold–S bonds, and attached thiolated linkers usually allow a further attachment of biomolecules in a

controlled way. Click-chemistry reactions are useful and effective, they have been applied for proteins [248], enzymes [249], fluorophores [250], polymers [251] coupling to NPs. The copper(I)-catalyzed azide-alkyne cycloaddition (CuAAC) click reaction between azides and alkynes has a tremendous popularity. It occurs at room temperature with high chemoselectivity, it is fast, simple and has an acceptable degree of insensitivity to solvent and pH.

4.5.2. Non-covalent functionalization

Non-covalent strategies (*Fig. 20*) are easy and neither the biomolecules nor the NPs require a modification of their structure [144]. However, conjugation is less stable compared to covalent methods and it is also less reproducible, so it is difficult to control the amount and the orientation of immobilized molecules.

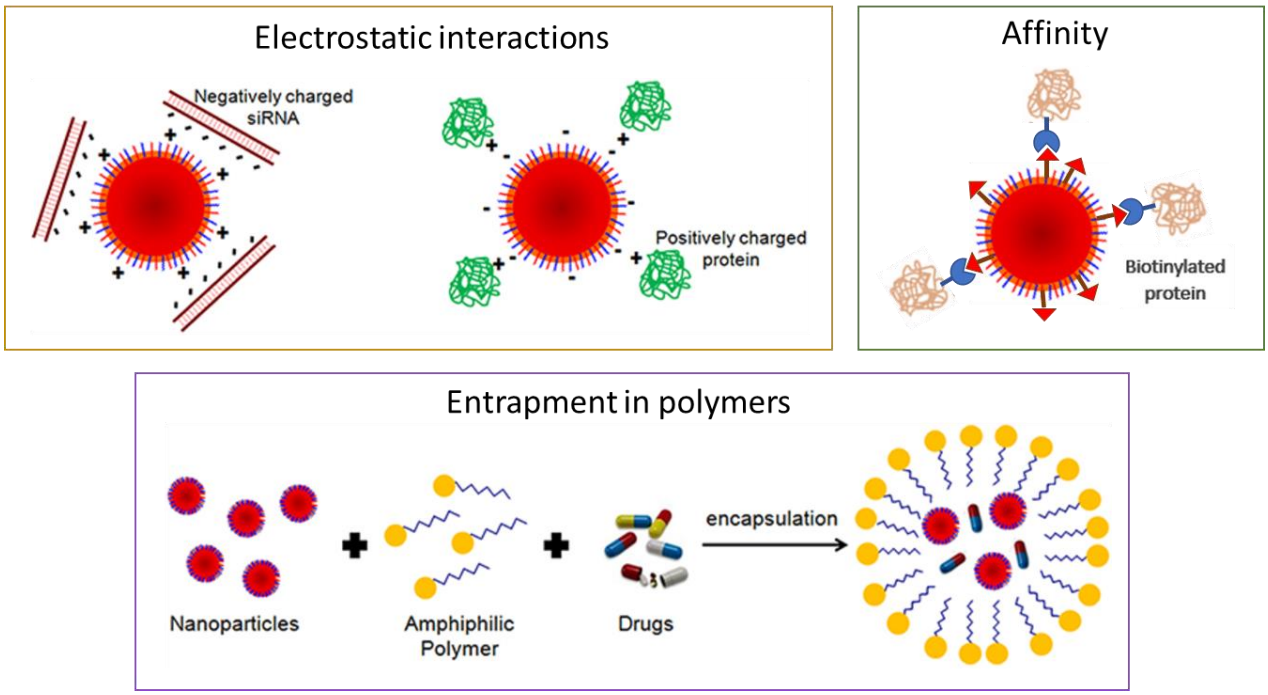

Fig. 20: examples of non-covalent strategies used for nanoparticle functionalization. Adapted from Ref. [243].

Polymeric species and biological molecules with an opposite charge can be coupled to NPs via electrostatic interactions. However, any changes to the pH or ionic strength may induce desorption.

Amphiphilic polymers or cyclodextrins can be used to encapsulate NPs and drugs in a microenvironment improving their solubility. Functionalization based on supramolecular or coordinative (affinity) interactions are also highly employed. The most classic example is

biotin-avidin/streptavidin-biotin system (K_a around 10^{15} L mol^{-1}). Nowadays several companies offer biomolecules and NPs already modified with biotin or avidin groups [252]. The advantage of the non-covalent interactions for the fabrication of NPs-based biosensors is the possibility of regeneration of the transducer element [144].

5. Bibliography

(1) Assad, Humira, Savas Kaya, P. Senthil Kumar, Dai-Viet N. Vo, Ajit Sharma, e Ashish Kumar. «Insights into the Role of Nanotechnology on the Performance of Biofuel Cells and the Production of Viable Biofuels: A Review». *Fuel.* (2022) 323, 124277.

(2) Grove, W. R. «XXIV. On voltaic series and the combination of gases by platinum». *The London, Edinburgh, and Dublin Philosophical Magazine and Journal of Science.* (1839) 14, 86, 127–130.

(3) Schœnbein C.F. «The voltaic polarization of certain solid and fluid substances». *Philosophical Magazine.* (1839) 14, 85, 43–45.

(4) EG & G Services, Ralph M. Parsons Company, and Science Applications International Corporation. «Fuel cell handbook». (2000)

(5) Warshay M., Prokopius P. R. «The fuel cell in space: yesterday, today and tomorrow.» *Grove Anniversary (1839-1989) Fuel Cell Symposium.* (1989) No. E-5084.

(6) Shukla A. K., Suresh P., Sheela B., Rajendran A. «Biological fuel cells and their applications». *Current science.* (2004) 87, 4, 455-468.

(7) Bullen R.A., Arnot T. C., Lakeman J. B., Walsh F. C. «Biofuel cells and their development». *Biosensors and Bioelectronics*. (2006) 21, 11, 2015–2045.

(8) Potter M. C. «Electrical effects accompanying the decomposition of organic compounds». *Proceeding of the Royal Society B.* (1911) 84, 260–276.

(9) Zhao C., Gai P., Song Rongbin, Chen Y., Zhang J., Zhu J. J. «Nanostructured Material-Based Biofuel Cells: Recent Advances and Future Prospects». Chemical Society Reviews. (2017) 46, 5, 1545–64.

(10) Rabaey, K., Lissenes, G., Siciliano, S. D. and Verstraete, W. «A microbial fuel cell capable of converting glucose to electricity at high rate and efficiency». *Biotechnol. Lett.* (2003) 25, 1531–1535.

(11) Logan B. E. et al. «Microbial Fuel Cells: Methodology and Technology». *Environ. Sci. Technol.* (2006) 40, 5181–5192.

(12) Bhatnagar D., Xu S., Fischer C., Arechederra L. R., Minteer S. D. «Mitochondrial biofuel cells : expanding fuel diversity to amino acids». *Physical Chemistry Chemical Physics.* (2011) 13, 86–92.

(13) Rasmussen M., Abdellaoui S., Minteer, S. D. «Enzymatic biofuel cells: 30 years of critical advancements». *Biosensors and Bioelectronics.* (2016) 76, 91–102.

(14) Quan X., Sun B., Xu H. «Anode decoration with biogenic Pd nanoparticles improved power generation in microbial fuel cells». *Electrochim Acta.* (2015) 182, 815-820.

(15) Colombo R., Sedenho G., Crespilho F. «Challenges in Biomaterials Science for Electrochemical Biosensing and Bioenergy». *Chemistry of Materials.* (2022) 5, 5, 2079-2092.

(16) Davis F., Higson S. P. J. «Biofuel cells—recent advances and applications». *Biosens. Bioelectron.* (2007) 22, 1224–1235.

(17) Moehlenbrock J. M., Minteer S. D. «Extended Lifetime Biofuel Cells». *Chemical Society Reviews.* (2008) 37, 6, 1188–96.

(18) Gil G.C., Chang I.S., Kim B.H., Kim M., Jang J.K., Park H.S., et al. «Operational parameters affecting the performance of a mediator-less microbial fuel cell». *Biosens Bioelectron.* (2003) 18, 4, 327-334.

(19) Das D., Khanna N., Veziroğlu N. «Recent developments in biological hydrogen production processes». *Chem Ind Chem Eng Quart.* (2008) 14, 2, 57-67.

(20) Yahiro A.T., Lee S.M., Kimble D.O. «Bioelectrochemistry. I. Enzyme utilizing biofuel cell studies». *Biochim Biophys Acta.* (1964) 88, 375-383.

(21) Kim J., Jia H., Wang P. «Challenges in Biocatalysis for Enzyme-Based Biofuel Cells». *Biotechnology Advances.* (2006) 24, 3, 296–308.

(22) Arechederra R., Minteer S. D. «Organelle-based biofuel cells: Immobilized mitochondria on carbon paper electrodes». *Electrochimica Acta.* (2008) 53, 6698–6703.

(23) Mano N., de Poulpiquet A. «O2 Reduction in Enzymatic Biofuel Cells». *Chemical Reviews.* (2018) 118, 5, 2392–2468.

(24) Yu H. E., Scott K. «Enzymatic Biofuel Cells—Fabrication of Enzyme Electrodes». *Energies.* (2010) 3, 1, 23–42.

(25) Degrand C., Miller L. L. «An electrode modified with polymer-bound dopamine which catalyzes NADH oxidation». *Journal of the American Chemical Society.* (1980) 102, 18, 5728-5732.

(26) Cooney M. J., Svoboda V., Lau C., Martin G., Minteer S. D. «Enzyme catalysed biofuel cells». *Energy & Environmental Science.* (2008) 1, 3, 320-337.

(27) Popescu I. C., Domínguez E., Narváez A., Pavlov V., Katakis I. «Electrocatalytic oxidation of NADH at graphite electrodes modified with osmium phenanthrolinedione». *Journal of Electroanalytical Chemistry.* (1999) 464, 2, 208-214.

(28) Sugiyama T., Goto Y., Matsumoto R., Sakai H., Tokita Y., Hatazawa, T. «A mediator-adapted diaphorase variant for a glucose dehydrogenase–diaphorase biocatalytic system». *Biosensors and Bioelectronics.* (2010) 26, 2, 452-457.

(29) Cosnier S., Fontecave M., Innocent C., Niviere V. «An original electroenzymatic system: Flavin reductase-riboflavin for the improvement of dehydrogenase-based biosensors. Application to the amperometric detection of lactate». *Electroanalysis.* (1997) 9, 9, 685-688.

(30) Marcus R. A., Sutin N. «Electron transfers in chemistry and biology». *Biochimica et Biophysica Acta (BBA) - Reviews on Bioenergetics.* (1985) 811, 265–322.

(31) Masa J., Schuhmann W. «Electrocatalysis and bioelectrocatalysis – Distinction without a difference». *Nano Energy.* (2016) 29, 466–475.

(32) Reuillard B. et al. «High power enzymatic biofuel cell based on naphthoquinone-mediated oxidation of glucose by glucose oxidase in a carbon nanotube 3D matrix». *Physical Chemistry Chemical Physics.* (2013) 15, 14, 4892-4896.

(33) Clark W. M. «Oxidation-reduction potentials of organic systems». (1960)

(34) Durand F., Stines-Chaumeil C., Flexer V., André I., Mano, N. «Designing a highly active soluble PQQ–glucose dehydrogenase for efficient glucose biosensors and biofuel cells». *Biochemical and biophysical research communications*. (2010) 402, 4, 750-754.

(35) Milton D. R., Giroud F., Thumser A. E., Minteer S. D., Slade T. R. C. «Hydrogen peroxide produced by glucose oxidase affects the performance of laccase cathodes in glucose/oxygen fuel cells: FAD-dependent glucose dehydrogenase as a replacement». *Physical Chemistry Chemical Physics.* (2013) 15, 44, 19371–19379.

(36) Karyakin A. A., Karyakina E. E., Schmidt H.-L. «Electropolymerized Azines: A New Group of Electroactive Polymers». *Electroanalysis.* (1999) 11, 149–155.

(37) Salaj-Kosla U., Scanlon M. D., Baumeister T., Zahma K., Ludwig R., Conghaile P. Ó, ..Magner, E. «Mediated electron transfer of cellobiose dehydrogenase and glucose oxidase at osmium polymer-modified nanoporous gold electrodes». *Analytical and bioanalytical chemistry.* (2013) 405, 11, 3823-3830.

(38) Di J., Cheng J., Xu Q., Zheng H., Zhuang J., Sun Y., …Bi, S. «Direct electrochemistry of lactate dehydrogenase immobilized on silica sol–gel modified gold electrode and its application». *Biosensors and Bioelectronics.* (2007) 23, 5, 682-687.

(39) Arechederra R. L., Minteer S. D. «Complete oxidation of glycerol in an enzymatic biofuel cell». *Fuel Cells.* (2009) 9, 1, 63-69.

(40) Deng L., Shang L., Wen D., Zhai J., Dong, S. «A membraneless biofuel cell powered by ethanol and alcoholic beverage». *Biosensors and Bioelectronics.* (2010) 26, 1, 70-73.

(41) Vincent K. A., Parkin A., Armstrong F. A. «Investigating and exploiting the electrocatalytic properties of hydrogenases». *Chemical reviews.* (2007) 107, 10, 4366-4413.

(42) De Lacey A. L., Fernandez V. M., Rousset M., Cammack R. «Activation and inactivation of hydrogenase function and the catalytic cycle: spectroelectrochemical studies». *Chemical reviews.* (2007) 107, 10, 4304-4330.

(43) Plumeré N. et al. «A redox hydrogel protects hydrogenase from high-potential deactivation and oxygen damage». *Nature Chemistry.* (2014) 6, 9, 822–827.

(44) Palmore G. T. R., Kim H. H. «Electro-enzymatic reduction of dioxygen to water in the cathode compartment of a biofuel cell». *Journal of Electroanalytical Chemistry*. (1999) 464, 1, 110–117.

(45) Le Goff A., Holzinger M., Cosnier, S. «Recent progress in oxygen-reducing laccase biocathodes for enzymatic biofuel cells». *Cellular and Molecular Life Sciences*. (2015) 72, 5, 941–952.

(46) Mano N., Edembe L. «Bilirubin oxidases in bioelectrochemistry: Features and recent findings». *Biosensors and Bioelectronics.* (2013) 50, 478–485.

(47) Giroud F., Gondran C., Gorgy K., Vivier V., Cosnier S. «An enzymatic biofuel cell based on electrically wired polyphenol oxidase and glucose oxidase operating under physiological conditions». *Electrochimica Acta.* (2012) 85, 278–282.

(48) Katz E., Lioubashevski O., Willner I. «Magnetic field effects on bioelectrocatalytic reactions of surface-confined enzyme systems: enhanced performance of biofuel cells». *Journal of the American Chemical Society.* (2005) 127, 11, 3979-3988.

(49) Miura Y. et al. «Direct Electrochemistry of CueO and Its Mutants at Residues to and Near Type I Cu for Oxygen-Reducing Biocathode». *Fuel Cells.* (2009) 9, 1, 70–78.

(50) Heller A. «Integrated Medical Feedback Systems for Drug Delivery». *AIChE J.* (2005) 51, 4, 1054– 1066.

(51) Gamella M., Koushanpour A., Katz E. «Biofuel Cells-Activation of Micro- and Macro-Electronic Devices». *Bioelectrochem.* (2018) 119, 33-42.

(52) Amar A. B., Kouki A. B., Cao H. «Power Approaches for Implantable Medical Devices». *Sensors.* (2015) 15, 28889–28914.

(53) Danaei G. et al. «National, regional, and global trends in fasting plasma glucose and diabetes prevalence since 1980: systematic analysis of health examination surveys and epidemiological studies with 370 country-years and 2·7 million participants». *The Lancet.* (2011) 378, 9785, 31–40.

(54) Khonsary S. A. «Guyton and Hall: Textbook of Medical Physiology». *Surg Neurol Int.* (2017) 8.

(55) Mano N., Mao F. Heller A. «Characteristics of a Miniature Compartment-less Glucose−O2 Biofuel Cell and Its Operation in a Living Plant». *J. Am. Chem. Soc.* (2003) 125, 6588–6594.

(56) MacVittie K., Halamek J., Halamkova L., Southcott M., Jemison W. D., Lobel R., Katz E. «From "Cyborg" Lobsters to a Pacemaker Powered by Implantable Biofuel Cells». *Energy Environ. Sci.* (2013) 6, 81-86.

(57) Cinquin P. et al. «A Glucose BioFuel Cell Implanted in Rats». *PloS One.* (2010) 5, e10476.

(58) El Ichi S., Zebda A., Alcaraz J. P., Laaroussi A., Boucher F., Boutonnat J., Reverdy-Bruas N., Chaussy D., Belgacem M. N., Cinquin P. et al. «Bioelectrodes Modified with Chitosan for Long-Term Energy Supply from the Body». *Energy Environ. Sci.* (2015) 8, 1017-1026.

(59) Reuillard B., Abreu C., Lalaoui N., Le Goff A., Holzinger M., Ondel O., Buret F., Cosnier S. «One-Year Stability for a Glucose/Oxygen Biofuel Cell Combined with pH Reactivation of the Laccase/Carbon Nanotube Biocathode». *Bioelectrochemistry*. (2015) 106, 73-76.

(60) Jia W., Valdés-Ramírez G., Bandodkar A. J., Windmiller J. R. Wang J. «Epidermal Biofuel Cells: Energy Harvesting from Human Perspiration». *Angewandte Chemie International Edition*. (2013) 52, 7233–7236.

(61) Reid R. C., Minteer S. D., Gale B. K. «Contact lens biofuel cell tested in a synthetic tear solution». *Biosensors and Bioelectronics*. (2015) 68, 142–148.

(62) Morady F. «Electrophysiologic interventional procedures and surgery». *In Goldman's Cecil Medicine. WB Saunders.* (2012) 369-373.

(63) Xiao X., Xia H. Q., Wu R., Bai L., Yan L., Magner E., Cosnier S., Lojou E., Zhu Z., Liu A. «Tackling the challenges of enzymatic (bio) fuel cells». *Chemical reviews.* (2019) 119, 16, 9509-9558.

(64) Shleev S. «Quo Vadis, Implanted Fuel Cell?». *ChemPlusChem.* (2017) 82, 522-539.

(65) Lowe C.R. «Biosensors». *Trends in Biotechnology.* (1984) 2, 3, 59–65.

(66) Naresh V., Lee N. «A Review on Biosensors and Recent Development of Nanostructured Materials-Enabled Biosensors». *Sensors.* (2021) 21, 4, 1109.

(67) Kumar N., Shetti N. P., Jagannath S., Aminabhavi T. M. «Electrochemical sensors for the detection of SARS-CoV-2 virus». *Chemical Engineering Journal*. (2022) 430, 132966.

(68) Sarkar P., Pal P.S., Ghosh D., Setford S. J. Tothill I. E. «Amperometric biosensors for detection of the prostate cancer marker (psa)». *International Journal of Pharmaceutics.* (2002) 238, 1-2, 1–9.

(69) Patris S., Vandeput M., Kauffmann J.-M. «Antibodies as Target for Affinity Biosensors». *TrAC Trends Anal. Chem.* (2016) 79, 239–246.

(70) Haab B.B. «Applications of antibody array platforms». *Current Opinion in Biotechnology.* (2006) 17, 4, 415–421.

(71) Chambers J. P., Arulanandam B. P., Matta L. L., Weis A., Valdes J. J. «Biosensor recognition elements». *Current issues in molecular biology.* (2008) 10, 1-2, 1-12.

(72) Ellington A. D., Szostak J. W. «Invitro selection of rna molecules that bind specific ligands». *Nature.* (1990) 346, 6287, 818–822.

(73) Grieshaber D., MacKenzie R., Vörös J., Reimhult E. «Electrochemical Biosensors - Sensor Principles and Architectures». *Sensors.* (2008) 8, 3, 1400–1458.

(74) Skladal P. «Piezoelectric biosensors». *TrAC Trends Anal. Chem.* (2016) 79, 127–133.

(75) Hooda V., Gahlaut A., Gothwal A., Hooda V. «Bilirubin Enzyme Biosensor: Potentiality and Recent Advances towards Clinical Bioanalysis». *Biotechnology Letters.* (2017) 39, 10, 1453–62.

(76) Chen C., Wang J. «Optical biosensors: An exhaustive and comprehensive review». *Analyst*. (2020) 145, 1605–1628.

(77) Mansouri M., Fathi F., Jalili R., Shoeibie S., Dastmalchi S., Khataee A., Rashidi M. R. «SPR enhanced DNA biosensor for sensitive detection of donkey meat adulteration». *Food Chem.* (2020) 331, 127163.

(78) Peña-Bahamonde J., Nguyen H. N., Fanourakis S. K., Rodrigues D. F. «Recent Advances in Graphene-Based Biosensor Technology with Applications in Life Sciences». *Journal of Nanobiotechnology*. (2018) 16, 1, 75.

(79) Chaubey A., Malhotra B.D. «Mediated biosensors». *Biosensors & Bioelectronics*. (2002) 17, 6-7, 441–456.

(80) Shishkanova T. V., Volf R., Krondak M., Kral V. «Functionalization of PVC membrane with ss oligonucleotides for a potentiometric biosensor». *Biosensors and Bioelectronics*. (2007) 22, 11, 2712-2717.

(81) Bahadır E. B., Sezgintürk M. K. «A review on impedimetric biosensors». *Artificial cells, nanomedicine, and biotechnology*. (2016) 44, 1, 248-262.

(82) Heineman W. R., Jensen W. B. «Leland C. Clark Jr. (1918–2005)». *Biosens. Bioelectron.* (2006) 8, 21, 1403–1404.

(83) Guilbault G. G., Montalvo J. G. Jr. «Urea-specific enzyme electrode». *J. Am. Chem. Soc.* (1969) 91, 2164–2165.

(84) Mosbach K., Danielsson B. «An enzyme thermistor». *Biochim. Biophys. Acta.* (1974) 364, 1, 140–145.

(85) Lübbers D.W., Opitz N. «The pCO_2-/pO_2-optode: A new probe for measurement of pCO_2 or pO in fluids and gases (transl)». *Z. Naturforsch C Biosci.* (1975) 30, 4, 532–533.

(86) Geyssant A., Dormois D., Barthelemy J. C., Lacour J. R. «Lactate determination with the lactate analyser LA 640: a critical study». *Scandinavian journal of clinical and laboratory investigation*. (1985) 45, 2, 145-149.

(87) Liedberg B., N Nylander, Lundstrom I. «Biosensing with surface plasmon resonance-how it all began». *Biosensors and Bioelecironics.* (1995) 10.

(88) Fang A. P., Ng H. T., Li S. F. Y. «A high-performance glucose biosensor based on monomolecular layer of glucose oxidase covalently immobilised on indium-tin oxide surface». *Biosensors & Bioelectronics*. (2003) 19, 1, 43–49.

(89) Azevedo A., Martins V., Prazeres D., Vojinovic V., Cabral J., Fonseca L. «Horseradish peroxidase: a valuable tool in biotechnology». *Biotechnology annual review*. (2003) 9, 199–247.

(90) Raymundo-Pereira P. A., Silva T. A., Caetano F. R., Ribovski L., Zapp E., Brondani D., ... Fatibello-Filho O. «Polyphenol oxidase-based electrochemical biosensors: A review». *Analytica Chimica Acta.* (2020) 1139, 198-221.

(91) Wong, C. M., Wong, K. H., Chen, X. D. «Glucose oxidase: natural occurrence, function, properties and industrial applications». *Appl. Microbiol. Biotechnol.* (2008) 78, 927–938.

(92) Hecht H. J., Schomburg D., Kalisz H., Schmid R. D. «The 3D structure of glucose oxidase from Aspergillus niger. Implications for the use of GOD as a biosensor enzyme». *Biosensors and Bioelectronics.* (1993) 8, 197–203.

(93) Hecht H. J., Schomburg D., Kalisz H., Schmid R. D. «The 3D structure of glucose oxidase from Aspergillus niger. Implications for the use of GOD as a biosensor enzyme». *Biosensors and Bioelectronics.* (1993) 8, 197–203.

(94) Veitch N. C. «Horseradish peroxidase: a modern view of a classic enzyme». *Phytochemistry.* (2004) 65, 3, 249-259.

(95) Yoruk R., Marshall M. R. «Physicochemical properties and function of plant polyphenol oxidase: a review». *Journal of food biochemistry.* (2003) 27, 5, 361-422.

(96) Research T. M. Biosensors Market. https://www.grandviewresearch.com/industry-analysis/biosensors-market

(97) Winer N., Sowers J. R. «Epidemiology of diabetes. The Journal of Clinical Pharmacology». (2004) 44, 4, 397-405.

(98) Clark L. C. Jr., Lyons C. «Electrode system for continuous monitoring in cardiovascular surgery». *Ann. NY Acad. Sci.* (1962) 102, 29–45

(99) Newman J. D., Setford, S. J. «Enzymatic biosensors». *Molecular biotechnology.* (2006) 32, 3, 249-268.

(100) Wang J. «Glucose biosensors: 40 years of advances and challenges». *Electroanalysis.* (2001) 13, 12, 983–988.

(101) Clemens A. H., Chang P. H., Myers R. W. «Development of an automatic system of insulin infusion controlled by blood sugar, its system for the determination of glucose and control algorithms». *Proc. Journes Ann. de Diabtologie de l'Htel-Dieu.* (1976) 269–278.

(102) Cass A. E. G., Francis D. G., Hill H. A. O., et al. «A ferrocene-mediated enzyme electrode for amperometric glucose determination». *Anal. Chem.* (1984) 56, 667–671.

(103) Renneberg R., Pfeiffer D., Lisdat F., Wilson G., Wollenberger U., Ligler F., Turner A. P. «Frieder Scheller and the short history of biosensors». *Biosensing for the 21st Century.* (2007) 1-18.

(104) Shichiri M., Kawamori R., Yamaski R., Hakai Y., Abe H. «Wearable artificial endocrine pancreas with needle-type glucose sensor». L*ancet.* (1982) 2, 1129–1131.

(105) Otero F., Magner E. «Biosensors—Recent Advances and Future Challenges in Electrode Materials». *Sensors.* (2020) 20, 12, 3561.

(106) Yang W., Ratinac K. R., Ringer S. P., Thordarson P., Gooding J. J., Braet F. «Carbon Nanomaterials in Biosensors: Should You Use Nanotubes or Graphene?». *Angew. Chem. Int. Ed. Engl.* (2010) 49 , 12 , 2114–2138.

(107) Benedetti T. M., Andronescu C., Cheong S., Wilde P., Wordsworth J., Kientz M., Tilley R. D., Schuhmann W., Gooding J. J. «Electrocatalytic Nanoparticles That Mimic the Three-Dimensional Geometric Architecture of Enzymes: Nanozymes». *J. Am. Chem. Soc.* (2018) 140, 41.

(108) Ahmad O. S., Bedwell T. S., Esen C., Garcia-Cruz A., Piletsky S. A. «Molecularly Imprinted Polymers in Electrochemical and Optical Sensors». *Trends Biotechnol.* (2019) 37, 3, 294–309.

(109) Purohit B., Vernekar P. R., Shetti N. P., Chandra P. «Biosensor nanoengineering: Design, operation, and implementation for biomolecular analysis». *Sensors International.* (2020) 1, 100040.

(110) Lineweaver H., Burk D. «The determination of enzyme dissociation constants». *Journal of the American chemical society.* (1934) 56, 3, 658-666.

(111) Borgmann S., Schulte A., Neugebauer S., Schuhmann W. «Amperometric biosensors». *Advances in Electrochemical Science and Engineering.* (2011) 2.

(112) Peveler W. J., Yazdani M., Rotello V. M. «Selectivity and specificity: pros and cons in sensing». *ACS Sens.* (2016) 1, 1282-1285,

(113) Sassolas A., Blum L. J., Leca-Bouvier B. D. «Immobilization strategies to develop enzymatic biosensors». *Biotechnology advances.* (2012) 30, 3, 489-511.

(114) Yang X.-Y., Tian G., Jiang N., Su B.-L. «Immobilization technology: a sustainable solution for biofuel cell design». *Energy Environ. Sci.* (2012) 5, 2, 5540-5563.

(115) Spahn C., Minteer S. D. «Enzyme immobilization in biotechnology». *Recent patents on engineering.* (2008) 2, 3, 195-200.

(116) Nguyen H. H., Kim M. «An Overview of techniques in enzyme immobilization». *Appl. Sci. Converg. Technol.* (2017) 26, 157–163.

(117) Armstrong F. A., Wilson G. S. «Recent developments in faradaic bioelectrochemistry». *Electrochimica Acta*. (2000) 45, 2623–2645.

(118) Novick S. J., Rozzell J. D. «Immobilization of enzymes by covalent attachment». *Microbial enzymes and biotransformations.* Humana Press. (2005) 247-271.

(119) Kolb H. C., Finn M. G., Sharpless K. B. «Click chemistry: diverse chemical function from a few good reactions». *Angewandte Chemie International Edition*. (2001) 40, 11, 2004-2021.

(120) Kowalewska B., Jakubow K. «The impact of immobilization process on the electrochemical performance, bioactivity and conformation of glucose oxidase enzyme». *Sensors and Actuators B: Chemical.* (2017) 238, 852–861.

(121) Cosnier S., Holzinger M. «Electrosynthesized polymers for biosensing». *Chemical Society Reviews.* (2011) 40, 5, 2146-2156.

(122) Choi D., Lee W., Park J., Koh W. «Preparation of poly (ethylene glycol) hydrogels with different network structures for the application of enzyme immobilization». *Bio-medical materials and engineering*. (2008) 18, 6, 345-356.

(123) Rother C., Nidetzky B. «Enzyme immobilization by microencapsulation: methods, materials, and technological applications». *Encyclopedia of Industrial Biotechnology: Bioprocess, Bioseparation, and Cell Technology.* (2009) 1-21.

(124) Moore C. M., Akers N. L., Hill A. D., Johnson Z. C., Minteer S. D. «Improving the Environment for Immobilized Dehydrogenase Enzymes by Modifying Nafion with Tetraalkylammonium Bromides». *Biomacromolecules.* (2004) 5, 1241–1247.

(125) Ichi S. EI., Zebda A., Laaroussi A., Reverdy-Bruas N., Chaussy D., Belgacem M. N.... & Martin D. K. «Chitosan improves stability of carbon nanotube biocathodes for glucose biofuel cells». *Chem. Commun.* (2014) 50, 14535–14538.

(126) Ionescu R. E., Abu-Rabeah K., Cosnier S., Marks R. S. «Improved enzyme retention from an electropolymerized polypyrrole-alginate matrix in the development of biosensors». *Electrochemistry Communications.* (2005) 7, 1277–1282.

(127) Švancara I., Vytřas K., Barek J., Zima J. «Carbon paste electrodes in modern electroanalysis». *Critical Reviews in Analytical Chemistry*. (2001) *31*, 4, 311-345.

(128) Zebda A., Gondran C., Le Goff A., Holzinger M., Cinquin P., Cosnier, S. «Mediatorless high-power glucose biofuel cells based on compressed carbon nanotube-enzyme electrodes». *Nature communications.* (2011) 2, 1, 1-6.

(129) Nadar S. S., Vaidya L., Rathod V. K. «Enzyme embedded metal organic framework (enzyme–MOF): De novo approaches for immobilization». *International journal of biological macromolecules*. (2020) 149, 861-876.

(130) Richards F. M.; Knowles J. R. «Glutaraldehyde as a protein cross-linking reagent». *J. Mol. Biol.* (1968) 37, 1, 231–233.

(131) MacAodha D., Ferrer M. L., Conghaile P. Ó., Kavanagh P., Leech D. «Crosslinked redox polymer enzyme electrodes containing carbon nanotubes for high and stable glucose oxidation current». *Physical Chemistry Chemical Physics*. (2012) 14, 42, 14667-14672.

(132) Wong S. S., Wong L. J. C. «Chemical crosslinking and the stabilization of proteins and enzymes». *Enzyme and Microbial Technology.* (1992) 14, 11, 866-874.

(133) Anzai J. I., Takeshita H., Kobayashi Y., Osa T., Hoshi T. «Layer-by-layer construction of enzyme multilayers on an electrode for the preparation of glucose and lactate sensors: elimination of ascorbate interference by means of an ascorbate oxidase multilayer». *Analytical chemistry*. (1998) *70*, 4, 811-817.

(134) Bucur B., Danet A. F., Marty J.-L. «Versatile method of cholinesterase immobilisation via affinity bonds using Concanavalin A applied to the construction of a screen-printed biosensor». *Biosensors and Bioelectronics.* (2004) 20, 217–225.

(135) Buzzetti P. H. M., Carrière M., Brachi M., Gorgy K., Mumtaz M., Borsali R., Cosnier S. «Organic β-cyclodextrin Nanoparticle: An Efficient Building Block Between Functionalized Poly (pyrrole) Electrodes and Enzymes». *Small*. (2022) 18, 10, 2105880.

(136) Haddour N., Cosnier S., Gondran C. «Electrogeneration of a poly (pyrrole)-NTA chelator film for a reversible oriented immobilization of histidine-tagged proteins». *Journal of the American Chemical Society.* (2005) 127, 16, 5752-5753.

(137) Kimple M. E., Brill A. L., Pasker R. L. «Overview of affinity tags for protein purification». *Current protocols in protein science*. (2013) 73, 1, 9-9.

(138) Balland V., Hureau C., Cusano A. M., Liu Y., Tron T., Limoges B. «Oriented immobilization of a fully active monolayer of histidine-tagged recombinant laccase on modified gold electrodes». *Chemistry–A European Journal*. (2008) 14, 24, 7186-7192.

(139) Bourourou M., Elouarzaki K., Lalaoui N., Agnès C., Le Goff A., Holzinger M., ... & Cosnier S. «Supramolecular immobilization of laccase on carbon nanotube electrodes functionalized with (methylpyrenylaminomethyl) anthraquinone for direct electron reduction of oxygen». *Chemistry–A European Journal*. (2013) 19, 28, 9371-9375.

(140) Zhang Y., Wei Q. «The role of nanomaterials in electroanalytical biosensors: A mini review». *Journal of Electroanalytical Chemistry.* (2016) 781, 401-409.

(141) Moniz E. J. «Nanotechnology for the energy challenge». *John Wiley & Sons.* (2010)

(142) De Poulpiquet A., Ciaccafava A., Lojou, E. «New trends in enzyme immobilization at nanostructured interfaces for efficient electrocatalysis in biofuel cells». *Electrochimica Acta*. (2014) 126, 104-114.

(143) Zhang X., Guo Q., Cui D. «Recent Advances in Nanotechnology Applied to Biosensors». *Sensors.* (2009) 9, 2, 1033–53.

(144) Holzinger M., Le Goff A., Cosnier S. «Nanomaterials for biosensing applications: a review». *Frontiers in chemistry*. (2014) 2, 63.

(145) Săndulescu R., Tertis M., Cristea C., Bodoki E. «New materials for the construction of electrochemical biosensors». *Biosensors-Micro and Nanoscale Applications*. (2015) 1-36.

(146) Wang J., Musameh M. «Carbon nanotube/teflon composite electrochemical sensors and biosensors». *Analytical chemistry*. (2003) 75, 9, 2075-2079.

(147) Barnes T. M., van de Lagemaat J., Levi D., Rumbles G., Coutts T. G., Weeks C. L. «Optical characterization of highly conductive single-wall carbon-nanotube transparent electrodes». *Phys. Rev. B.* (2007) 75, 23, 23541001-22354110.

(148) Novoselov K. S., Geim A. K., Morozov S. V., Jiang D. E., Zhang Y., Dubonos S. V., ... & Firsov A. A. «Electric field effect in atomically thin carbon films». *Science*. (2004) 306, 5696, 666-669.

(149) Hernandez Y., Nicolosi V., Lotya M., Blighe F. M., Sun Z., De S., ... Coleman J. N. «High-yield production of graphene by liquid-phase exfoliation of graphite». *Nature nanotechnology*. (2008) 3, 9, 563-568.

(150) Hummers W. S, Offeman R. E. «Preparation of graphitic oxide». *J. Am. Chem. Soc*. (1958) 80, 1339–1339.

(151) Zhu Y., Murali S., Cai W., Li X., Suk J. W., Potts J. R., Ruoff R. S. «Graphene and graphene oxide: synthesis, properties, and applications». *Advanced materials*. (2010) 22, 35, 3906-3924.

(152) Martins M. V, Pereira A. R., Luz R. S., Iost R. M.; Crespilho F. N. «Evidence of ShortRange Electron Transfer of a Redox Enzyme on Graphene Oxide Electrodes». *Phys. Chem. Chem. Phys.* (2014) 14, 33, 17426–17436.

(153) Radushkevich L. V., Lukyanovich V. M. «The structure of carbon forming in thermal decomposition of carbon monoxide on an iron catalyst». *Russian Journal of Physical Chemistry*. (1952) 26, 88–95.

(154) Iijima S. «Helical microtubules of graphitic carbon». *Nature.* (1991) 354, 56–58.

(155) Mintmire J. W., Dunlap B. I., White C. T. «Are fullerene tubules metallic?» *Physical Review Letters.* (1992) 68, 631–634.

(156) Hu C., Hu S. «Carbon nanotube-based electrochemical sensors: Principles and applications in biomedical systems». *Journal of Sensors.* (2009) 2009, 187615.

(157) Awasthi K., Srivastava A., Srivastava O. N. «Synthesis of carbon nanotubes». *J Nanosci Nanotechnol.* (2005) 5, 10, 1616-1636.

(158) Thostenson E. T., Ren Z., Chou T. W. «Advances in the science and technology of carbon nanotubes and their composites: a review». *Composites science and technology*. (2001) 61, 13, 1899-1912.

(159) Journet C. et al. «Large-scale production of single-walled carbon nanotubes by the electric-arc technique». *Nature.* (1997) 388, 756–758.

(160) Thess A. et al. «Crystalline Ropes of Metallic Carbon Nanotubes». *Science.* (1996) 273, 483–487.

(161) Kroto H. W., Heath J. R., O'Brien S. C., Curl R. F., Smalley R. E. «C60: Buckminsterfullerene». *Nature*. (1985) 318, 6042, 162-163.

(162) Guo T., Nikolaev P., Thess A., Colbert D. T., Smalley R. E. «Catalytic growth of single-walled manotubes by laser vaporization». *Chemical physics letters*. (1995) 243, 1-2, 49-54.

(163) Flahaut E., Laurent Ch., Peigney A. «Catalytic CVD synthesis of double and triple-walled carbon nanotubes by the control of the catalyst preparation». *Carbon.* (2005) 43, 375–383.

(164) Gohier A., Ewels C. P., Minea T. M., Djouadi M. A. «Carbon nanotube growth mechanism switches from tip-to base-growth with decreasing catalyst particle size». *Carbon*. (2008) 46, 10, 1331-1338.

(165) Treacy M. M. J., Ebbesen T. W., Gibson J. M. «Exceptionally high Young's modulus observed for individual carbon nanotubes». *Nature.* (1996) 381, 678.

(166) Odom T. W., Huang J. L., Kim P., Lieber C. M. «Structure and electronic properties of carbon nanotubes». *The Journal of Physical Chemistry B.* (2000) 104, 13, 2794-2809.

(167) Odom T. W., Huang J.-L., Kim P. Lieber C. M. «Atomic structure and electronic properties of single-walled carbon nanotubes». *Nature.* (1998) 391, 62–64.

(168) Feng J., Sui J., Cai W., Gao Z. «Microstructure and mechanical properties of carboxylated carbon nanotubes/poly (L-lactic acid) composite». *Journal of composite materials.* (2008) 42, 16, 1587-1595.

(169) Dai H., Wong E. W., Lieber C. M.. «Probing electrical transport in nanomaterials: conductivity of individual carbon nanotubes». *Science.* (1996) 272, 5261, 523-526.

(170) O'Connell M. J. «Carbon Nanotubes: Properties and Applications». *CRC Press.* (2006)

(171) de las Casas C., Li W. «A review of application of carbon nanotubes for lithium ion battery anode material». *Journal of Power Sources.* (2012) 208, 74–85.

(172) Mukherjee S., Bates A., Lee S. C., Lee D.-H., Park S. «A Review of the Application of CNTs in PEM Fuel Cells». *International Journal of Green Energy.* (2015) 12, 787–809.

(173) Niu Z. et al. «Compact-designed supercapacitors using free-standing single-walled carbon nanotube films». *Energy & Environmental Science.* (2011) 4, 1440–1446.

(174) Wang J. «Carbon-nanotube based electrochemical biosensors: a review». *Electroanalysis.* (2005) 17, 7–14.

(175) Gruner G. «Carbon nanotube transistors for biosensing applications». *Anal. Bioanal. Chem*. (2006) 384, 322–335.

(176) Holzinger M., Vostrowsky O., Hirsch A., Hennrich F., Kappes M., Weiss R., Jellen F. «Sidewall functionalization of carbon nanotubes». *Angewandte chemie international edition*. (2001) 40, 21, 4002-4005.

(177) Hirsch A. «Functionalization of single-walled carbon nanotubes». *Angewandte Chemie International Edition*. (2002) 41, 11, 1853-1859.

(178) Pereira A. R., Souza J. C. P., Gonçalves A. D., Pagnoncelli K. C., Crespilho F. N. «Bioelectrooxidation of Ethanol Using NAD-Dependent Alcohol Dehydrogenase on Oxidized Flexible Carbon Fiber Arrays». *J. Braz. Chem. Soc.* (2017) 28, 1698–1707.

(179) Tobias G., Mendoza E., Ballesteros B. «Functionalization of carbon nanotubes». *Encyclopedia of Nanotechnology, 2nd ed.; Bhushan B., Ed*. (2016) 1281-1291.

(180) Singh P. et al. «Organic functionalisation and characterisation of single-walled carbon nanotubes». *Chemical Society Reviews.* (2009) 38, 2214–2230.

(181) Holzinger M. et al. «Functionalization of Single-Walled Carbon Nanotubes with (R-)Oxycarbonyl Nitrenes». *J. Am. Chem. Soc*. (2003) 125, 8566–8580.

(182) Salice P. et al. «An insight into the functionalisation of carbon nanotubes by diazonium chemistry: Towards a controlled decoration». *Carbon.* (2014) 74, 73–82.

(183) Zhao Y. L., Stoddart J. F. «Noncovalent functionalization of single-walled carbon nanotubes». *Accounts of chemical research*. (2009) 42, 8, 1161-1171.

(184) Ramasamy R. P., Luckarift H. R., Ivnitski D. M., Atanassov P. B., Johnson G. R. «High electrocatalytic activity of tethered multicopper oxidase–carbon nanotube conjugates». *Chemical Communications*. (2010) 46, 33, 6045-6047.

(185) Le Goff A. et al. «Facile and tunable functionalization of carbon nanotube electrodes with ferrocene by covalent coupling and π-stacking interactions and their relevance to glucose bio-sensing». *Journal of Electroanalytical Chemistry.* (2010) 641, 57–63.

(186) Star A., Stoddart J. F., Steuerman D., Diehl M., Boukai A., Wong E. W., ... & Heath J. R.. «Preparation and properties of polymer-wrapped single-walled carbon nanotubes». *Angewandte Chemie*. (2001) 113, 9, 1771-1775.

(187) Matarredona O., Rhoads H., Li Z., Harwell J. H., Balzano L., Resasco D. E. «Dispersion of single-walled carbon nanotubes in aqueous solutions of the anionic surfactant NaDDBS». *The Journal of Physical Chemistry B.* (2003) 107, 48, 13357-13367.

(188) Pelaz B., Jaber S., De Aberasturi D. J., Wulf V., Aida T., de la Fuente J. M., ... & Parak W. J. «The state of nanoparticle-based nanoscience and biotechnology: progress, promises, and challenges». *ACS Publications.* (2012) 6, 10, 8468-8483.

(189) Jesus M. D. L. F., Grazu V. «Nanobiotechnology: inorganic nanoparticles vs organic nanoparticles». *Elsevier.* (2012)

(190) Jia F., Liu X., Li L., Mallapragada S., Narasimhan B., Wang Q. «Multifunctional nanoparticles for targeted delivery of immune activating and cancer therapeutic agents». *Journal of Controlled Release.* (2013) 172, 3, 1020-1034.

(191) Niemeyer C. M. «Nanoparticles, proteins, and nucleic acids: biotechnology meets materials science». *Angewandte Chemie International Edition*. (2001) 40, 22, 4128-4158.

(192) Zhao P., Li N., Astruc D. «State of the art in gold nanoparticle synthesis». *Coordination Chemistry Reviews*. (2013) 257, 3-4, 638-665.

(193) Martinkova P., Kostelnik A., Válek T., Pohanka M. «Main streams in the construction of biosensors and their applications». *International Journal of Electrochemical Science*. (2017) 12, 8.

(194) Walcarius A., Minteer S. D., Wang J., Lin Y., Merkoçi A. «Nanomaterials for Bio-Functionalized Electrodes: Recent Trends». *Journal of Materials Chemistry B 1*. (2013) 38, 4878–4908.

(195) Holland J. T., Lau C., Brozik S., Atanassov P., Banta S. «Engineering of glucose oxidase for direct electron transfer via site-specific gold nanoparticle conjugation». *Journal of the American Chemical Society*. (2011) 133, 48, 19262-19265.

(196) Salimi A., Sharifi E., Noorbakhsh A., Soltanian S. «Immobilization of glucose oxidase on electrodeposited nickel oxide nanoparticles: direct electron transfer and electrocatalytic activity». *Biosensors and Bioelectronics*. (2007) 22, 12, 3146-3153.

(197) Assad H., Kaya S., Kumar P. S., Vo D. V. N., Sharma A., Kumar A. «Insights into the Role of Nanotechnology on the Performance of Biofuel Cells and the Production of Viable Biofuels: A Review». *Fuel.* (2022) 323, 124277.

(198) Katz E., Willner I. «Integrated nanoparticle–biomolecule hybrid systems: synthesis, properties, and applications». *Angewandte Chemie International Edition*. (2004) 43, 45, 6042-6108.

(199) Shipway A. N., Katz E., Willner I. «Nanoparticle arrays on surfaces for electronic, optical, and sensor applications». *ChemPhysChem*. (2000) 1, 1, 18-52.

(200) Li Y., Schluesener H., Xu S. «Gold nanoparticle-based biosensors». *Gold Bull*. (2010) 43, 29–41.

(201) Yang L., Zhang X., Ye M., Jiang L., Yang R., Fu T. et al. «Aptamer-conjugated nanomaterials and their applications». *Adv. Drug Deliv. Rev.* (2011) 63, 14-15, 1361-1370.

(202) Chen G., Tong H., Gao T., Chen Y., Li G. «Direct application of gold nanoparticles to one-pot electrochemical biosensors. *Anal. Chim. Acta.* (2014) 849, 1-6.

(203) Yin T., Qin W. «Applications of nanomaterials in potentiometric sensors». *TrAC Trends Anal. Chem.* (2013) 51, 79-86.

(204) Wang X., Falk M., Ortiz R., Matsumura H., Bobacka J., Ludwig R., Bergelin M., Gorton L., Shleev S. «Mediatorless sugar/oxygen enzymatic fuel cells based on gold nanoparticle-modified electrodes». *Biosens Bioelectron.* (2012) 31, 1, 219-225.

(205) Yang G., Chen D., Lv P., Kong X., Sun Y., Wang Z., Yuan Z., Liu H., Yang J. «Core-shell Au-Pd nanoparticles as cathode catalysts for microbial fuel cell applications». *Sci Rep.* (2016) 6, 35252.

(206) Medina-Orta R., Labrada-Delgado G. J., Silva-Pereyra H. G., Ortega E. M., Pérez-Herranz V., Sánchez-Loredo M. G. «Synthesis of Gold Nanoparticles and Incorporation to a Porous Nickel Electrode to Improve its Catalytic Performance Towards the Hydrogen Evolution Reaction». *Electrocatalysis*. (2022) 13, 1, 47-61.

(207) Feng J. J., Li A. Q., Wang A. J., Lei Z., Chen J. R. «Electrodeposition of monodispersed platinum nanoparticles on a glassy carbon electrode for sensing methanol». *Microchim Acta.* (2011) 173, 383–9.

(208) Zhang Y., Huang B., Ye J., Ye J. «A sensitive and selective amperometric hydrazine sensor based on palladium nanoparticles loaded on cobalt-wrapped nitrogen-doped carbon nanotubes». *J. Eelctroanal. Chem.* (2017) 801, 215–223.

(209) Li J., Tang J., Wei L., He S., Ma L., Shen W., Kang F. et al. «Preparation and performance of electrochemical glucose sensors based on copper nanoparticles loaded on flexible graphite sheet». *New Carbon Materials.* (2020) 35, 4, 410-419.

(210) Haun J. B., Yoon T. J., Lee H., Weissleder R. «Magnetic nanoparticle biosensors. *Wiley Interdiscip. Rev*. (2010) 2, 291–304.

(211) Zhang X. F., Dong X. L., Huang H., Lv B., Zhu K. G., Lei J. P. et al. «Synthesis, structure and magnetic properties of SiO_2-coated Fe nanocapsules». *Mater. Sci. Eng. A.* (2007) 454-455, 211-215.

(212) Gruttner C., Rudershausen S., Teller J. J. «Improved properties of magnetic particles by combination of different polymer materials as particle matrix». *J. Magn. Magn. Mater.* (2001) 225, 1-2, 1-7.

(213) Rosensweig R. E. «Heating magnetic fluid with alternating magnetic field». *J. Magn. Magn. Mater*. (2002) 252, 370–374.

(214) Yoo D., Lee J. H., Shin T. H., Cheon J. «Theranostic magnetic nanoparticles. *Acc. Chem. Res*. (2011) 44, 863–874.

(215) Gutierrez A. M., Dziubla T. D., Hilt J. Z. «Recent advances on iron oxide magnetic nanoparticles as sorbents of organic pollutants in water and wastewater treatment». *Reviews on environmental health*. (2017) 32, 1-2, 111-117.

(216) Zhang H. W., Liu Y., Sun S. H. «Synthesis and assembly of magnetic nanoparticles for information and energy storage applications». *Frontiers of Physics in China*. (2010) 5, 4, 347-356.

(217) Rocha-Santos T. A. «Sensors and biosensors based on magnetic nanoparticles». *TrAC Trends in Analytical Chemistry*. (2014) 62, 28-36.

(218) Gautam S., Hoque S., Gooding J. J. «Gold-Coated Magnetic Nanoparticles as Dispersible Electrochemical Biosensors for Ultrasensitive Biosensing». *Biochemical Sensors: Nanomaterial-Based Biosensing and Application In honor of the 90th birthday of Prof. Shaojun Dong*. (2021) 59–83.

(219) Direnzo F., Cambon H., Dutartre R. «A 28-year-old synthesis of micelle-templated mesoporous silica». *Micropor. Mater.* (1997) 10, 283-286.

(220) Chen W. H., Luo G. F., Lei Q., Cao F. Y., Fan J. X., Qiu W. X., ... & Zhang X. Z. «Rational design of multifunctional magnetic mesoporous silica nanoparticle for tumor-targeted magnetic resonance imaging and precise therapy». *Biomaterials*. (2016) 76, 87-101.

(221) Bharti C., Nagaich U., Pal A. K., Gulati N. «Mesoporous silica nanoparticles in target drug delivery system: A review». *International journal of pharmaceutical investigation*. (2015) 5, 3, 124.

(222) Fan D., et al. «Electrochemical immunosensor for detection of prostate specific antigen based on an acid cleavable linker into MSN-based controlled release system». *Biosens Bioelectron.* (2016) 85, 580–586.

(223) Medintz I. L., Uyeda H. T., Goldman E. R., Mattoussi H. «Quantum dot bioconjugates for imaging, labelling and sensing». *Nat. Mater.* (2005) 4, 435–446.

(224) Petryayeva E., Algar W. R., Medintz I. L. «Quantum dots in bioanalysis: a review of applications across various platforms for fluorescence spectroscopy and imaging». *Appl. Spectrosc*. (2013) 67, 215–252.

(225) Ray P. C., Fortner A., Darbha G. K. «Gold nanoparticle based FRET assay for the detection of DNA cleavage». *J. Phys. Chem. B.* (2006) 110, 20745–20748.

(226) Freeman R., Girsh J., Willner I. «Nucleic acid/Quantum dots (QDs) hybrid systems for optical and photoelectrochemical sensing». *ACS Appl. Mater. Interfaces.* (2013) 5, 2815–2834.

(227) Malic L., Sandros M. G., Tabrizian M. «Designed biointerface using near-infrared quantum dots for ultrasensitive surface plasmon resonance imaging biosensors». *Anal. Chem.* (2011) 83, 5222–5229.

(228) Xu Y., Cai H., He P. G., Fang Y. Z. «Probing DNA hybridization by impedance measurement based on CdS-oligonucleotide nanoconjugates». *Electroanal.* (2004) 16, 1-2, 150–155.

(229) Kumar R., Lal S. «Synthesis of organic nanoparticles and their applications in drug delivery and food nanotechnology: a review». *J Nanomater Mol Nanotechnol.* (2014) 11, 2.

(230) Vauthier C., Bouchemal K. «Methods for the preparation and manufacture of polymeric nanoparticles». *Pharmaceutical research*. (2009) 26, 5, 1025-1058.

(231) Laridi R., Kheadr E. E., Benech R. O., Vuillemard J. C., Lacroix C., Fliss, I. «Liposome encapsulated nisin Z: optimization, stability and release during milk fermentation». *International dairy journal*. (2003) 13, 4, 325-336.

(232) Were L. M., Bruce B. D., Davidson P. M., Weiss J. «Size, stability, and entrapment efficiency of phospholipid nanocapsules containing polypeptide antimicrobials». *Journal of agricultural and food chemistry*. (2003) 51, 27, 8073-8079.

(233) Grimaudo M. A., Concheiro A., Alvarez-Lorenzo C. «Nanogels for regenerative medicine». *Journal of Controlled Release*. (2019) 313, 148-160.

(234) Zha L., Banik B., Alexis F. «Stimulus responsive nanogels for drug delivery». *Soft Matter*. (2011) 7, 13, 5908-5916.

(235) Bertrand N., Leroux J. C. «The journey of a drug-carrier in the body: an anatomo-physiological perspective». *J. Control. Release.* (2012) 161, 152–163.

(236) Sperling R. A., Parak W. J. «Surface modification, functionalization and bioconjugation of colloidal inorganic nanoparticles». *Philos. Trans. A Math. Phys. Eng. Sci*. (2010) 368, 1333–1383.

(237) Daou T. J., Li L., Reiss P., Josserand V., Texier I. «Effect of poly(ethylene glycol) length on the *in vivo* behavior of coated quantum dots». *Langmuir.* (2009) 25, 3040–3044.

(238) Maldiney T., Richard C., Seguin J., Wattier N., Bessodes M., Scherman D. «Effect of core diameter, surface coating, and PEG chain length on the biodistribution of persistent luminescence nanoparticles in mice». *ACS Nano.* (2011) 5, 854–862.

(239) Graf N., Bielenberg D. R., Kolishetti N., Muus C., Banyard J., Farokhzad O. C., Lippard S. J. «αVβ3 integrin-targeted PLGA-PEG nanoparticles for enhanced anti-tumor efficacy of a Pt (IV) prodrug». *ACS nano*. (2012) 6, 5, 4530-4539.

(240) Ding Y., Su S., Zhang R., Shao L., Zhang Y., Wang B., Li Y., Chen L., Yu Q., Wu Y., Nie G. «Precision Combination Therapy for Triple Negative Breast Cancer via Biomimetic Polydopamine Polymer Core-Shell Nanostructures». *Biomaterials.* (2017) 113, 243–252.

(241) Harmatys K. M., Chen J., Charron D. M., MacLaughlin C. M., Zheng G. «Multipronged Biomimetic Approach To Create Optically Tunable Nanoparticles». *Angew. Chem. Int. Ed.* (2018) 57, 8125–8129.

(242) Zhang S. X., Wang N., Yu, H. J., Niu Y. M., Sun C. Q. «Covalent attachment of glucose oxidase to an Au electrode modified with gold nanoparticles for use as glucose biosensor». *Bioelectrochemistry.* (2005) 67, 15–22.

(243) Khoshnevisan K., Bordbar A. K., Zare D., Davoodi D., Noruzi M., Barkhi M., et al. «Immobilization of cellulase enzyme on superparamagnetic nanoparticles and determination of its activity and stability». *Chem. Eng. J.* (2011) 171, 669–673.

(244) Dyal A., Loos K., Noto M., Chang S. W., Spagnoli C., Shafi K.V. P. M., et al. «Activity of candida rugosa lipase immobilized on g-Fe2O3 magnetic nanoparticles». *J Am Chem Soc.* (2003) 125, 1684-1685.

(245) Conde J., Dias J. T., Grazú V., Moros M., Baptista P. V., de la Fuente J. M. «Revisiting 30 years of biofunctionalization and surface chemistry of inorganic nanoparticles for nanomedicine». *Frontiers in chemistry*. (2014) 2, 48.

(246) Brinkley M. «A brief survey of methods for preparing protein conjugates with dyes, haptens, and cross-linking reagents». *Bioconjug. Chem*. (1992) 3, 2–13.

(247) Pumera M., Castaneda M. T., Pividori M. I., Eritja R., Merkoçi A., Alegret S. «Magnetically trigged direct electrochemical detection of DNA hybridization using Au67 quantum dot as electrical tracer». *Langmuir*. (2005) 21, 21, 9625-9629.

(248) Zhu K., Zhang Y., He S., Chen W. W., Shen J. Z., Wang Z., et al. «Quantification of proteins by functionalized gold nanoparticles using click chemistry». *Anal. Chem*. (2012) 84, 4267–4270.

(249) Brennan J. L., Hatzakis N. S., Tshikhudo T. R., Dirvianskyte N., Razumas V., Patkar S., et al. «Bionanoconjugation via click chemistry: the creation of functional hybrids of lipases and gold nanoparticles». *Bioconjug. Chem*. (2006) 17, 1373–1375.

(250) Voliani V., Ricci F., Signore G., Nifosi R., Luin S., Beltram F. «Multiphoton molecular photorelease in click-chemistry-functionalized gold nanoparticles». *Small*. (2011) 7, 3271–3275.

(251) Boisselier E., Salmon L., Ruiz J., Astruc D. «How to very efficiently functionalize gold nanoparticles by “click” chemistry». *Chem. Commun.* (2008) 44, 5788–5790.

(252) Wilchek M., Bayer E. «The avidin-biotin complex in bioanalytical applications». *Anal. Biochem*. (1988) 171, 1–32.

Chapter II

Functionalization of carbon nanotubes by thiol-yne chemistry for enzyme electrocatalysis

Summary

1. The Thiol–yne “click” reaction at carbon nanotubes

1.1 Overview of thiol-ene and thiol-yne “click” reactions

Click chemistry reactions are known for their attractive characteristics: simplicity, regioselectivity, high reaction rate, mild reaction conditions, functionality tolerance [1]. Thiol-based reactions are dominated by thiol–ene chemistry, which is described as the addition of a thiol to carbon–carbon double bonds. It was first observed in 1905 [2] but its systematic investigation and adoption in polymer chemistry and material science begun in the late 1930s [3]. According to literature, the reaction appears to proceed under mild reaction conditions, rapidly giving high yields with the concomitant formation of few or no side products thus owing some of the attributes which are typical of the click reactions. At the same time, the efficiency seems to vary depending on the particular system and in certain circumstances it fails to meet the typical criteria of click reactions [3]. The analogous thiol-yne reaction, which involves the addition of a thiol to a carbon carbon triple bond is instead much less studied and documented [2].

One great advantage of both these reactions is that they don’t require a metal catalyst, thus eliminating the issue of its potential toxicity for biological and biomedical applications and environmental issues linked to the necessity of its removal. On the contrary, this is the case in the Cu(I)-catalyzed Huisgen 1,3-dipolar cyclo-addition of alkynes and azides (CuAAC), which is probably the most employed and characterized click reaction. In addition, the triazole moiety that is formed is similar to the natural amide moiety and it can forms hydrogen bondings or π-π stacking interactions with the aminoacidic residues of peptides and proteins complicating the experimental outcome [4]. So there is a need for the use of alternative coupling procedures especially for biological applications.

In recent years, thiol-based chemistry has emerged as a new ligation tool not only for the synthesis of small molecules but also complex molecular systems, such as linear, highly branched, functional (co)polymers, polymer-based gels, cross-linked materials and dendrimers for applications such as drug delivery, imaging, catalytic supports, and viscosity modifiers [5]. Furthermore, it is employed for the post-functionalization of materials containing alkene/alkyne or thiol functional groups to target a specific function.

Thiol-based reactions have clearly demonstrated potential in the bio-organic field, and especially as a tool for glycosylation and biomolecule functionalization [3]. The natural

abundance of the thiol-based amino acid cysteine on proteins can be directly exploited for thiol-reactions circumventing the use of further modification of the biomolecule. On the other hand, it is relatively easy to modify biomolecules, proteins or polymers introducing a thiol or alkyne group. As an example, Lo Conte M. et al. described an approach for the double glycosylation of cysteine-containing peptides. In a first step some alkyne functional groups were left to react with the cysteines via a base-mediated nucleophilic substitution and in a second step a glucosyl, galactosyl or lactosyl thiol was reacted with the alkyne-modified substrate under irradiation in presence of a photoinitiator [6]. Li Y. et al. used thiol-yne chemistry for the labelling of proteins after a first incorporation of alkyne- pyrrolysines and their subsequent reaction with thiol-containing fluorophores [7].

Similarly to its analog thiol-ene reaction, thiol-yne reaction have emerged as a versatile reaction, since it can proceed through both nucleophile and radical-based route and it is supposed to work in both organic and aqueous media [8]. In general, some compounds, such as amines, phosphine or β-cyclodextrins, can promote the formation of a thiolate anion that act as a nucleophile able to react with the alkyne. UV light, elevated temperatures, peroxides and in general any other species able to form radicals, promotes the reaction via a radical mechanism [9]. Apart from those, the general addition process can also be catalysed by a variety of transition metals and main group elements, especially Pd, Pt, Ni or Rh complexes [3].

The possibility of carrying out the thiol-ene and thiol-yne chemistries under photo-induced conditions, is a really convenient aspect. In case of electron-deficient alkenes susceptible to chain growth polymerization such as allyl acrylates, methacrylates and acrylamides the addition process can also initiate a chain polymerization reaction. Importantly, the polymerization triggered by radical photoinitiation may benefit from both spatially- and temporally-controlled functionalizations [2].

Differently from the thiol-ene reaction that can give only two possible products from the addition reaction to unsymmetrical alkenes (the Markovnikov and anti-Markovnikov species), the thiol-yne reaction involving a terminal alkyne bond can generate six different products depending on the experimental conditions (*Fig. 1*). It is known that the nature of the substrates and the reaction conditions play an important role in determining the nature of the products and their distribution and among them, the steric bulkiness of the coupling reagents seems to particularly influence mono- or bis-addition selectivity [3]. To provide some examples, the mono-additive products are easily obtained when the reaction is carried out between thiols

and aromatic alkynes, while the 1,2-addition product (F in *Fig. 1*) is more likely to be obtained under radical-mediated conditions with two or more equivalents of thiols [3].

The possibility to form bis-additive products confers the thiol-yne reaction a great advantage compared to the analogous thiol-ene because dually functionalised conjugates and highly branched or cross-linked polymeric structures can be more efficiently produced by thiol-yne chemistry. Furthermore, the radical additions to alkynes are slower than those to alkene but the latter usually occurs in a reversible manner and therefore is necessary to work an excess of the reagents or high thiol concentrations to shift the equilibrium of the reaction towards the formation of the products. Instead, the radical thiol-yne reaction is more efficient when equimolar amounts of reagents are employed and it is basically irreversible since the vinyl radicals intermediates are formed in a irreversible manner [4].

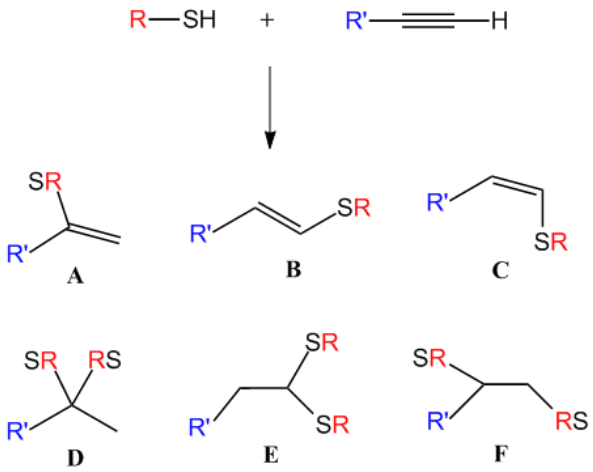

Fig. 1: possible addition products for the mono- and bis-hydrothiolation of a terminal alkyne bond.

1.2 The thiol-ene and thiol-yne reactions on surfaces and nanomaterials

The different aspects and the advantages of the thiol-based reactions described above, make them reactions appealing as functionalization strategies for the preparation of dendrimers, polymers, polymer–protein conjugates and glycopolymers.

Chen G. et al. recently described the preparation of a diblock copolymer via a thiol-ene coupling reaction between ene-functional precursor copolymers and glucothiose under photochemical conditions [10].

Due to their caracteristics of efficiency, velocity, orthogonality, thiol-based click chemistries are, in both their radical and nucleophilic forms, powerful and convenient tools for surface

and nanomaterial modification. They can promote high-density and oriented functionalization of surfaces and overcome limitations caused by bulkyness of the substituents and the presence of multiple reactive groups on the ligands that diminish the reaction selectivity [11]. Other functionalization strategies require in fact the protection and deprotection of reactive groups to achieve a proper orientation and selectivity, which can be detrimental for nanomaterial substrates.

The thiol-ene click reaction is an interesting route for organic–inorganic NPs functionalization. A photo-induced thiol−ene click chemistry has been applied for the controlled and directed deposition of multifunctional ligands on metal oxide NPs [11]. But recently, the reaction has been applied also for the functionalization of polymeric and silica NPs [11]. Connal L. A. and co-workers recently described the formation of multilayer-coated silica particles by crosslinking of adiacent layers of ene or thiol functionalized polyvinylpyrrolidone (PVP) and poly(methacrylic acid) (PMAA) induced by thiol-ene coupling under UV irradiation [12]. Short thiol-terminated PEG chains were grafted to the surface of hybrid inorganic-organic NPs via thiol-ene coupling to improve their dispersability in solvent [13]. A variety of thiol-containing peptidic targeting species were conjugated to allyl-functional nanoparticles by Harth and co-workers by thiol-ene chemistry for establishing a conjugation protocol utilizable for cancer targeting/delivery applications [14].

Thiol–ene click reactions have been also used to functionalize the surface of amorphous carbon films, which is a promising material for the preparation of biosensors and chemically modified electrodes [10]. Thiol-modified amorphous carbon films were irradiated in presence of vinylferrocene leading to a ferrocene-modified material potentially suitable to be used as mediator substrate. The authors demonstrated the potentiality of the UV-catalyzed reaction for the preparation of chemical and biochemolecule arrays [15]. This feature has been highlighted also by other authors that created a patterned surface by coupling of ene-functional biotin onto a thiol-modified silicon oxide surface under irradiation using a photomask. The pattern was visualized by treatment with a Cy5-labeled streptavidin [16].

A deeper understanding of the conditions influencing the thiol-yne reaction is crucial to extend the knowledge about it and the range of its possible applications. Nowadays there is no report in the literature of the thiol-yne reaction applied to carbon nanotube-functionalized surfaces for enzyme electrocatalysis.

Carbon nanotubes (CNTs) are an ideal substrate for their use in CNT-based enzyme biofuel cells and biosensors because of their structure, they possess a diameter (ranging from 1 nm for SWCNTs to 10 nm for MWCNTs) that can approach closely the redox active sites of the enzymes. They have high conductivity and high electron transfer rate. Furthermore, electrodes modified with CNTs have improved electroactive surface and porosity that in turn allows the immobilization of a high surface concentration of enzymes and redox mediators maximizing the current densities of the bioanodes and biocathodes [17]. Following the efforts of the BIOCEN group in the investigation of click reaction such as CuAAC [18, 19] and oxime ligation [20] at carbon nanotubes, the present work is devoted to the functionalization of multiwalled carbon nanotubes **(**MWCNTs) by thiol-yne reaction via both covalent and non-covalent strategies in order to introduce alkyne functional groups on their sidewalls. The thiol-yne reaction has been then investigated by cyclic voltammetry upon immobilization of ferrocene derivatives containing a thiol terminal group on the alkyne modified nanotubes.

2. Investigation of the thiol-yne reaction on MWCNTs with ferrocene derivatives

Ferrocene and its derivatives form a class of attractive organometallic compounds, which can be considered as model systems due to ferrocene structural stability, aromaticity, ease of modification. Ferrocene is a metal complex consisting of an iron(II) atom sandwiched between two cyclopentadienyl rings, it undergoes one electron oxidation to form ferrocenium cation (*Fig. 2*) and the heterogeneous electron transfer at the solid electrode is fast and reversible with excellent charge/discharged properties [21]. Furthermore, the electrochemical behaviour is not greatly affected by solvent effects. They are well-known and they have been extensively used as standard reference in electrochemical studies [22]. Different examples of the use of ferrocene as electrochemical probe are present in the literature. In particular, ferrocene has been used as a redox probe to investigate the efficiency of reactions at surfaces and electrodes such as the CuAAC performed at azido-modified CNTs [19]. In general, substituted ferrocene derivatives and ferrocene-based polymers and dendrimers count several applications.They have been used in molecular recognition and in electrochemical sensors [23] In bioelectrochemistry, ferrocene acts as a redox mediator for several enzymatic reactions, such as bioelectrocatalytic oxidation of glucose by GOx [24].

Therefore, ferrocene is an ideal redox probe for both assessing the thiol-yne reaction by electrochemical means and provide attached redox mediators for electron transfers between enzymes and MWCNTs.

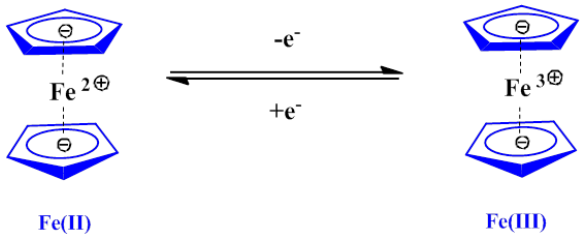

Fig. 2: reversible mono electronic oxidation of ferrocene.

2.1. Covalent functionalization of MWCNTs with aryldiazonium chemistry

2.1.1. Principles of diazonium grafting

Diazonium chemistry is a recognized method for the covalent modification of surfaces with an organic layer [25]. This functionalization method was first introduced by Pinson and coworkers and then employed largely in the past decade [26]. It has many advantages: the compatibility on a wide range of materials, since it can be applied to various metals (Al, Cr, Fe, Co, Pt, Ni, Zn, Cu, and Au), all sort of carbon surfaces (like glassy carbon, graphite, carbon nanotubes and diamond), silicon, indium tin oxide [25]. Other characteristics include the ease and rapidity of modification and the huge versatility of the organic chemistry of the aryl moiety that allows a pletora of possibilities in terms of functional groups that can be grafted using this method.

Two general approaches can be contemplated for modifying surfaces by diazonium chemistry: the grafting of pre-synthetized aryldiazonium salts or in situ generation of aryldiazonium salts. In both cases the grafting mechanism proceeds through an homolytic dediazoniation to give an highly reactive aryl radical that reacts with the underlying electrode to yield a covalent bond [27]. Proofs of the presence of the covalent bond as well as the lost of the diazonium group have been provided by XPS and infrared spectroscopy [26, 28].

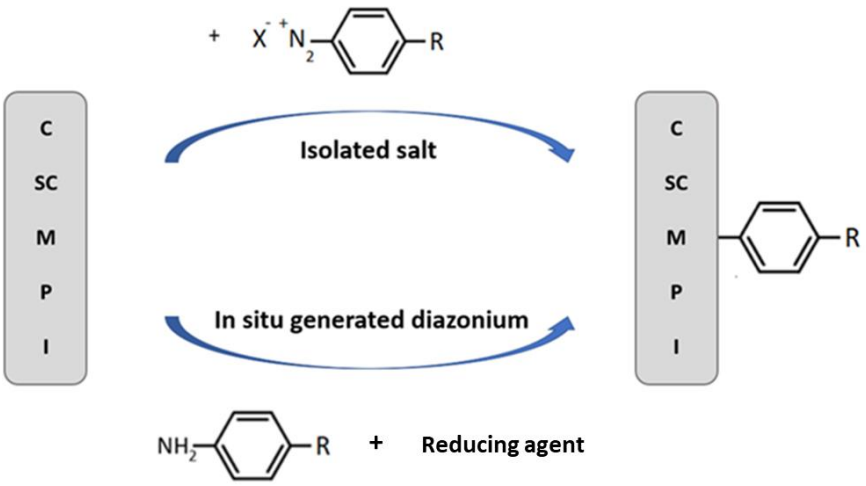

Fig. 3: schematic representation of the grafting process of aryldiazonium salts on different surfaces: C = carbon, SC = semi-conductor, M = metal, P = polymer, I = insulating.

The grafting of diazonium salts can lead to the formation of multilayers, that have the general structure of a polyphenylene [29]. Actually, the structure is often complex and disorganized, as not all the substitutions appear at para positions and also azo bonds (– N = N –) can be found in XPS spectra (*Fig. 4*).

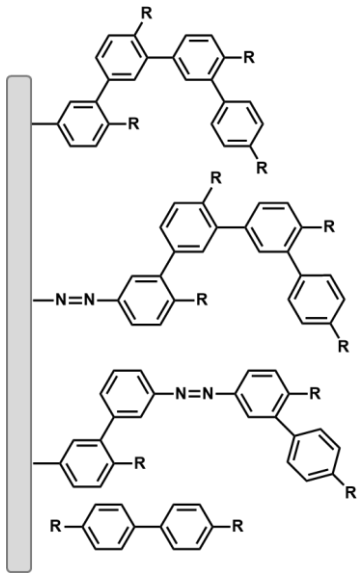

Fig.4: scheme of the possible complex structure of an aryl multilayer.

In general, the process is less controlled than other coupling chemistry, like the formation of self-assempled monolayers from alkanethiols on gold surfaces. Also, during the grafting, dimers and oligomers can be formed by radicals reacting with each other and then they deposit on the grafted surface, although they can be easily desorbed by a careful rinsing

procedure [30, 31]. The mechanism of formation of a multilayer is schematized in *Fig. 5*. After the formation of the first monolayer, a radical polymerization process takes place via aromatic homolytic substitution [29]. An aryl radical attacks at the ortho position the already grafted para-substituted aryl molecules forming a cyclohexadienyl radical. Then, the cyclohexadienyl radical reacts with another diazonium cation forming a new aryl radical. This electron exchange process continues the growth of a pure polyphenyl layer. A possible side reaction that can occur during the grafting process is the bonding to the surface without loss of the diazonium group to give a hydrazine attached to the surface [29]. Mixed grafted surfaces can be also obtained by reduction of mixtures of aryl diazonium salts, altough the final composition of the layer is not easily predictable since it will be enriched by the diazonium salt that is more prone to reduction [29].

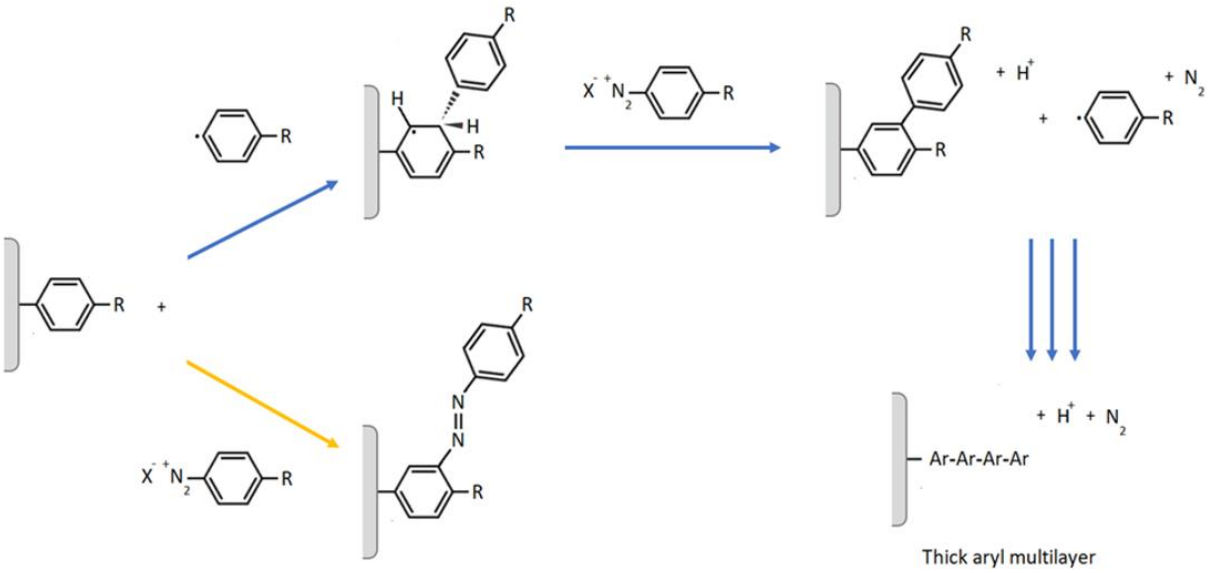

Fig.5: the mechanism for the formation of a multilayer during the grafting of diazonium salts.

Since aryldiazonium salts are easily reduced, the aryl radicals can be generated by a spontaneous electron transfer between the compounds and surfaces with a sufficient reducing power, such as gold, copper or carbon surfaces [31]. The spontaneous dediazonation can also occurr by increasing the pH of an aqueous solution which causes the conversion of the diazonium cation into a diazohydroxide (Ar-N=N-OH) and diazoate (Ar-N=N-O-) which are highly unstable. Alternatively, electrochemistry or a number of reducent agents, even very mild ones such as hypophosphorous acid, iron powder and ascorbic acid, are able to form aryl

radicals. Lastly, the grafting of aryl layers can be triggered by photochemistry, ultrasound or microwave assistance and even by localized surface plasmon excitation [31].

Each method has its advantages and drawbacks and depending on the desired application some are more suitable than others. For instance, the spontaneous reduction is very simple but there is a limitation to the growth of the layer so that only a thin film will be formed on the surface. By using the chemical reduction the process is less controllable than in the case of electroreduction but with the first method, the process is efficient with low conductive or even insulating surfaces such as Teflon or glass [30].

2.1.2. Covalent modification of CNTs by diazonium chemistry

The grafting of a series of diazonium salts produced in situ from the aniline precursors on CNTs has been described by Bahr J. L. et al. in 2001 [32]. The free-radical chain mechanism for the reaction of diazonium with SWNTs has been proposed by Schmidt G. et al. [33]. In the initiation step, the diazonium salt is reduced to an aryl radical by a single electron transfer (SET) from the SWNTs and then, the aryl radical reacts with SWNTs to a form an aryl-CNT radical. During the propagation, the aryl-CNT radical reacts with another diazonium salt regenerating an aryl radical by SET. In the termination steps, the various formed radicals can react with each other. The popularity of this method for the covalent functionalization of carbon materials is linked to its high efficiency and yield and the rich and well known chemistry of the phenyl group. The grafted phenyl groups can be further modified or coupled with other molecules.

CNTs have been functionalized in the past by immobilization of an activated ester Fc derivative on amine groups covalently grafted on CNTs sidewalls by electrogeneration of aryl radicals from the reduction of diazonium salts giving a reliable and stable glucose sensor electrode material [34]. CNTs have been covalently modified by anthracene and anthraquinone groups by diazonium chemistry for biobatteries and biofuel cells [35]. Different carbon-based materials have been previously covalently modified by using aryldiazonium salts by the BIOCEN group to promote enzyme wiring and electrocatalysis. MWCNT/reduced graphene oxide (RGO) hybrid electrodes were covalently functionalized by the in situ generation and reduction of anthraquinone diazonium salt for the electrical wiring and the direct electrocatalytic reduction of oxygen by laccase enzymes [36]. As another example, MWCNTs electrodes have been modified by electrografting of aryldiazonium salts, 2-amino-4-

ethylphenyldiazonium and 6-carboxynaphthalenediazonium tetrafluoroborate salts, to study the influence of the incorporation of positive or negative charges on MWCNTs for the orientation of bilirubine oxidase at the electrode [37]. The negative charges provided by the carboxynaphtalene groups improved the enzyme orientation and thus the direct electron transfer (DET) and enzyme catalytic activity at the electrode [37]. Electrografting of 4-azidobenzene diazonium tetrafluoroborate was performed either by spontaneous or electrochemical grafting of the corresponding diazonium salt for the control-oriented immobilization of an alkynated laccase via alkyne–azide Huisgen 1,3-dipolar cycloaddition reaction [19].

2.1.3. Electrografting of 4-ethynylbenzene diazonium tetrafluoroborate on MWCNTs

The electroreduction of diazonium salts on conductive surfaces has been the privileged method for decades [27]. After dissolving an diazonium salt in an aprotic medium with a supporting electrolyte or in an acidic aqueous medium (for example H_2SO_4 0.1 M), a potential is applied and the aryl radical is formed in close proximity of the surface followed by its grafting on the surface [30]. The electrografting can be pursued by repetitive cyclic voltammetry or by chronoamperometry at a potential equal or negative to the reduction potential of the diazonium. Alternatively, the use of potential pulses (0.1-1 s) can be also efficient for the growth of the layers [30].

One drawback of this method is the formation of an high amount of aryl radicals that leads to a disorganized film, usually a multilayer which can range from a few nanometeres to microns. Many advances have been done in the last past decade concerning the control over thickness of the final aryl layers. For some applications, such as the development of supercapacitors or electrocatalysis toward oxygen reduction, thick multilayers are generally preferred. Instead, for protein film voltammetry (PFV), biosensors and fuel cells, monolayers or thin layers (3-5 nm) are advisable to provide a faster and uniform electron transfer [38]. It is possible to have good control over the final thickness of the film by varying some experimental factors such as the applied potential, the charge passed during the deposition process and the sweep rate. Some tricks can be used to obtain a thin layer or a monolayer like the use of ionic liquids that are more viscous than the usual solvents used in electrochemistry, the use of radical scavengers or the use of aryldiazonium salts bearing two bulky tert-butyl groups in meta positions of the benzene ring that prevent the growth of the film by steric hindrance [39].

Relatively to electrochemical reduction, it is known that choosing a low number of cycles and a potential not excessively negative produce thinner and more porous films [31].

A diazonium compound with a terminal alkyne, 4-ethynylbenzendiazonium tetrafluoroborate, was synthetized following the procedure of Limoges B. et al. [40]. The formation of the correct product was confirmed by ^{1}H NMR, mass spectrometry and ATR spectroscopy.

MWCNT-GC electrodes were prepared by dissolution of the MWCNTs (Nanocyl 3100, >95% purity) in NMP and then dropcasting 20 µL of a 5 mg mL^{-1} suspension of MWCNTs onto each electrode surface. NMP is removed under reduced pressure until completely dry. The process leads to the formation of a uniform film of MWCNTs (5 µm thickness) onto the electrode surface (*Fig. 6*). Prior to electrografting, all the electrodes were cleaned by mechanical polishing with 2 µm alumina slurry, followed by sonication in distilled water to remove any residual alumina powder and then in ethanol for 5 minutes.

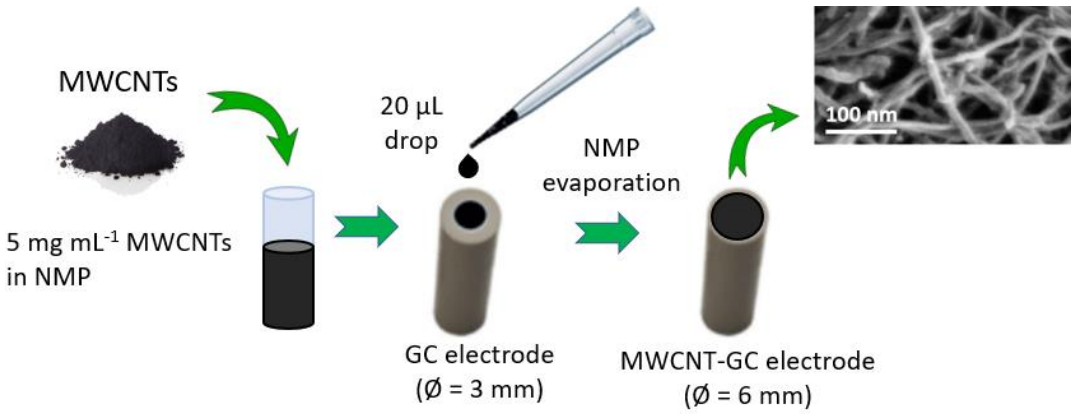

Fig. 6: preparation of MWCNT-GC electrodes and SEM image of a pristine MWCNT film (Ref. for SEM image: Lalaoui et al. ACS Catalysis. 2016, 6, 3, 1894–1900).

Tipically the reduction of the diazonium compound is visible in cyclic voltammetry as a single, broad one-electron irreversible wave, sometimes accompagnied by a pre-peak. In *Fig. 7* the electroreduction of 2 mM 4-ethynylbenzene diazonium tetrafluoroborate is performed on GC electrodes or on MWCNT-based electrodes. The electrografting was performed by recording two consecutive cycles with the potential varying from +0.5 V to −0.4 V vs Ag/Ag^{+} in TBAP 0.1M MeCN. On GC electrodes (*Fig. 7A*) the reduction wave of the diazonium salt of the first cycle, completely disappears during the second cycle since an insulating organic layer is formed on the electrode preventing the access of the diazonium cations to the electrode surface. On MWCNT electrodes (*Fig. 7B*) the reduction wave, which is detected at more positive potentials at around +0.18 V vs Ag/Ag^{+}, is only slightly decreased in the

second cycle compared to the first one. This effect is attributed to the enhanced electroactive area of MWCNTs, avoiding the blocking effect of the polyphenylene layer. The process of the electrografting is very reproducible and the cyclic voltammograms of all the electrodes functionalized in this way were almost identical.

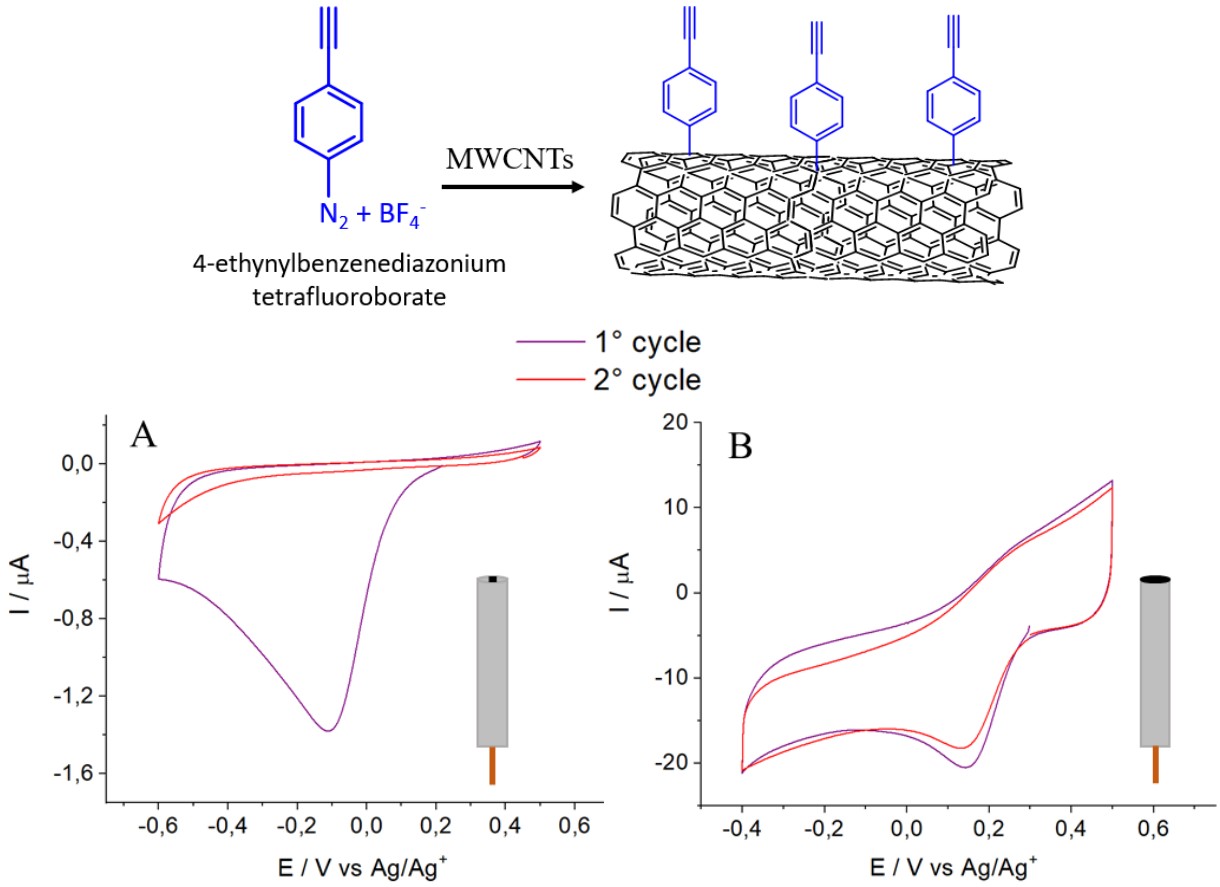

Fig. 7: schematization of the electrografting of 4-ethynylbenzendiazonium tetrafluoroborate on multiwalled carbon nanotubes. Electrografting on A) a GC electrode and B) on a MWCNTs-GC electrode in 2mM 4-ethynylbenzene diazoniumin TBAP 0.1M MeCN. Ref. electrode: Ag/Ag^+ in TBAP 0.1 M MeCN. Scan rate 10 mV s^{-1}.

2.1.4. Assessment of the thiol-yne reaction under different conditions

- **TCEP**

After the electrografting, MWCNT-GC electrodes were incubated with 6-ferrocenyl hexanethiol (6-FcSH) as a redox probe. The thiol-yne reaction was assessed under different conditions: in presence of tris(2-carboxyethyl)phosphine (TCEP), β-cyclodextrins (β-CDs) or under UV irradiation (*Fig. 8*).

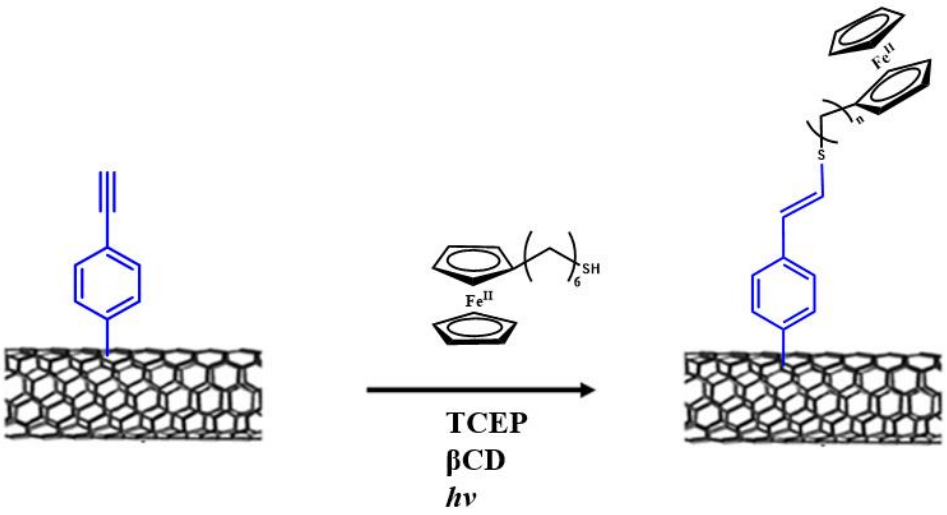

Fig. 8: thiol-yne reaction between the grafted ethynylbenzene groups and 6-ferrocenyl hexanethiol.

Cyclic voltammetry is a major electroanalytical method for monitoring the redox characteristics of a compound [41], and it was used in the following analyses to probe the electrochemical properties of the immobilized ferrocene on the electrode surface.

Both TCEP and β-CDs are supposed to promote the reaction through a nucleophilic addition substitution, through the generation of a thiolate anion which is a good nucleophile and can form a covalent bond with an electron-poor unsaturated system such as alkene or alkyne group.

Tris(2-carboxyethyl)phosphine (TCEP) is a water soluble phosphine, often used as a reducing agent in biochemistry applications to prevent the formation of disulfide bonds, but it was also used specifically as a catalyst for a thiol-ene click chemistry by the group of Zhang L. et al [42]. For the reaction, the electrodes were immersed into a solution containing 2 mM 6-FcSH in a mixture of H_2O/methanol (3:7) v/v% and 2 mM TCEP for 3 hours. Then, the electrodes were thoroughly rinsed in methanol and water and subsequently dried.

A reversible redox system corresponding to an immobilized redox specie is observed at the potential attributed to Fc. Comparing the functionalization with or without TCEP, TCEP caused lower redox peaks and thus a lower amount of ferrocenyl immobilized on the surface. It is noteworthy that CVs of control electrodes that were incubated in presence of 2 mM ferrocene (without the terminal thiol-alkyl- chain) gave no signal after 3 hours of incubation.

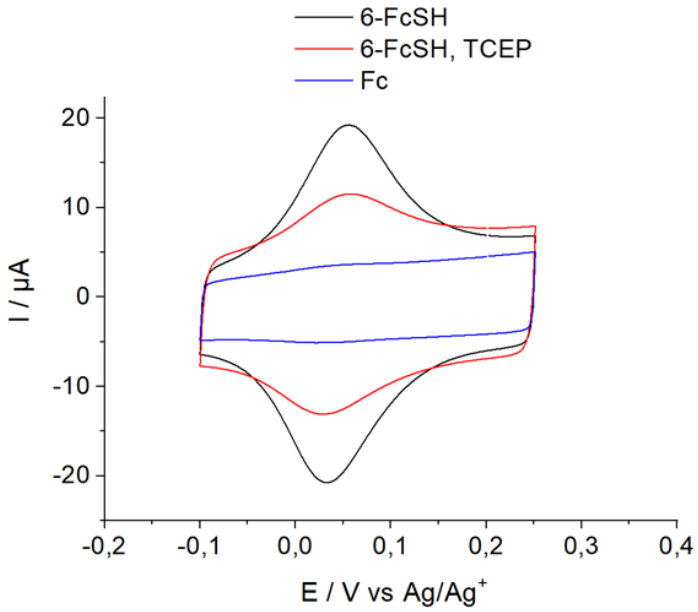

Fig. 9: CVs were carried out after a 3 hours incubation of the electrodes with 6-(ferrocenyl)hexanethiol in presence (red line) or absence (black line) of TCEP. The electrodes were modified with 4-ethynylbenzendiazonium salt by electrografting. The blue lines are relative to electrodes incubated in the same condition with ferrocene. Ref. electrode: Ag/Ag^+ in TBAP 0.1 M MeCN. Scan rate: 10 mV s^{-1}.

- **β-CD**

Cyclodextrins (CDs) are naturally-occurring cyclic oligosaccharides consisting of several (6, 7, 8) glucose units. They are torus shaped molecules that possess a hydrophilic outer shell and a hydrophobic interior cavity. This structure enables the formation of reversible host–guest complexes by the reversible interaction of hydrophobic molecules with the inner cavity. CDs can promote reactions in aqueous environment by supramolecular catalysis [43, 44]. Complexation depends on the size, shape and hydrophobicity of the guest molecule [45]. A good advantage of the use of β-CDs compared to more stronger bases is their biocompatibility that makes them an ideal candidate for bioconjugation. There are several examples of their use as catalyst for thiol-based reaction occurring at the surface. Kostić et al. described the modification of lignocellulosic materials, by introduction of vinyl groups on their surfaces followed by a thiol-ene reaction using β-CDs as catalyst with the purpose of increase the hydrophobic properties of wood materials [46]. The mechanism for the supramolecular addition of thiols to unsaturated compounds promoted by β-CDs was postulated by Sridhar R. et al. [47] based on the evidence obtained from ^{1}H NMR spectroscopy. The reaction starts with the sulfur atom of the S-H bond becoming a better nucleophile after the formation of hydrogen bonds between the thiol and the hydroxyl groups onto the β-CD cavity, which enhances its

reactivity towards alkenes. A similar mechanism could be thus imagined for the addition of thiols to alkynes (*Fig. 10*).

In order to investigate this possible route, MWCNTs-GC electrodes were functionalized with 4-ethynylbenzene diazonium by electrografting as described before and then they were immersed for 3 hours in a mixture of H_2O/DMF (1:1 v/v%) able to dissolve both 2mM 6-(ferrocenyl)hexanethiol and 2 mM β-CDs while stirring and lastly probed by cyclic voltammetry (*Fig. 10*).

β-CD was able to only slightly increase the peak currents of ferrocene as compared to the control (without β-CD). Peak current intensities are similar to that obtained previously in the presence of TCEP. The reduced peak current intensities of the control compared to the precedent control without TCEP, could be explained with the lower solubility of 6-FcSH in a more aqueous environment. Also in this case, the nature of the reagents can also play a considerable role and while some authors obtained high yields by starting from various unactivated alkynes [48], for others the reaction with β-CDs appeared to work only when thiophenols and arylacetylenes are used [47]. Though, the reaction with reagents grafted on the surface is also described [46], the interaction with the β-CDs cavity is likely more favoured when the reagents have more degrees of freedom in solution.

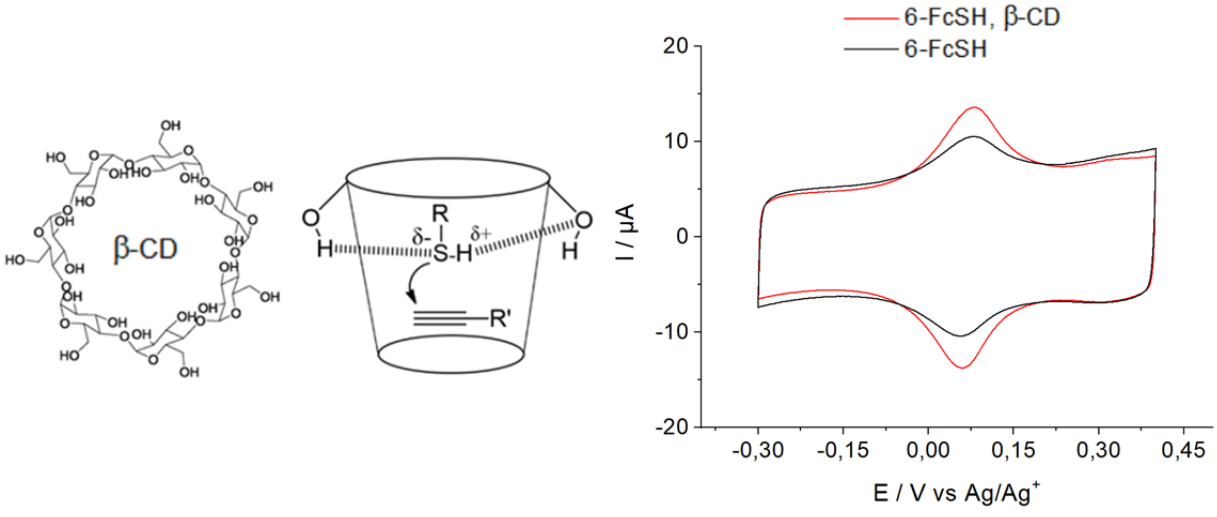

Fig. 10: mechanism of the thiol-yne reaction mediated by ß-cyclodextrins and CVs obtained after a 3 hours incubation of 6-(ferrocenyl)hexanethiol in presence or absence of 2mM ß-CDs on MWCNTs-GC electrodes that were previously electrochemically grafted with 4-ethynylbenzendiazonium. Ref. electrode: Ag/Ag^+ in TBAP 0.1 M MeCN. Scan rate 10 mV s^{-1}.

- **UV irradiation**

UV radiation (with or without photoinitiator) can promote a thiol-yne reaction through a radical mechanism, which is schematized briefly in *Fig. 11*. A thiyl radical adds across the triple bond to form a carbon-centered vinyl sulfide radical, which abstracts a hydrogen from a thiol forming a vinyl sulfide and regenerating a new thiyl radical that sustains the chain. The mechanism is analogous to that of thiol-ene chemistry, but each alkyne functional group is theorically capable of two consecutive reactions with two thiol functional groups. Thus, depending on the nature of the alkyne, mainly its molecular size and bulkyness, a subsequent addition of a thiyl radical to the double bond of the vinyl sulfide may occurr or not, to afford fully saturated bis-sulfide bis-adducts [4].

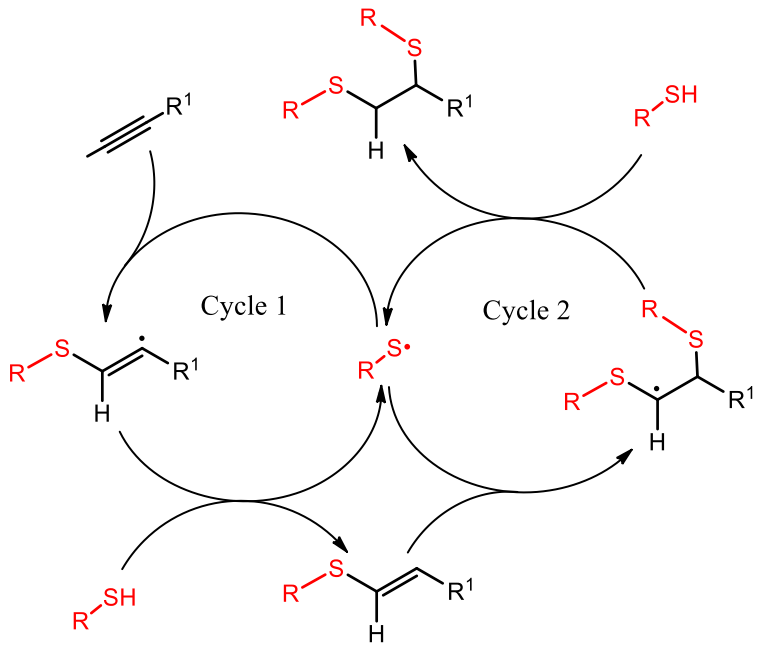

Fig. 11: generalized radical thiol−yne reaction mechanism. Cycle 1 represents the initial addition of a thiol to an alkyne while cycle 2 represents the subsequent addition of another thiol to the vinyl sulfide product.

The radical addition of thiols to alkynes has been recently utilized for the synthesis of polyfunctional materials, dendrimers, polymer brushes or cross-linked polymers [49]. As already stated, the possibility of bisfunctionalization of the vinyl moiety, which occurs especially via the radical route, renders the thiol-yne reaction more advantageous over the thiol-ene reaction for obtaining polymers with high cross-link density. The radical initiated thiol-yne chemistry offers the advantage to spatially and temporally control the modification of a surface by controlling the light exposure thus is suitable for photolithography applications. As an example, Hensarling R. M. et al. [50] created a micropatterned surface

composed of two different areas with different properties, hydrophilic and hydrophobic, on propargyl methacrylate brushes by application of a photomask using a library of commercially available thiols under irradiation in presence of 2,2-Dimethoxy-2-phenylacetophenone (DMPA).

After the electrografting of the diazonium salt as described before, MWCNTs-GC electrodes were dipped in a glass vial containing 2 mM 6-FcSH in degassed chlorophorm for 50 min under UV irradiation (240-400 nm, 200 W). 0.2 equivalents of a photoinitiator, DMPA, were added in the solution to facilitate the reaction. A tip was placed on the top of the vial to exclude oxygen. The electrodes were then rinsed in solvent and water to remove the possible residual ferrocenyl molecules remaining on the electrodes prior testing. The electroactive area relative to Fc is approximatively twice compared to that originated in the same conditions without UV irradiation. Also, 20 consecutive cycles were applied at 10 mV s^{-1}, showing a good stability of the cathodic and anodic peaks.

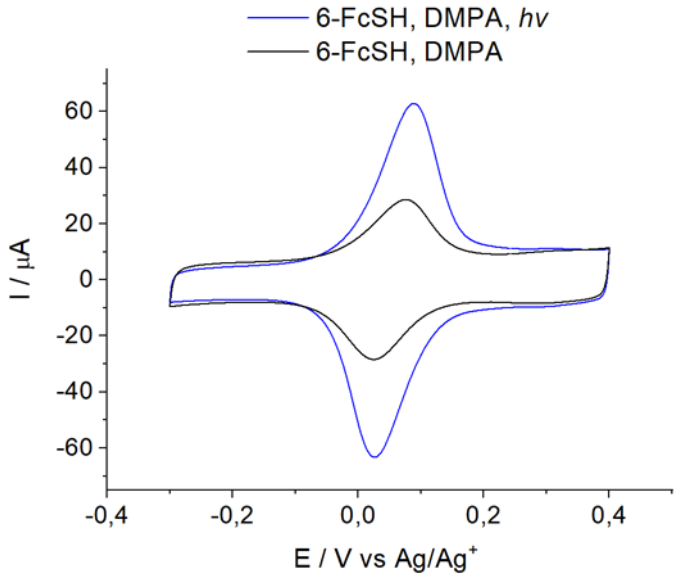

Fig. 12: CVs of 6-(ferrocenyl)hexanethiol in presence of 0.2 eq. of DMPA under (blue line) and without (black line) UV irradiation. Working electrodes: MWCNTs-GC electrodes electrochemically grafted with 4-ethynylbenzendiazonium salt. Ref. electrode: Ag/Ag^+ in TBAP 0.1 M MeCN. Scan rate: 10 mV s^{-1}.

Fig. 13 and *Table 1* below summarize the results of the immobilization of 6-FcSH onto MWCNTs-GC electrodes functionalized with ethynylbenzene groups by electrografting under three different conditions: TCEP, β-CDs and UV radiation. An average value of electroactive surface coverage (Γ) of the electroactive center was extimated from multiple experiments, using the same cycle (15° cycle) for the calculations. The electroactive surface coverage was

calculated by using *Equation 1.* where Q is the total charge that is obtained by integration of anodic peak areas, A is the geometric surface area of the electrode (0.28 cm^2 for MWCNTs-GC electrodes), n is the number of electrons involved (1) and F is the Faraday constant (96485 C mol^{-1}).

$$\Gamma = \frac{Q}{nFA} \qquad \textit{Equation 1.}$$

For all conditions, the anodic and cathodic peak-to-peak separation (ΔE) is close to zero, which is indicative of immobilized species. UV irradiation appeared to be the best condition and hugely increased the amount of ferrocene on the electrode. If we compare experiments performed with β-CDs and TCEP with control experiments without catalyts, we can conclude that the immobilization is closed to a simple adsorption of the ferrocene derivative on MWCNTs and that the thiol-yne reaction is inefficient. On the contrary, the increase generated by UV irradiation compared to other conditions strongly suggest that ferrocene thiol is efficiently coupled to the alkyne groups. It might be also possible that a double conjugation of the vinyl disulfide occurs owing to the generation of high amounts of reactive thiyl radicals by irradiation. For comparison, the surface coverage (220 pmol cm^{-2}) is approximatevely 5 times lower than that estimated after immobilization of ethynylferrocene on MWCNTs modified by electrografting of 4-azidobenzene diazonium tetrafluoroborate via CuAAC [19].

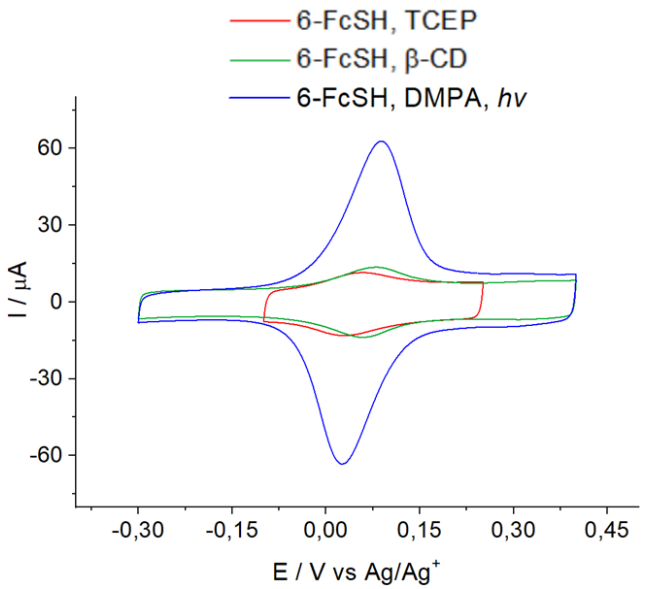

Fig. 13: comparison of the cyclic voltammograms of electrodes functionalized with 4-ethynylbenzendiazonium salt by electrografting and then 6-(ferrocenyl)hexanethiol in different conditions (15° cycle). Ref. electrode: Ag/Ag^+ in TBAP 0.1 M MeCN. Scan rate: 10 mV s^{-1}.

	$E_{1/2}$ (V) vs Ag/Ag^+	ΔE(V) vs Ag/Ag^+	Γ_{max}
6-FcSH, TCEP	+0.07	0.02	21 pmol cm^{-2}
6-FcSH, βCDs	+0.04	0.03	33 pmol cm^{-2}
6-FcSH, DMPA, *hv*	+0.05	0.06	220 pmol cm^{-2}

Table 1

2.1.5. UV-promoted thiol-yne reaction with different ferrocene thiol probes

The effectiveness of the immobilization under UV irradiation was further confirmed using other two ferrocenyl redox probes: 11-ferrocenyl(undecanethiol) (11-FcSH) and ferrocenyl methanethiol (FcSH) (*Fig. 14*). In both cases the redox peaks of ferrocene are significantly enhanced when the electrodes are subjected to UV irradiation compared to the controls that were kept in the dark. It cannot be excluded that a fraction of the thiols could react spontaneously with the ethynyl groups on the surface, and this could explain also why the controls exhibit redox peaks. The use of ferrocenyl methanthiol resulted in a lower surface coverage than the other ferrocenyl thiols with longer alkyl chains (*Table 2*), while a higher surface coverage was obtained with 11-FcSH.

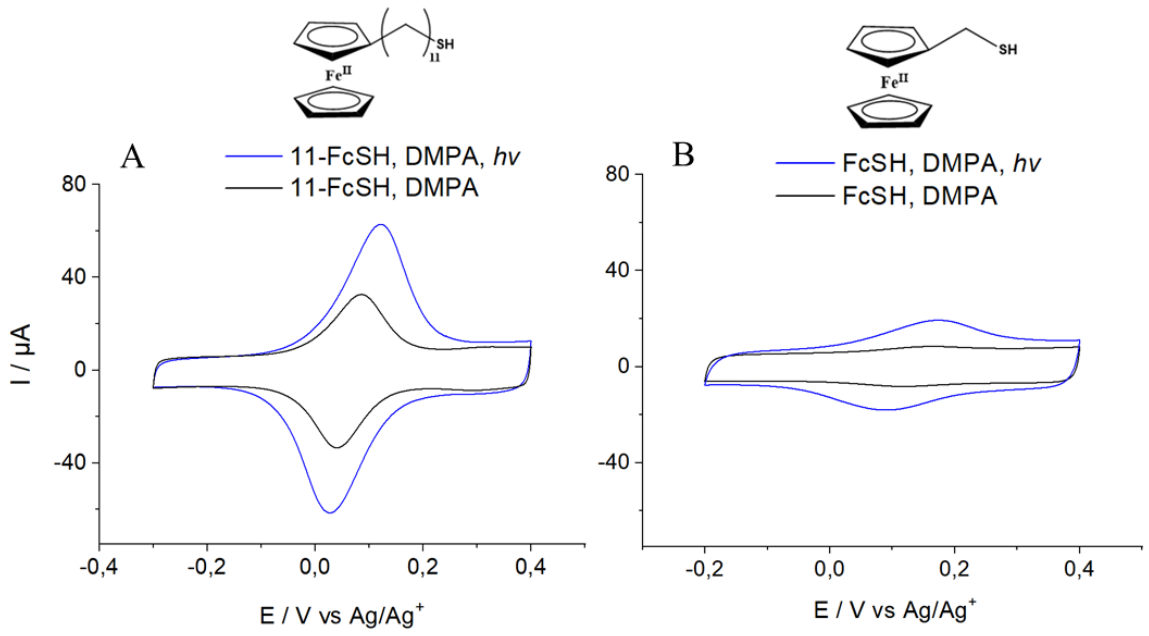

Fig. 14: CVs of A) 11-(ferrocenyl)undecanethiol and B) ferrocenyl methanethiol in presence of 0.2 eq. DMPA with or without UV irradiation. Working electrodes: MWCNT-GC functionalized with 4-ethynylbenzendiazonium tetrafluoroborate by electrografting. Ref. electrode: Ag/Ag^+ in TBAP 0.1 M MeCN. Scan rate: 10 mV s^{-1}.

	UV	$E_{1/2}$ vs Ag/Ag^+	ΔE	Γ_{max}	STD dev.
6-FcSH	✓	0.05	0.06	220 pmol cm^{-2}	60 pmol cm^{-2}
6-FcSH	×	0.05	0.05	103 pmol cm^{-2}	11 pmol cm^{-2}
11-FcSH	✓	0.07	0.09	304 pmol cm^{-2}	40 pmol cm^{-2}
11-FcSH	×	0.06	0.05	120 pmol cm^{-2}	16 pmol cm^{-2}
FcSH	✓	0.12	0.08	70 pmol cm^{-2}	10 pmol cm^{-2}
FcSH	×	0.13	0.05	6 pmol cm^{-2}	4 pmol cm^{-2}

Table 2

The flexibility of the alkyl is likely playing a role.The presence of longer alkyl chains induces higher flexibility and less steric hindrances, which might improve the efficiency of the thiol-yne reaction at the surface of MWCNT sidewalls. A contribution of the alkyl chain to the adsorption of ferrocene on nanotubes can be also postulated, which is very low when ferrocenyl methanethiol, with a only a single methyl group, is used.

The immobilization of FcSH was evaluated by varying the scan rate from 10 to 150 mV s^{-1} to probe the reversibility of the redox process and the surface confinement of ferrocene. For a reversible electron transfer process involving freely diffusing redox species, cyclic voltammetry shows a linear relationship between peak current and the square root of the scan rate, as demonstrated by the Randles-Sevcik equation (*Equation 2.*) where i_p is the peak current, n is the number of electrons, F is Faraday's constant, Γ is the surface coverage, A is the area of the electrode, v is the scan rate, R and T are the ideal gas constant and temperature [51]. If the species is confined to a surface (adsorbed or attached) the diffusion model is not longer applicable and a linear relationship with the scan rate can be established instead, as stated from *Equation 3.* [52].

$$i_p = 0.4463nFAC\left(\frac{nFvD}{RT}\right)^{1/2} \qquad \textit{Equation 2.}$$

$$i_p = \frac{n^2F^2\Gamma Av}{4RT} \qquad \textit{Equation 3.}$$

A linear relationship between the peak current and the scan rate, but not the square root of the scan rate, was observed (*Fig. 14*), as expected from the theoretical model for a species that has been immobilized to an electrode surface.

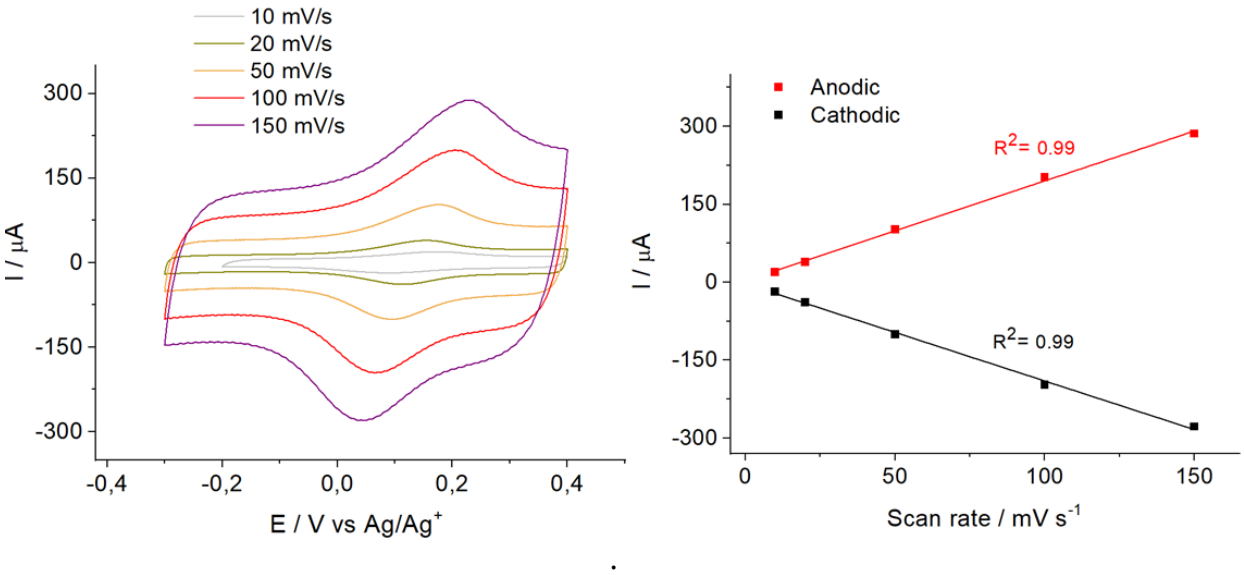

Fig. 14: cyclic voltammetries at variable scan rates of ferrocenyl methanethiol on a functionalized electrode after UV irradiation and the corresponding plot of anodic and cathodic peak currents versus scan rate.

2.1.6. A comparison with pristine MWCNTs

Some additional experiments have been done on pristine non-functionalized MWCNTs as controls. Actually, the direct functionalization of pristine CNTs through a radical initiated thiol-ene reaction between mercaptans with the double bond groups of the CNTs skeleton has been reported by some authors [53]. The radicals formed upon irradiation are supposed to have the strenght to break the carbon skeleton of the nanotubes and consequently be grafted. It could also be imagined that the generated thiyl radicals could react with defects which are naturally present on the outer walls of the nanotubes, the ones present at the edges or originating from the purification procedures or during the sonication treatment necessary to their dissolution in NMP.

In order to test also these possibilities and verify the specificity of the reaction in absence of any alkyne functional groups on the nanotubes, MWCNT-GC electrodes were incubated for 50 min with 2 mM 6-FcSH in presence of DMPA as already done with the alkyne-modified nanotubes. In this case, the difference in surface coverage values of the electrodes subjected or not to UV is not as significant as the one observed on alkyne-nanotubes. Thus, it could be stated that the presence of ethynyl functionalities is decisive for the immobilization of the thiols via the radical thiol-yne reaction while the immobilization via other mechanism is negligible. The photo-initiated conditions are not suitable for producing a significant

immobilization of 6-FcSH through a thiol-ene reaction with the double bonds of pristine nanotubes or by reaction with the nanotubes defects.

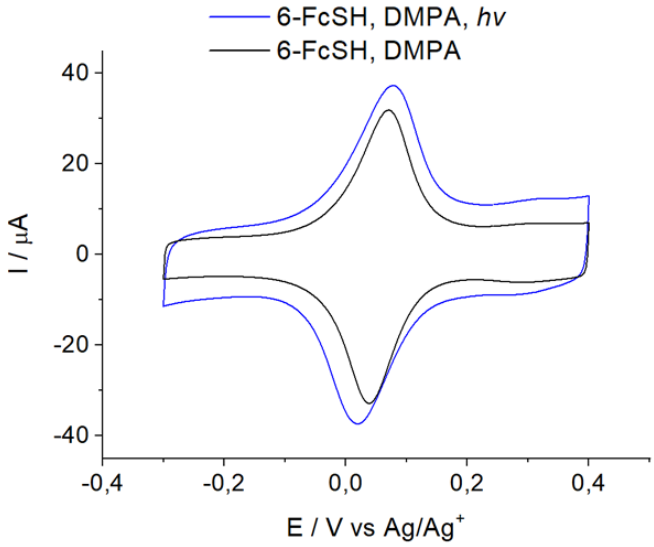

Fig. 25: CVs of GC and GDL electrodes containing a pristine MWCNTs film functionalized with 6-(ferrocenyl)hexanethiol (15° cycle) with/without 50 min UV irradiation. Ref: Ag/Ag^+ in TBAP 0.1M MeCN. Scan rate 10 mV s^{-1}.

	UV	$E_{1/2}$ vs Ag/Ag^+	ΔE	Γ_{max}
MWCNT-GC	✓	0.05	0.05	120 pmol cm^{-2}
MWCNT-GC	×	0.05	0.04	100 pmol cm^{-2}

Table 4

2.1.7. Chemical grafting of in situ generated 4-ethynylbenzene diazonium salt

Another way to covalently graft ethynyl groups onto MWCNTs using diazonium chemistry is the chemically driven reduction of the aryldiazonium salt generated in situ. This method was found to be an effective means for the decoration and solubilization of graphene and CNTs [54]. In general, it is also very useful when electrochemical means are not practicable, thus for low-conductive and insulating surfaces or for highly non planar substrates. Also, the method is sometimes preferred with non commercially available aryldiazonium compounds or to skip their synthesis and purification which is often not easy, since particular attention need to be taken being the diazonium group thermally instable and light-sensitive [55].

By this method, the aryldiazonium salt is produced by diazotization from its aniline or triazene precursor [54]. Various options exist for promoting the conversion from the aniline precursors, for instance the use of t-butylnitrite or $NOBF_4$ in organic solvent or $NaNO_2$ in

aqueous acidic medium. A treatment with HF or HBF_4 was instead proposed by Tour et al. [56] for the generation of aryldiazonium salt from triazene groups.

The grafting of the in situ generated 4-ethynylbenzene diazonium onto MWCNTs followed by thiol-yne reaction was investigated as a complementary method. The followed procedure for the chemical generation of 4-ethynylbenzene diazonium has been taken from et Lalaoui N. et al. [56] and it is schematized in *Fig. 15*. 50 mg of MWCNTs (Nanocyl 3100, >95% purity) were dispersed in 150 mL of DMF using an ultrasonic bath for 30 min. The dispersion was then placed under argon atmosphere and heated up to 80 °C. The precursor of the diazonium salt, 4-ethynylaniline (0.9 g, 8 mmoL) and a reducing agent, isopentyl nitrite (1.1 mL, 8 mmoL), were added in the dispersion that was stirred overnight at 80 °C and under reflux. During this process, the aryl radicals are produced continuously in solution followed by their spontaneous grafting to MWCNTs. Finally, the reaction mixture was filtered through 0.45 µm PTFE membrane filters, washed several times with hot DMF and finally with acetone to remove unreactant species and dried under reduced pressure to obtain a granular powder of MWCNTs.

Fig. 15: modification of MWCNTs from in situ generated 4-ethynylbenzendiazonium salt.

Subsequently, the obtained carbon nanotubes were characterized by Raman spectroscopy to look for any trace of structure modification that occurred during the reaction. Raman spectroscopy is a valuable technique for obtaining vibrational and crystallographic information as well as information about the electronic state of small quantities of materials or small regions whitin a material, including non transparent solids and nano-objects [57]. MWCNTs have unique spectroscopic properties. The G-band (tangential mode), located at 1580 cm^{-1}, originates from the graphitic nature of CNTs. It is related to vibrations that can be

found in all sp^2 carbon materials. The D-band (disordered mode), located at 1350 cm^{-1}, can reveal the presence of impurities or defects which breaks the basic symmetry of the graphene sheet and the tubular structure of CNTs. It is indicative of the presence of sp^3 bonding or broken sp^2 bonds in the sidewalls. Finally, the G′-band (d-band overtone), at 2700 cm^{-1}, which is dependent upon chirality and diameter of the CNTs [58].

For the analysis, CNTs were dispersed in ethanol and drop-dried on a microscope glass slice covered with a gold film (50 nm thickness). Raman spectra of a sample containing the modified MWCNTs were acquired at different locations within the sample and compared to that of pristine MWCNTs used as standard. As a consequence of the grafting of the aryl diazonium salt, some sp^2 bonded carbon atoms are converted into sp^3 bonded carbon atoms leading to a consequent increase in the D-band (*Fig. 16*). To have a relative estimation, the I_D/I_G ratio was calculated from an average of the maxima intensities of the corresponding bands from different spectra. The ratio is increased from 0.53 to 0.87 for the modified MWCNTs testifying the effective functionalization. While the spectra obtained from different areas of the pristine nanotubes were almost identical and overlapping, some areas of the sample of the modified nanotubes showed a clearly increased D-band while others were assimilable to that of pristine MWCNTs. Thus the modification was not homogeneously distributed on MWCNTs.

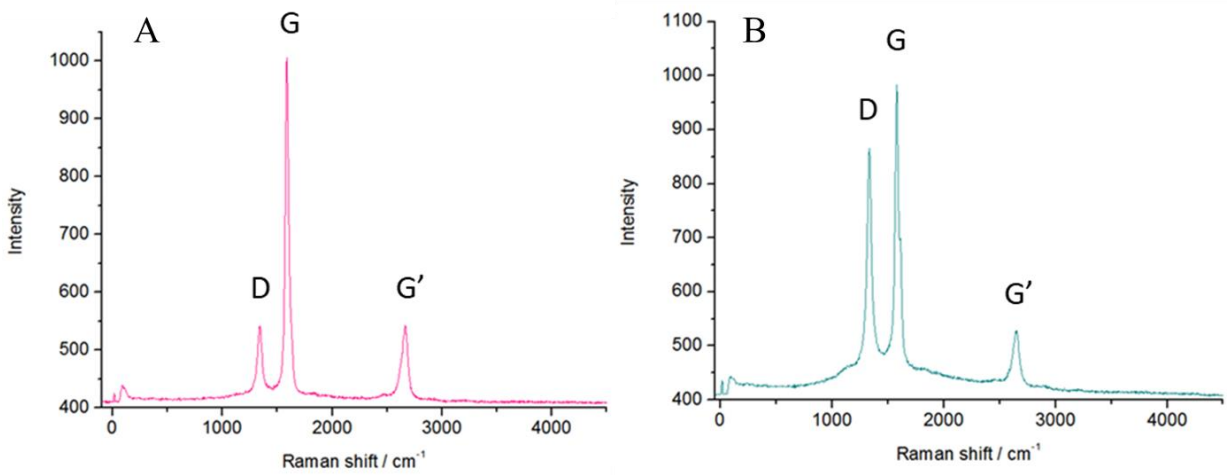

Fig. 16: a Raman spectrum of A) pristine MWCNTs and B) MWCNTs modified with in situ generated aryldiazonium salts. A laser at 633 nm and 3 mW power was focused on the sample surface using a 50% objective.

The modified MWCNTs were then tested with 6-FcSH under UV irradiation. A new type of working electrodes was used for the electrochemical assessment of the thiol-yne reaction: carbon paper with a Microporous Layer (MPL). MPL electrode is made from a porous

composite material containing carbon and a dense array of carbon fibers, is often used in fuel cell systems and, given its rough and porous structure, is more suitable for the adhesion of MWCNTs. In *Fig. 17* is reported an image of a MPL electrode and the electrochemical cell used. In particular, MWCNTs were deposited on a circular area of 6 mm diameter on the MPL electrode.

Also in this case, though the capacitative current is relatively large due to the high surface area of the porous MPL structure, it appears clear that the irradiation produced a higher signal relative to 6-FcSH than the control. The calculated surface coverage, obtained after proper background subtraction, is 916 pmol cm^{-2} for UV while 264 pmol cm^{-2} for the control (*Fig. 17*).

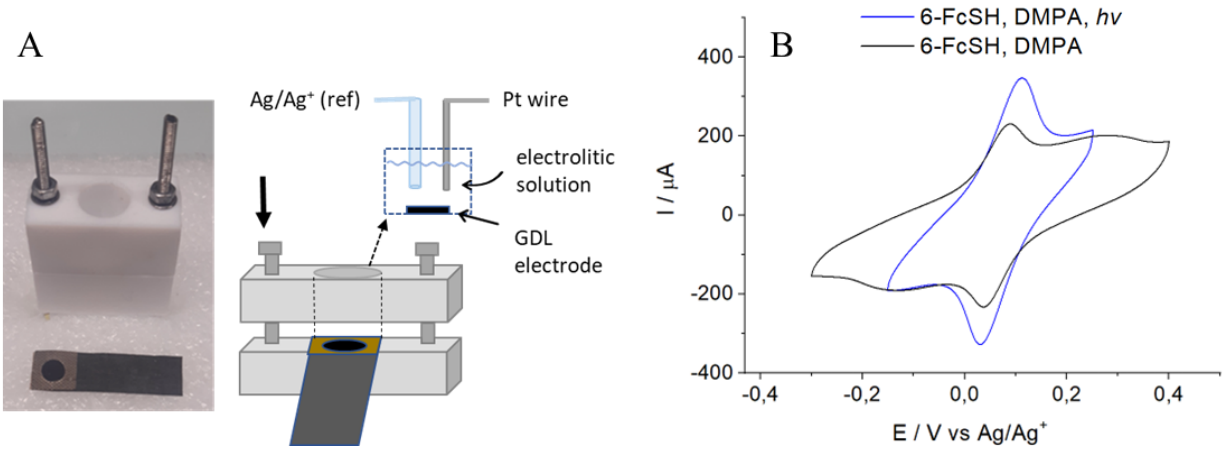

Fig. 17: A) picture of a MPL electrode covered with MWCNTs modified from in situ generation of 4-ethynylbenzene and the electrochemical cell set-up used for electrochemical experiments. B) CVs of MWCNTs-MPL electrodes incubated with 6-FcSH with/without UV irradiation. Ref. electrode: Ag/Ag^+ in TBAP 0.1 M MeCN. Scan rate: 10 mV s^{-1}.

2.2. Non-covalent functionalization of MWCNTs with pyrene

Another complementary route for the introduction of alkyne- groups on the sidewalls of carbon nanotubes has been explored, the non-covalent functionalization using a pyrene derivative, 1-ethynylpyrene. It is known that pyrene and its derivatives are effective for the stable functionalization of CNTs through the establishment of non-covalent stable π–π stacking interactions [59]. In general, these interactions are a specific type of intermolecular attraction typical of aromatic molecules (carbon nanotubes, graphite, anthracene, pyrene) and are so named because they occur when the plane of aromatic rings are stacked parallel to one another [60]. These interactions are stronger with the number of π electrons thus, MWCNTs are ideal substrates for non-covalent functionalization.

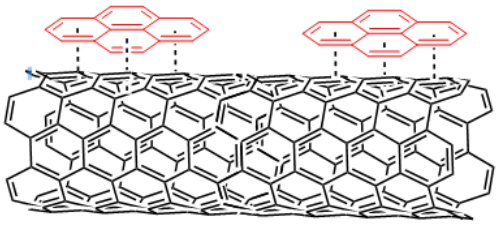

Fig. 18: schematization of the π–π stacking interactions between carbon nanotubes and pyrene.

The immobilization of ferrocenyl derivatives onto ethynylpyrene-functionalized MWCNTs was then assessed again on both GC and MPL electrodes.

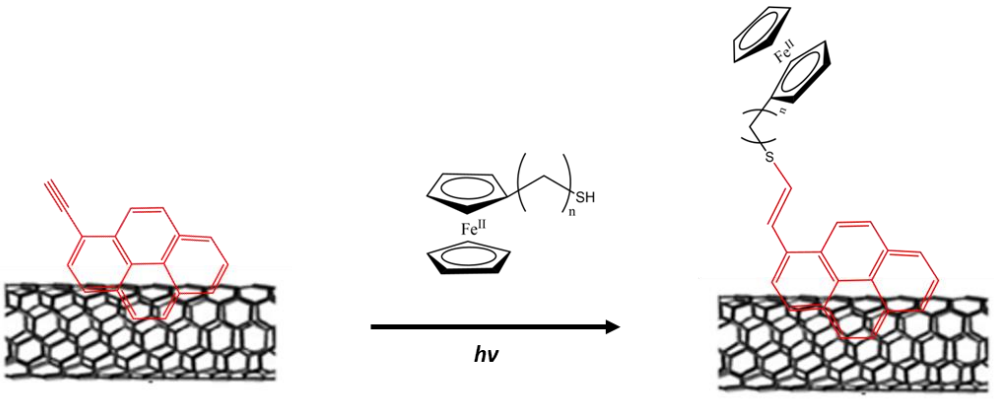

Fig. 19: thiol-yne reaction between 1-ethynylpyrene and ferrocenyl thiols.

A drop of 20 µL of a 10 mM solution of 1-ethynylpyrene in DMF was dropcasted onto the pristine MWCNTs film on both GC and MPL electrodes and evaporated completely under vacuum. Finally the electrodes were dipped in a glass vial containing 2 mM solutions of different ferrocenyl derivatives bearing a carbon chain spacer with different lengths and the effectiveness of their coupling under UV irradiation, in the same conditions described previously for the covalent modified electrodes, was verified.

The peak currents of the cyclic voltammograms are significantly increased after UV irradiation compared to the controls that were not irradiated for all the three ferrocenyl derivatives used (*Fig. 20, 21*). Multicyclic experiments showed that the ferrocenyl/ferrocenium ($Fc^{+/0}$) redox couple was stable.

The electrochemical data of all the ferrocenyl derivatives are summarized in *Table 3*. The electroactive areas calculated from the total charge obtained by integration of the anodic peaks, which are indicative of the amount of ferrocene, are also similar and just slighly lower to that calculated previously for the electrochemically grafted electrodes with the diazonium compound. Also in this case, the surface coverages are dependent on the length of the carbon chain spacer of the ferrocenyl thiol, with a major length related to an higher amount of

immobilized ferrocene, similarly to the diazonium functionalized electrodes. Again, the role of the irradiation is undoubted, determining a significantly higher ferrocene immobilization with all the analyzed ferrocenyl probes.

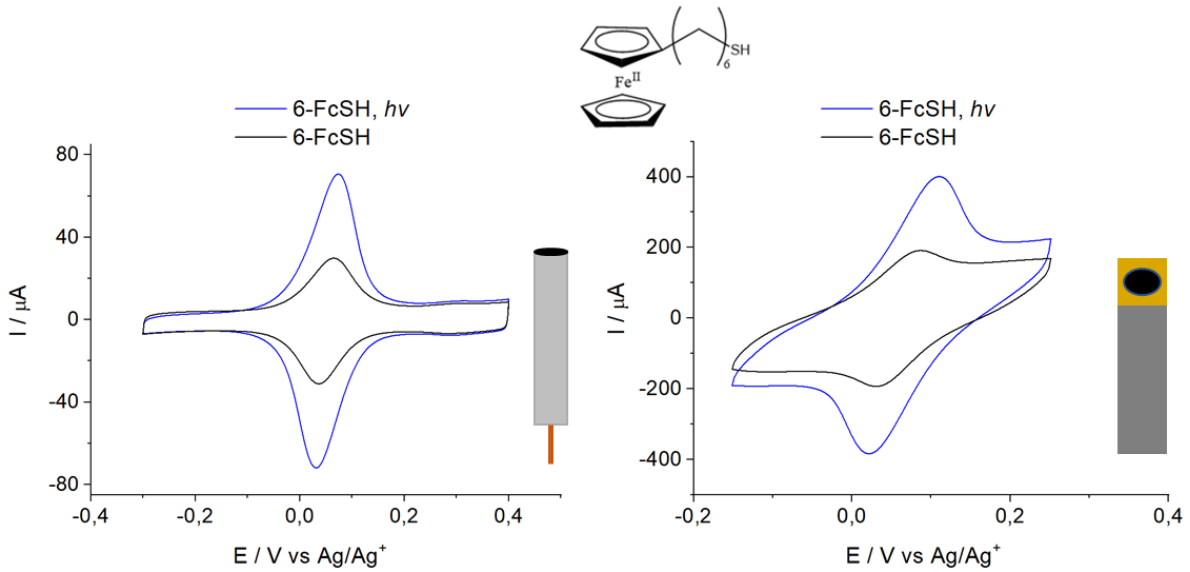

Fig. 20: cyclic voltammogram of MWCNT-GC electrodes (left) and MWCNT-MPL electrodes (right) functionalized with 6-(ferrocenyl)hexanethiol with or without UV irradiation (15° cycle). Ref: Ag/Ag^+ in TBAP 0.1 M MeCN. Scan rate: 10 mV s^{-1}.

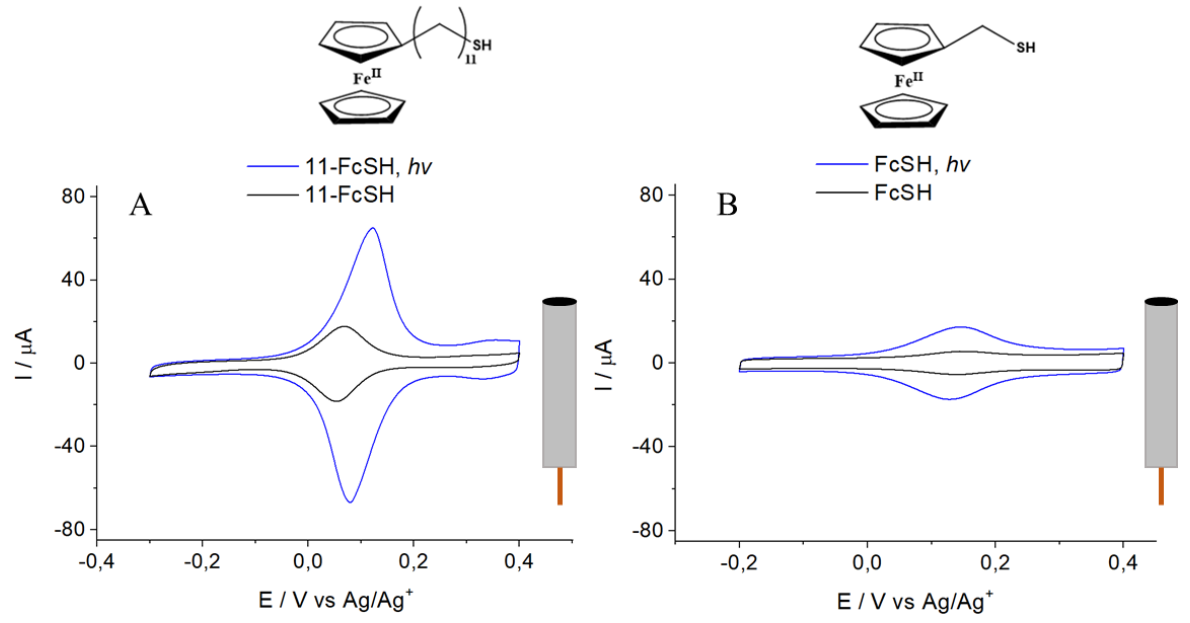

Fig. 21: cyclic voltammetry data for MWCNT-GC electrodes functionalized with A) 11-(ferrocenyl)undecanethiol and B) ferrocenyl metanethiol with or without UV irradiation (15° cycle). Ref: Ag/Ag+ in TBAP 0.1 M MeCN. Scan rate: 10 mV s^{-1}.

MWCNTs-GC	UV	DMPA	$E_{1/2}$ vs Ag/Ag^+	ΔE	Γ_{max}	STD dev.
6-FcSH	✓	✓	0.05	0.04	210 pmol cm^{-2}	38 pmol cm^{-2}
6-FcSH	×	✓	0.05	0.02	75 pmol cm^{-2}	20 pmol cm^{-2}
11-FcSH	✓	✓	0.09	0.04	230 pmol cm^{-2}	60 pmol cm^{-2}
11-FcSH	×	✓	0.06	0.02	60 pmol cm^{-2}	-
FcSH	✓	✓	0.13	0.02	64 pmol cm^{-2}	7 pmol cm^{-2}
FcSH	×	✓	0.14	0.01	8 pmol cm^{-2}	5 pmol cm^{-2}

Table 3

2.2.1. Role of DMPA

A deeper investigation, in particular on the role of the UV-activated radical photoinitiator, DMPA, was carried out using ferrocenyl methanethiol (*Fig. 22*). The irradiation in absence of DMPA produced only a minor decrease of the electroactive surface coverage relative to ferrocenyl methanethiol (44 pmol cm^{-2}) compared to the irradiation carried out in its presence (60 pmol cm^{-2}). Apparently, the role of the photoinitior is marginal in promoting the radical thiol-yne reaction which appears to be triggered simply by UV light. This outcome is not surprising, since also in the literature it is stated that the presence of the photoinitiatior is not always necessary, especially when irradiation with low wavelengths around 254 nm are used [61]. As expected, a control electrode made using 2mM of ferrocene, without the alkyl chain and the terminal thiol group in the same experimental conditions, in presence of DMPA and UV light, gave no redox peaks.

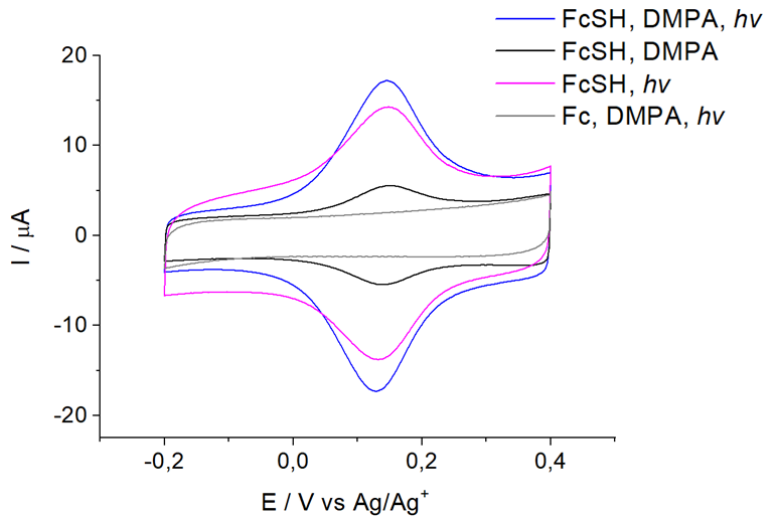

Fig.22: cyclic voltammetry data for MWCNT-GC electrodes functionalized with ferrocenyl metanethiol in different conditions (15° cycle). Ref: Ag/Ag+ in TBAP 0.1 M MeCN. Scan rate: 10 mV s^{-1}.

2.2.2. Role of the irradiation time

The effect of the time of irradiation on the reaction was explored as well using FcSH on the ethynylpyrene functionalized nanotube electrodes. The electrodes were immersed in a 2 mM solution of FcSH in chloroform and exposed at UV light for different times (ranging from 1 min to 50 min). The cyclic voltammograms show redox peaks that increase with the exposure time of irradiation. After 1 min, no difference in the surface coverages are observed between irradiated electrodes and controls, while after 5 min, the photo-induced reaction produced bigger peaks and the difference is increaed over time. A good linear fitting of the charge under the anodic peaks versus time was found up to 30 min, while after 50 min the charge still increases but the linearity is lost (*Fig. 23*).

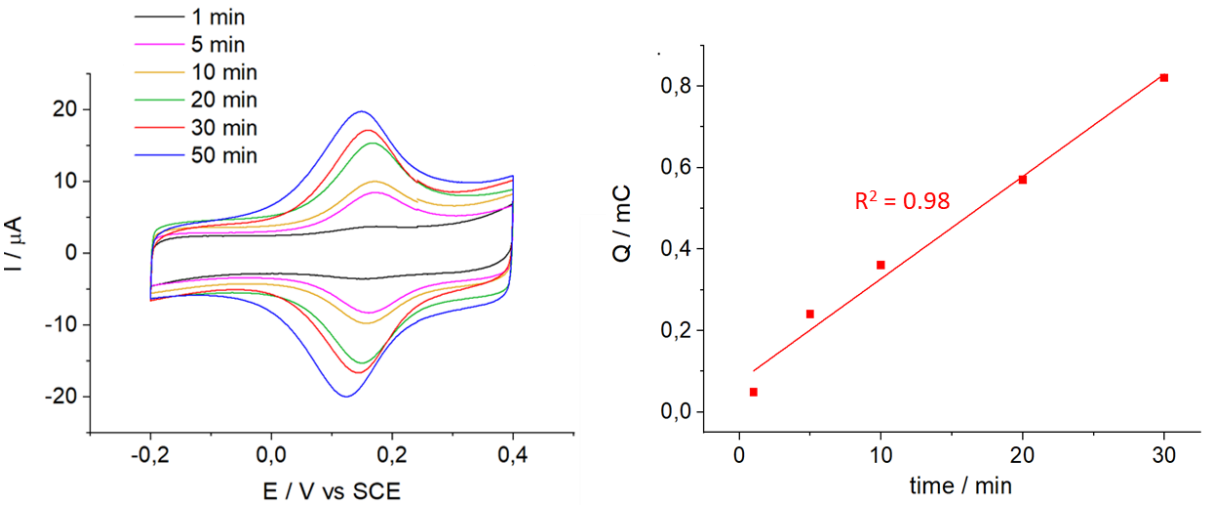

Fig. 23: CVs of ferrocenyl methanethiol in presence of 0.2 equivalents of DMPA after different UV exposure times (240-400 nm, 200 W) and plot of the charge under anodic peaks vs time. MWCNT-GC electrodes modified with ethynylpyrene served as working electrodes. Ref. electrode: Ag/Ag$^+$ in TBAP 0.1 M MeCN. Scan rate: 10 mV s^{-1}.

$$\Delta E_{fwhm} = \frac{3.53RT}{nF} \quad (90.6/n \text{ mV at } 25\ ^\circ C) \qquad \textit{Equation 4.}$$

It is also possible to note a shift of about 0.05 V of the mid point potential of the $Fc^{+/0}$ redox couple towards lower potentials over time of irradiation. It can be hypothesized that the increase in the number of immobilized ferrocene moieties and their subsequent aggregation driven by hydrophobic interactions on the electrode surface, could be responsible of this behaviour. The ideal full-width at half-maximum of the anodic or cathodic voltammetric wave, ΔE_{fwhm}, when no interactions take place between the redox centers is given by *Equation 4.* and it is equal to 90 mV for non interacting ferrocene molecules. Deviations toward higher

and smaller values are often linked to aggregated state of ferrocene [37, 46]. The ΔE_{fwhm} calculated from the anodic wave is 96 mV after 5 min, thus similar to the theorical expected value, while it has a value of 130 mV after 50 min of irradiation indicating a degree of interaction between redox centers.

2.3. XPS analysis of the functionalized electrodes

Further analyses were performed by using x-ray photoelectron spectroscopy (XPS) in order to evaluate the surface composition and the chemical changes at the surface of the MWCNTs as a consequence of the functionalization process. The technique provides a simple elemental analysis of solid surfaces, except for hydrogen and helium, as well as information on chemical shifts and chemical bondings. It is probably the most readily interpretable, informative and quantitative technique for chemical surface characterization [62]. XPS spectra are generated by interaction of a photon with an atomic orbital electron, as a result the electron is ejected from the atom with a kinetic energy which is the difference between the photon energy and the binding energy of the electron in the atom. An X-ray source provides the incident photons while the analyzer measures the number of electrons with different kinetic energies generating a spectrum in which the phoelectronic intensities are correlated to the binding energies. The binding energy position of the peaks allows the elemental identification [63].

A small film of MWCNTs has been formed on small and flat silicium supports for the successive XPS analyses by dropcasting 5 µL of the MWCNTs suspension (5mg mL^{-1}) in NMP and evaporated under vacuum. The electrodes have been modified by deposition of a 5 µL of a 10 mM solution of 1-ethynylpyrene to the formation of stacking interactions. Subsequently, the electrodes were immersed in a second solution containing 2 mM of FcSH with or without irradiation for 50 min and finally rinsed several times. The XPS spectra are reported in *Fig. 24*.

On both spectra a main peak can be observed at about 284 eV, which is generated by photoelectrons emitted from the C 1s core level. A second peak that appears at about 540 eV, is also present in both spectra, which is generated by photoelectrons emitted from the O 1s core level. These peaks can be found on samples containing MWCNTs [64]. The presence of oxygen can be attributed to the presence of C=O and C–O–C functional groups on the nanotubes that are more likely generated during the purification of MWCNTs, which generally involves acid washings to separate the nanotubes from the amorphous carbon and the metallic impurities used as catalysts. These treatments create defects in the structure of

nanotubes which are stabilised by –COOH and –OH groups [64]. Alternatively the oxidized groups are formed during UV treatment, although the procedure of degassing with argon has been always carried out to exclude oxygen. In the sample that was not irradiated, only these two elements, carbon and oxygen, are detected in the XPS spectum. The XPS data support the electrochemical data, in which FcSH is barely absorbed on ethynylpyrene-MWCNTs electrodes in absence of UV irradiation. On the contrary, both iron and sulfur are detected in the spectrum of the irradiated sample, demonstrating the presence of FcSH on the surface of the MWCNTs. In particular, the Fe 2p region confirms the presence of Fe(II) with the two principal spin-orbit components at 707.5 eV ($2p_{3/2}$) and at 720.2 eV - 725 eV ($2p_{1/2}$) accompanied with satellite peaks at 718.3 and 727.7 eV. The binding energies observed in this spectrum are in agreement with those described in the literature [65, 66]. The presence of Fe(III) species with broad peaks at 710.2 and 722.9 indicates that ferrocene is partially oxidized, likely upon irradiation. The two components of the S 2p core levels at 163.3 and 164.3 eV are consistent with the formation of a thioether bond upon coupling of FcSH [67]. Traces of oxidized thiol is observed at 169.2 eV.

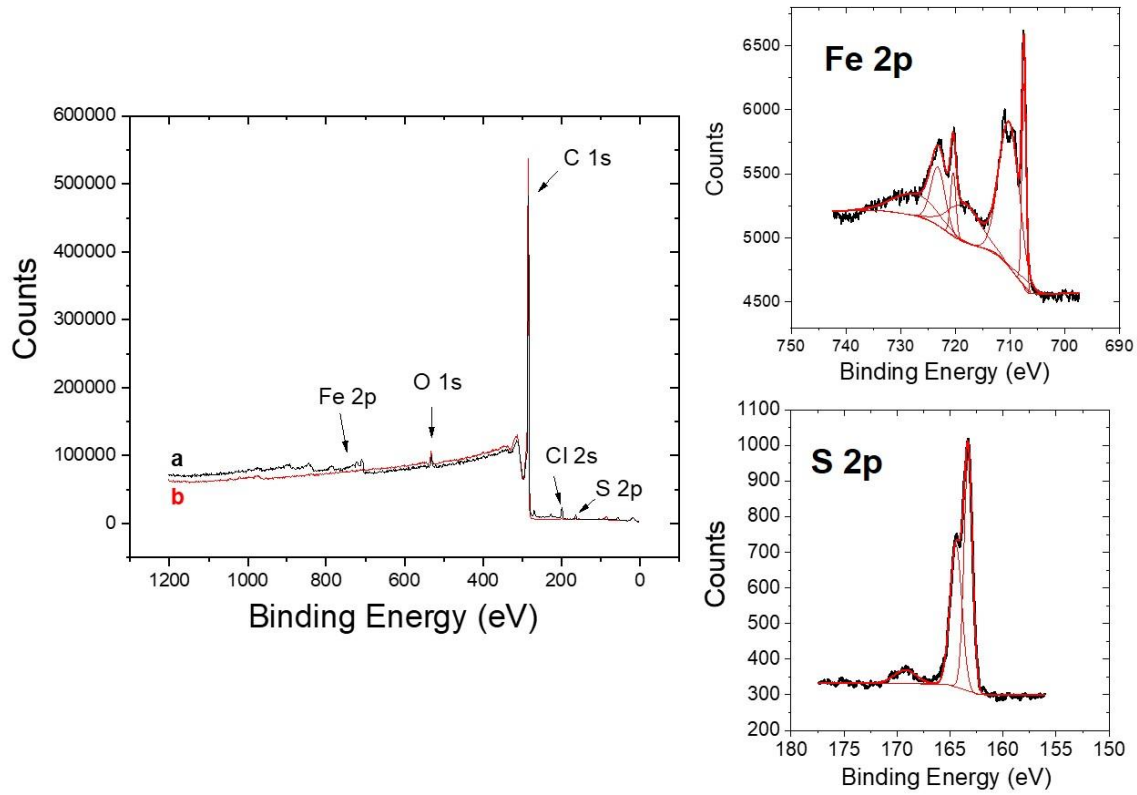

Fig. 24: XPS Survey spectra of MWCNTs modified with ethynylpyrene and then incubated for 50 min with 2 mM FcSH (a) in the presence and (b) absence of irradiation accompanied with XPS spectra at Fe2p and S 2p core levels for ethynylpyrene-MWCNTs incubated with 2 mM FcSH after 50 min UV irradiation.

3. Photoinitiated thiol-yne reaction with a phenanthroline thiol derivative

The immobilization of other redox thiol compounds by thiol-yne reaction was then assessed. A compound with a terminal thiol, 8-mercapto-N-(1,10-phenanthrolin-5-yl) octanamide (PLSH), was synthetized following the procedure reported by Elmes R. B. P. et al. [68]. The obtained product was characterized by NMR.

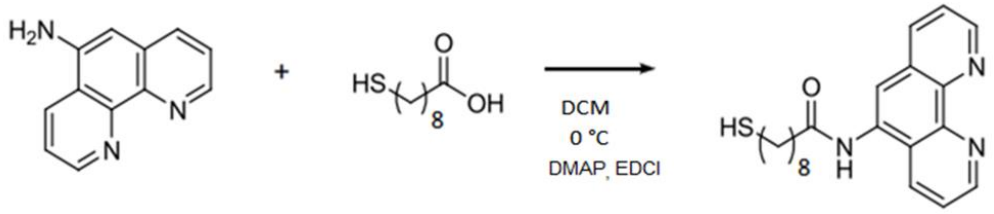

Fig. 26: reaction scheme for the synthesis of 8-mercapto-N-(1,10-phenanthrolin-5-yl) octanamide. Adapted from Ref. [68].

MWCNT-GC electrodes were prior functionalized with ethynylpyrene then immersed in 2 mM solution of the synthetized PLSH and 0.4 mM of DMPA and placed under UV lamp for 50 min in the same conditions used for the ferrocenyl probes. After the reaction, the electrodes were rinsed carefully in chloroform and water. The electrodes were then cycled 30 times in phosphate buffer at pH 7 from -0.4 V to +1.2 V vs SCE (saturated calomel reference electrode) at 100 mV s^{-1}. This process is aimed at generating phenanthrolinequinone by electrooxidation. The as produced quinone is redox-active and can be detected by electrochemistry (the phenanthroline is electroactive only at very negative potential) [69]. The electro-oxidation in aqueous solvent to form quinones has been already used for different polycyclic aromatic hydrocarbons including naphthalene, pyrene and phenanthrene [70]. A mechanism for the electro-synthesis of the phenanthroline quinone derivative (PLQSH), similar to that described for the electro-synthesis of pyrenediones, can be postulated [59]. The electro-oxidation generates a radical and a water molecule is incorporated during the process giving an hydroxylic functionality. During a second oxidation step, which probably occurs simultaneously to the first, a second hydroxylic group is formed in an adjacent position. These dihydroxylic functionalities are reversibly oxidized during cyclic voltammetry. While in aprotic medium, two reversible one-electron-reduction waves are visible in the CV corresponding to the formation of the semiquinone anion and then the fully reduced dianion species, in aqueous medium a single wave corresponding to the reduction of the quinone to the hydroquinone by a two-electron and two-proton process (*Fig. 26*) is instead observed [69].

After the first oxidation, a couple of reversible redox peaks appeared in the cyclic voltammograms with mid point potential at -0.018 V vs SCE along with a second small irreversible oxidation peak at around +0.4 V vs SCE. Upon consecutive cycling, the redox peaks were increasing slightly after each cycle due to the formation of new quinone functionalities (*Fig. 27*). The redox current peaks showed a linear dependence with respect to the scan rate confirming the immobilization of PLQSH (*Fig. 28*).

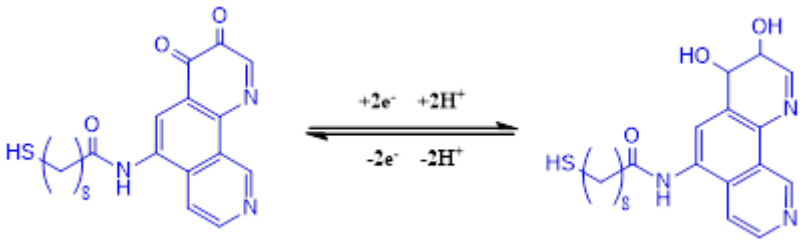

Fig. 26: redox equation of the electrosynthesized quinones for a 2 electron / 2 proton process.

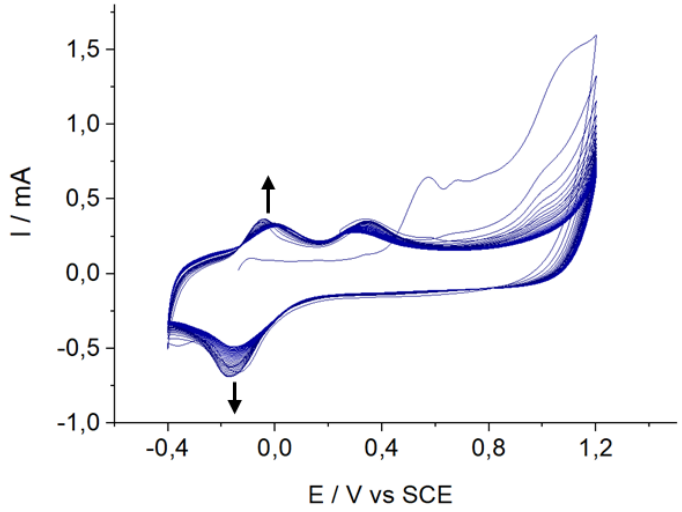

Fig. 27: electro-synthesis of the oxidized 8-mercapto-N-(1,10-phenanthrolin-5-yl) octanamide (PLQSH) in 0.1 M phosphate buffer pH 7 by 30 cycles. Scan rate: 100 mV s^{-1}.

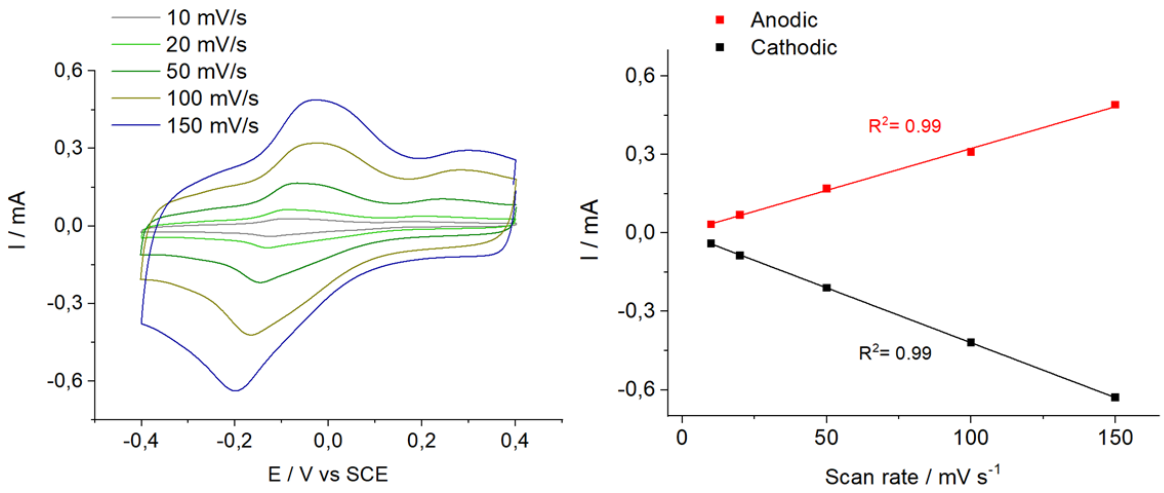

Fig. 28: CVs at variable scan rates of 8-mercapto-N-(1,10-phenanthrolin-5-yl) octanamide at a pyrene-functionalized electrode after UV irradiation followed by electro-oxidation at pH 7 and corresponding plot of anodic and cathodic peak currents versus scan rate.

Since protons take part in the electro-oxidation, the pH of the solution affects the extent of the process. Electrodes previously functionalized with the phenanthroline thiol derivative under UV and then electro-oxidized by 30 cycles in phosphate buffer at different pH (2, 7 and 12) are tested again in phosphate buffer pH 7 (*Fig. 29*).

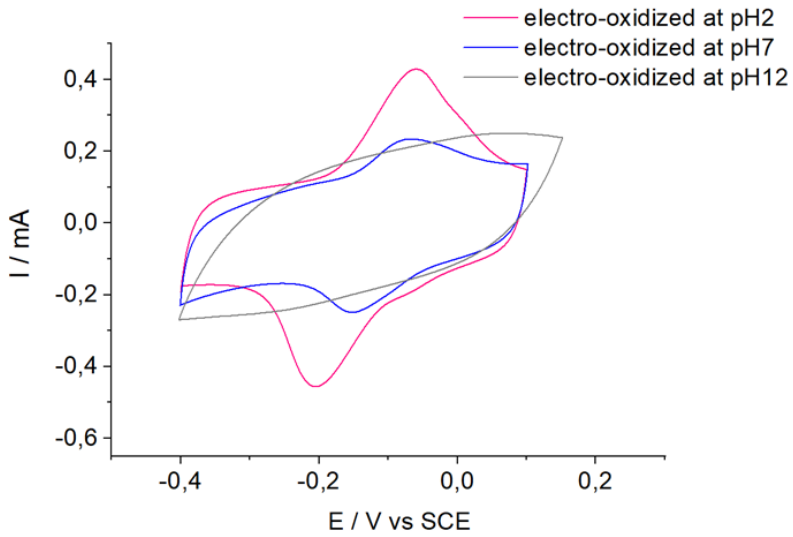

Fig. 29: cyclic voltammograms of electrodes functionalized with 8-mercapto-N-(1,10-phenanthrolin-5-yl) octanamide under UV and then oxidized at pH 2, pH 7 and pH 12 and finally cycled again in phosphate buffer at pH 7.

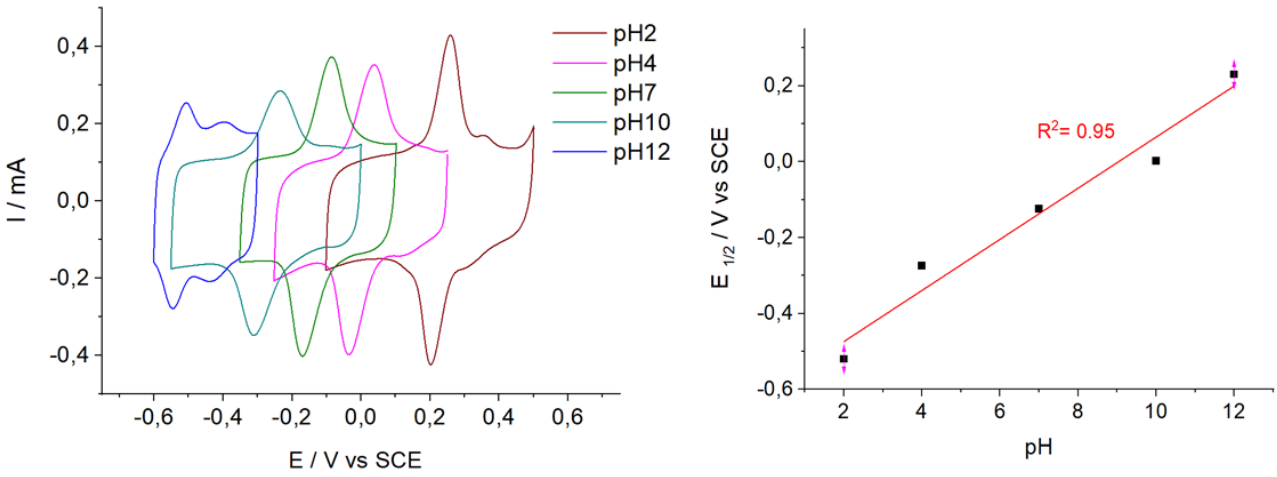

Fig. 30: cyclic voltammograms of one electrode functionalized with 8-mercapto-N-(1,10-phenanthrolin-5-yl) octanamide under UV and electro-oxidized in phosphate buffer at pH 2 then cycled again at different pH. Plot of the dependence of the mid point potential versus pH of the electrolytic buffer used. Scan rate: 100 mV s^{-1}.

An acidic pH led to a clearly higher electroactive area of the redox peaks relative to PLQSH while at ph 12 no redox peaks are observed at the end of the electro-synthesis process. Also, since the reversible electrochemical reaction of PLQSH involves two electrons and two protons, an increase of pH from pH 2 to 12 led to a negative shift of both oxidation and reduction peak potentials and an almost linear dependence of the formal potential of the compound with the pH value of the buffer could be found (*Fig. 30*).

To test the stability of the electrogenerated compound, the electrodes were then cycled multiple times between +0.4 V and -0.4 V vs SCE in fresh phosphate buffer and the redox peaks appeared very stable over the number of scan with no loss in current intiensietis after more than 30 cycles.

4. The phoinitiated thiol-yne reaction for enzyme electrocatalysis applications

The development of bioelectrodes based on the immobilization of redox mediators and enzymes on CNTs is of great interest for the development of enzymatic biofuel cells (EFCs), in particular those that that rely on glucose oxidation at the bioanode and oxygen reduction at the biocathode [71]. Much effort has been devoted to find novel strategies of immobilization of both enzyme and redox mediators to improve the EFCs performance and stability, enzyme loading and electron transfer between the biological component and the electrode [72]. The immobilization is important for the design of a miniaturazed and membraneless biofuel cell configuration without the necessity to separate the catalyst from the fuel [73]. Moreover, the immobilization of the redox mediators at the electrode surface via adsorption, π–π stacking interactions or covalent linkage is fundamental for promoting the mediated electron transfer (MET) bioelectrodes in which the redox mediators are essential to channel the electrons from the redox centers of the enzyme and the electrode [74]. Among the different immobilization strategies, a covalent and stable attachment of the mediator is preferred to reduce leaching from the electrode surface, thus avoiding toxicity issues for in vivo applications and extending the lifetime of the EFCs [75, 76].

4.1. Mediated catalytic oxidation of glucose by FAD-GDH with immobilized redox thiol derivatives

Fungus-derived FAD-GDH is a glucose-oxidizing enzyme with a tightly bound FAD as cofactor. FAD-GDH has emerged as a valuable alternative to GOx. GOx has been the most

widely used catalyst for the bioelectrocatalytic oxidation of glucose in glucose biosensors and biofuel cells due to its high thermal stability and glucose selectivity [77]. FAD-GDH is a more convenient choice for EFCs applications since differently from GOx, it catalyzes the oxidation of glucose to gluconolactone without delivering electrons to oxygen molecules. Thus, it can operate in the presence of O_2 and the power ouput is not affected by oxygen fluctuations [77]. Furthermore, the production of hydrogen peroxide, that has an inhibitory effect on the enzymatic activity of many enzymes and especially of the multicopper oxidase generally employed at the O_2-reducing biocathode, is avoided [74]. Moreover, FAD-GDH displays good turnover rates, stability and substrate specificity to glucose [78]. However, FAD-GDH requires a a redox partner or a redox mediator for the regeneration of the FAD cofactor since the enzyme-electrode distance necessary for the direct electron transfer is too large [70]. Thus, the immobilization of the redox mediators at the electrode surface is fundamental for the construction of a bioanode based on FAD-GDH (*Fig. 32*).

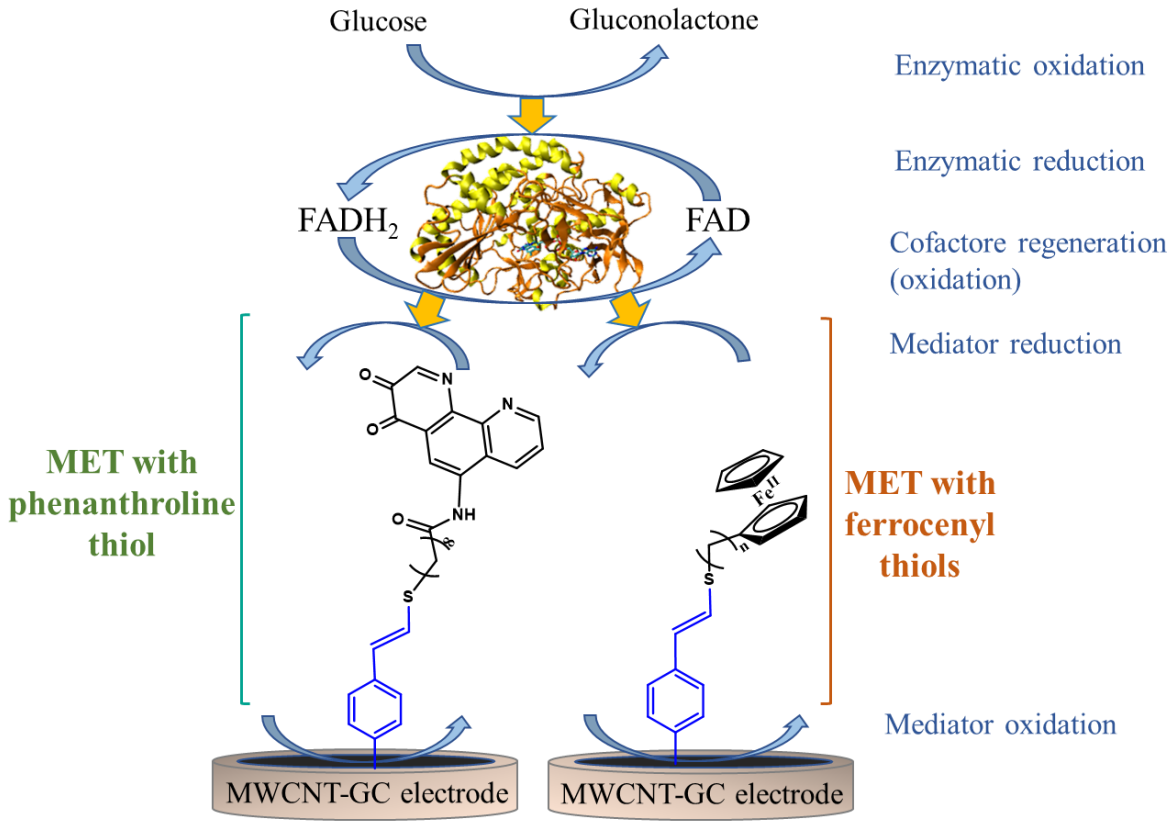

Fig. 32: scheme of the FAD-GDH mediated glucose oxidation with the thiol redox mediators immobilized onto MWCNT-GC electrodes. Glucose is oxidized by FAD-GDH while the FAD cofactor is reduced to $FADH_2$ followed by the $FADH_2$-mediated reduction of an artificial electron acceptor (mediator). The mediator is then re-oxidized at the electrode.

The most employed redox mediators have been metal complexes like osmium- and ruthenium- based complexes and quinone derivatives like 1,2 and 1,4 naphthoquinone, 1,10-phenanthroline-5,6-dione and 1,6 and 1,8 pyrenedione [71].

The catalytic performance of MWCNTs modified by ferrocene and phennthrolinequinone via thiolyne covalent coupling has been evaluated after their specific immobilization under UV irradiation or after their simple absorption in absence of any irradiation.

4.1.1 Electrocatalysis of FAD-GDH with immobilized ferrocenyl-thiol

The first use of ferrocene as redox mediator for the enzymatic determination of glucose dated back to 1984 [79]. Ferrocene and its derivatives have been already used with both glucose oxidase and glucose dehydrogenase [80]. In a relatively recent work, aminoferrocene was covalently grafted on the epoxy gropus of a porous carbon surface for the construction of a biofuel cell employing FAD-GDH [81].

Although both the functionalization with ethynylbenzene and ethynylpyrene were effective as substrates for the immobilization of the redox thiols under UV irradiation, the electrografting of 4-ethynylbenzene diazonium on nanotubes, that has high reproducibilty and gave a slighty higher surface coverage, was chosen for the further immobilization of the ferrocenyl thiols.

- **Effect of the irradiation on the electrocatalytic oxidation of glucose**

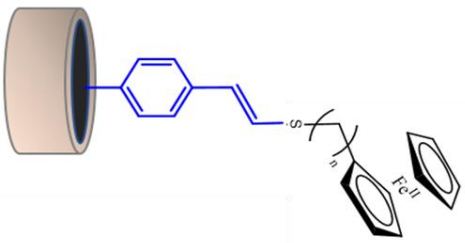

Ferrocenyl methanethiol was immobilized on ethynylbenzene-modified MWCNT-GC electrodes under UV light as already described. After a careful rinsing, 40 µL of a 5 mg mL^{-1} solution of FAD-GDH (1150 U mg^{-1} from Sekisui) solid in phosphate buffer pH 7 were deposited onto the surface of the electrodes that were then incubated for 3 hours at 4 °C. Enzyme catalysis was evaluated by cyclic voltammetry. A first cycle was carried out in a deareated buffer at pH 7 in absence of glucose and no catalysis is observed (*Fig. 33A*). In absence of FcSH, no catalytic current is observed upon addition of a saturating concentration of glucose (200 mM) proving the importance of the presence of a redox mediator. Instead, the

catalytic current in presence of FcSH that was immobilized under UV light is gretly enhanced compared to electrode in which FcSH was not subjected to UV treatment (*Fig. 33B,C*). The improved catalysis is a result of the covalent immobilization of FcSH at the electrode.

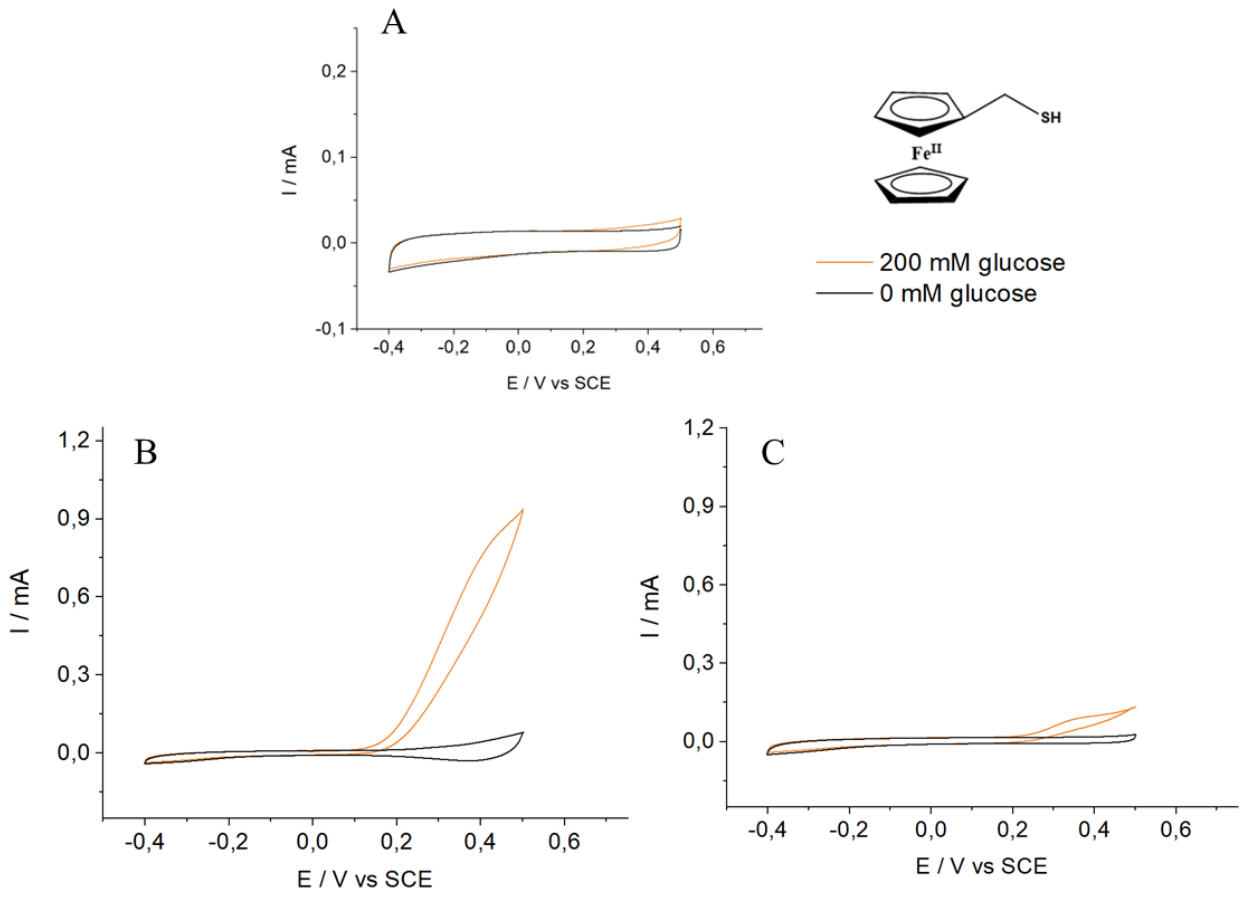

Fig. 33: cyclic voltammograms of MWCNT-GC electrodes functionalized by electrografting of 4-ethynylbenzene diazonium and then with 40 µL of FAD-GDH without any ferrocenyl methamethiol (A), or in presence of ferrocenylmethanethiol after its incubation for 50 min with (B) or without (C) UV irradiation prior to enzyme immobilization. Phosphate buffer 0.1 M pH 7. Ref: SCE. Scan rate: 20 mV s^{-1}.

Since a relationship between the amount of immobilized FcSH and the time of incubation was previously highlighted, the catalytic current by FAD-GDH was recorded on electrodes that were incubated with FcSH under UV light for different times: 10, 20 or 50 minutes. The results are resumed in *Fig. 34*, it is clear that a higher incubation time for FcSH produced the higher catalytic current, although the difference between 20 and 50 minutes is not very pronounced. An increase of the immobilized redox mediator above a certain surface coverage, does likely not affect further the catalysis because there is a limit on the number of redox mediators that can productively interact with the active center of FAD-GDH.

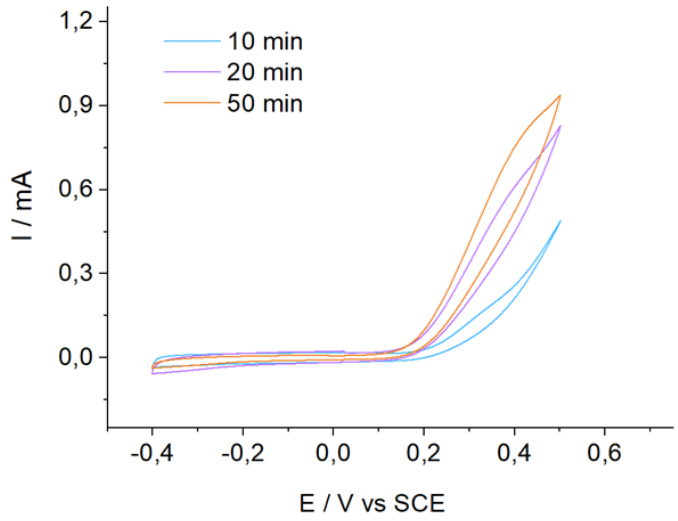

Fig. 34: CVs for the catalytic oxidation of glucose (200 mM) by FAD-GDH of electrodes containing FcSH that was upon different exposure times of UV irradiation. Phosphate buffer 0.1 M pH 7. Ref: SCE.

- **Effect of the chain length on the electrocatalytic oxidation of glucose**

Schuhmann et al. [82] showed that the length of the ferrocene derivatives can have has an impact on the catalysis of GOx. In that case, the ferrocenyl compounds were bounded to sugar residues of the enzyme, a longer spacer chain was able to favour the catalysis allowing ferrocene to penetrate sufficiently deeply through the outer shell of the protein and interact with the redox center, which is buried and electrically insulated by a thick glycoprotein shell. Thus, an increase in the electrocatalytic current with increase in chain length of ferrocene was observed by the authors. Since FAD-GDH has an overall structure similar to that of GOx, the electrocatalytic oxidation of glucose by FAD-GDH was thus also probed with other immobilized ferrocenyl derivatives, 6-FcSH and 11-FcSH, to evaluate the existance of a similar influence of the alkyl chain length on the catalysis.

Similarly to FcSH, when the ferrocenyl derivatives are immobilized via the photo-induced reaction, the oxidation current generated by the enzyme is much higher (*Fig. 35*). The catalytic behaviour of FAD-GDH and in particular the average value of the oxidation current estimated by multiple experiments (*Table 6,7*) and it is not significantly affected by the type of ferrocenyl derivative used, differently from what reported by the authors for GOx [82]. When CVs are runned in absence of glucose, the redox systems attributed to ferrocene are observed and the electroactive surface coverages can be calculated. Thus, the differences observed in

the electrocatalysis by FAD-GDH are associated to the amount of mediator immobilized on the electrode.

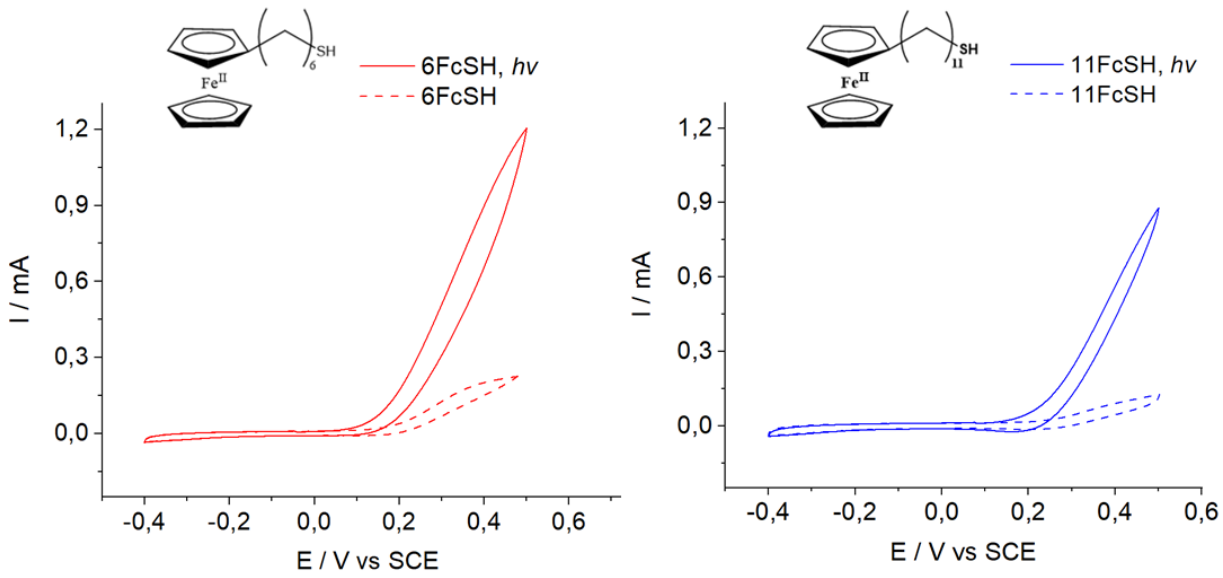

Fig. 35: cyclic voltammograms for the catalytic oxidation of glucose (200 mM) by FAD-GDH after immobilization of 6-ferrocenyl(hexanethiol) and 11-ferrocenyl(undecanethiol) onto ethynylbenzene-MWCNT-GC electrodes upon UV treatment (full lines) or without irradiation (dashed lines) recorded in 0.1 M phosphate buffer pH 7. All potentials are referrred vs SCE, scan rate 20 mV s^{-1}.

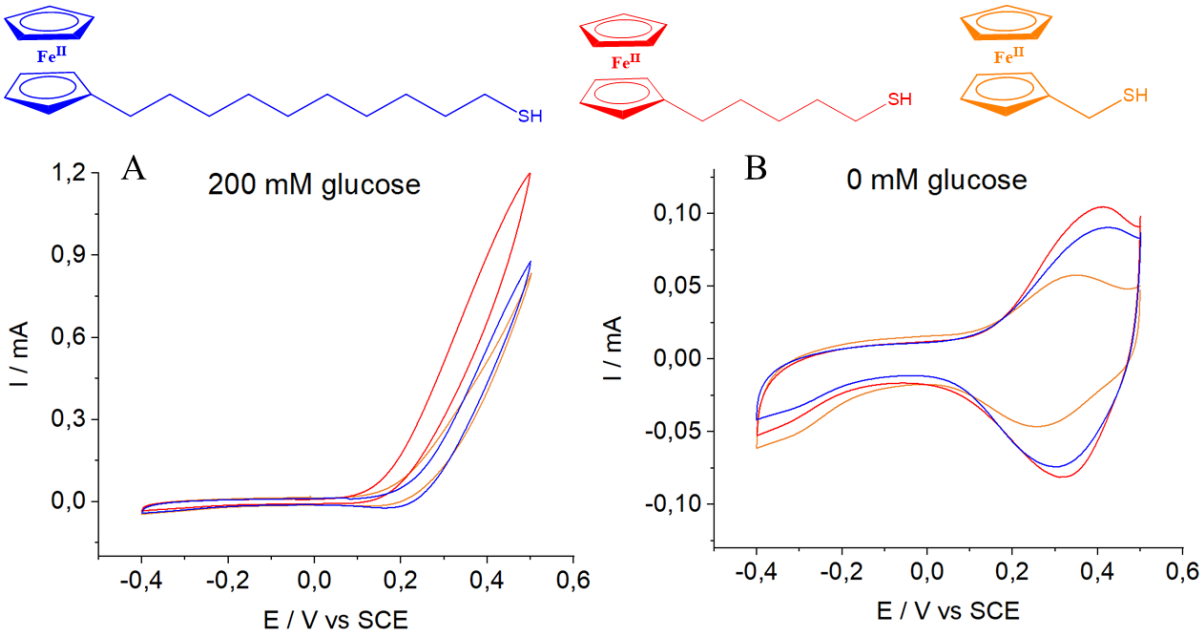

Fig. 36: comparison of the cyclic voltammograms of the catalysis by FAD-GDH in presence of three different ferrocenyl derivatives immobilized under UV irradiation with A) 200 mM glucose and B) in absence of glucose. CVs are recorded in 0.1 M phosphate buffer pH 7. All potentials vs SCE; scan rate 20 mV s^{-1}.

mediator	UV	Catalytic current at +0.4 V vs SCE, 200 mM glucose (mA)
FcSH	✓	0.61
6-FcSH	✓	0.91
11-FcSH	✓	0.67

Table 6

mediator	UV	Catalytic current at +0.4 V vs SCE, 200 mM glucose (mA)
FcSH	×	0.09
6-FcSH	×	0.20
11-FcSH	×	0.09

Table 7

4.1.2 Electrocatalysis of FAD-GDH with phenanthroline-thiol

Quinone derivatives have previously been reported to act as a mediator for NAD/NADP-and FAD-dependent enzymes [83]. In particular, a phenanthroline derivative, 1,10-phenanthroline-5,6-dione, has shown to be an effective redox mediator for FAD-GDH [84].

The effect of immobilization of the synthetized phenanthroline thiol compound on enzyme biocatalysis was investigated.

MWCNTs-GC electrodes was functionalized with 4-ethynylbenzene diazonium tetrafluoroborate by electrografting, then immersed in a 2 mM solution of PLSH in degassed chloroform under UV lamp at 200W for 50 minutes. CV was then performed scanning 30 times between -0.4 V to +1.2 V vs SCE in phosphate buffer at pH 7 or pH 2 to form the corresponding quinones functionalities that are essential for the electron exchange with the enzyme. 40 µL of a 5 mg mL^{-1} solution of FAD-GDH (1150 U mg^{-1}) solid were deposited onto the surface of the electrodes and stored for 3 hours at 4 °C.

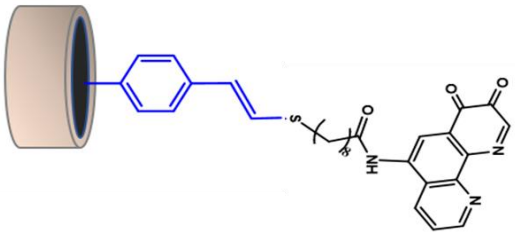

The catalytic activity of the phenanthroline mediating system of electrodes, subjected to UV irradiation and electro-oxidized at pH 7, was evaluated and compared.

Clearly, UV treatment, similarly to what observed for the ferrocenyl mediators, determined an higher amount of mediator immobilized at the electrode surface and thus an improved catalytic current for the oxidation of glucose.

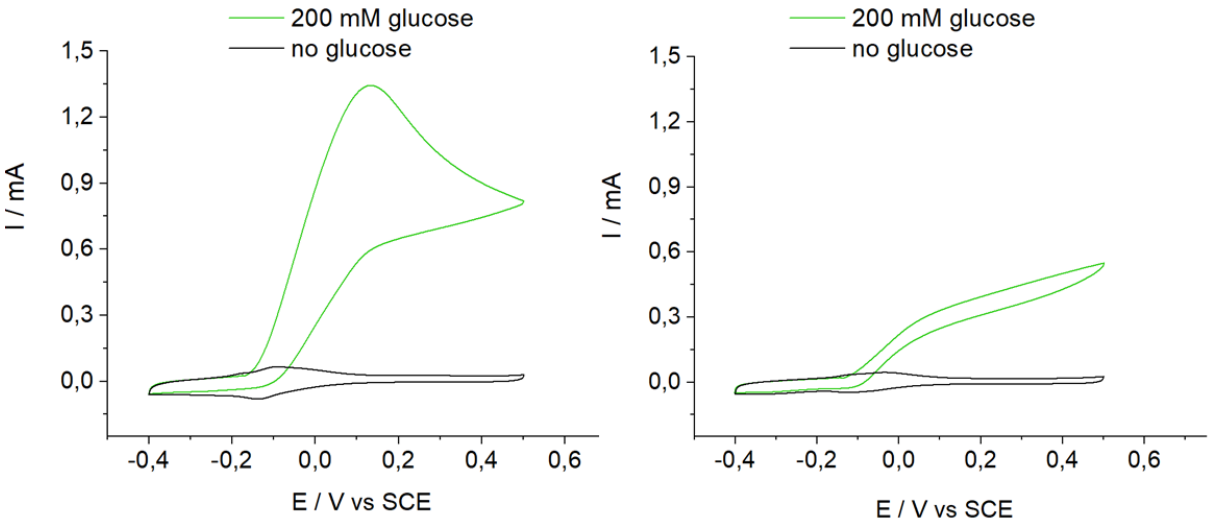

Fig. 37: cyclic voltammograms of MWCNT-GC electrodes functionalized by 4-ethynylbenzene diazonium and then with 8-mercapto-N-(1,10-phenanthrolin-5-yl) octanamide with (left) or without UV irradiation (right). Electro-oxidation of both electrodes was conducted at pH 7 prior enzyme incubation. Cyclic voltammograms are recorded in absence of glucose or in presence of 200 mM glucose. Scan rate: 20 mV s^{-1}.

This result is confirmed by an overlay of the cyclic voltammograms obtained in absence of glucose (*Fig. 38*). In absence of glucose the redox system typical of the phenanthroline compound with two main redox peaks with $E_{1/2}$ at -0.011 V vs SCE is visible. The area of the peaks is significantly bigger after irradiation, as expected.

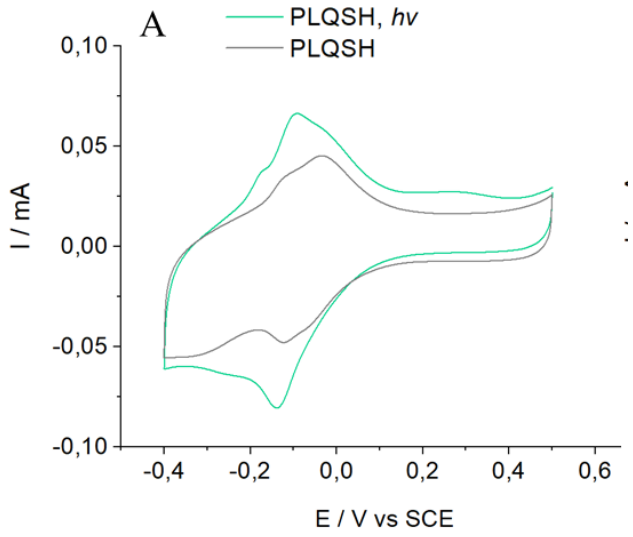

Fig. 38: cyclic voltammograms obtained in absence of glucose after immobilization of FAD-GDH at electrodes functionalized by 4-ethynylbenzene diazonium first and then with 8-mercapto-N-(1,10-phenanthrolin-5-yl) octanamide with or without UV irradiation. Prior to enzyme incubation, the electro-oxidation of the immobilized phenanthroline derivative was conducted A) at pH 7. Scan rate: 20 mV s^{-1}.

UV	pH during electro-synthesis	$E_{1/2}$ mediator (V) vs SCE	Γ_{max} mediator (0 mM glucose)	Catalytic current at +0.4 V vs SCE, 200 mM glucose (mA)
✓	7	-0.11	146 pmol cm^{-2}	0.90
×	7	-0.08	90 pmol cm^{-2}	0.50

Table 8

Ferrocene has a quite positive formal potential and since the one of FAD-GDH is comprised between -0.49 V and -0.277 V [58], a bigger difference between the mediator and enzyme potential exists, that leads to voltage losses. The formal potential of phenanthroline instead is more negative than ferrocene and closer to that of the FAD cofactor and thus is more favourable for biofuel cells applications. The determination of glucose is of great importance in biological and clinical fields. The use of phenanthroline as mediating system is better also for the construction of a glucose biosensor compared to ferrocene, because the oxidation of glucose at lower potential can avoid the concomitant oxidation of interfering species like uric acid, dopamine, ascorbic acid.

4.1.3 Glucose biosensing

An evaluation of the analytical performances of the phenanthrolinequinone mediator applied to a glucose biosensor was investigated by using electrodes modified by PLQSH immobilized under UV irradiation and electro-oxidized at pH 2. After incubation with FAD-GDH, chronoamperometric measurements at -0.2 V vs. SCE were carried out upon successive glucose injections until saturation (200 mM). In *Fig. 40A* is reported the typical current response on successive injections of glucose to the buffer solution. In order to determine the linear range of the biosensor, a calibration curve was built plotting the steady-state current versus glucose concentration (*Fig. 40B*).

The biosensor exhibited a rapid response to the addition of glucose. The current density increases with the addition of glucose until 100 mM, then it reaches the plateau. The response time, defined as the time when 95% of the steady-state current is reached, is about 6-7 s. The apparent Michaelis–Menten constant (K_M^{app}) was extimated by the analysis of the slope and the intercept of the plot of the reciprocals of the steady-state current versus glucose concentration and has a value of 23 mM. The biosensor response to glucose is linear in the range from 1 to 5 mM glucose. The sensitivity in the linear region is 0.125 mA M^{-1} cm^{-2}, which is is in good agreement with other amperometric glucose biosensors reported in the

literature based on FAD-GDH confined in a mixture of MWCNTs and polyoxometalates as redox mediators [85].

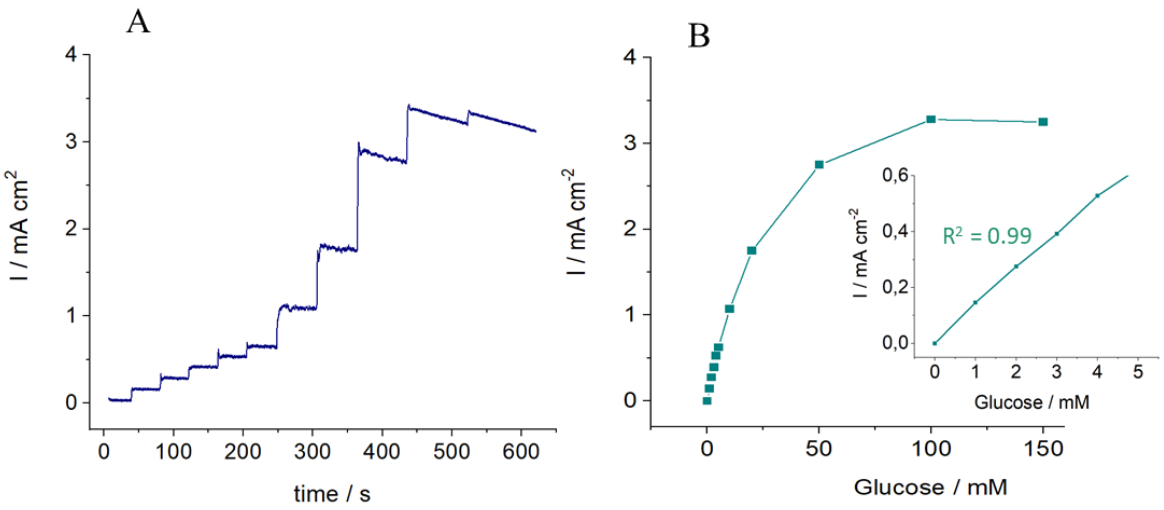

Fig.40: A) Current-time plot of a biosensor based on FAD-GDH with PLQSH immobilized on MWCNTs-GC electrodes under UV and electro-oxidized at pH 2 with applied potential of −0.2 V vs SCE. B) Plot of the steady-state current versus glucose concentration.

4.2 Applications of the photoinitiated thiol-yne chemistry to the grafting of alginates

An important aspect to consider in the construction of enzymatic biofuel cells with potential in vivo applications is their biocompatibility. Confining the biological catalyst and mediators as well as the nano-objects of the biofuel cell avoiding their dispersion in body tissues is essential to avoid inflammatory reactions and toxicity in vivo [86]. On of the route that can be followed for this purpose, is the use of biocompatible polymers such as collagen, chitosan and alginate, although their use reduce glucose diffusion and the power output [86].

Alginates are unbranched co-polymers, derived mainly from brown algae and bacteria, constituted by β-D-mannuronic (M blocks) and α-L-guluronic (G blocks) acid residues in varying proportions, order and molecular weight [87].

Alginate forms gels quite easily after the addition of divalent cations which act as ionic cross-linkers. In general, Ca^{2+} ions are the most frequently employed ion because of their low toxicity [87]. Cations cooperatively bind the carboxylic groups G blocks of adjacent alginate chains, creating ionic interchain bridges which cause gelling of aqueous alginate solutions (*Fig. 41*).

Because of their properties of biocompatibility, non-toxicity and biodegradability, alginates have been widely employed in various biomedical applications: as hydrophilic drug carriers and as matrix materials for tissue engineering [88]. The hydrogel that is formed upon addition of calcium to an alginate solution can be used to entrap the enzyme and redox mediators within a network that allows the diffusion of glucose while retaining all the organic components inside [89]. Although, a strong drawback is the poor mechanical stability of the hydrogel that limit the retention toward the biomolecules causing leaching over time [90].

Chemical or physical modifications of alginates, exploiting the hydroxyl and carboxyl groups of the backbone, is essential to improve their mechanical properties. Cross-linking strategies are often employed to strenghten the hydrogel network, although many of these strategies require the use of toxic and unfriendly catalysts that reduce the intrinsic biocompatibility of the polymer. Attempts to improve the stability of the alginates, as well as the conductivity, have been made also by incorporation of multi-walled carbon nanotubes prior to gelation as a reinforcing phase and as a mean to improve the conductivity of the system [90].

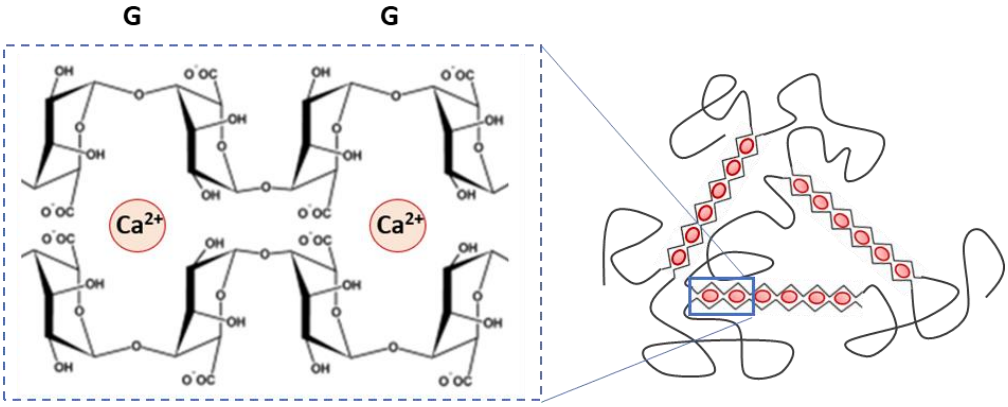

Fig. 41: structure of a gel of alginate upon addition of Ca^{2+} ions.

The covalent grafting of alginates to the surface of carbon nanotubes could be a strategy to improve the adhesive properties of the electrode and the biocompatibility of the microenvironment for enzyme immobilization. Studies with "click" hydrogels created by functionalization of alginate with pendant alkyne or azide groups have been already conducted [91]. The possibility to graft alginate via the photoinduced reaction was thus assessed using a functionalized alginate containing a poly(ethylene glycol) (PEG) linker terminating with a thiol group (Alg-PEG-SH). The structure of the functionalized alginate, obtained from École Polytechnique Fédérale of Lausanne, is reported in *Fig. 42*.

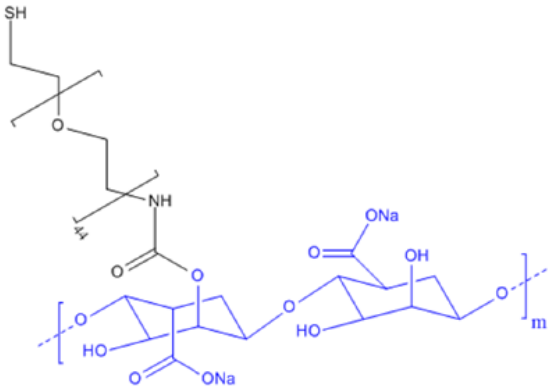

Fig.42: Alg-PEG-SH

An alginate-based film was created onto the surface of MWCNT-GC electrodes previously non-covalently functionalized with ethynylpyrene, by depositing a drop 15 µL of a mixture of alginate in water (2% w/v) and addition of a very small volume of DMPA (0.2 eq) in DMF onto the electrodes. The surface of the electrodes were irradiated by UV light for 30 minutes. Controls have been made in the same way but without irradiating the electrodes. After 30 minutes, all the electrodes were rinsed several times in water to remove adsorbed species. Then, a drop of $CaCl_2$ 0.1 M was then deposited on the electrode that were rinsed again in water after 5 minutes. A thin translucent gel was thus formed on the electrodes.

The mechanical stability of the resulting gel was tested by cycling the electrodes in a phosphate-free buffer, Tris HCl pH 7, containing 2 mM of 1,1-ferrocenedicarboxylic acid as a redox probe. $CaCl_2$ was also added to the electrolytic solution to reach a final concentration of 1 mM to prevent leakage of the calcium from the alginate network over time. The presence of the hydrogel coating onto the electrodes is demonstrated by the decrease of the reversible redox peaks of the ferrocene probe in the first cycle compared to the controls without any alginate. In case of an increased immobilization of alginates after irradiation and thus a final thicker gel, a bigger and more persistent decrease of the redox system of Fc could be expected compared to the control not irradiated. Altough, the anodic peak of Fc appeared more decreased for the electrode subjected to irradiation in the first cycle, no differences in the current intensities were found upon multiple cycling between the two electrodes. In both cases, the redox peaks of Fc were increasing over time as a result of the permeation of Fc through the polymer network or a partial dissolution of the gel in the electrolytic solution.

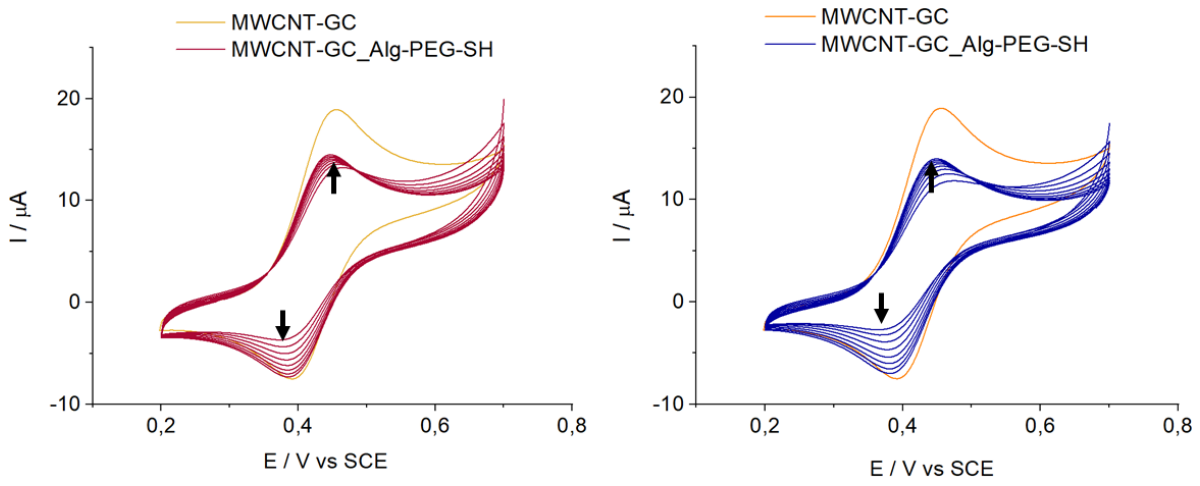

Fig. 43: cyclic voltammograms of 2 mM ferrocene dicarboxylic acid in 0.1 M Tris-HCl (pH 7) containing 1 mM $CaCl_2$. MWCNT-GC electrodes have been functionalized with ethynylpyrene and then with a gel of Alg-PEG-SH without UV (on the left) and after UV irradiation (on the right).

An improved stability for biocathodes based on direct electron transfer-type enzymes coated with biocompatible hydrogel has been reported [92, 93]. The activity over time of Bilirubin oxidase from *Myrothecium verrucaria* (BOx) (11.5 U mg^{-1} from Sigma Aldrich), after its immobilization on the MWCNTs in presence of the alginate gel, was explored. BOx is a multicopper enzyme often used for the bioelectrocatalytic reduction of oxygen at the cathode. It has two distinct redox centers, one is a trinuclear 2 and 3 type (T2/T3) center that reduces oxygen to water in a four electron process, and the other one is a mononuclear 1 type (T1) center that is involved in the oxidation of its natural substrate, which are mostly phenolic compounds [94]. It is a small protein capable of DET since the active center is close to the protein surface [94].

Differerent configurations of electrodes were prepared, the enzymatic activity of the electrode containing Alg-PEG-SH immobilized under irradiation was compared to that of controls made in absence of alginate and on pristine non-functionalized carbon nanotubes. In all the cases, after the immobilization of Alg-PEG-SH, a solution of the BOx enzyme (40 µL of 5 mg mL^{-1}) was drop-casted onto the surface of the electrodes that were kept for 2 hours at 4 °C. Before testing, a drop of $CaCl_2$ 0.1 M was deposited on the electrode to start the gelation process. After 5 minutes the electrodes were rinsed and tested for the catalytic activity of BOx in Tris HCl pH 7. The first CV was runned in buffer deareated with argon and no catalytic activity was observed as expected. The ability of the enzyme to reduce oxygen in water was verified after saturating the cell with oxygen and in presence of 10 mM of 2,2′-azino-bis(3-ethylbenzothiazoline-6-sulfonic acid (ABTS). Although, BOx is able of direct electron

transfer (DET), ABTS improves the catalysis especially in those situations where the DET is not optimal. In this case, it was used to circumvent eventual limitations in the electron exchange given by the presence of the gel. The electrodes were then stored in buffer at 4 °C and the electrocatalytic performance was evaluated again after 3 days in presence of oxygen and ABTS to check the residual activity (*Fig.45*). Overall, enzyme catalysis did not vary significantly after a period of 3 days between all the different configurations. The decrease in the catalytic current at 0 V vs SCE after 3 days was only slightly smaller (47%) after irradiation of Alg-PEG-SH on ethynylpyren-MWCNTs electrodes compared to the controls.

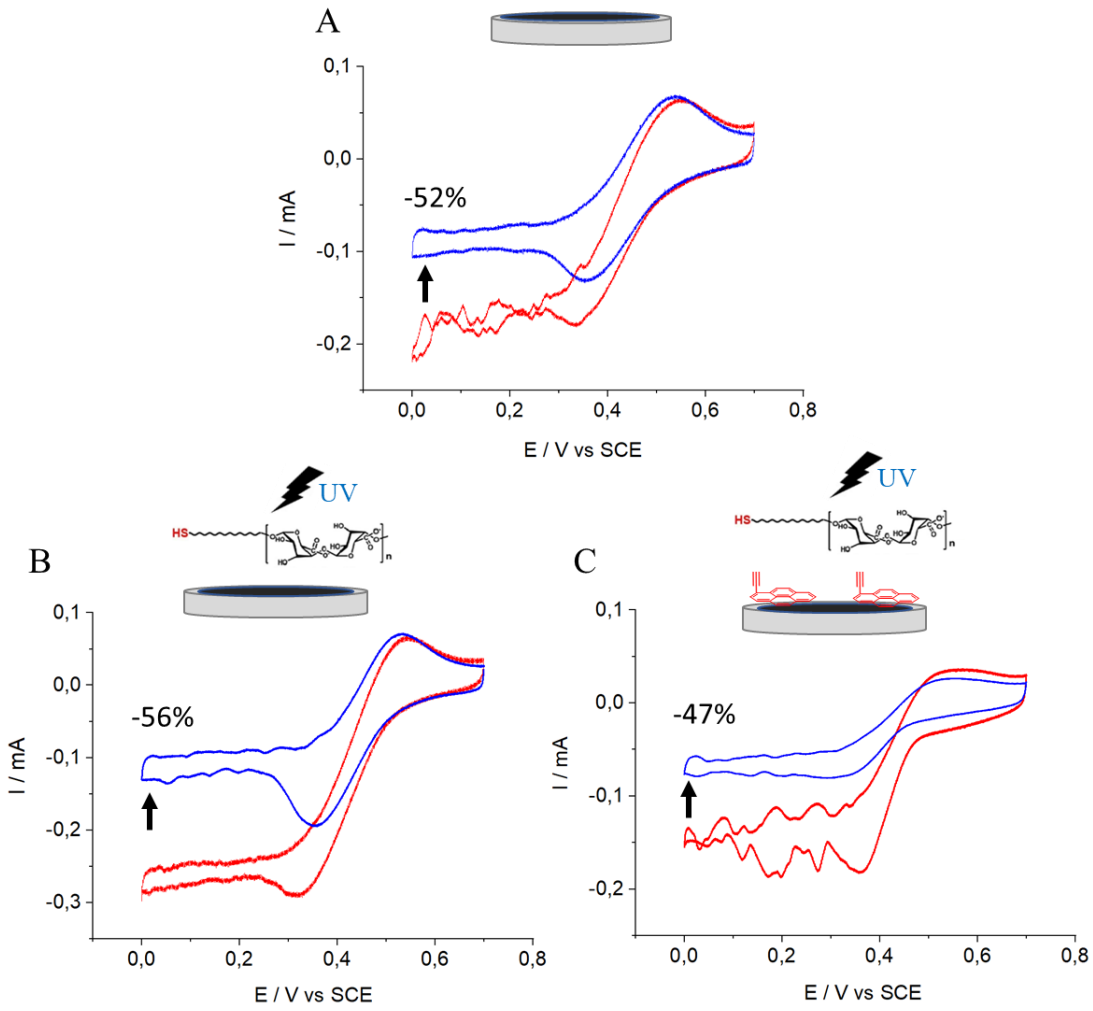

Fig. 45: cyclic voltammograms of the catalytic reduction of O_2 by BOx under saturating O_2 and 10 mM ABTS on A) pristine MWCNTs, B) Alg-PEG-SH on pristine MWCNTs after 30 minutes of UV irradiation and C) Alg-PEG-SH on ethynylpyrene-MWCNTs after 30 minutes of UV irradiation. The curves colored in blue are recorded after 3 days.

In conclusion, the comparative test of the permeation of Fc on Alg-PEG-SH functionalized electrodes and evaluation of BOx catalysis over time, did not evidence noteworthy and remarkable differences. Since the evaluation of the enzyme activity is only an indirect

measure of the immobilization of alginate, it is still uncertain if the observed poor outcome originates from a low efficiency of the photoinduced reaction when a bigger macomolecule, like alginate, is involved, or it is as a consequence of the poor stability of the gel itself even after successful covalent grafting of alginate. A possibility could be that the entrapment of the enzymes is also not very efficient as a result of the large pore size of the gel matrix. Thus, an additional crosslinking strategy would be necessary to reinforce the mechanical stability of the gel for future investigations, especially considering the necessity of retaining the entrapped molecules for a prolonged time for potential future applications in biosensors and EFCs.

5. Conclusions and future perspectives

A thiol-yne reaction has been investigated on MWCNT-based electrodes as a covalent coupling strategy. The photo-induced reaction, triggrered by UV light, has been proven to be effective for the immobilization of ferrocenyl thiol redox probed on two different types of alkyne-decorated MWCNTs, both of diazonium covalently and ethynylpyrene non-covalently modified MWCNTs. The electrochemical data were corroborated by XPS analysis. The immobilization of both ferrocene and phenanthroline quinone redox mediators onto the modified electrodes via this method, led to a considerable improvement in the mediated electrocatalysis by the immobilized FAD-GDH. In particular, the phenanthroline thiol, for its formal potential close to that of FAD-GDH, has good suitability for its use in biosensors and EFCs. The photo-induced thiol-yne reaction can be used as a coupling strategy, an eco-friendly and metal-catalyst free alternative to other click chemistry reactions, to increase the amount of redox mediators onto the electrode in order to prevent their desorption, leaching and favour the orientation and the electron transfer with the biocatalysts. The method is simple and it is easily controllable by light exposure both in a spatial and temporal way. Furthermore, this thiol-yne surface reaction can be further extended to other types of thiol or cysteine-modified molecules and biomolecules. Despite the fact that it is still unclear if this approach could be used to directly graft bigger macromolecules, such as polymers like alginates, this technique could be further extended to the grafting of redox molecules such as molecular catalysts or enzymes which could possess cysteine-tags. This type of technique could be highly efficient to control the efficiency and stabilization of the immobilized enzymes while also providing specific orientations at the surface of electrodes. Further investigations are thus still necessary to elucidate these perspectives.

Bibliography

(1) Kolb H. C., Finn M. G., Sharpless K., Angew B. «Click chemistry: diverse chemical function from a few good reactions». *Chemie International Edition*. (2001) 40, 2004-2021.

(2) Ruhemann S., Stapleton H. E. «CIX. Condensation of Phenols with Esters of the Acetylene Seyies. Part III. Synthesis of Benxoy-pyrone». *Journal of the Chemical Society*. (1990) 77, 1179-1185.

(3) Lowe A. B. «Thiol-Yne 'Click'/Coupling Chemistry and Recent Applications in Polymer and Materials Synthesis and Modification». *Polymer*. (2014) 55, 22, 5517–5549.

(4) Massi A., Nanni D. «Thiol–Yne Coupling: Revisiting Old Concepts as a Breakthrough for up-to-Date Applications». *Organic & Biomolecular Chemistry*. (2012) 10, 12, 3791–3807.

(5) Hu X., Tan H., Wang X., P. Chen. «Surface Functionalization of Hydrogel by Thiol-Yne Click Chemistry for Drug Delivery». *Colloids and Surfaces A: Physicochemical and Engineering Aspects.* (2016) 489, 297–304.

(6) Lo Conte M., Pacifico S., Chambery A., Marra A., Dondoni A. «Photoinduced Addition of Glycosyl Thiols to Alkynyl Peptides: Use of Free-Radical Thiol-Yne Coupling for Post-Translational Double-Glycosylation of Peptides». *The Journal of Organic Chemistry*. (2010) 75, 13, 4644–4647.

(7) Li Y., Pan M., Li Y., Huang Y., Qingxiang G. «Thiol –Yne Radical Reaction Mediated Site-Specific Protein Labeling via Genetic Incorporation of an Alkynyl- l -Lysine Analogue». *Organic & Biomolecular Chemistry*. (2013) 11, 16, 2624–29.

(8) Daglar O., Luleburgaz S., Baysak E., Gunay U. S., Hizal G., Tunca U., Durmaz H. «Nucleophilic Thiol-Yne Reaction in Macromolecular Engineering: From Synthesis to Applications». *European Polymer Journal*. (2020) 137, 109926.

(9) Bicheng Y., Mei J., Li J., Wang J., Wu H., Sun Z. J., Qin A., Tang B. Z. «Catalyst-Free Thiol–Yne Click Polymerization: A Powerful and Facile Tool for Preparation of Functional Poly(vinylene sulfide)s». *Macromolecules.* (2014) 47, 4, 1325–1333.

(10) Chen G., Amajjahe S., Stenzel M. H. «Synthesis of thiol-linked neoglycopolymers and thermo-responsive glycomicelles as potential drug carrier». *Chemical communications.* (2009) 10, 1198-1200.

(11) McKenas C. G., Fehr J. M., Donley C. L., Lockett M. R. «Thiol–Ene Modified Amorphous Carbon Substrates: Surface Patterning and Chemically Modified Electrode Preparation». *Langmuir.* (2016) 32, 41, 10529-10536.

(12) Connal L. A., Kinnane C. R., Zelikin A. N., Caruso F. «Stabilization and functionalization of polymer multilayers and capsules via thiol− ene click chemistry». *Chemistry of materials.* (2009) 21, 4, 576-578.

(13) van Berkel K. Y., Piekarski A. M., Kierstead P. H., Pressly E. D., Ray P. C., Hawker C. J. «A simple route to multimodal composite nanoparticles». *Macromolecules.* (2009) 42, 5, 1425-1427.

(14) van der Ende A., Croce T., Hamilton S., Sathiyakumar V., Harth E. «Tailored polyester nanoparticles: post-modification with dendritic transporter and targeting units via reductive amination and thiol-ene chemistry». *Soft Matter*. (2009) 5, 7, 1417-1425.

(15) McKenas C. G., Fehr J. M., Donley C. L., Lockett M. R. «Thiol–Ene Modified Amorphous Carbon Substrates: Surface Patterning and Chemically Modified Electrode Preparation». *Langmuir*. (2016) 32, 41, 10529-10536.

(16) Jonkheijm P., Weinrich D., Köhn M., Engelkamp H., Christianen P. C., Kuhlmann J., ... & Waldmann H. «Photochemical surface patterning by the thiol-ene reaction». *Angewandte Chemie.* (2008) 120, 23, 4493-4496.

(17) Holzinger M., Le Goff A., Cosnier S. «Carbon Nanotube/Enzyme Biofuel Cells». *Electrochimica Acta*. (2012) 82, 179–190.

(18) Lalaoui N., Rousselot-Pailley P., Robert V., Mekmouche Y., Villalonga R., Holzinger M., ... & Le Goff A. «Direct electron transfer between a site-specific pyrene-modified laccase and carbon nanotube/gold nanoparticle supramolecular assemblies for bioelectrocatalytic dioxygen reduction». *Acs Catalysis.* (2016) 6, 3, 1894-1900.

(19) Gentil S., Rousselot-Pailley P., Sancho F., Robert V., Mekmouche Y., Guallar V., ... & Le Goff A. «Efficiency of Site-Specific Clicked Laccase–Carbon Nanotubes Biocathodes towards O2 Reduction». *Chemistry–A European Journal*. (2020) 26, 21, 4798-4804.

(20) Gentil S., Pifferi C., Rousselot-Pailley P., Tron T., Renaudet O., Le Goff A. «Clicked bifunctional dendrimeric and cyclopeptidic addressable redox scaffolds for the functionalization of carbon nanotubes with redox molecules and enzymes». *Langmuir*. (2021) 37, 3, 1001-1011.

(21) Deng, L., Wang, L., Yu, H., Dong, X., Huo J. «Recent progress in synthesis of ferrocenyl dendrimers and their application in anion recognition». *Designed Monomers and Polymers.* (2007) 10, 2, 131– 143.

(22) Fabbrizzi L. «The Ferrocenium/Ferrocene Couple: A Versatile Redox Switch». *ChemTexts*. (2020) 6, 4, 22.

(23) Sun R., Wang L., Yu H., Abdin Z., Chen Y., Huang J., Tong R. «Molecular Recognition and Sensing Based on Ferrocene Derivatives and Ferrocene-Based Polymers». *Organometallics.* (2014) 33, 18, 4560–4573.

(24) Nguyen K. V., Holade Y., Minteer S. D. «DNA Redox Hydrogels: Improving Mediated Enzymatic Bioelectrocatalysis». *ACS Catalysis.* (2016) 6, 4, 2603–2607.

(25) Menanteau T., Levillain E., Breton T. «Electrografting via Diazonium Chemistry: From Multilayer to Monolayer Using Radical Scavenger». *Chemistry of Materials*. (2013) 15, 14, 2905–2909.

(26) Pinson J., Fetah P. «Attachment of Organic Layers to Conductive or Semiconductive Surfaces by Reduction of Diazonium Salts». *Chemical Society Reviews*. (2005) 34, 5, 429–439.

(27) Gooding J. J. «Advances in Interfacial Design for Electrochemical Biosensors and Sensors: Aryl Diazonium Salts for Modifying Carbon and Metal Electrodes». *Electroanalysis*. (2008) 20, 6, 573-582.

(28) Boukema K., Chehimi M. M., Pinson J., Blomfield C. «X-ray Photoelectron Spectroscopy Evidence for the Covalent Bond between an Iron Surface and Aryl Groups Attached by the Electrochemical Reduction of Diazonium Salts». *Langmuir*. (2003) 19,15, 6333–6335.

(29) Randriamahazaka H., Ghilane J. «Electrografting and Controlled Surface Functionalization of Carbon Based Surfaces for Electroanalysis». *Electroanalysis*. (2016) 28, 1, 13–26.

(30) Chehimi M. M. «Aryl Diazonium Salts: New Coupling Agents in Polymer and Surface Science». *John Wiley & Sons*. (2012)

(31) Mahouche-Chergui S., Gam-Derouich S. S., Mangeney C., Chehimi M. M. «Aryl Diazonium Salts: A New Class of Coupling Agents for Bonding Polymers, Biomacromolecules and Nanoparticles to Surfaces». *Chemical Society Reviews.* (2011) 40, 7, 4143–4166.

(32) Bahr J. L., Yang J., Kosynkin D. V., Bronikowski M. J., Smalley R. E., Tour J. M. «Functionalization of carbon nanotubes by electrochemical reduction of aryl diazonium salts: a bucky paper electrode». *J. Am. Chem. Soc.* (2001) 123, 27, 6536.

(33) Schmidt G., Gallon S., Esnouf S., Bourgoin J. P., Chenevier P. «Mechanism of the coupling of diazonium to single-walled carbon nanotubes and its consequences». *Chemistry–A European Journal.* (2009) 15, 9, 2101-2110.

(34) Le Goff A., Moggia F., Debou N., Jegou P., Artero V., Fontecave M., ... & Palacin S. «Facile and tunable functionalization of carbon nanotube electrodes with ferrocene by covalent coupling and π-stacking interactions and their relevance to glucose bio-sensing». *Journal of Electroanalytical Chemistry.* (2010) 641, 1-2, 57-63.

(35) Stolarczyk K., Łyp D., Żelechowska K., Biernat J. F., Rogalski J., Bilewicz R. «Arylated carbon nanotubes for biobatteries and biofuel cells». *Electrochimica Acta.* (2012) 79, 74-81.

(36) Lalaoui N., Le Goff A., Holzinger M., Mermoux M., Cosnier S. «Wiring Laccase on Covalently Modified Graphene: Carbon Nanotube Assemblies for the Direct Bio-electrocatalytic Reduction of Oxygen». *Chemistry–A European Journal.* (2015) 21, 8, 3198-3201.

(37) Gentil S., Carrière M., Cosnier S., Gounel S., Mano N., Le Goff A. «Direct Electrochemistry of Bilirubin Oxidase from Magnaporthe orizae on Covalently-Functionalized MWCNT for the Design of High-Performance Oxygen-Reducing Biocathodes». *Chemistry–A European Journal.* (2018) 24, 33, 8404-8408.

(38) Cao C., Zhang Y., Jiang C., Qi M., Liu G. «Advances on Aryldiazonium Salt Chemistry Based Interfacial Fabrication for Sensing Applications». *ACS Applied Materials & Interfaces*. (2017) 9,6, 5031-5049.

(39) Bousquet A., Ceccato M., Hinge M., Pedersen S. U., Daasbjerg K. «Redox Grafting of Diazotated Anthraquinone as a Means of Forming Thick Conducting Organic Films». *Langmuir*. (2012) 28, 2, 1267–1275.

(40) Evrard D., Lambert F., Policar C., Balland V., Limoges B. «Electrochemical Functionalization of Carbon Surfaces by Aromatic Azide or Alkyne Molecules: A Versatile Platform for Click Chemistry». *Chemistry – A European Journal*. (2008) 14, 3, 9286–9291.

(41) Bitter S., Schilling M., Brahm J. P., Polarz S., Winter R. F.. «Voltammetry as a Tool to Monitor the Aggregation Behavior of a Zwitterionic Ferrocene Surfactant». *Langmuir*. (2021) 37, 14, 4183–4191.

(42) Zhang L., Vilà N., Klein T., Kohring G., Mazurenko I., Walcarius A., Etienne M. «Immobilization of Cysteine-Tagged Proteins on Electrode Surfaces by Thiol–Ene Click Chemistry». *ACS Applied Materials & Interfaces*. (2016) 8, 27, 17591-17598.

(43) Dalal D. S., Patil D. R., Tayade Y. A. «β-Cyclodextrin: A Green and Efficient Supramolecular Catalyst for Organic Transformations». *The Chemical Record*. (2018) 18, 11, 1560–1582.

(44) Srilakshmi Krishnaveni N., Surendra K., Rama Rao K.. «Study of the Michael Addition of β-Cyclodextrin–Thiol Complexes to Conjugated Alkenes in Water». *Chemical Communications*. (2005) 5, 669–671.

(45) Arslan M., Gevrek T. N., Sanyal R., Sanyal A. «Fabrication of Poly(Ethylene Glycol)-Based Cyclodextrin Containing Hydrogels via Thiol-Ene Click Reaction». *European Polymer Journal*. (2015) 62, 426–434.

(46) Kostić S., Berg J. K. , Casdorff K., Merk V., Burgert I., Cabane E. «A Straightforward Thiol–Ene Click Reaction to Modify Lignocellulosic Scaffolds in Water». *Green Chemistry*. (2017) 19, 17, 4017–4022.

(47) Sridhar R., Surendra K., Srilakshmi Krishnaveni N., Srinivas B., Rama Rao K. «Stereoselective Synthesis of E-Vinyl Sulfides from Alkynes in Water under Neutral Conditions Using β-Cyclodextrin». *Synlett*. (2006) 20, 3495–3497.

(48) Bhadra S., Ranu B. C. «Water-promoted regioselective hydrothiolation of alkynes». *Canadian Journal of Chemistry*. (2009) 87, 11, 1605–1609.

(49) Fairbanks B. D., Sims E. A., Anseth K. S., Bowman C. N. «Reaction Rates and Mechanisms for Radical, Photoinitated Addition of Thiols to Alkynes, and Implications for Thiol−Yne Photopolymerizations and Click Reactions». *Macromolecules*. (2010) 43,9, 4113–4119.

(50) Hensarling R. M., Doughty V. A., Chan J. W., Patton D. L. «"Clicking" Polymer Brushes with Thiol-yne Chemistry: Indoors and Out». *Journal of the American Chemical Society*. (2009) 131, 41, 14673–14675.

(51) Elgrishi N., Rountree K. J., McCarthy B. D., Rountree E. S., Eisenhart T. T., Dempsey J. L. «A Practical Beginner's Guide to Cyclic Voltammetry». *Journal of Chemical Education*. (2018) 95, 2, 197–206.

(52) Bard, A. J., Faulkner L. R. «Electrochemical Methods: Fundamentals and Applications». *John Wiley & Sons*. (2001)

(53) Duan Q., Wang Y., Chen S., Miao M., Chen S., Zhang D. «Functionalized carbon nanotube films by thiol-ene click reaction». *Applied Surface Science.* (2019) 486, 144-152.

(54) Hetemi D., Noël V., Pinson J. «Grafting of Diazonium Salts on Surfaces: Application to Biosensors». *Biosensors.* (2020) 10, 1, 4.

(55) Carvahlo Padilha J., Noël J. M., Bergamini J. F., Rault-Berthelot J., Lagrost C. «Functionalization of Carbon Materials by Reduction of Diazonium Cations Produced in Situ in a Brønstedt Acidic Ionic Liquid». *ChemElectroChem*. (2015) 3, 4, 572–580.

(56) Lalaoui N., de Poulpiquet A., Haddad R., Le Goff A., Holzinger M., Gounel S., Mermoux M. « A Membraneless Air-Breathing Hydrogen Biofuel Cell Based on Direct Wiring of Thermostable Enzymes on Carbon Nanotube Electrodes ». *Chemical Communications.* (2015) 51, 35, 7447-7450.

(57) Mulvaney S. P., Keating C. D. «Raman Spectroscopy». *Analytical Chemistry*. (2000) 72, 12, 145–158.

(58) Bokobza L., Zhang J. «Raman spectroscopic characterization of multiwall carbon nanotubes and of composites». *Express Polymer Letters*. (2012) 6, 7, 601‑608.

(59) Blanchard P. Y., Buzzetti P. H. M., Davies B., Nedellec Y., Girotto E. M., Gross A., Le Goff A., Nishina Y., Cosnier S., Holzinger M. «Electrosynthesis of pyrenediones on carbon nanotube electrodes for efficient electron transfer with FAD-dependent glucose dehydrogenase in biofuel cell anodes». *ChemElectroChem.* (2019) 6, 20, 5242–5247.

(60) Thakuria R., Nath N. K., Saha B. K. «The nature and applications of π–π interactions: a perspective».*Crystal Growth & Design.* (2019) 19, 2, 523-528.

(61) Cramer N. B., Scott J. P., Bowman C. N. «Photopolymerizations of Thiol−Ene Polymers without Photoinitiators». *Macromolecules.* (2002) 35, 14, 5361–5365.

(62) Peng Z., Qu X., Dong S. «Co-Assembly of Ferrocene-Terminated and Alkylthiophene Thiols on Gold and Its Redox Chemistry Modulated by Surfactant Adsorption». *Journal of Electroanalytical Chemistry*. (2004) 563, 2, 291–298.

(63) Andrade J. D. «X-Ray Photoelectron Spectroscopy (XPS)». *Surface and Interfacial Aspects of Biomedical Polymers.* (1985) 1, 105–195.

(64) Felten A., Bittencourt C., Pireaux J. J. «Gold clusters on oxygen plasma functionalized carbon nanotubes: XPS and TEM studies». *Nanotechnology.* (2006) 17, 1954.

(65) Barber M., Connor J. A., Derrick L. M. R., Hall M. B., Hillier I. H. J. «High energy photoelectron spectroscopy of transition metal complexes». *Chem. Soc.* (1973) 69, 559, 21973.

(66) Ciampi S., Le Saux G., Harper J. B., Gooding J. J. «Optimization of Click Chemistry of Ferrocene Derivatives on Acetylene-Functionalized Silicon (100) Surfaces». *Electroanalysis.* (2008) 20, 14, 1513–1519.

(67) Angelova P., Solel E., Parvari G., Turchanin A., Botoshansky M., Gölzhäuser A., Keinan E. «Chemisorbed monolayers of corannulene penta-thioethers on gold». *Langmuir.* (2013) 29, 7, 2217-2223.

(68) Elmes R. B. P., Orange K. N., Cloonan S. M., Williams D. C., Gunnlaugsson T. «Luminescent ruthenium (II) polypyridyl functionalized gold nanoparticles; their DNA binding abilities and application as cellular imaging agents». *Journal of the American Chemical Society.* (2011) 133, 40, 15862–15865.

(69) Goss C. A., Abruna H. D. «Spectral, Electrochemical and Electrocatalytic Properties of 1,10-Phenanthroline-5,6-Dione Complexes of Transition Metals». *Inorganic Chemistry*. (1985) 24, 25, 4263–4267.

(70) Buzzetti P. H. M., Blanchard P. Y., Girotto E. M., Nishina Y., Cosnier S., Le Goff A., Holzinger M. «Insights into Carbon Nanotube-Assisted Electro-Oxidation of Polycyclic Aromatic Hydrocarbons for Mediated Bioelectrocatalysis». *Chemical Communications.* (2021) 57, 71, 8957–8960.

(71) Gross A. J., Tanaka S., Colomies C., Giroud F., Nishina Y., Cosnier S., Tsujimura S., Holzinger M. «Diazonium Electrografting vs. Physical Adsorption of Azure A at Carbon Nanotubes for Mediated Glucose Oxidation with FAD-GDH». *ChemElectroChem*. (2020) 7, 22, 4543-4549.

(72) Kim J., Jia H., Wang P. «Challenges in biocatalysis for enzyme-based biofuel cells». *Biotechnology Advances.* (2006) 24, 3, 296-308,

(73) Yang X.Y., Tian G., Jiang N., Su B. L. «Immobilization technology: a sustainable solution for biofuel cell design». *Energy & Environmental Science.* (2012) 5, 5540-5563.

(74) Milton R. D., Giroud F., Thumser A. E., Minteer S. D., Slade R. C. T. «Hydrogen Peroxide Produced by Glucose Oxidase Affects the Performance of Laccase Cathodes in Glucose/Oxygen Fuel Cells: FAD-Dependent Glucose Dehydrogenase as a Replacement». *Physical Chemistry Chemical Physics*. (2013) 15, 44, 19371–19379.

(75) Kim J., Jia H., Wang P. «Challenges in biocatalysis for enzyme-based biofuel cells». *Biotechnology Advances.* (2006) 24, 3, 296-308.

(76) Hou C., Lang Q., Liu A. «Tailoring 1,4-Naphthoquinone with Electron-Withdrawing Group: Toward Developing Redox Polymer and FAD-GDH Based Hydrogel Bioanode for Efficient Electrocatalytic Glucose Oxidation». *Electrochimica Acta*. (2016) 211, 663–670.

(77) Ferri S., Kojima K., Sode K. «Review of Glucose Oxidases and Glucose Dehydrogenases: A Bird's Eye View of Glucose Sensing Enzymes». *Journal of Diabetes Science and Technology*. (2011) 5, 5, 1068–1076.

(78) Filipiak M. S., Vetter D., Thodkar K., Gutiérrez-Sanz O., Jönsson-Niedziółka M., Tarasov A. «Electron Transfer from FAD-Dependent Glucose Dehydrogenase to Single-Sheet Graphene Electrodes». *Electrochimica Acta.* (2020) 330, 134998.

(79) Cass A. E., Davis G., Francis G. D., Allen H., Hill O., Aston W. J., Higgins I. J., Plotkin E. V., Scott L. D., Turner A. P. « Ferrocene-mediated enzyme electrode for amperometric determination of glucose». *Anal. Chem.* (1984) 56, 4, 667-671.

(80) Chen C., Xie Q., Yang D., Xiao H., Fu Y., Tan Y., Yao S. «Recent Advances in Electrochemical Glucose Biosensors: A Review». *RSC Advances.* (2013) 3, 14, 4473–4791.

(81) Suzuki R., Shitanda I., Aikawa T., Tojo T., Kondo T., Tsujimura S., Itagaki M., Yuasa M. «Wearable Glucose/Oxygen Biofuel Cell Fabricated Using Modified Aminoferrocene and Flavin Adenine Dinucleotide-Dependent Glucose Dehydrogenase on Poly(Glycidyl Methacrylate)-Grafted MgO-Templated Carbon». *Journal of Power Sources*. (2020) 479, 228807.

(82) Schuhmann W., Ohara T. J., Schmidt H. L., Heller A. «Electron Transfer between Glucose Oxidase and Electrodes via Redox Mediators Bound with Flexible Chains to the Enzyme Surface». *J. Am. Chem. Soc.* (1991) 113, 1394-1397.

(83) Junior D. F., Haddad R., Giroud F., Holzinger M., Maduro de Campos C. E. M., Acuña J. J. S., Domingos J. B., Cosnier S. «Cubic PdNP-based air-breathing cathodes integrated in glucose hybrid biofuel cells». *Nanoscale*. (2016) 8, 10433– 10440.

(84) Gross A. J., Chen X., Giroud F., Abreu C., Le Goff A., Holzinger M., Cosnier S. «A high power buckypaper biofuel cell: exploiting 1, 10-phenanthroline-5, 6-dione with FAD-dependent dehydrogenase for catalytically-powerful glucose oxidation». *ACS Catalysis.* (2017) 7, 7, 4408-4416.

(85) Boussema F., Gross A. J., Hmida F., Ayed B., Majdoub H., Cosnier S., Maaref A., Holzinger M. «Dawson-Type Polyoxometalate Nanoclusters Confined in a Carbon Nanotube Matrix as Efficient Redox Mediators for Enzymatic Glucose Biofuel Cell Anodes and Glucose Biosensors». *Biosensors and Bioelectronics*. (2018) 109, 20–26.

(86) Cosnier S., Gross A. J., Le Goff A., Holzinger M. «Recent Advances on Enzymatic Glucose/Oxygen and Hydrogen/Oxygen Biofuel Cells: Achievements and Limitations». *Journal of Power Sources.* (2016) 325, 252–263.

(87) García-Astrain C., Avérous L. «Synthesis and evaluation of functional alginate hydrogels based on click chemistry for drug delivery applications». *Carbohydrate polymers.* (2018) 190, 271-280.

(88) Raus R. A., Nawawi W. M. F. W., Nasaruddin R. R. «Alginate and Alginate Composites for Biomedical Applications». *Asian Journal of Pharmaceutical Sciences.* (2021) 16, 3, 280–306.

(89) Han E., Li X., Cai J. R., Cui H. Y., Zhang X. A. «Development of Highly Sensitive Amperometric Biosensor for Glucose Using Carbon Nanosphere/Sodium Alginate Composite Matrix for Enzyme Immobilization». *Analytical Sciences.* (2014) 30, 9, 897–902.

(90) Joddar B., Garcia E., Casas A., Stewart C. M. «Development of functionalized multi-walled carbon-nanotube-based alginate hydrogels for enabling biomimetic technologies». *Scientific reports.* (2016) 6, 32456.

(91) Breger J. C., Fisher B., Samy R., Pollak S., Wang N. S., Isayeva I. «Synthesis of "click" alginate hydrogel capsules and comparison of their stability, water swelling, and diffusion properties with that of Ca+2 crosslinked alginate capsules». *Journal of Biomedical Materials Research Part B: Applied Biomaterials*. (2014) 103, 5, 1120-1132.

(92) Jain D., Karajic A., Murawska M., Goudeau B., Bichon S., Gounel S., ... & Barthélémy P. «Low-molecular-weight hydrogels as new supramolecular materials for bioelectrochemical interfaces». *ACS Applied Materials & Interfaces.* (2017) 9, 1, 1093-1098.

(93) El Ichi-Ribault S., Zebda A., Laaroussi A., Reverdy-Bruas N., Chaussy D., Belgacem M. N., ... & Martin D. K. «Laccase-based biocathodes: Comparison of chitosan and Nafion». *Analytica chimica acta.* (2016) 937, 43-52.

(94) Solène G., Carrière M., Cosnier S., Gounel S., Mano N., Le Goff A. «Direct Electrochemistry of Bilirubin Oxidase from Magnaporthe orizae on Covalently-Functionalized MWCNT for the Design of High-Performance Oxygen-Reducing Biocathodes». *Chemistry – A European Journal.* (2018) 24, 33, 8404–8408.

Chapter III

Functionalization and characterization of Trialkoxyheptazine-glyconanoparticles derived from polystyrene-*block*-β-cyclodextrin copolymer

Summary

1. Glyconanoparticles (GNPs) derived from β-cyclodextrin-based amphiphilic block copolymer (PS-b-βCD)

1.1. Biotechnological applications of cyclodextrins

Cyclodextrins (CDs) are a family of cyclic oligosaccharides composed by glucopyranose units connected at 1 and 4 carbon atoms that form torus-like macro-rings (truncated cones) [1]. They were discovered for the first time by Villiers in 1881 from the degradation of starch by a transglycosylation reaction by cyclodextrin glucanotransferase (CGTase) enzyme of *Bacillus amylobacter* and their structure was demonstrated later in 1903 by Schardinger [2]. Three main classes of cyclodextrins exist: α-CDs composed of six glucopyranose units, β-CDs composed of seven such units, and γ-CDs which possess eight units. Apart from those, other larger CDs (δ, ε, etc.) with up to twelve glucose units, have been isolated and studied [1]. Among the CDs, β- CDs is the most accessible and the lowest-priced [3]. The interior of the cavity is essentially hydrophobic due to the presence of the CH_2 groups and ether-like oxygens of the skeleton of the CD, while the cavity entrances and the outside are hydrophilic due to the presence of hydroxylic groups, allowing the dissolution of the CDs in water [4]. In particular, secondary hydroxyl groups are situated on the edge of the larger cavity whereas the primary ones are placed on the narrow edge. The sizes and dimensions of CDs are shown in *Fig. 1*.

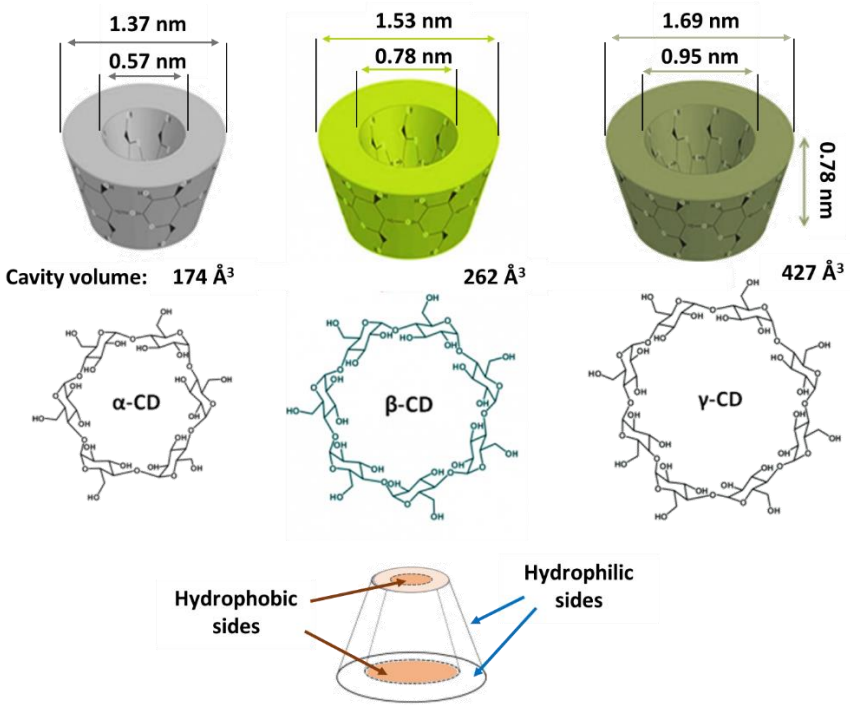

Fig. 1: structure and geometric dimensions of CDs. Representation of hydrophilic and hydrophobic regions of a CD.

As a consequence of their particular morphology, the CDs have the ability to form inclusion complexes with various solid, liquids and gaseous compounds by a phenomenon of molecular complexation [2]. A 'guest' molecule with appropriate size is held fully or partially within the cavity of the CDs. The formation of different inclusion complexes (host–guest complexes) with several compounds was demonstrated by the study of X-ray structures and by analysis of NMR or FTIR spectra [3,5]. Complexation can occur either in solution or in the crystalline state, typically in water, but it can be also accomplished in mixtures of solvents containing one non-polar solvent [2]. In aqueous solution the non-polar cavity of the CDs is in fact occupied by water molecules. A guest molecule less polar than water, causes the displacement of the water molecules inside the cavity and a decrease of the CD ring strain resulting in a more energetically favourable state [1]. The release of water molecules located inside the cavity is the principal driving force for the formation of the inclusion complexes in aqueous solution [3]. The most frequent ratio between the host and the guest is 1:1 but in some cases, two or even three CDs can form complexes with one or two guest molecules [1]. The fit of a guest molecule into the CD cavity depends thus on its relative size compared to that of the CD and on the presence of some key functional groups within the guest. Straight or branched chain aliphatics, aromatics, aldehydes, ketones, alcohols, organic acids, fatty acids, and polar compounds such as halogens and amines can be hosted in CDs [3]. Taking into account the CDs size, α-CD can typically host compounds with low molecular weight molecules, including azobenzene and its derivatives, β-CD are more likely to host aromatics and heterocycles, like anthraquinone, pyrene, ferrocene and adamantane, while γ-CD larger molecules such as steroids and macrocycles [3]. The molecular complexation does not involve the formation of covalent bonds, but intermolecular interactions instead: van der Waals forces and hydrogen bondings, hydrophobic interactions and electrostatic interactions. The binding of the guest molecules is regulated by a dynamic equilibrium which is dependent upon the strenght of the interactions between the guest and the CDs. For a single guest molecule (D) that forms a complex with a CD, the equilibrium is expressed by the association constant or K_a by *Equation 1.* [3].

$$C + D \rightleftharpoons CD \qquad K_a = \frac{[CD*D]}{[C][D]} \qquad \textit{Equation 1.}$$

As a result of the molecular complexation, some of the chemical and physical properties of the guest molecules can be changed. The solubility in aqueous solvent can be improved, as

well as the stabilization from oxidants, UV light or heat and the protection from micro-organisms. Other modifications include the reduction of the volatility and sublimation of the guest and variation of its chromatographic mobility, a shifts in UV/vis absorbance and fluorescence spectroscopic characteristics and changes in the chemical reactivity [3]. Thus, the range of applications of CDs derivatives is vast: food [6], packing and textiles [7], cosmetics [8], pharmaceuticals [9], analytical chemistry, environment protection and bioconversion [10,11]. Since CDs have low toxicity, immunogenicity and good biocompatibility, their applications in biomedicine and in the pharmaceutical field are very attractive, since they can enhance the solubility and stability of drugs, improve their permeability across biological membranes, protect them from degradation and reduce their toxicity, they can mask odors and tastes [12]. Furthermore, liquid pharmaceuticals can be transformed in powders after complexation [13]. Currently, over 30 commercial pharmaceutical products are based on inclusion complexes of drugs with CDs [12]. Moreover, CDs are often used in separation science immobilized in chromatographic columns, and since the CD ring has chirality, they can be used for the separation of enantiomers from a racemic mixture [13]. One issue encountered in bioconversion and fermentation applications is the different solvent preference of the biocatalysts compared to the substrate (generally while an aqueous medium is more suitable for the biocatalysts, the organic substrates can be lipophilic) which limit the substrate accessibility [2]. CDs can be very useful indeed on this matter. For instance, the bioconversion rate of the microbial transformation of cholesterol to androst-4-ene-3,17-dione can be increased from 40% to up 90% in presence of β-CDs [14]. Also in some cases, β-CDs can be employed as chelating agents for the in situ detoxification of the fermentation medium from the products formed during bioconversion that have an inhibitory effect to the micro-organism used as catalyst [14]. In environmental science and bioremediation, CDs can be used to favour the solubilization and removal of organic pollutants like phenol, p-chlorophenol and benzene from industrial effluent, or to increase the water solubility of fungicides making them more available to soil and thus more effective [14]. CDs can act as catalyst in chemical reactions and even as enzyme mimics, the production of a chymotrypsin mimic [15] and a transamine mimic [16] are two examples. The catalytic reaction can be promoted by specific functional groups of the CD cavity after the molecular complexation or favoured by their enantiomeric specificity that promote the reagent attack only on one side [14]. Additionally, CDs are used to increase dye uptake by the fabric tissues, for instance a tosyl β-CD derivative is able to hugely increase the uptake of a fluorescent dye of a polyester fiber [17].

In electrochemistry, the use of CDs dissolved in the electrolytic solutions or attached to the electrode surface can be beneficial for organic electrosynthesis and electrocatalytic reactions via formation of inclusion complexes. Thus, the immobilization of catalysts or redox mediators or even the preconcentration of trace analytes by accumulation on the surface of the electrode can be used for the development of sensors.[18]. For instance, a glassy carbon electrode has been modified with carboxylic acid functionalized SWCNTs and amino functionalized β-CDs for an electrochemical sensor for dopamine detection in the presence of ascorbic acid exploiting the formation of supramolecular inclusion complexes between dopamine and the β-CDs [19]. The electrochemical chiral recognition of triptophan enantiomers at a glassy carbon electrode modified with β-CDs was applied for the determination of the ratio of triptophan enantiomers in samples [20]. Various non-electrochemical sensors have been created as well, for instance fluorescent chemical sensors, in which the complexation of guest molecules with chromophore modified CDs was able to switch on and off the fluorescence intensity [21].

1.2. Amphiphilic block copolymers in nanotechnology

Block glycopolymers (BCPs) are by definition molecules composed by two or more blocks with different physical and chemical properties which are covalently linked [22]. They are a class of materials which are very interesting for their intrinsic ability to form supramolecular structures in water with various sizes and morphologies by self-direct assembly: spherical and worm-like micelles, lamellar structures, hexagonally packed cylinders, core-shell nanoparticles, vesicles [22]. Thus, diverse and modular structures can be formed from the choice of the starting building block constituents. The properties of the components are merged in a single macromolecule and in some cases, the assemblies acquire novel and unique properties from the synergistic combination of the different blocks that could not be obtained simply by mixing the individual constituents [23]. The advances made in recent years in polymer chemistry and polymer functionalization enables the synthesis and investigation of a wide and expanding number of block copolymers [23].

Regarding the synthesis of BCPs, three are the main routes that can be followed: sequential polymerization, macroinitiation and coupling chemistries [23, 24]. The synthetic routes are important since premature termination, contaminants and inefficient coupling will impact the macromolecular self-assembly [23]. Sequential polymerization methods include ring-opening polymerization, atom-transfer radical polymerization or reversible-addition-fragmentation

chain-transfer polymerization [23, 25, 26]. Post-polymerization coupling approaches include the copper(I)-catalyzed azide–alkyne cycloaddition reaction, Diels-Alder reaction or thiol-based reactions [27].

Amphiphilic block copolymers are a class of BCPs that contain a hydrophobic polymer and a hydrophilic block [22]. They can be synthetized with a linear, dendritic, star-like, bottle-brush, hyperbranched, and cyclic structure (*Fig. 2*) [28]. The properties of the final self-assembled structure can be tailored by varying some of the copolymer properties, for instance the hydrophilic to hydrophobic ratio, the length of the linear blocks and the number of peripheral groups displayed by the branched copolymers [23].

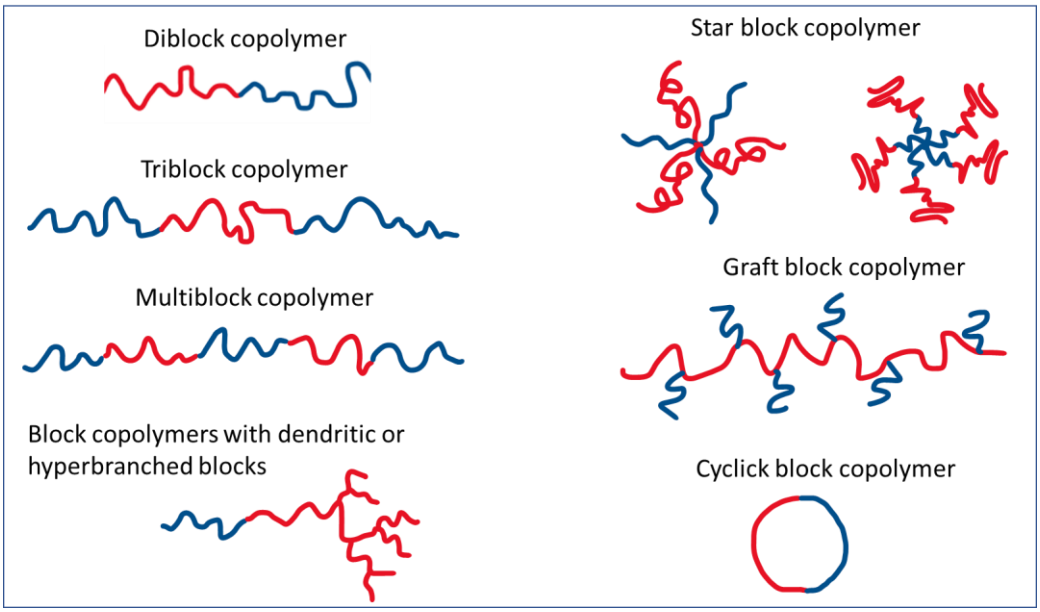

Fig. 2: different architectures for amphiphilic block copolymers.

While organic BCPs may contain only synthetic derived polymers, bio-hybrid BCPs contain at least a nature-inspired block such as a peptide, a protein, nucleic acid or sugar [29]. The use of end-functional polymers with saccharide residues has attracted great attention due to their biocompatibility, biodegradability and biorecognition properties [30]. These self-assembled nanostructures have shown promising applications in biomaterials, cosmetics, bioassays, imaging, drug delivery and even gene and cancer therapy [30, 31, 32]. The copolymers provide an easy and versatile method for the decoration of the corona of the nano-objects with various molecules and for the incorporation of therapeutic agents, like drugs, genes or siRNA in the hydrophobic blocks. They increase the solubility of hydrophobic drugs in water and they can protect the genes/RNAs from enzymatic digestion and reduce their side effects [34, 35, 36]. As an

example, glyconanoparticles made from a maltoheptaose-block-polyisoprene copolymer entrapping an anticancer drug, curcumin, showed good stability in gastric and intestinal fluids demonstrating their suitability as drug delivering systems [37]. Some copolymers have the ability to switch morphology and undergo conformational changes in response to an external stimulus like a change in temperature and pH. These stimuli-responsive assemblies are particularly interesting for nanomedicine since they can favour the drug transfer from a polar environment such as blood to non-polar lipidic membranes [38]. The carbohydrate hybrid assemblies can be used to modulate or mimick the interactions between natural carbohydrates and their receptors in biological systems and thus create targeted materials [39]. Many biological processes like cell adhesion, tissue growth and repair, signaling transductions, are based on recognition between cell surface glycoconjugates and their respective ligands. The recognition based on carbohydrate-proteins interactions is characterized by lower production cost and immunogenicity compared to those based on antibodies/antigens, and for this reason they have attracted a lot of interest in biomedicine [34]. Different examples of nano-objects derived from amphiphilic block glycocopolymers as therapeutic agents can be found in literature, for instance copolymers bearing methyl acrylate as hydrophobic part and mannose as hydrophilic block have been self-assembled in solution to form glyconanoparticles with a binding affinity towards lectins for potential biomedical applications in cell-targeted drug-delivery [22]. Others are able to function as inhibitors or bacterial and viral infections [40, 41]. Other applications, outside the biomedical field, include the use of amphiphilic block copolymers as templates for the preparation of metallic, semiconductor nanoparticles and mesoporous materials inside their micelle cores [42]. By this method, the copolymers provide control over the size of the nanoparticles and avoid their aggregation during synthesis.

1.3. Self-assembly process of amphiphilic block copolymers

Amphiphilic BCPs undergo a self-assembly process or micellization in solution, when the copolymer is dissolved in a large volume of a solvent which is selective for one of the blocks [43]. The monodisperse copolymers rearrange in minimum free energy configurations, the block which is more soluble in the medium will be oriented towards it by creating the corona of the final micelles. The insoluble part will try to minimize the interactions with the solvent by forming the core of the structure [43]. This occurs when two different parameters are reached: the critical micelle temperature (CMT) and the critical micelle concentration (CMC). Afterwards, a thermodynamic equilibrium between the micelle and the single copolymer units

is established [43]. An additional process called gelation can also occur when the micelles form highly ordered structures during the transition from diluted to high concentrated copolymer solutions [43]. Thus, the type of assemblies will depend upon the sum of two main opposing forces: the repulsion between the hydrophilic head groups forming the corona due to electrostatic or steric interactions and the hydrophobic attractions between the hydrophobic moieties that form the core. In addition, the interfacial energy between the molecules of the solvent and those forming the corona, and inter-aggregate forces that are established between different aggregates, will also play a role in determining the final size and shape of the assemblies [43]. The balance between those forces and the final geometry of the assemblies can be described by some parameters and in particular, by the packing parameter or shape factor, p, which is related to the interfacial area (a_o), the length of the hydrophobic chains (l_c) and the volume they occupy (v) according to the *Equation 2.* [44].

$$p = \frac{v}{l_o a_o} \qquad \textit{Equation 2.}$$

If the shape factor is less than 1, the micelles will have a spherical shape with an hydrophobic interior surrounded by polar head-groups. If p is approximatively 1, bilayers will form from lamellar structures or vesicles, the latter characterized by two aqueous domains, one forming the core and the other the outer corona. Finally, inverted structures with a water core and hydrophobic corona will be formed when p value is greater than 1 in non-polar solvents [43].

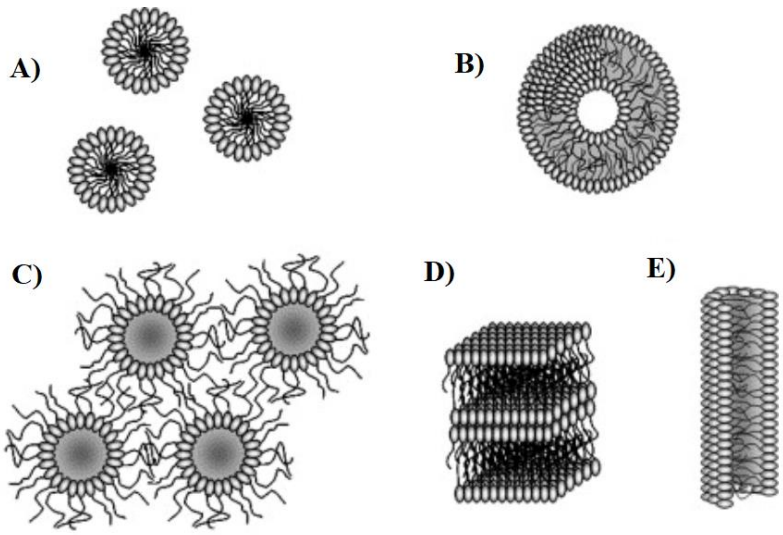

Fig. 3: some examples of the possible structures formed from block copolymers, A) micelles, B) vesicles, C) inverted micelles, D) lamellar structures and E) cylindrical or tubular micelles. The image has been adapted from: Israelachvili J. N. «Intermolecular and surface forces». Academic Press. (1992).

Two different procedures can be followed for the preparation of the micelles. The first relies on the introduction of the copolymer in a non selective solvent and the micelle formation will be driven by the manipulation of some experimental parameters, such as temperature, or the use of a co-solvent [43]. Otherwise, after the initial dissolution of the copolymer in a solvent or in a combination of solvents suitable for both hydrophilic and hydrophobic segments, the formation of the micelles will be driven by the addition of a solvent which is selective for only one of the block of the copolymer, followed by the removal of the common solvent by dialysis or evaporation [43]. This technique is called nanoprecipitation or solvent displacement method and was patented by Fessi H. et al. in 1988 [45]. The standard method of nanoprecipitation also called solvent-to-water method involves the addition of the copolymer solution in a large volume of a polar solvent, usually water, while in the inverted nanoprecipitation or water-to-solvent method, the aqueous phase is added slowly at the copolymer solution under stirring.

Both methods have been used to form glyconanoparticles, which tend to have smaller diameters when the inverted nanoprecipitation is followed [46]. In both cases, water acts as a precipitant, driving the copolymer chains aggregation. The choices of solvents, the copolymer composition and initial copolymer concentration can affect the process, as well as the presence of co-solutes and additives in the solution [46].

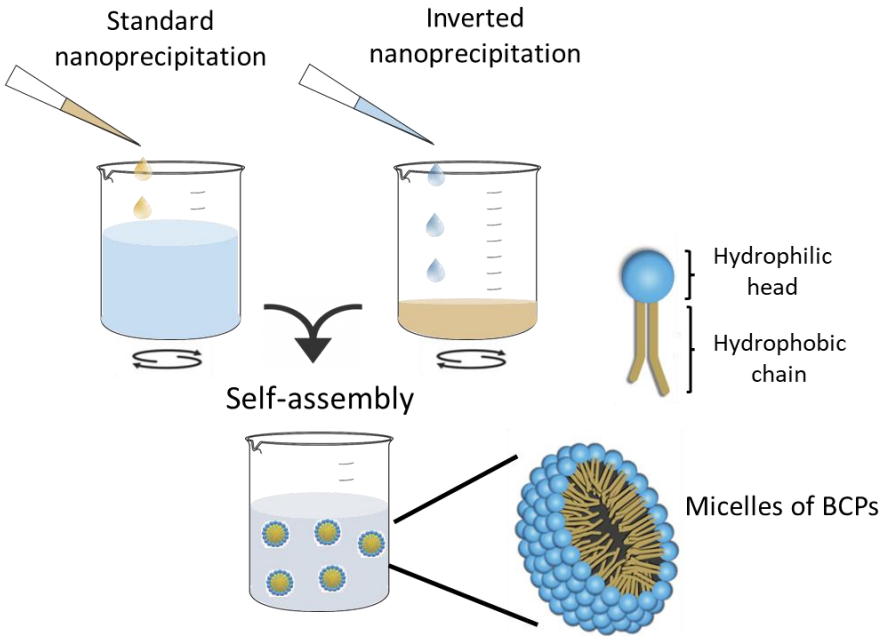

Fig. 4: preparation of micelles of block copolymer by nanoprecipitation.

1.4. Self-assembly of GNPs from an amphiphilic PS-b-βCD copolymer

Due to their specific property of forming host-guest complexes, CDs are ideal building blocks for the formation of supramolecular aggregates and nano-objects. The formation of nanoparticles from amphiphilic block copolymers composed of a β-CD block can offer several advantages compared to the single β-CDs. In particular, a large interaction surface and the compact presence of several functionalizable β-CD sites within the same macrostructure generates a versatile entity that can lead to the enhanced encapsulation of molecules within the core or the corona domain of the nanoparticles [47].

In the present work, β-cyclodextrin-decorated glyconanoparticles (GNPs) have been obtained from an amphiphilic diblock copolymer, polystyrene-block-β-cyclodextrin (PS-b-βCD), by nanoprecipitation. The hydrophobic part of the block polymer (*Fig. 5*) is a polystyrene chain while β-CD is the hydrophilic one. The synthetic procedure of the copolymer is described in the work of Carrière M. and coworkers [48] and it involves a click chemistry reaction between azido functionalized polystyrene (1 eq, 4 g, 0.89 mmol) and mono-6-N-propargylamino-6-deoxy-β-cyclodextrin (1.2 eq, 1.25 g, 1.07 mmol) in the presence of 2 equivalents of copper nanopowder in DMF (30 mL) at 65 °C for 72 h. The product (4.5 g, 85 % yield) was characterized by ^{1}H NMR and SEC [48].

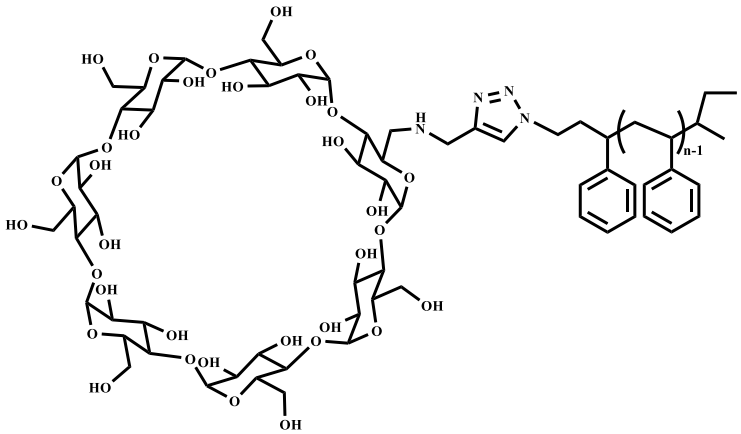

Fig. 5: structure of the polystyrene-block-β-cyclodextrin copolymer.

The first syntesis of NPs derived from PS-b-βCD copolymer by inverted nanoprecipitation was carried out by the team of Borsali (Giacomelli C. et al. in 2009) [49]. In that work, the copolymer was dissolved in DMF followed by the slow addition of water up to 80% w/w DMF/water. Finally, the organic solvent was removed by extensive dialysis against pure

water [49]. The method allowed the formation of GNPs with a dense core of polystyrene chains surrounded by a thin shell of β-cyclodextrins. Some parameters of the nanoprecipitation have proven to be of great importance in the final outcome, in particular the initial concentration of the copolymer in the organic phase, the rate of water addition and the final volume of water before dialysis [49]. The nanoprecipitation to form GNPs was subsequently optimized and a new procedure has been developed and adopted in successive works [48]. The subsequent characterization of the obtained GNPs showed the efficacy and reproducibility of this optimized method. The process is schematized in *Fig. 6*.

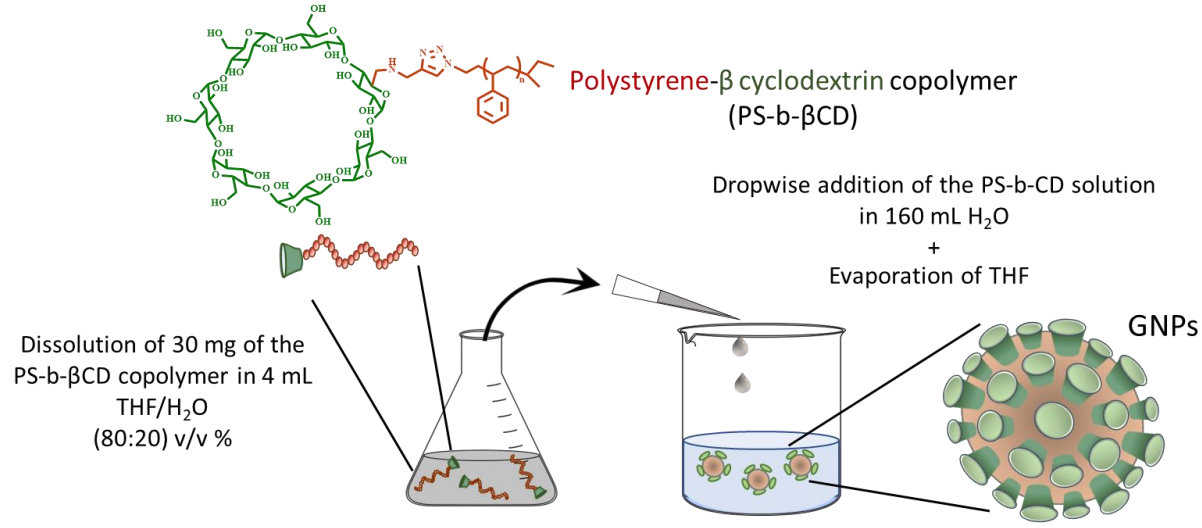

Fig. 6: scheme of the nanoprecipitation process used for the formation of β-cyclodextrin-polystyrene glyconanoparticles.

Following the recent optimized procedure, 30 mg of copolymer PS-b-βCD were dissolved in a 4 mL of a mixture of an organic solvent, THF and MilliQ water (80: 20)% w/w. Preliminary solubility tests carried out by Carrière M. combined with static light scattering (SLS) analysis, indicated that this combination of solvents and this ratio are ideal to allow the complete dissolution of both blocks, polystyrene and βCD, avoiding the formation of aggregates. Pre-existing aggregates of styrene and βCD blocks can in fact hindering chain mobility during self-assembling [48]. The solution containing the copolymer with a concentration of 7.5 mg mL^{-1} was stirred at 1000 rpm for 24 h at 25 °C. The following day, the copolymer solution was added drop by drop to a large amount of water (160 mL) using a siringe pump. The syringe pump debit was setted at 10.2 mL h^{-1} to provide a controlled flow, while the suspension was stirred at 500 rpm. During this process, the solution which is initially clear and transparent, becomes progressively opaque with a milky colour due to the formation of micelles. The final

suspension was left for another 2 hours under stirring. In the last step, THF was evaporated under reduced pressure at 36 °C and the final volume was adjusted to 160 mL by adding MilliQ water. The final concentration of the copolymer in the suspension is thus 0.1875 mg L^{-1}. The suspension containing the GNPs was kept at 4 °C. At this temperature, it showed good stability up to a period of two months. A detailed morphological and dimensional characterization of the GNPs obtained by this method has been already carried out by Carrière M. et al. [48].

2. Functionalization of GNPs with tris((adamantan-1-yl)-methoxy)-heptazine (HTZ-Ad)

2.1. Overview on the functionalization of the GNPs derived from PS-b-βCD

In general, NPs self-assembled from amphiphilic block copolymers can be further functionalized with compounds that have an affinity with the core or the shell of the NPs. Two main strategies can be pursued for the functionalization: the incorporation of compounds during the self-assembly process or the post-functionalization of the already assembled NPs with compounds that have an affinity for the groups of the corona. In the first case, the compounds are co-dissolved with the copolymer solution and during the nanoprecipitation, they can be entrapped in the core or enter into the composition of the corona depending on their relative polarity [48, 50, 51]. In the second case, the suspension of pre-formed GNPs are mixed with the compound which is able to interact with the groups of the corona leading to decorated GNPs.

Thus, the GNPs obtained from PS-b-βCD copolymer have two abilities: the one to encapsulate hydrophobic species in the polystyrene core and the ability to bind compounds through β-CDs molecular complexation. The post-functionalization of GNPs derived from PS-b-βCD has been already demonstrated in previous works [48, 50]. In particular, electroactive GNPs have been obtained by their post-functionalization with anthraquinone sulfonate (AQS) in aqueous solvent [49]. Interestingly, the authors showed that is possible to modulate the surface densities of the β-CDs by creation of hybrid GNPs by mixing two different amphiphilc block copolymers in different proportions during the nanoprecipitation [49]. In particular, hybrid GNPs have been formed by a mixture of PS-b-βCD and polystyrene-b-maltoheptaose (PS-b-MH). The modulation of the β-CDs sites allowed in turn to modulate the electroactivity of the AQS-functionalized GNPs [49].

The complexation of redox mediators into the βCDs cavity has shown promising applications in enzyme electrocatalysis. In particular, our group demonstrated the functionalization of GNPs with bis-pyrene-ABTS (P_2ABTS) by formation of inclusion complexes between the pyrene groups and the βCDs [50]. These GNPs improved the electrocatalytic reduction of oxygen to water by BOx when used in solution with the freely diffusing enzyme. Interestingly, the catalytic current was considerably higher than that observed for the configuration where the P_2ABTS mediator is in solution without GNPs. The improvement in enzyme catalysis can be attributed to the improved solubilization of the hydrophobic redox mediator in aqueous environment and also to a redox hopping effect resulting from the presence of several redox mediators in close proximity within the same GNP and between different GNPs that facilitates the electron transfer from the enzyme to the electrode [50]. Similarly, redox GNPs have been formed by encapsulation of phenanthrene-quinone (PQ) in the core of the GNPs during the self-assembly [51]. Both types of redox GNPs have been used for the fabrication of a solubilized enzymatic fuel cell (SEFC).

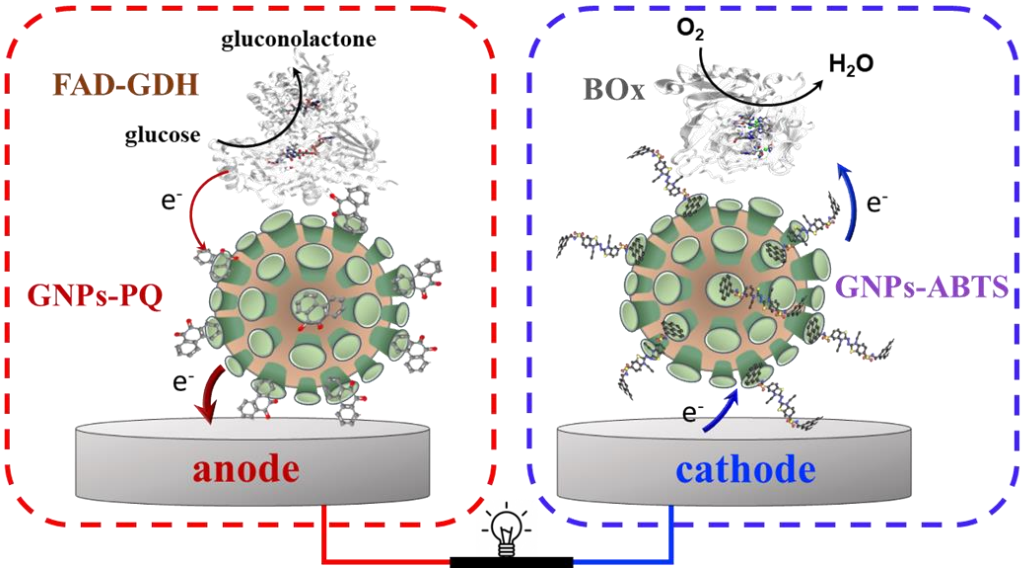

Fig. 7: the concept of a solubilized EFC used for glucose and oxygen conversion based on redox functionalized GNPs and freely diffusing enzymes.

In particular, the GNPs functionalized with PQ have been used in combination with a glucose dehydrogenase (FAD-GDH) at the anode while those functionalized with P_2ABTS were associated with BOx at the cathode for glucose and oxygen conversion respectively. In this cell setup, both the freely diffusing enzymes and the GNPs are retained in permselective dialysis membranes that allow the diffusion of substrates and protons while retaining the

catalyst and the GNPs inside each compartment. The fuel supply is assured by a peristaltic pump. The performances of the SEFC was good with a power loss of only 26.3% after 7 days of continuous cycling [51].

Redox and fluorescent GNPs have been similarly obtained by formation of inclusion complexes with tetrazine−naphthalimide [52]. In this case, similarly to P_2ABTS, the tetrazines have been encapsulated in the β-CDs during nanoprecipitation. The different analyses conducted confirmed the presence of aggregates of tetrazine at the surface of the GNPs [52].

Despite the good fluorescence yield and the high redox potential in the excited state of the tetrazine, their moderate chemical stability reduces their potential use for long term applications [29]. For this reason, the possibility to functionalize the GNPs with a different fluorescent compound with higher chemical stability, 2,5,8-tris((adamantan-1-yl)methoxy)-heptazine, has been explored with the aim of developing novel class of materials that can be adopted for energy conversion, storage or environmental applications. The results have been published [51] and are described in the present work.

2.2. Structure, properties and synthesis of heptazines

The discovery of heptazines was reported by Justus von Liebig in the 19th century [53] and attributed to a Swedish chemist, Jons Jakob Berzelius, that obtained a compound, cyameluric derivative, by ignition of mercury thiocyanate [54]. Despite that, research into heptazines have been rare in history essentially because of solubility issues and their low chemical reactivity which made their characterization and modification quite challenging [55]. In the last years, the interest in heptazines is growing due to considerations about their peculiar properties and their interesting applications in various fields. Heptazines are a family characterized by a polycyclic aromatic core, a s-heptazine (tri-s-triazine) moiety consisting of three fused s-triazine rings (*Fig. 8*). The structure of heptazine is planar and relatively rigid, the delocalized π-conjugated system has a high nitrogen to carbon ratio (heptazine core: N/C = 1.17) which make them strongly electron deficient compounds, similarly to triazines and tetrazines [56]. In contrast to tetrazines, these compounds show a large HOMO-LUMO gap (in the near UV-blue region) and they have a slightly lower redox reduction potential in the fundamental state [56].

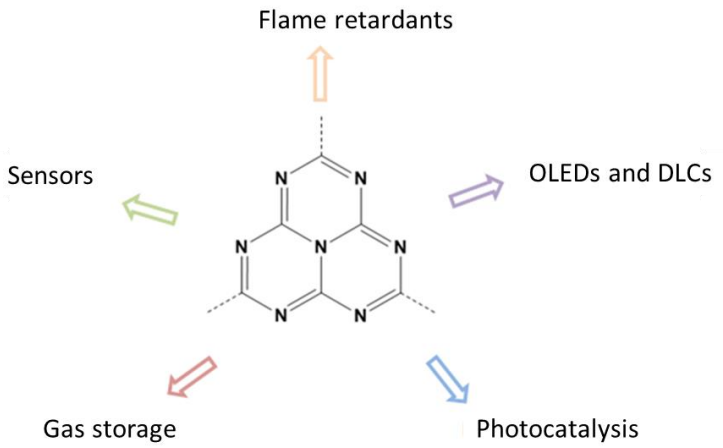

Fig. 8: the s-heptazine core and some of the principal applications of heptazines.

These characteristics make heptazines suitable for applications in optoelectronics [57]. Heptazines have been recently used as building blocks to synthesize chemically and thermally stable microporous polymer networks, covalent organic frameworks (COFs) and metal organic framework (MOFs) that can be used in different applicative domains such as gas storage [58]. Heptazine polymers have demonstrated remarkable metal-free photocatalytic properties for hydrogen evolution [59, 60], CO_2 reduction [61], photocatalytic degradation of organic pollutants [62] and artificial photosynthesis [63]. The heptazine core might be one of the rare molecular platforms able to perform water splitting via molecular catalysis [56]. Moreover, they possess very high thermal and chemical stability (the decomposition temperature can exceed 500 °C) [56]. Beside that, heptazine derivatives are fluorescent, so they are promising candidates for the development of organic light-emitting diodes (OLEDs), furthermore s-heptazine-based assemblies linked via intermolecular hydrogen-bonding interactions gave rise to semiconductor materials that have been employed for the fabrication of DLCs discotic liquid crystals (DLCs) [64]. Therefore, the synthesis and characterization of new heptazines has recently attracted a lot of interest.

Heptazines derivatives can be synthetized from precursors with exchangeable groups. The most utilized precursor has been trichloroheptazine, also designated as cyameluric chloride. The chloride groups can be efficiently replaced by various mild nucleophiles, including amines, thiols and phosphines. This synthetic pathway, which was originally described by Schwarzer A. et al. [65], presents some drawbacks: the preparation of trichloroheptazine is difficult and dangerous so that very delicate equipment is required and the precursor is easily hydrolized and is only mildly soluble in most common solvents [58]. To overcome these issues,

an alternative synthetic route that relies on the use of 2,5,8-tris(3,5-diethyl-pyrazol-1-yl)-heptazine (3PyHept) as precursor is preferred. 3PyHept can be obtained from trihydrazinoheptazine in the presence of an excess of the pure diketone and an acidic catalyst and it possesses diethylpyrazolyl leaving groups that can be replaced by nucleophilic substitution giving several heptazines derivatives (*Fig. 9*) [58].

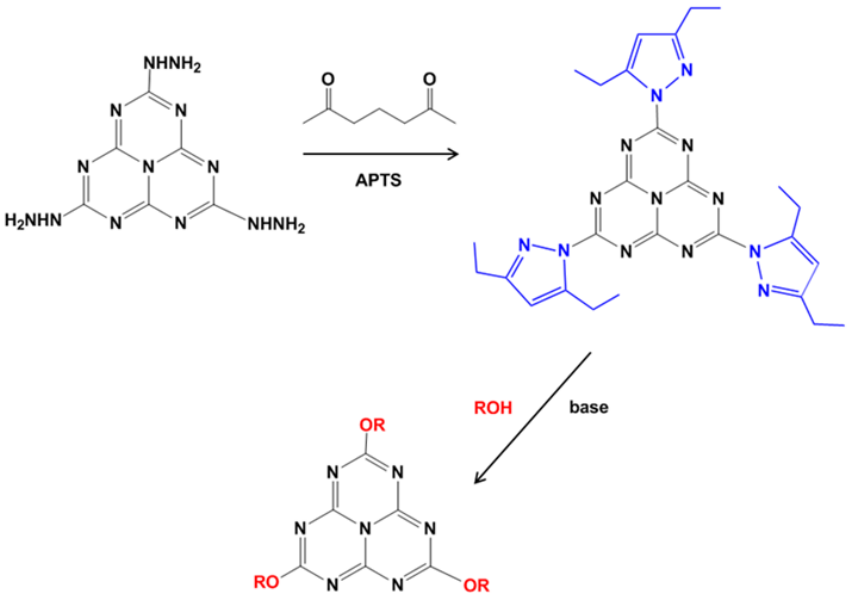

Fig. 9: synthesis of alkoxyheptazines from 2,5,8-tris(3,5-diethyl-pyrazol-1-yl)-heptazine.

2,5,8-tris((adamantan-1-yl)methoxy)-heptazine (HTZ-Ad or tris(O-CH2-Ad)heptazine), an heptazine derivative with three methoxy-adamantanyl substituents at the corners of the heptazine core (*Fig. 10*), has been obtained by Audebert P. et al. [66] by a nucleophilic substitution reaction, using a base, collidine, for the first substitution step and DMAP for the second one. In more detail, in the second step, the precursor, (tris-(diethylpyrazolyl)-heptazine) (TDPH), was mixed with an equimolar amount of DMAP in a pressure tube with a 3-fold excess of (adamantan-1-yl)-methanol. The tube, completely sealed, was stored at 100°C for 3 h. The product was finally purified by flash chromatography [66].

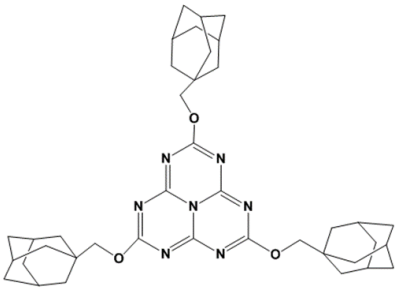

Fig. 10: 2,5,8-tris((adamantan-1-yl)methoxy)-heptazine (HTZ-Ad).

Adamantane (Ad) has a cage-like structure with high stability and a diameter of about 7 Å and a volume of approximately 180 $Å^3$, which are close to the hydrophobic cavity of β-CD [67]. Ad is well known to form stable supramolecular complexes with β-CDs (1: 1) [68, 69], while it can form a 2: 1 inclusion complexes with α-CD with a stability constant of only about 10^2 mol^{-1} L because of the small size of α-CD cavity [67]. The association constant (K_a) between β-CD and Ad has been calculated to be instead much higher and equal to 10^5 mol^{-1} L [70]. The possibility to functionalize the GNPs decorated with a shell of β-CDs with HTZ-Ad has been examined.

2.3. Characterization of HTZ-Ad

Prior to GNPs functionalization, the properties of the synthetized HTZ-Ad were investigated. First, the solubility and spectroscopic characteristics of HTZ-Ad were verified. In order to favour the contact between the GNPs and heptazine, an appropriate solvent should be used to dissolve both reagents and more preferably, a mixture of water and a solvent miscible in water. In general, the solubility of heptazine derivatives depends strongly on the nature of the substituents. Except melem, that can be protonated and solubilized in strong aqueous acids, all heptazines are generally almost insoluble in water. In particular, trialkoxyheptazines, especially those with large substituents, like HTZ-Ad, have a really low solubility in water while they are very soluble in organic solvents. However, the use of organic solvents should be reduced as far as possible when working on GNPs to reduce the possibility of their disassembling. In *Fig. 11*, the same amount of HTZ-Ad (0.66 mg mL^{-1}) was dispersed in water or in a mixture of EtOH/H_2O (70:30) v/v% after 20 min sonication, the picture has been taken under ambient light or under UV lamp at 365 nm. Even after the sonication treatment, the sample dispersed in water presented a solid deposit and visible aggregates. In contrast, the presence of a volume fraction of 70% of EtOH in the aqueous solution greatly improved the dissolution of HTZ-Ad, producing a more homogeneous mixture with a more brighter fluorescence.

Similarly to what reported by Audebert P. et al. [66] in dichloromethane (DCM), HTZ-Ad showed an intense band around 270 nm and a slight absorption tail or shoulder in the visible range (due to a charge transfer band of very low intensity). The positions and intensities of the absorption bands are supposed to only weakly depend on the nature of the alkoxy substituent [66]. Although the maximum absorption peak of HTZ-Ad is located at 270 nm, HTZ-Ad is able to absorb a wider range of wavelengths around the maximum, including 365 nm. As expected, the supernatant of the sample in the mixture of EtOH/H_2O showed also an higher absorbance

intensity in the UV-vis spectrum compared to that recorded in pure water (λ_{abs} = 2.7 at 270 nm vs λ_{abs} = 0.3 at 270 nm respectively).

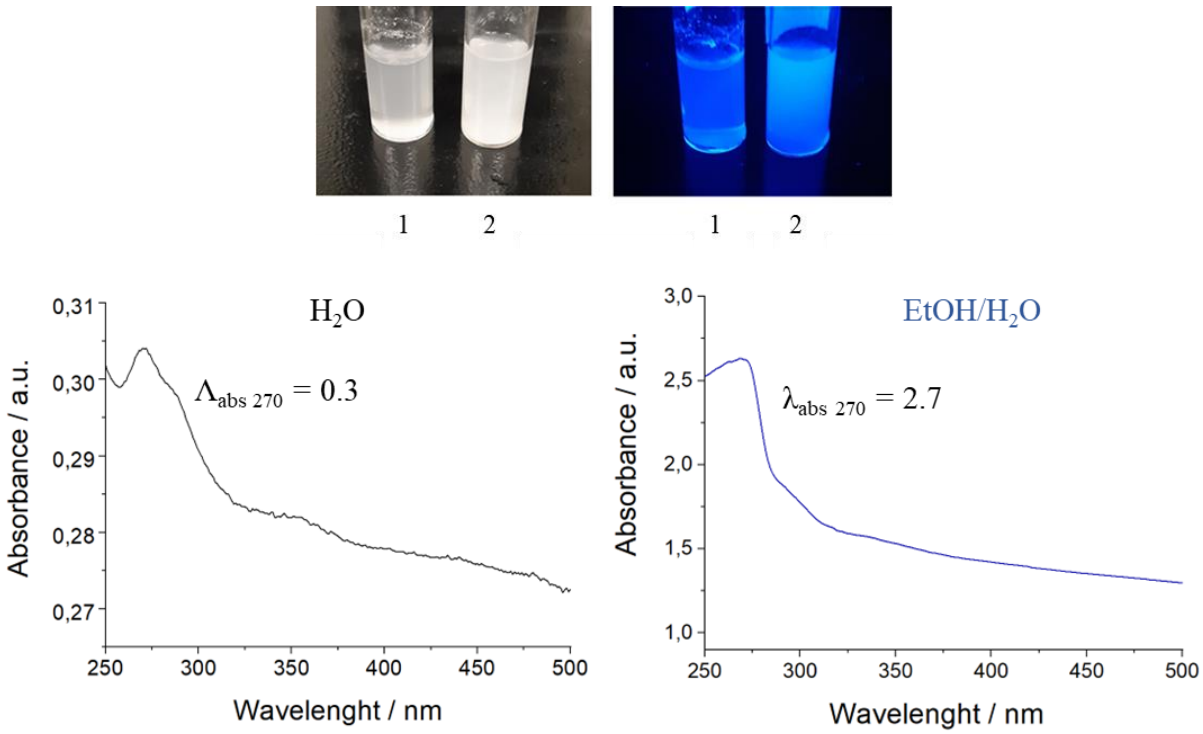

Fig. 11: Images of two samples of HTZ-Ad (0.66 mg mL^{-1}) in water (1) and in a mixture of ethanol/water (70:30) v/v% (2) after 20 min sonication under light and under irradiation at 365 nm. UV-vis absorbance spectra background corrected of the supernatants of the two samples.

In general, fluorescence occurs in organic compounds with planar and rigid structures, containing polyaromatic hydrocarbons or heterocycles (fluorophores) [71]. When a fluorophore adsorbs a photon, one electron is excited to an higher energy level, an excited electronic singlet state (S1'), by a transition from the highest occupied molecular orbital (HOMO) to lowest unoccupied molecular orbital (LUMO). After a certain interval, called fluorescence lifetime (usually 1–10 nanoseconds), the fluorophore undergoes conformational changes and dissipates energy by interactions with the surrounding molecules forming a relaxed singlet excited state (S1) (vibrational relaxation). When S1 returns to the molecule's ground state (S0), a photon is emitted with lower energy and longer wavelength than the excitation photon causing fluorescence emission. In some cases, the electron in the S1 electronic state can decay to a triplet excited state (T1) via a non-fluorescent phenomenon called intersystem crossing [71].

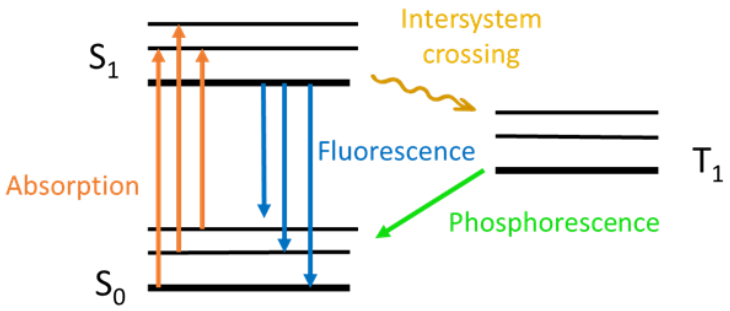

Fig. 12: Jablonski diagram depicting processes of absorption, fluorescence, intersystem crossing, and phosphorescence.

If the separation of π-electron densities of HOMO and LUMO is sufficiently high without overlap, the energy gap between the S1 and T1 states, termed Δ_{EST}, will be small. In this condition, intersystem crossing both from S1-to-T1 states and reverse intercrossing from T1-to-S1 states have fast reaction rates establishing an equilibrium between those state populations. Consequently, these compounds will display a broad fluorescence emission originating from the initial population in the S1 state and those electrons in the T1 state which are reversely converted to S1 over time (delayed fluorescence) [72]. All trialkoxyheptazines, for their peculiar and rigid nuclear geometry, fall into this category (with Δ_{EST} near to zero [73]), and show a broad fluorescence emission band located in the near UV-visible region depending on the type of substituents [66].

The spectroscopic properties of HTZ-Ad in combination with β-CDs in water have been then explored. Two samples, one containing only HTZ-Ad in water (0.66 mg mL^{-1}) and one containing the same amount of HTZ-Ad plus an excess of free β-CDs (5-fold molar excess), were immersed in an ultrasonic bath for 2 hours followed by overnight stirring. The UV-vis spectra of the samples were recorded after a 1:50 dilution while the fluorescence emission spectra were recorded at the excitation wavelength of 270 nm after a 1:1000 dilution. The UV-vis spectra of both samples showed an intense band around 270 nm, which is typical of HTZ-Ad, and clearly the intensity of the maximum absorption peak is considerable higher in presence of β-CDs. A similar outcome was observed for the fluorescence emission (*Fig. 10*). The maximum fluorescence emission of HTZ-Ad in water is localized at around 420 nm, similarly to what previously reported in the literature [66], and also in this case the intensity was more than 7 times higher in presence of β-CDs.

Thus, the improved absorption and fluorescence emission observed in presence of β-CDs can be explained by the molecular complexation of HTZ-Ad with the hydrophobic cavity of β-CDs that has the effect of improving greatly its solubilization in water. The solubilization with CDs allowed the first characterization of an alkoxy-heptazine derivative in water. This result demonstrates the importance of β-CDs which can overcome the solubility problems of heptazine derivatives and thus extend their applicability, for instance their use as catalyst for water splitting reaction. Furthermore, it also proves that the functionalization of GNPs via formation of inclusion complexes between the adamantane residues of HTZ-Ad and β-CDs is feasible.

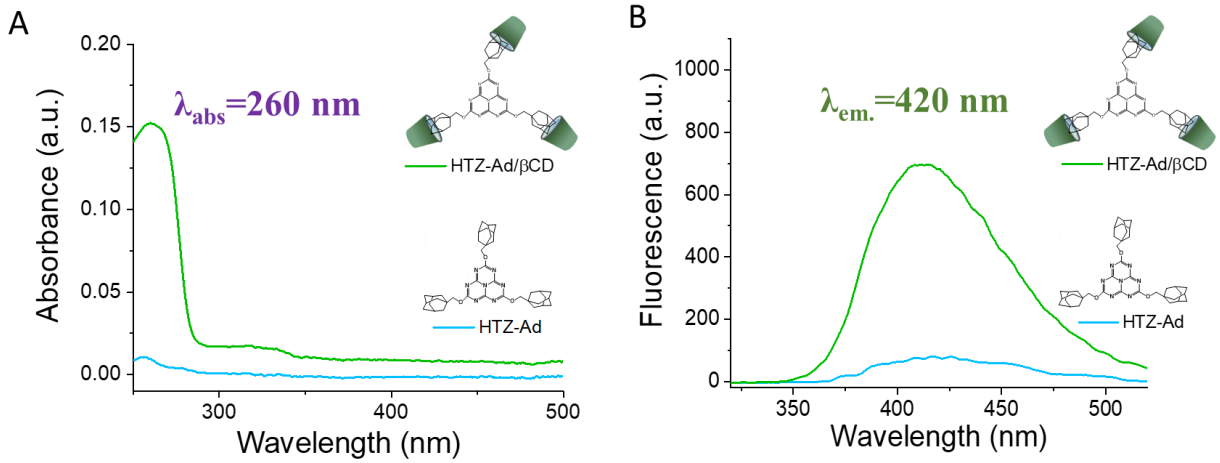

Fig. 13: A) UV–vis absorption spectra and B) fluorescence emission spectra in water of the supernatants of HTZ-Ad in the presence or absence of β-CDs (HTZ-Ad/β-CDs equivalent ratio: 1/5).

The electrochemical characterization of HTZ-Ad in aqueous medium was instead not feasible, even after its dissolution with β-CDs, because the compound is electroreducible in the form of reduced dianion, but at a very negative potential incompatible with the potential window of aqueous electrolytes. Thus, the electrochemical characterization has been done in an aprotic medium, DCM. The reduction of heptazine can be almost reversible or irreversible depending on the substituents [74]. The characterization of heptazines by cyclic voltammetry in aprotic solvent is described in the work of Dubois et al. [75] which reports a reversible peak at -2.17 V vs SCE for tris-(diisobutylamino)-s-heptazine in DMSO. Audebert et al. [74] reported a first almost reversible wave at -1.3 V vs Ag/AgCl and a second irreversible wave at around –1.9 V for the electrochemical behaviour of 2,5,8-tris(3,5-diethyl-pyrazolyl)-heptazine in DCM containing 0.1 M of tetrabutylammonium hexafluorophosphate (TBFP) as supporting electrolyte. For glassy carbon (GC) electrodes tested in a solution of HTZ-Ad in DCM

(previously dried using molecular shieves) containing 0.1 M of TBFP, a tiny irreversible peak at -1.43 V vs Ag/Ag^+ (0.01 M $AgNO_3$ + 0.1 M TBFP in DCM) and a second sharp irreversible peak at -2.32 V vs Ag/Ag^+ were observed. (*Fig. 14*).

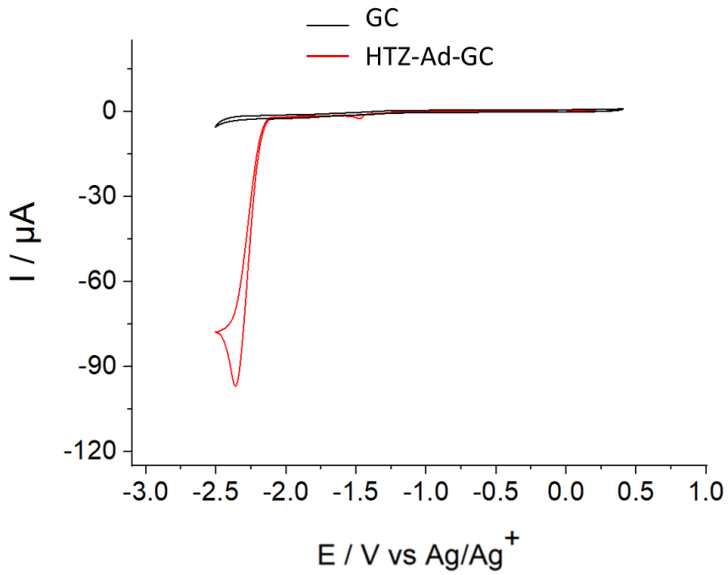

Fig. 14: Cyclic voltammogram recorded at a glassy carbon (GC) electrode (3 mm diameter disc) of degassed DCM + 0.1 M TBFP in absence and presence of HTZ-Ad (5 mmol L^{-1}), scan rate 20 mV s^{-1}, Ref: Ag/Ag^+ (potentials are referred to the ferrocene/ferrocenium (Fc/Fc^+) redox couple tested in the same conditions).

2.4. Post-functionalization of the GNPs with HTZ-Ad

For the functionalization of the GNPs, previously self-assembled from PS-b-βCD, with HTZ-Ad, a procedure similar to that described by Carrière et al. [48] for the functionalization of the GNPs with AQS was followed. Since after some days, the GNPs in the suspension tend to sediment, the suspension was sonicated for 10 min before usage. 3.2 mg HTZ-Ad were dispersed in 1 mL of EtOH/H_2O (70:30, v/v%) and the solution was added dropwise to a larger volume (5 mL) of the GNPs suspension. The final concentration of HTZ-Ad in the mixture was thus 0.66 mg mL^{-1}, the molar fold is in excess compared to βCDs which are associated with the GNPs (estimated from the concentration of PS-b-βCD in the suspension of GNPs). The mixture was then immersed for 2 hours in a ultrasound bath and left under stirring at 500 rpm overnight (>12 hours) and finally transferred in a dialysis bag with a membrane cut off of 3.5 kDa immersed in pure water (4 L).

While for the functionalization of the GNPs with AQS, which is partially soluble in water, the role of dialysis was to slowly separate the unreacted reagent by diffusion outside of the

dialysis bag from the GNPs retained inside the bag [48], in this case the dialysis was used to remove the small volume of EtOH from the solution to cause the slow precipitation of HTZ-Ad. As a consequence of the poor solubility of HTZ-Ad in water, all the unreacted HTZ-Ad are collected in the form of a white solid at the bottom of the dialysis bag after one day of dialysis. A volume of supernatant containing GNPs still dispersed in the aqueous suspension above the heptazine deposit (4 mL) was thus collected and stored at 4° C for the further characterization.

The efficiency of the separation of the HTZ-Ad by precipitation was verified by acquiring of UV-vis spectra of the supernatant of a sample containing 0.66 mg mL^{-1} of HTZ-Ad in water starting the initial 2h sonication treatment (from t = 0). A decrease of the intensity of the absorption maximum (λ_{abs}) at 270 nm over time occurred. The decrease was already very pronounced after 8 hours and after 24 hours was close to zero (0.03), while measurements taken after longer times (48 h) did not show a further significant decrease. Thus, a time of 24 hours is sufficient for obtaining a good separation (*Fig. 15*). A scheme of the process used for the functionalization of the GNPs with HTZ-Ad is reported in *Fig. 16*.

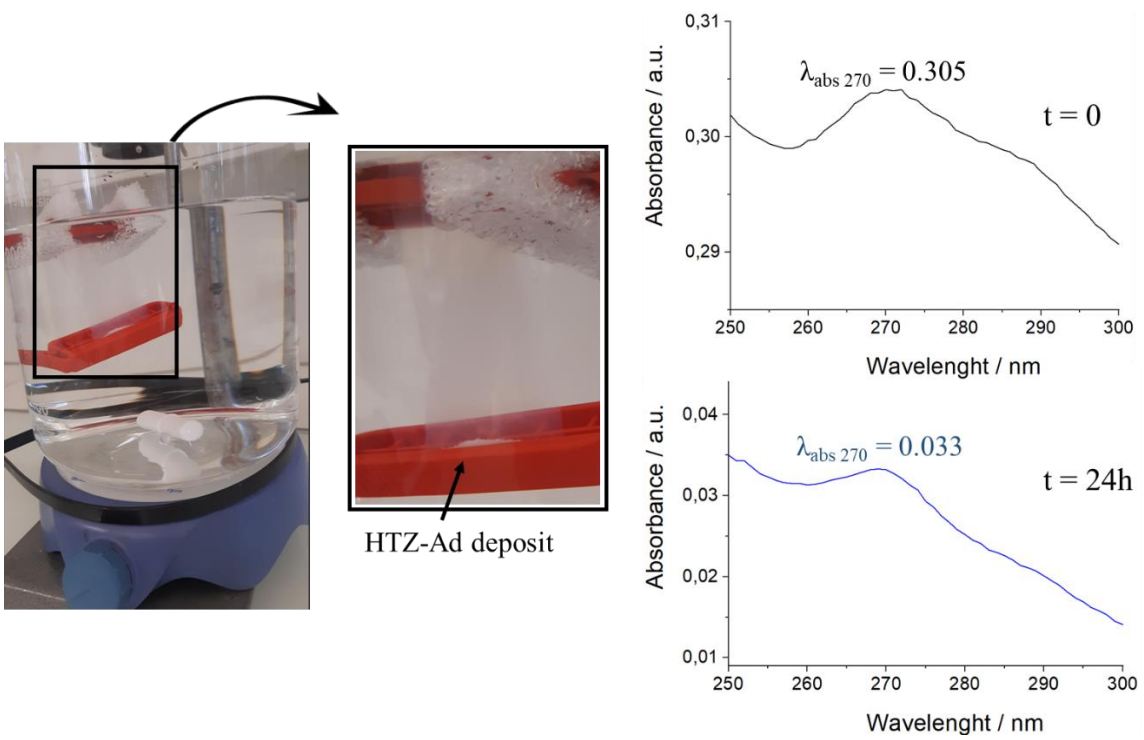

Fig.15: a picture of the dialysis bag after 24 of dialysis showing the white HTZ-Ad deposit. On the right, UV-vis absorbance spectra of the supernatants of a samples of HTZ-Ad (0.66 mg mL^{-1}) in water just after 2h sonication and after 24h of HTZ-Ad precipitation.

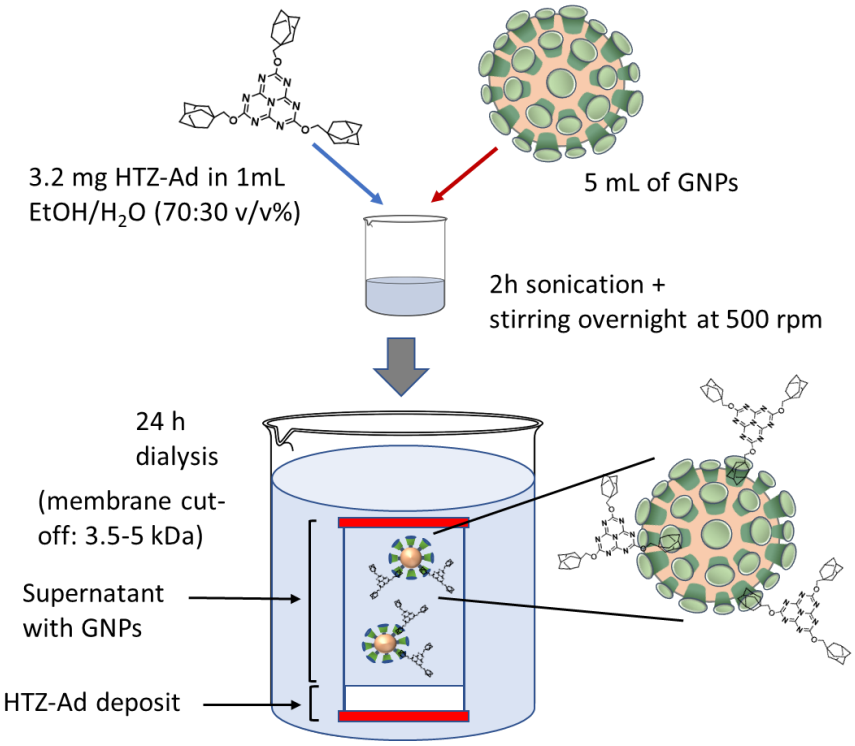

Fig.16: scheme of the functionalization process of the GNPs with HTZ-Ad.

3. Characterization of the aqueous suspension of the functionalized GNPs (HTZ-Ad-GNPs)

3.1. Determination of the morphology and size of the functionalized HTZ-Ad-GNPs

The supernatant collected at the end of the dialysis was characterized to check the presence and the morphological characteristics of the NPs. A number of techniques are available for this purpose. In particular, the morphology and size of the GNPs can be measured with great detail at the single-particle level using high-resolution microscopy techniques, such as scanning electron microscope (SEM), transmission electron microscopy (TEM) and nanoparticle tracking analysis (NTA) [76]. Other techniques such as dynamic light scattering (DLS) are rather useful to evaluate phenomena that occur in solution such as swelling or aggregation [76].

Both SEM and TEM images revealed the presence of spherical nanoparticles in the supernatant (*Fig. 17* and *Fig. 18*). The particle size distribution of the post-functionalized GNPs (HTZ-Ad-GNPs) was determined by using ImageJ software from the analysis of multiple TEM images and compared to that calculated from the images of the original suspension of GNPs prior the functionalization process. The software is able to process the

images and calculate the diameter of several nanoparticles allowing the realization of histograms that represent the percentages of NPs with a certain diameter range. The curve distribution do not follow a normal distribution, instead it was fitted by a log-normal model so that the correlation coefficient is above 0.9. Although a narrowed distribution of size is preferred, in real samples the NPs present a certain degree of variation and the samples are usually polydisperse [76]. The particle size distributions are similar before and after the functionalization, with the biggest proportion of GNPs showing diameters ranging from 40 to 60 nm.

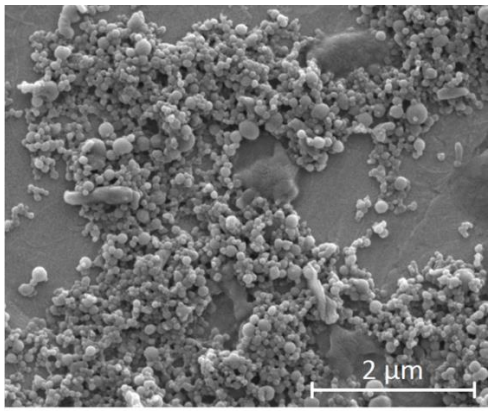

Fig.17: a SEM image of the HTZ-Ad-GNPs.

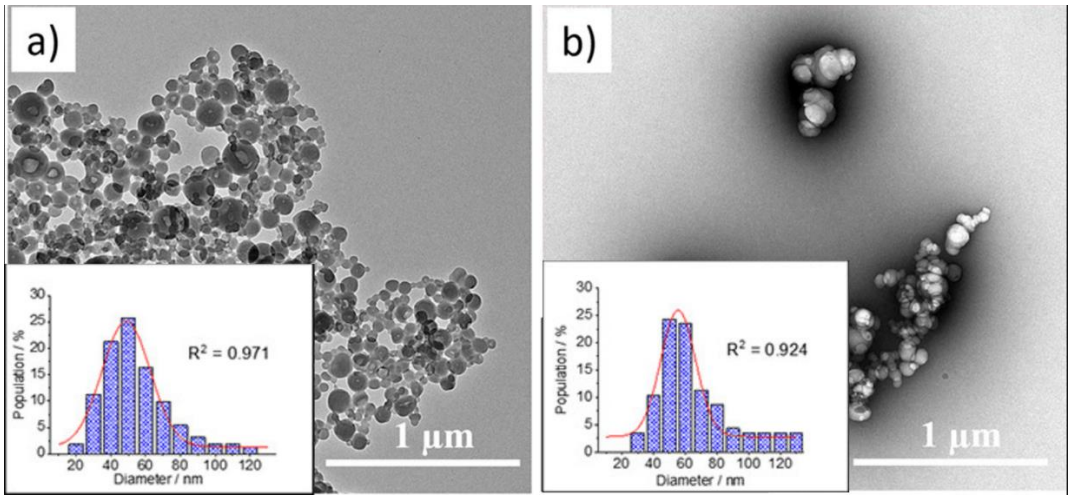

Fig.18: A TEM image of the GNPs A) prior and B) after functionalization with the relative nanoparticle size distribution fitted by a log-normal model.

The particle size distribution was evaluated also by using DLS technique, which is very suitable for the analysis of NPs dispersed in solvents and the detection of agglomerates and aggregates [77]. The NPs dispersed in a solvent (dispersant) are subjected to Brownian motions

that originate from interactions with the solvent molecules in the surrounding. NPs scatter the light of an incident laser and the scattered light coming from different NPs creates a constructive or destructive interference. This phenomenon leads to time-dependent fluctuations in the intensity of the scattered light which is measured in DLS. In particular, the rate of fluctuations is dependent upon the diffusion coefficient (D) of the NPs, which is related to the particle hydrodynamic radius (D_h) by the Stokes-Einstein equation:

$$D_h = \frac{k_B T}{3\pi\eta D} \qquad \textit{Equation 3.}$$

where D_h is the hydrodynamic radius, k_B is the Boltzmann constant, T is the absolute temperature, η is the viscosity, D the diffusion coefficient [78]. Smaller particles diffuse faster, causing more rapid fluctuations, and viceversa. As indicated by *Equation 3.*, the viscosity and the temperature affect the motion of the NPs, thus these parameters need to be known and controlled during DLS measurements. The measurement of the intensity of the scattered light is used to generate an autocorrelation function (G(τ)) that describes the motion of the molecules under investigations and is expressed as an integral of the product of the intensities at a time (t) and a delayed time (t + τ):

$$G_2(\tau) = \langle I(t) I(t+\tau) \rangle \qquad \textit{Equation 4.}$$

The smaller is the delayed time, the higher the correlation between the two measures. In general, the correlation decreases exponentially over time and the exponential decay describes how long a particle is located at the same spot within the sample. If the particles are small and moving rapidly the correlation will decrease more quickly. A more extended decay reflects a greater sample polydispersity. Different algorithms can be used to obtain the particle size distribution from the correlation function [78]. Since light does not pass through the entire sample in the cuvette and large particles and contaminants scatter light mainly in the forward direction compared to smaller size particles, it is important to perform the analysis using also a backscatter detecting system [50].

Thus in the present work, DLS analysis was carried out from different scattering angles in order to unmask the scattered light signals of low intensity that originate from smaller particles and thus have a more accurate result. The correlation functions and the relaxation time distributions (particle size distributions) of the suspension of GNPs prior and after the functionalization are reported in *Fig. 19*. The distributions are not dissimilar, both evidenced three populations of NPs, as already reported in previous works [48]. In particular, the mean

hydrodynamic radii estimated by the first distribution, which is related to single NPs and also the more represented, is almost identical between the unmodified and modified NPs (87 nm and 84 nm respectively). It could be noted that the size inferred by DLS is bigger than that estimated previously by the particle size distributions calculated from TEM images. This difference is understandable since the former includes the degree of solvatation of the NPs whereas TEM images are produced from dry samples [51].

Changes can be observed instead in the second and third size distributions which are linked to the presence of aggregates. These aggregates are quite common in samples containing micelles and they are produced by hydrophobic interactions between the cores of the micelles [81]. In particular, the average value of R_h inferred from the second particle size distribution decreases from 312 nm for the sample of unmodified GNPs to 235 nm for HTZ-Ad-GNPs. This could be induced by a shrinkage of the functionalized NPs caused by hydrophobic interactions between adamantane groups of HTZ-Ad and the core of single micelles [56]. A more consistent increase of R_h (from 1490 nm to 2480 nm) occurred in the third distribution, which is indicative of the formation of aggregates and clusters of NPs of bigger dimensions. The cause is probably a crosslinking between different functionalized NPs caused by the Ad groups exposed at the surface of the GNPs that form inclusion complexes with the β-CDs of adjacent NPs.

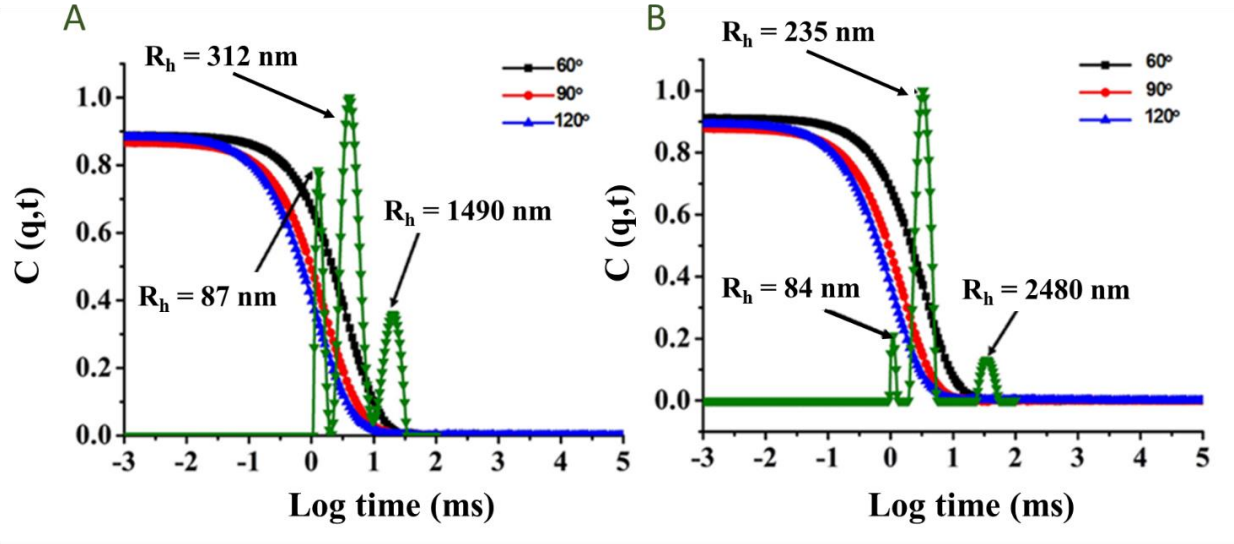

Fig. 19: autocorrelation functions and particle size distributions of A) unmodified and B) modified GNPs measured using DLS for the shown scattering angles.

The scattering vector (q) is a fundamental parameter in DLS and is defined as the difference between the vectors of the incident and scattered waves, expressed by:

$$q = \frac{4\pi\eta}{\lambda} \sin\left(\frac{\theta}{2}\right) \qquad \textit{Equation 5.}$$

where n is the index of refraction of water at 25 °C, λ is the wavelength of the incident light (633 nm) and θ is the scattering angle. A proportional dependence of the relaxation frequency (r) as a function of the square of the scattering vector (q^2) indicates that the size distributions are originated from the NPs translational diffusion [48]. The plots of the inverse of the relaxation frequency versus q^2 for the first and second size distributions do not show large differences before and after the functionalization (*Fig. 20*).

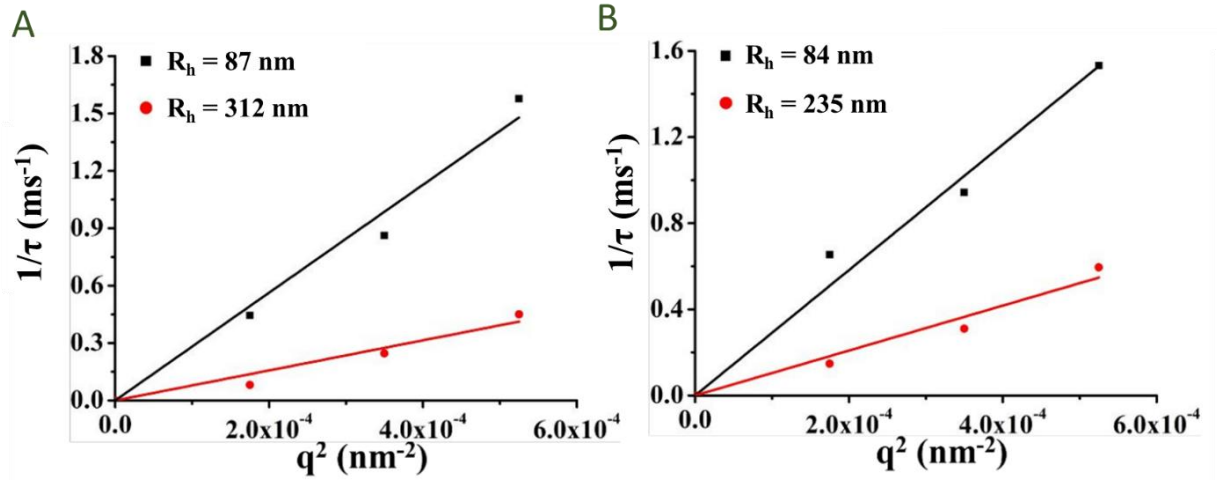

Fig. 20: variation of the relaxation frequency versus q^2 of the GNPs A) prior and B) after functionalization.

In conclusion, the analysis conducted by SEM, TEM imaging and DLS did not show any significant morphological changes or significant alterations in the size of the GNPs after the functionalization process.

3.2. Absorption and fluorescence spectroscopic investigation of HTZ-Ad-GNPs

The spectroscopic properties of the functionalized GNPs have been then investigated, the UV-vis absorption and the fluorescence emission spectra of the GNPs prior and after functionalization are overlayed in *Fig. 21A* for comparison.

A broad absorption band between 200 nm and 300 nm is observed in the UV-vis spectrum of the unmodified GNPs. As already reported in the literature [82], this spectroscopic characteristic is attributed to the polystyrene chains of GNPs. The latter was also confirmed indirectly by the absence of an absorption peak in this range for a sample containing only free β-CDs dissolved in water. Due to the presence of this absorption band, UV-vis spectroscopy did not

provide any evidence for the presence of HTZ-Ad in the NPs since the peak of HTZ-Ad, that falls in this range, is masked and not detectable. It could be noted that the spectrum of the functionalized GNPs has a less intense and narrowed band. This difference is likely attributed to the different concentration of the two samples. During the dialysis indeed, not only the unreacted HTZ-Ad is deposited at the bottom of the dialysis bag, but also some GNPs that tend to sediment for gravity over time. Thus, since only the supernatant was collected at the end of the dialysis, the suspension of functionalized GNPs is less concentrated than the inital suspension of unmodified GNPs.

The GNPs collected after functionalization, exhibited a broad fluorescence emission with a maximum at 420 nm, typical of HTZ-Ad. As expected, the untreated GNPs displayed a negligible fluorescence emission, very close to that of the baseline obtained with only water (*Fig. 21B*).

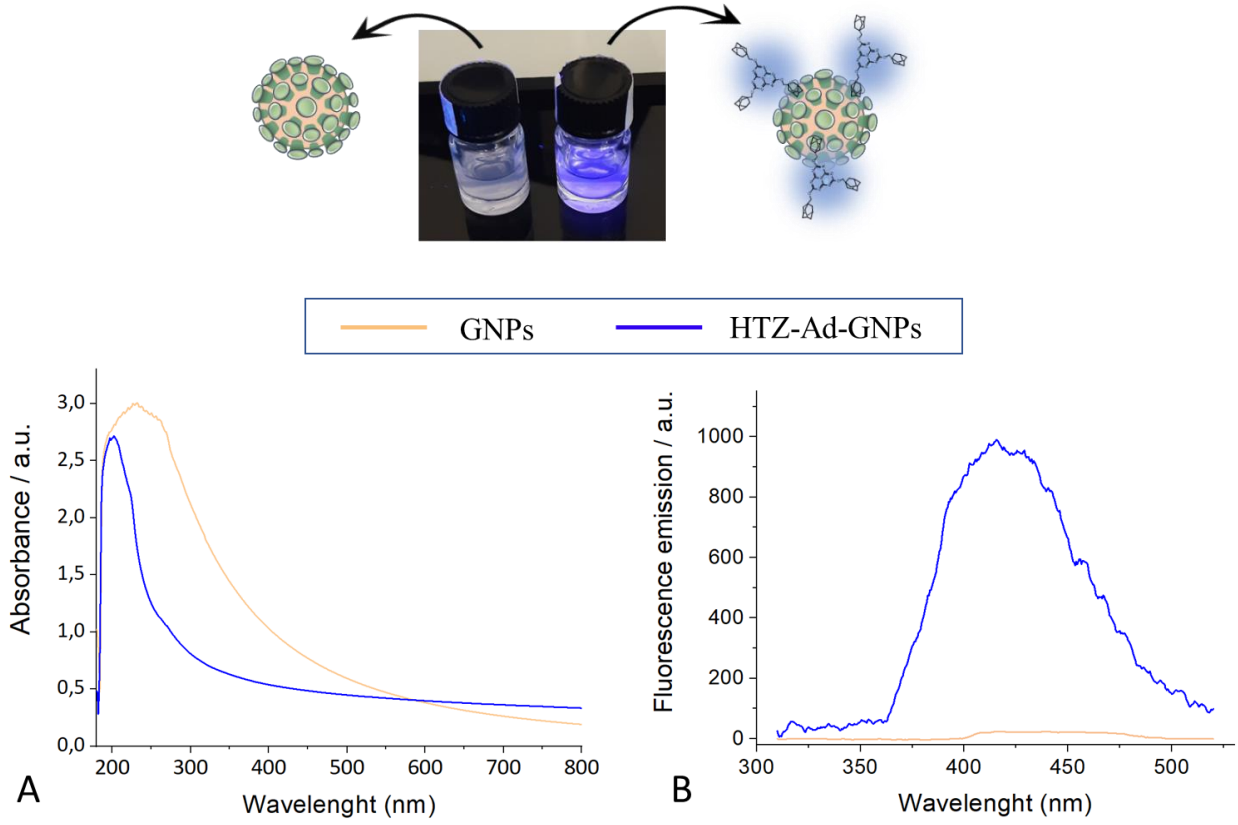

Fig. 21: A picture of the GNPs prior (left) and after functionalization (right) under UV irradiation (λ = 365 nm). A) UV-vis spectra (1:50 dilution) and B) fluorescence emission spectra collected at the excitation wavelength of 270 nm (1:1000 dilution) of the GNPs and HTZ-Ad-GNPs.

The fluorescence properties of the GNPs have been also investigated after their deposition on a solid support, in particular on a indium tin oxide (ITO) electrode. This electrode consists of a thin layer of ITO (100 nm) deposited on a quartz or borosilicate glass substrate (0.5 mm). A polytetrafluoroethylene (PTFE) adhesive with a cut-out circular area of 3 mm diameter was attached on the surface of the ITO electrodes, in order to deposit NPs only in the delimited circular area (0.07 cm^2).

An image of ITO electrodes containing GNPs and HTZ-Ad-GNPs (50 µL) under UV lamp is reported in *Fig. 22*. Fluorescence microscopy was then carried out by acquisition of images from different spots of the surface of the two modified ITO supports. The microscope was equipped with a 4′,6-diamidino-2-phenylindole (DAPI) filter characterized by an excitation wavelengh of 340–380 nm and emission between 450–490 nm. This filter was used because its excitation and emission bands most closely match the ones of HTZ-Ad, and even though the excitation maximum of HTZ-Ad is centered at 270 nm, its absorption profile is rather wide with a long 'tail', as already mentioned earlier. As expected, the GNPs prior functionalization did not show any florescence. Conversely, the ITOs containing the GNPs functionalized with HTZ-Ad showed a bright blue fluorescence.

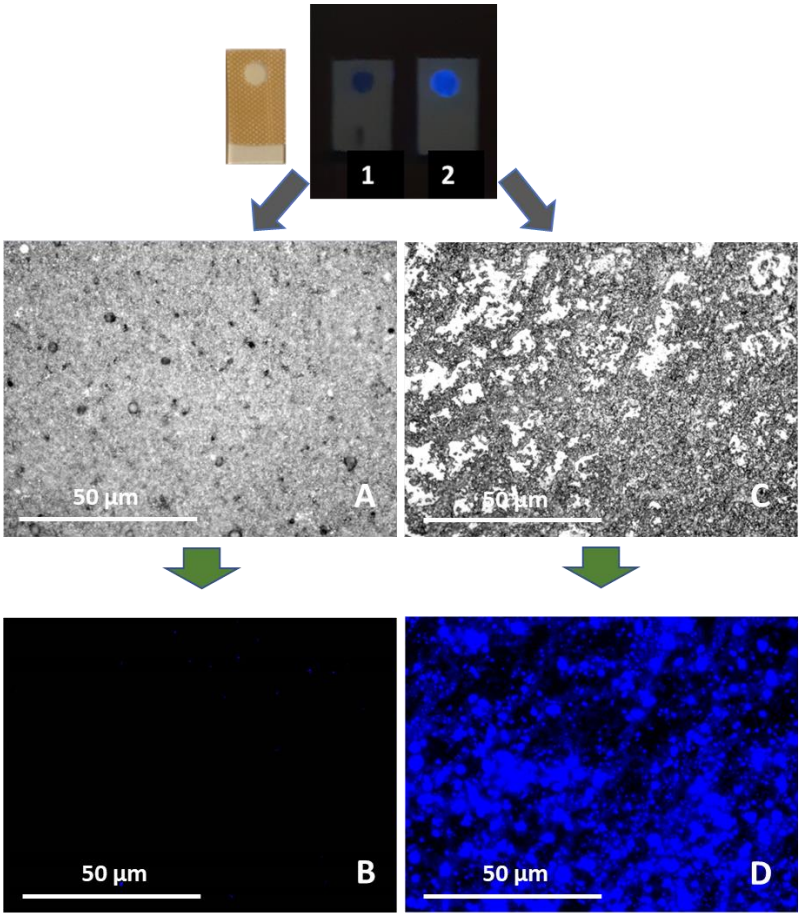

Fig. 21: a photo of ITO electrodes modified with a volume of 50 µL/0.07 cm^2 of 1) GNPs and 2) HTZ-Ad GNPs under irradiation at 254 nm. Below brightfield and fluorescence images were carried out with a DAPI filter and an exposition time of 5000 ms. A) Brightfield and B) fluorescence image of unmodified GNPs; C) brightfield and D) fluorescence images of HTZ-Ad-GNPs.

By observation of the brightfield images, obtained by deposition of the same volume of the respective suspensions (50 µL), it is clear once again that the concentration of the GNPs and HTZ-Ad in the aqueous suspension is different as a consequence of the sedimentation of some GNPs during the dialysis after functionalization. In particular, in the first case a complete coverage of the area of ITO surface is obtained. Other images were taken using a smaller volume of HTZ-Ad-GNPs (5 µL) deposited on ITOs to have a better spatial resolution. In these new set of images (*Fig. 22*), it is easier to note the overlap between the areas covered by the GNPs in the brightfield images and the fluorescent areas.

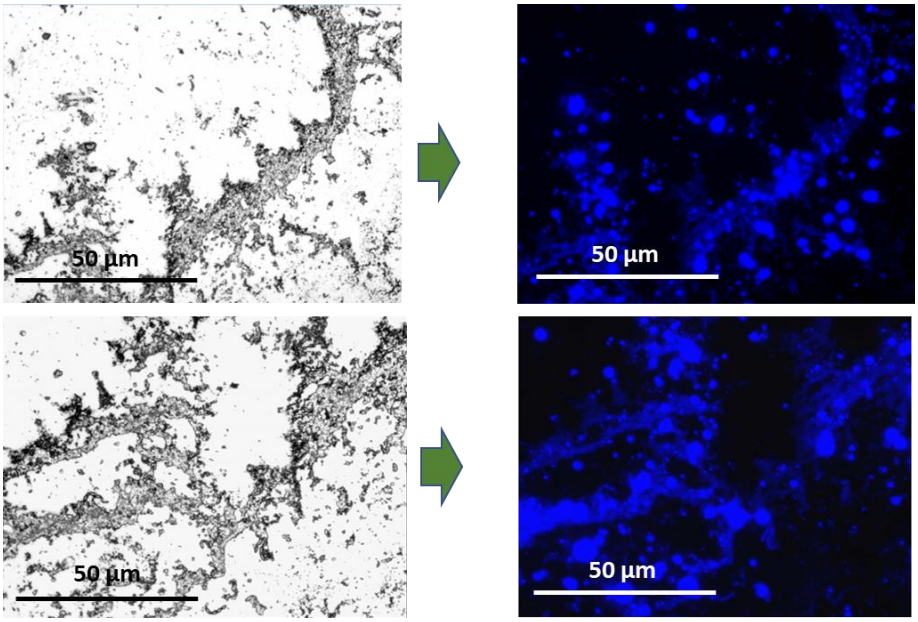

Fig. 22: brightfield and relative fluorescence images of HTZ-Ad-GNPs (5 µL/0.07 cm^2) carried out with a DAPI filter and an exposition time of 5000 ms.

Overall, the fluorescence of the HTZ-Ad-GNPs in suspension and on surface is a confirmation of the successfull functionalization of the GNPs with HTZ-Ad.

4. Immobilization of HTZ-Ad-GNPs on electrogenerated conductive polymers

The interaction of β-CD and Ad was also investigated in order to immobilize GNPs on a solid support. The concept envisaged consists in creating a polymer layer with Ad functional groups offering a possibility of fixing GNPs on the electrode surface. A poly(pyrrole-adamantane) film (PPY-Ad) has been already used by our team for the anchoring of gold nanoparticles modified by β-CDs [83]. The ability of the PPY-Ad film to anchor the GNPs derived from PS-b-βCD copolymer via host-guest interactions on the electrode and the possibility to use the immobilized NPs as a molecular platform for a further functionalization was thus explored.

4.1. Electropolymerization of N-substituted pyrrole monomers: overview

Conjugated and redox organic conducting polymers and copolymers are formed by oxidation of the monomeric constituents: heterocyclic compounds such as pyrrole, thiophene, thianaphthene, indole, furan and benzenoid and nonbenzenoid hydrocarbons such as pyrene, azulene, fluorene, fluoranthene [84]. They have been studied for years since their discovery in 1977 [85] in both academia and industrial research for their various applications in energy conversion and storage systems, opto-electronic devices [86]. In particular, conducting polymers such as poly(thiophene), poly(para-phenylene vinylene), poly(carbazole), polyaniline and polypyrrole, have been employed for the formation of anti-corrosion and anti-static coatings [87], for the constitution of batteries [88], supercapacitors [89], sensors [90] photovoltaic cells [91] and light emitting diodes [92]. They offer adavantages related to their chemical diversity, tunable structural flexibility and electronic properties and the possibility to control their architectures at the nanoscale [86].

Due to their noteworthy properties, conductive polymers have definitely become one of the most promising electrode material. Conducting polymers are generated on the electrode surface with good adhesion and electrical contact either by chemical or electrochemical polymerization [93]. In the second case, the polymer is formed directly on the electrode from the monomeric constituents by anodic oxidation. Electrochemistry is generally preferred because it enables a better control over the morphology and thickness and enables spatial addressing on conductive surfaces regardless of their size and shape [93]. This can be achieved using different methods [94]: potentiostatic, galvanostatic and potentiodynamic (cyclic voltammetry) using a three electrodes system. The film properties can be controlled by varying some

parameters, for instance the type of counter ion in the electrolytic medium, the potential applied, the number of scan and potential window in the case of cyclic voltammetry, or the electrolysis charge in the case of chronoamperometry. The electrogeneration of films can be carried out both in aprotic solvents, like acetonitrile, or in protic ones, like water, at neutral pH. Via the electrochemical polymerization, the modified electrode is ready for usage, differently from the chemical polymerization that requires additional procedures (such as the use of blinders) for the attachment of the layer on the electrode surface.

Some polymers contain redox organic compounds as pendant groups covalently bound to the backbone, like polyvinylferrocene. In this case the electron transfer occurs by an electron hopping process, a process of sequential self-exchange steps between adjacent redox groups [94]. Otherwise, the conductivity of conjugated polymers that present an extensive alternation of double bonds, results from the presence of charged species that can move along the carbon chain of the polymer (charge delocalization) ensuring the charge transport [94]. These charges derive from the chemical treatment with oxidants, typically iodine or bromine, or reducing agents like alkali metals, or from the incorporation of charge species included those of the counter ion from the electrolytic solution during the electrochemical polymerization.

The polymers originated from pyrroles are the most extensively studied [95], they have good redox properties, high conductivity and environmental stability in the oxidized form [96]. Compared to other conducting polymers, polypyrrole (PPY) shows a better flexibility and higher mass density. For this reason, it is recently attracting increasing interest in the development of high performance, light-weight and flexible sensors and wearable devices [96].

During the electropolymerization, the pyrrole monomer, dissolved in an appropriate solvent containing an electrolyte, is oxidized at the electrode surface by application of an anodic potential forming a reactive π-radical cation. Acetonitrile or propylene carbonate are often used as medium because of their good ionic conductivity and very large potential windows. Importantly, both solvent and electrolyte should be stable at the oxidation potential of the monomer [92]. In the following step, the cation reacts with another neutral monomer, or monomeric or oligomeric radical cation, to form a dimeric radical cation by losing a proton [58]. Both dimers and oligomers are characterized by an oxidation potential lower than the one of the monomer thus, after the initiation or nucleation phase, the growth of the film tend to proceeds by a chain propagation via oxidation, coupling and deprotonation. When the length of the polymer and consequently its solubility overpasses a certain limit, the polycationic

polymer precipitates on the surface of the electrode [92]. The monomer units in the final PPY structure are linked primarily via their α,α′-positions [84]. During the polymerization, the counter anion in the electrolytic medium is incorporated in the film to ensure its electrical neutrality. Elemental analyses conducted on the film have shown that approximatively one anion every four pyrrole units is incorporated in the film and thus, the structure of the polymer is not neutral but cationic [92]. Other collateral reactions could take place, for instance crosslinking and/or over-oxidation of the polymer are common since the oxidation of the monomer occurs at a higher potential than the redox events linked with polymer growth. β-coupling can occur and determine a decrease in conductivity [84]. The mechanism responsible for the electropolymerization is reported in *Fig. 23*.

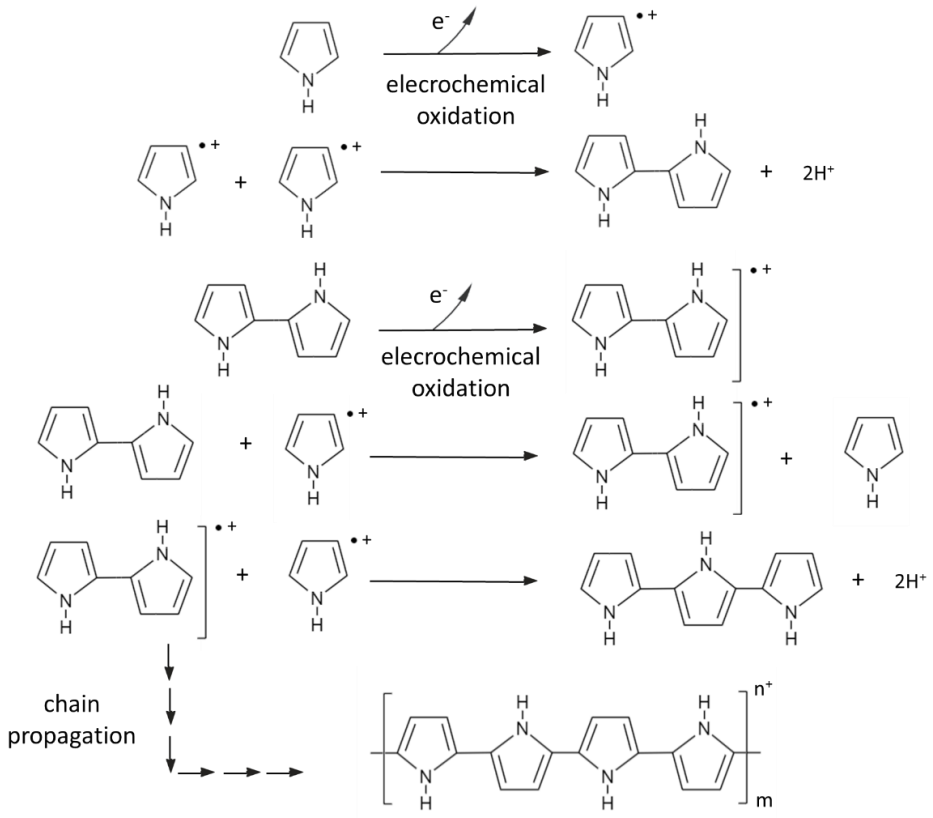

Fig. 23: mechanism of electropolymerization to form a polypyrrole film.

As already stated, the mechanical, electrical, optical, and physical properties of the film are highly dependent upon the chemical nature of the monomer and substituents, the type of electrolyte and solvent, the experimental conditions used for the polymerization [97], and of course, it is also possible to chemically modify the polymeric backbone after polymerization [92].

The size of the anion controls the structure, morphology and the porosity of the film [98]. For instance, surface roughness becomes higher when chloride and sulfate counter anions are used while it is smaller when perchlorate is used. Anions with higher basicity decrease the conductivity of the polymer because the interactions between the positive charges and the anions are reinforced decreasing the charge delocalization [92]. The presence of substituents can affect the electropolymerization reaction by either a steric effect or an electronic effect. For instance, substitution in the β-position prevents β-couplings determining a polymer with higher crystallinity. The presence of bigger substituents creates polymer with lower conductivity and lower mean conjugation length [99]. The presence of halogen atoms can increase the charge delocalization and thus the doping level [100].

4.2. Immobilization of GNPs on poly(pyrrole-adamantane) (PPY-Ad) electrogenerated on ITO electrodes

PPY films can be formed in a variety of electrodes: glassy carbon, platinum, gold and tin or indium–tin oxide (ITO) coated glass [92]. In order to promote the immobilization of the GNPs on the electrode, a pyrrole monomer containing a terminal adamantyl group was chosen for the electrepolymerization: adamantyl-11-pyrrolyl-1-undecyl carboxylic acid amide or pyrrole-adamantane (PY-Ad).

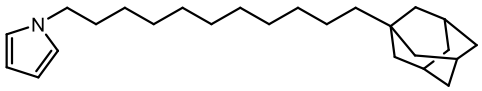

Fig.24: adamantyl-11-pyrrolyl-1-undecyl carboxylic acid amide (PY-Ad).

A poly(pyrrole-adamantane) film (PPY-Ad) was electrogenerated on ITO electrodes from a 3 mM solution of the PY-Ad monomer that was dissolved in acetonitrile containing 0.1 M $LiClO_4$ as electrolyte. This concentration of the monomer and type of electrolyte have been used previously by Holzinger et coworkers for modifying platinum electrode [83]. Initially, the oxidative electropolymerization was carried out by cyclic voltammetry in order to check the optimal experimental conditions and especially the oxidation potential suitable for the polymerization. The applied potential is critical for the formation of radical cations and for the nucleation reaction that allows the growth of the polymer, and it is strongly dependent on the electrode material so it should be determined experimentally.

For this reason, cyclic voltammetry was firstly conducted using a wide potential window (from 0 to +1.2 V/+1.3 V vs Ag/Ag^+ at 100 mV s^{-1}) using a platinum wire as the counter electrode, an Ag/Ag^+ (0.01 M $AgNO_3$ + 0.1 M $LiClO_4$) as a reference electrode. The cyclic voltammogram exhibits a sharp irreversible peak at +1 V corresponding to the oxidation of the pyrrole group and the formation of a film on the electrode, which is also visually observable as a light grey film on the ITO surface initially transparent.

If the potential chosen for the electropolymerization is too low, no polymeric film will be formed, but if it is too high, chemically irreversible follow-up reactions can occur. A potential located at approximatively one third of the height of the anodic oxidation wave is usually chosen for the electropolymerization (in this case +1 V). The PPY-Ad film was then formed by controlled potential electrolysis at +1 V with a limited electrolysis charge of 2.5 mC cm^{-2}.

The film was then characterized in fresh electrolytic solution free of monomer. The resulting electrode shows a reversible peak system at $E_{1/2}$ = +0.27 V with an anodic–cathodic peak separation of 0.04 V (*Fig. 25*) which corresponds to the electroactivity of the PPY-Ad film.

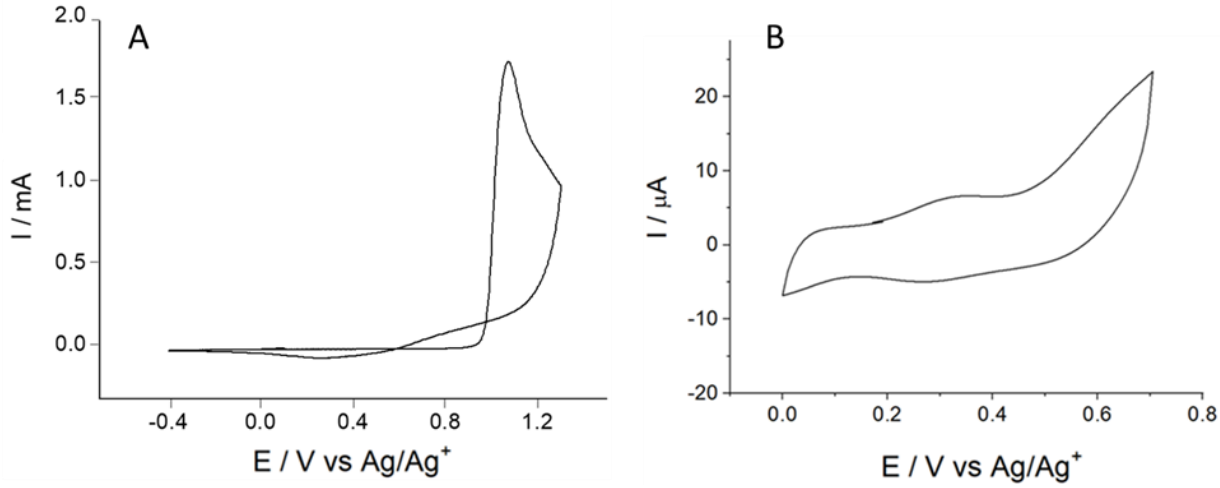

Fig. 25: A) oxidative electropolymerization of pyrrole-adamantane (3 mmol L^{-1}) in CH_3CN + $LiClO_4$ 0.1 mol L^{-1} by one cycle recorded at an ITO electrode. Scan rate: 100 mV s^{-1}.
B) Voltammogram of an ITO electrode that, after electropolymerization conducted with applied potential: +1 V vs Ag/Ag^+ and electrolysis charge: 2.5 mC cm^{-2}, was transfered in CH_3CN + $LiClO_4$ 0.1 mol L^{-1} free of monomer. Scan rate: 100 mV s^{-1}.

ITO electrodes were then prepared to study the anchoring of GNPs to the surface of the film via the inclusion of the polymerized adamantane groups with the β-CD shell of the GNPs. The immobilized layer of nanoparticles will then be applied to the immobilization of HTZ-Ad and the use of this dye as a bridge between nanoparticles.

After the formation of the PPY-Ad film, the ITO electrodes were covered with a PTFE adhesive in order to delimitate a circular area of 3 mm diameter (0.07 cm^2). GNPs (non functionalized) were deposited on the circular area of the ITO electrodes (50 µL) and after rinsing, the electrodes were immersed vertically in a glass vial containing 0.66 mg mL^{-1} of HTZ-Ad in EtOH/H_2O (70:30) v/v% for 1 hour under mild agitation followed by extensive rinsing. For some electrodes, the process of deposition of the GNPs and incubation with HTZ-Ad was repeated twice or three times. One control electrode, after the formation of the PPY-Ad film, was placed directly in the HTZ-Ad solution without deposition of GNPs. The fluorescence of the different ITO electrodes were verified under UV lamp at 254 nm (*Fig. 26*).

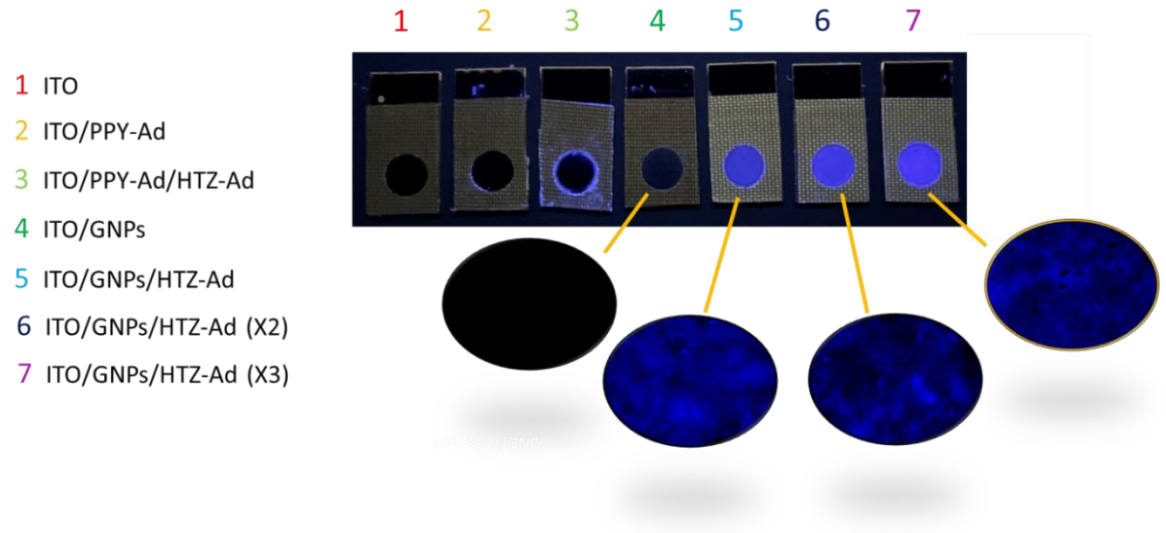

Fig. 26: different modified ITO electrodes under 254 nm:
1) a non-modified ITO, 2) an ITO covered only by a PPY-Ad film, 3) an ITO electrode that after the formation of the PPY-Ad polymer, was subsequently immersed in a solution of HTZ-Ad (0.66 mg mL^{-1}) for 1 hour. 4) after the electropolymerization of PY-Ad, 50 µL of the suspension of GNPs were deposited on the circular area. Then, the electrode was immersed in the solution of HTZ-Ad for 1 hour. The deposition of GNPs and incubation with HTZ-Ad was repeated 5) twice or 6) three times.
Below: fluorescence images of the surface of some differently modified ITO electrodes carried out with a DAPI filter.

No fluorescence was observed in the ITO electrode only modified by the PPY-Ad film. The incubation of the polymer with heptazine or the GNPs alone resulted in non fluorescent electrodes as well. In contrast, the electrodes containing the GNPs deposited on the polymer and incubated subsequently with HTZ-Ad showed a bright fluorescence. When the process of deposition of GNPs and heptazine incubation was repeated more than once, the fluorescence

appeared even brighter. Fluorescence images were acquired from the surface of some of the modified ITO electrodes using DAPI as a filter as described previously (*Fig. 26*).
These results demonstrate that HTZ-Ad can be stably attached to electrodes only when a layer of GNPs is present on the PPY-Ad surface while no adsorption of HTZ-Ad is observed on the PPY-Ad in absence of GNPs.

4.3. Immobilization of GNPs on PPY-Ad electrogenerated on interdigitated electrodes (IDEs)

The possibility to spatially control the immobilization of the GNPs on PPY-Ad was further investigated using a gold interdigitated microelectrode. A scheme of the structure of the interdigitated electrode, as well as an optical image of its surface, is reported in *Fig. 27*. The electrode is composed by two different working electrodes, each one is formed by a series of microbands (with 20 µm thickness) which are interdigitated in the central portion with a comb like arrangement. These type of electrodes (IDEs) are often used for sensing applications [100, 101] because of the increased area of contact and reduced distance between the electrodes. The modification of only one working electrode, that is one half of the interdigitated electrode array, with a PPY-Ad film and successively GNPs and heptazine, will offer a pattern with a spatial resolution and visual contrast between the functionalized and non functionalized areas.

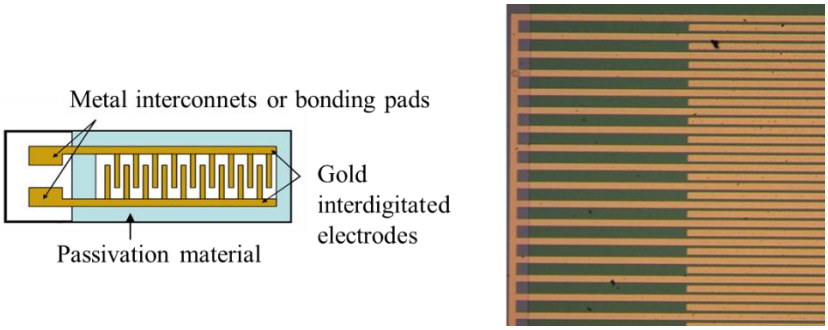

Fig. 27: representation of a gold interdigitated electrode. On the right, an optical image of a portion of the electrode showing one working electrode made with multiple microbands that is interdigitated with the working electrode of the opposite side in the central part of the electrode.

The electropolymerization of the PPY-Ad film was carried out from a 3 mM solution of the monomer, PY-Ad, in CH_3CN containing 0.1 M $LiClO_4$ by using only one of the working electrodes that compose the interdigitated array (by electrical connection of only one of the gold pads). As already done with ITO electrodes, a first characterization of the optimal

electropolymerization conditions was done by performing two cycles with a wide potential window (from 0 to +1.3 V vs Ag/Ag^+). During the first cycle, the anodic peak increases sharply starting from +0.8 V vs Ag/Ag^+ and then, a cathodic wave is generated at +0.8 V, similarly to what observed on ITO electrodes, due to the reduction of protons released during the polymerization process [84]. In the following cycle, the pyrrole oxidation wave is decreased due to the passivation of the electrode with a PPY-Ad film (*Fig. 28A*).

In this case, the PPY-Ad film was formed on novel IDEs electrodes by cyclic voltammetry in order to form a film with considerable thickness that could be clearly visible for further microscopy analysis. An upper potential of +0.84 V vs Ag/Ag^+ (which is the potential located approximately at one third of the anodic oxidation current in the first cycle of *Fig. 28A*) was set for the electropolymerization that was carried out by cycling 20 times between 0 V and +0.84 V vs Ag/Ag^+. Upon consecutive cycling, the reversible peak system at $E_{1/2}$ = +0.39 V, that is attributed to the electroactive PPY-Ad film, was increasing slightly after each cyle due to the continuous growth of the film (*Fig. 28B*).

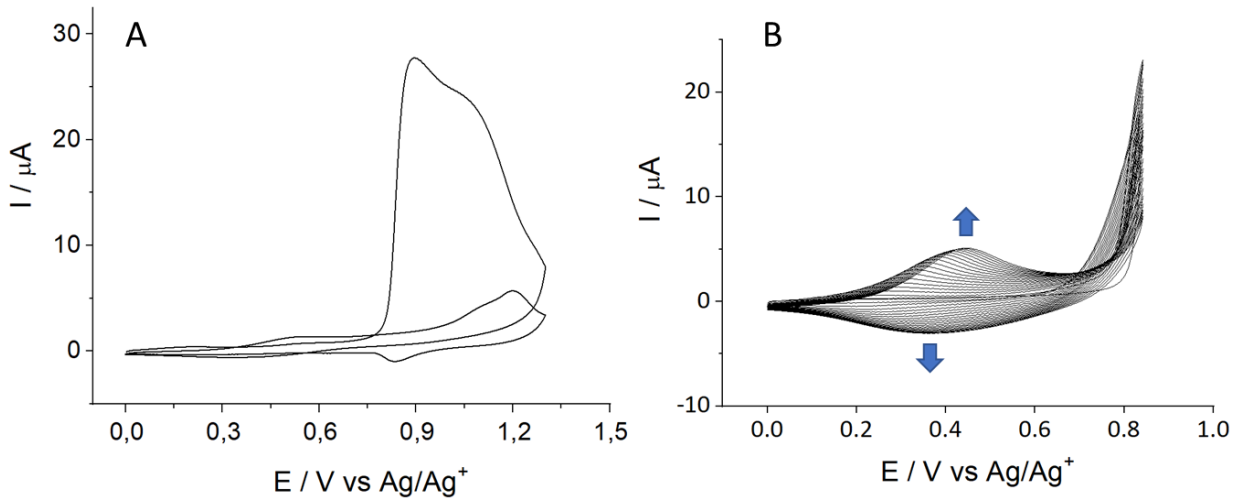

Fig. 28: Electropolymerization by cyclic voltammetry with wide potential window and B) oxidative electropolymerization by 20 cycles between 0 V and +0.84 V vs Ag/Ag^+ recorded at a gold interdigitated microelectrode in CH_3CN + $LiClO_4$ 0.1 mol L^{-1}. Scan rate: 100 mV s^{-1}.

After the electropolymerization, the IDEs have been analyzed by optical microscopy to check the correct formation of the polymer only on one side of the interdigitated array. The surface of the IDE displayed darker brown stripes, the portions covered by a thick polymer formed by cyclic voltammetry, alternated to lighter stripes which belong to the bare working electrode of the opposite side *(Fig. 29)*.

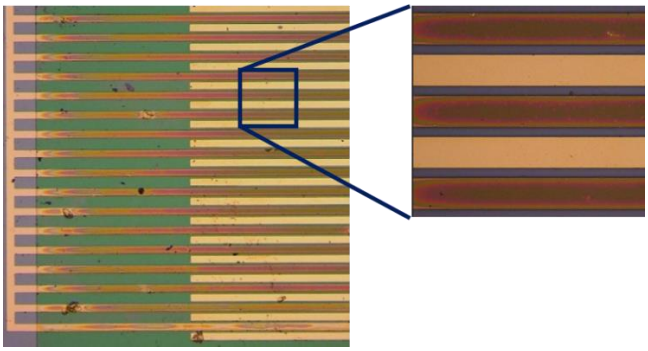

Fig. 29: an optical image of the surface of the interdigitated electrode after the formation of PPY-Ad only on one working electrode of the gold interdigitated electrode.

The IDEs modified in this way, have been further functionalized in successive steps. First, they were placed in a small eppendorf containing 300 µL of the suspension of GNPs and kept under mild agitation overnight. After rinsing with water, the electrodes were immersed in a solution containing 0.66 mg mL^{-1} of HTZ-Ad in EtOH/H_2O (70:30) v/v% for 1 hour under stirring and finally rinsed again with EtOH and water to remove traces of adsorbed heptazine. The electrodes were then analyzed by fluorescence microscopy in the same conditions described previously. In the brightfield images of *Fig. 30*, the darker stripes are the portions covered by the polymer while the white stripes belong to the bare electrode. When the fluorescence image is acquired, only the stripes covered by the polymer appeared as fluorescent.

This result is in agreement with those obtained on ITO electrodes and in particular, it is a confirmation of the specificity of the heptazine-adamantane interaction that requires the presence of the GNPs with β-CDs exposed at the surface. Moreover, the attachment of the GNPs on the polymer is also specific and determined by formation of host-guest interactions. The inclusion complexes are established during the incubation of the electrodes in the GNPs suspension under stirring, differently from the experiments done on ITO electrodes, where the GNPs were deposited on the polymer. Thus, the localized fluorescence is the result of host-guest interactions between HTZ-Ad on GNPs which in turn are immobilized on the polymer.

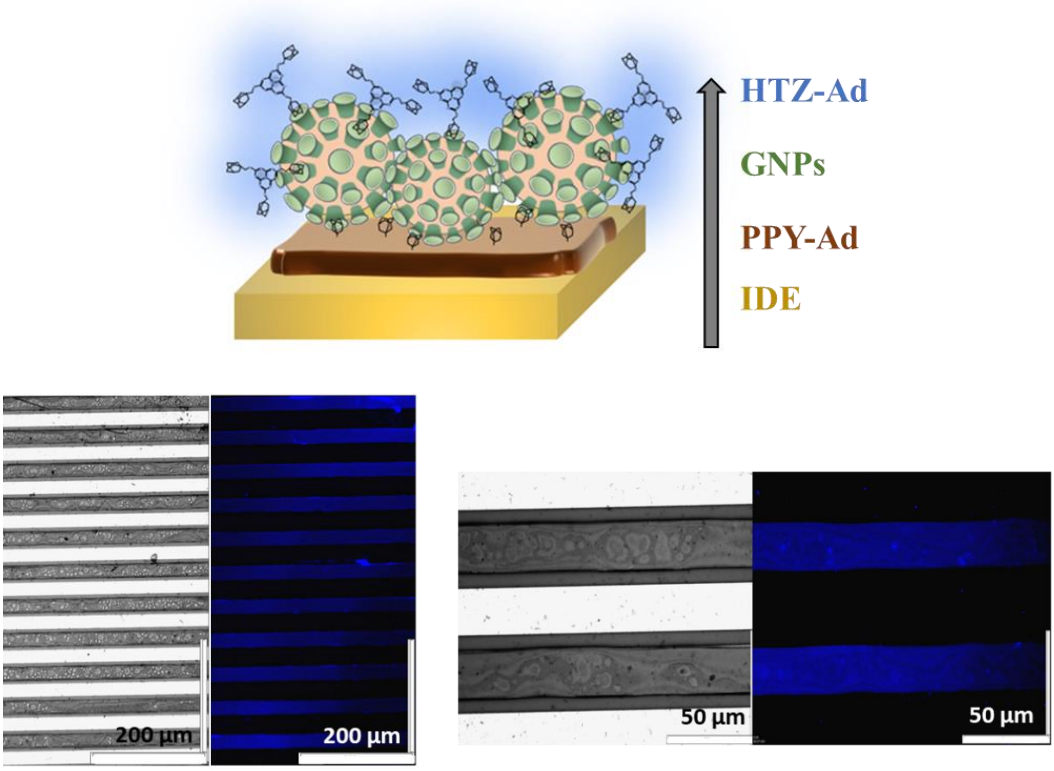

Fig. 30: on the top, a scheme of the three-dimesional architecture of the modified gold interdigitated electrode modified by the PPY-Ad polymer, GNPs and then HTZ-Ad. On the bottom, brightfield and fluorescence images of a portion of the interdigitated electrode. The fluorescence images have been carried out with a DAPI filter and an exposition time of 5000 ms.

The same concept was then applied to the immobilization of the functionalized HTZ-Ad-GNPs. One side of the interdigitated microelectrode modified with PPY-Ad, was immersed overnight in the suspension of unmodified GNPs and finally, after rinsing, in the suspension of HTZ-Ad-GNPs for a further night under mild agitation. The electrode was again rinsed with water and brightfield and fluorescence images were acquired from different spots of the electrode (*Fig. 31*).

The images are very similar to the ones obtained by incubation with HTZ-Ad. Only the darker stripes, corresponding to the areas covered by the polymer, exhibited a bright blue fluorescence. Again, the localized fluorescence can be explained by the binding of the heptazine-functionalized GNPs with the unmodified GNPs anchored by the Ad groups of the polymer. These unmodified GNPs indeed exhibit available β-CDs at the interface electrode-solution.

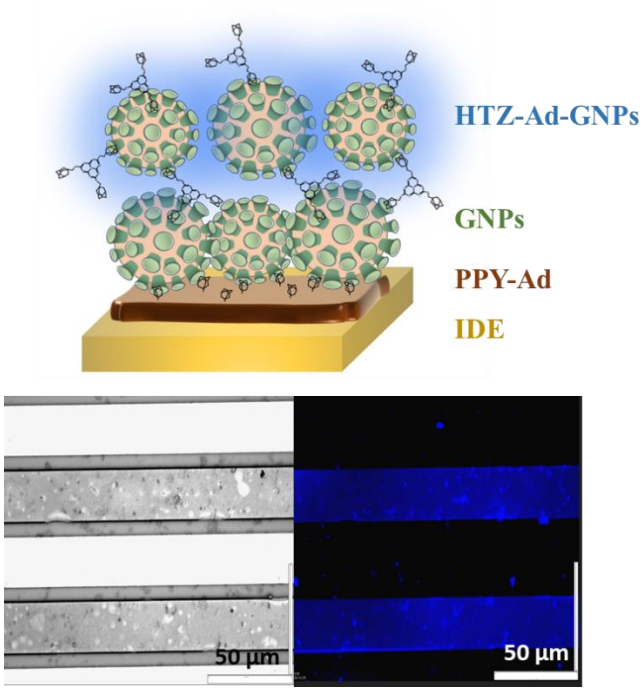

Fig. 31: on the top, a scheme of the three-dimensional structure of an interdigitated electrode modified successively by PPY-Ad polymer, GNPs and finally HTZ-Ad-GNPs. On the bottom, brightfield and fluorescence image of a portion of the modified electrode (using a DAPI filter and exposition time of 5000 ms).

Some control electrodes have been made as well. After the formation of the PPY-Ad polymer, one electrode has been incubated with the suspension of unmodified GNPs and then analyzed without any further modification (*Fig. 32A*). Another electrode was instead directly incubated with HTZ-Ad (0.66 mg mL^{-1} in ethanol/water (70:30) v/v%) after the formation of the PPY-Ad film, without the intermediate step of incubation with the GNPs (*Fig. 32B*).

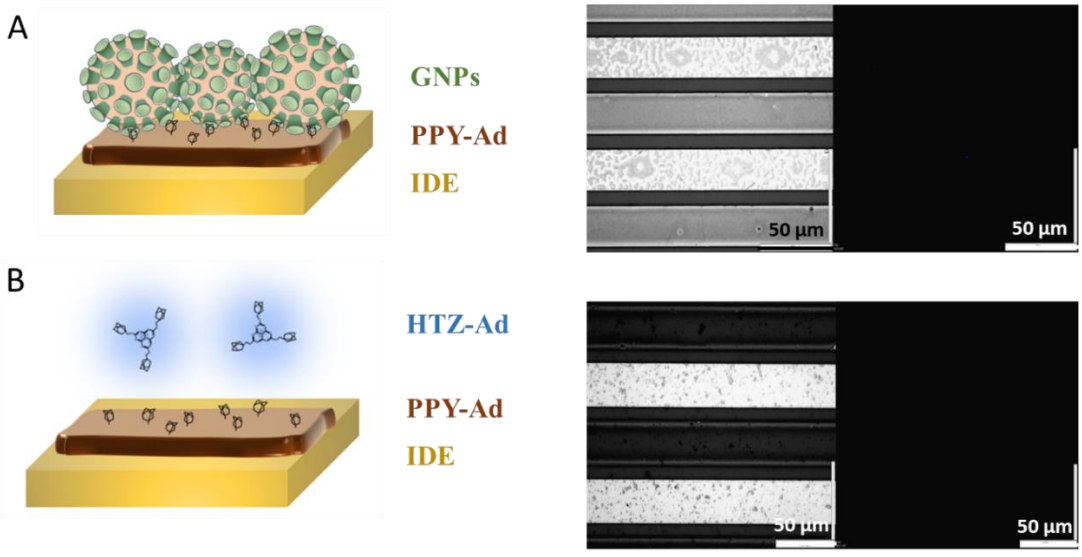

Fig. 32: brightfield and fluorescence image of a portion of the interdigitated electrode modified by A) PPY-Ad and then GNPs and by B) PPY-Ad film and then immersed for 1 hour with a solution of HTZ-Ad (0.66 mg mL^{-1} in ethanol/water (70:30) v/v%). Fluorescence imaging was carried out with a filter DAPI and an exposition time of 5000 ms.

In both cases, no fluorescence is displayed from the surface of the IDEs. While, the absence of fluorescence in absence of HTZ-Ad is expected, in the second case, it demonstrates that the presence of the GNPs, anchored on the polymer in the first modification step, is fundamental for the successive binding of HTZ-Ad on the electrode in the following step. Overall, the formation of specific affinity interactions between Ad and β-CDs result in the formation of a tridimensional structure that is located only on the PPY-Ad electrode areas.

In these experiments, 1 hour of incubation with HTZ-Ad followed by an overnight incubation with the GNPs were sufficient to produce a bright fluorescence that is distributed over the whole modified surface of the electrode stripes. Since the interaction between adamantane and β-cyclodextrin is characterized by a high affinity constant ($K_a = 10^5\ M^{-1}$), the chosen incubation time was sufficient to determine a complete coverage of the surface. To investigate the host-guest interaction in a bit more detail, a competition between two guest molecules for inclusion in the adamantane motifs was undertaken.

For this purpose, an IDE was modified successively by the polymer and the unmodified GNPs as already described, but then immersed in the following step in an aqueous solution containing a saturating concentration of biotin for 2 hours. Biotin has a binding affinity for β-CD, but with an association constant ($K_a = 10^2\ M^{-1}$) much lower than that of adamantane. The electrode was transferred in a vial containing HTZ-Ad (0.66 mg mL^{-1} in $EtOH/H_2O$ (70:30) v/v%) under mild stirring. The progressive substitution of biotin from the β-CDs of the GNPs with the Ad groups of HTZ-Ad has been followed by acquisition of fluorescence images of the surface of the electrode at different incubation times (*Fig. 33*).

After 15 minutes, the image appeared as almost dark and barely any fluorescence is detected. After 30 minutes, a weak fluorescence is observed in the areas covered by the polymer, it is not homogeneous but more appreciable in certain areas of the electrode stripes. Finally after 1 hour, the fluorescence was again bright and homogeneous, meaning that all the available sites have been bond by the excess of HTZ-Ad in the solution.

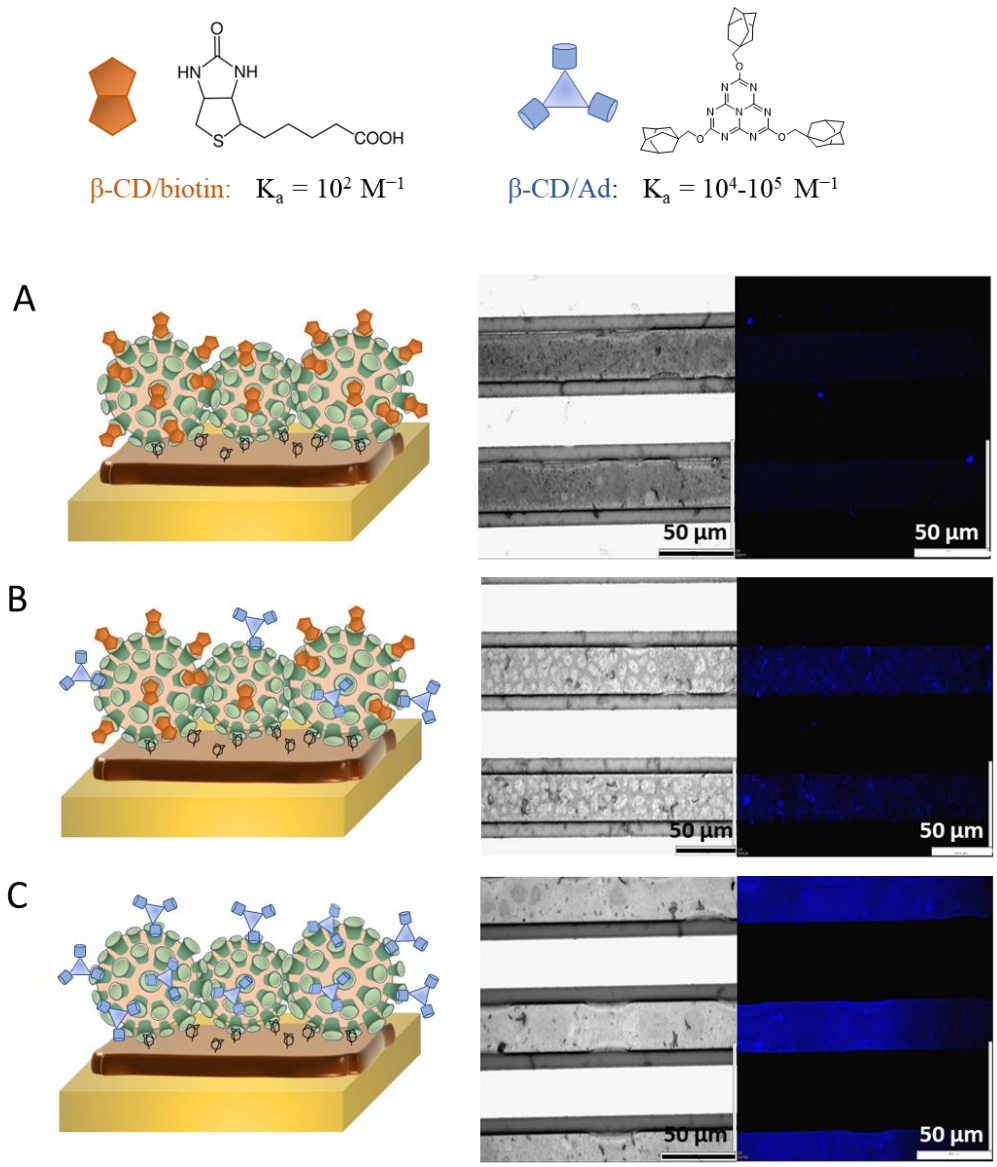

Fig. 33: A succession of brightfield and fluorescence images of an IDE acquired (with a DAPI filter and exposition time of 5000 ms) after A) 15minutes, B) 30 minutes or C) 60 minutes from the transfer inside the HTZ-Ad solution (0.66 mg mL^{-1} in ethanol/water (70:30) v/v%). Prior HTZ-Ad, the electrode had been immersed in a 1mM solution of biotin in water for 2 hours.

5. Conclusion

The formation of inclusion complexes between the Ad groups of a fluorescent compound, HTZ-Ad, and β-CDs led to the first spectroscopic characterization of HTZ-Ad in water by significant improvement of its solubility. Via β-CDs, the properties of heptazines can be transferred easily in aqueous medium opening future perpectives for applications in water splitting or photocatalysis. The β-CD/Ad interaction was then explored for the post-functionalization of GNPs obtained from the self-assembly of a polystyrene-block-β-

cyclodextrin copolymer. The poor solubility of the free HTZ-Ad in water provided a way to separate the unreacted compound from the GNPs during the procedure of functionalization. The successful functionalization of the GNPs with HTZ-Ad was confirmed by the acquisition of fluorescent properties by the GNPs, in particular by analysis of the fluorescence emission of the suspension of GNPs and by fluorescence imaging of the HTZ-Ad-GNPs deposited on a ITO electrode.

An approach for the functionalization of electrode surfaces with heptazine has been illustrated by using GNPs anchored on an electrogenerated polymer film, poly(pyrrole-adamantane) exploiting host-guest interactions. The functionalization with heptazine can also be confined in space as demonstrated by fluorescence imaging of some interdigitated electrodes that contain the poly(pyrrole-adamantane) film only on alternating portions of the electrode. In particular, GNPs anchored to the underlying polymer were able to bind both the free HTZ-Ad in solution and the HTZ-Ad associated with the post-functionalized GNPs. Thus, the construction of fluorescent nanostructured assemblies can be achieved using GNPs and organic functional polymeric films as substrates. More generally, this approach is a valuable tool for the design of functionalized patterned three-dimensional electrode surfaces.

Bibiliography

(1) József S. «Introduction and general overview of cyclodextrin chemistry». *Chemical reviews.* (1998) 98, 5, 1743-1754.

(2) Singh M., Sharma R., Banerjee U. C. «Biotechnological applications of cyclodextrins». *Biotechnology Advances.* (2002) 20, 5-6, 341-359.

(3) Del Valle E. M. «Cyclodextrins and Their Uses: A Review». *Process Biochemistry.* (2004) 39, 9, 1033–46.

(4) Nisar Ahmad K., Durakshan M. «Cyclodextrin: An Overview». *International Journal of Bioassays.* (2013) 2, 6, 858-865.

(5) Sambasevam K. P., Mohamad S., Sarih N. M., Ismail N. A. «Synthesis and Characterization of the Inclusion Complex of β-Cyclodextrin and Azomethine». *International Journal of Molecular Sciences.* (2013) 14, 2, 3671–3682.

(6) Fujishima N., Kusaka K., Umino T., Urushinata T., Terumi K. «Flour based foods containing highly branched cyclodextrins». *Japanese Patent JP.* (2001) 136, 898.

(7) Hedges R. A. «Industrial applications of cyclodextrins». *Chem. Rev.* (1998) 98, 2035-2044.

(8) Holland L., Rizzi G., Malton P. «Cosmetic compositions comprising cyclic oligosaccharides and fragrance». *PCT Int Appl WO.* (1999) 67,716.

(9) Bhardwaj R., Dorr R. T., Blanchard J. «Approaches to reducing toxicity of parenteral anticancer drug formulations using cyclo-dextrins». *J. Pharm. Sci. Technol.* (2000) 54, 233-239.

(10) Lezcano M., Ai-Soufi W., Novo M., Rodriguez-Nunez E., Tato J. V. «Complexation of several benzimidazole-type fungicides with alpha and beta-cyclodextrins» *J. Agric. Food Chem.* (2002) 50, 108-112.

(11) Dufosse L., Souchon I., Feron G., Latrasse A., Spinnler H. E. «In situ detoxification of the fermentation medium during gamma-decalactone production with the yeast Sporidiobolus salmonicolor» *Biotechnol. Prog.* (1999) 15, 135-139.

(12) Zhang J., Ma P.X. «Cyclodextrin-Based Supramolecular Systems for Drug Delivery: Recent Progress and Future Perspective». *Advanced Drug Delivery Reviews.* (2013) 65, 9, 1215–1233.

(13) Saenger W., Steiner T. «Cyclodextrin inclusion complexes: host–guest interactions and hydrogen-bonding networks». *Acta Crystallographica.* (1998) 54, 6, 798-805.

(14) Bar R. «Cyclodextrin aided bioconversions and fermentations». *Trends Biotechnol.* (1989) 7, 2-4.

(15) Ekberg B., Anderson L., Mosbach K. «The synthesis of an active derivative of cyclomalto hexose for the hydrolysis of esters and the formation of amide bonds». *Carbohydr. Res.* (1989) 192, 111-117.

(16) Atwood J. L. «Inclusion phenomenon and molecular recognition». *Springer Science & Business Media.* (2012)

(17) Hedges R. A. «Industrial applications of cyclodextrins». *Chem. Rev.* (1998) 98, 2035-2044.

(18) Ferancová A., Labuda, J. «Cyclodextrins as electrode modifiers». *Fresenius' journal of analytical chemistry*. (2001) 370, 1, 1-10.

(19) Gaied A., Jaballah N., Tounsi M., Braiek M., Jaffrezic-Renault N., Majdoub M. «Selective Detection of Dopamine in Presence of Ascorbic Acid by Use of Glassy-Carbon Electrode Modified with Amino-β-Cyclodextrin and Carbon Nanotubes». *Electroanalysis*. (2014) 26, 12, 2747-2753.

(20) Feng W., Liu C., Lu S., Zhang C., Zhu X., Liang Y., Nan J. «Electrochemical chiral recognition of tryptophan using a glassy carbon electrode modified with β-cyclodextrin and graphene». *Microchimica Acta*. (2014) 181, 5, 501-509.

(21) Ogoshi T., Harada A. «Chemical sensors based on cyclodextrin derivatives». (2008) *Sensors*. 8, 8, 4961-4982.

(22) Yilmaz G., Messager L., Gleinich A. S., Mitchell D., Battaglia G., Becer R. C. «Glyconanoparticles with controlled morphologies and their interactions with a dendritic cell lectin». *Polymer Chemistry.* (2016) 7, 6293-6296.

(23) Epps I. I. I. T. H., O'Reilly R. K. «Block Copolymers: Controlling Nanostructure to Generate Functional Materials – Synthesis, Characterization, and Engineering». *Chemical Science.* (2016) 7, 3, 1674–1689.

(24) Soeriyadi A. H., Boyer C., Nyström F., Zetterlund P. B., Whittaker M. R. «High-Order Multiblock Copolymers via Iterative Cu(0)-Mediated Radical Polymerizations (SET-LRP): Toward Biological Precision». *J. Am. Chem. Soc.* (2011) 133, 11128–11131.

(25) Nomura K., Abdellatif M. M. «Precise synthesis of polymers containing functional end groups by living ring-opening metathesis polymerization (ROMP): efficient tools for synthesis of block/graft copolymers». *Polymer*. (2010) 51, 1861–1881.

(26) Hadjichristidis N., Pitsikalis M., Iatrou H. «Synthesis of block copolymers». *Block Copolymers I*. (2005) 1-124.

(27) Golas P. L., Matyjaszewski K. «Marrying click chemistry with polymerization: expanding the scope of polymeric materials». *Chem. Soc. Rev.* (2010) 39, 1338–1354.

(28) Bates F. S., Hillmyer M. A., Lodge T. P., Bates C. M., Delaney K. T., Fredrickson G. H., «Multiblock Polymers: Panacea or Pandora's Box?». *Science*. (2012) 336, 434–440.

(29) Kedracki D., Safir I., Gour N., Ngo K., Vebert-Nardin C. «Bio-synthetic Polymer Conjugates». *Advances in Polymer Science. ed. Helmut Schlaad, Springer, Berlin Heidelberg*. (2013) 253, 181, 115–149.

(30) Li H., Mumtaz M., Isono T., Satoh T., Chen W. C., Borsali R. «Self-assembly of carbohydrate-based block copolymer systems: glyconanoparticles and highly nanostructured thin films». *Polymer Journal.* (2022) 54, 455–464.

(31) Luo Y., Liu L., Wang X., Shi H., Lv W., Li J. «Sugar-installed thermoresponsive micellar aggregates self-assembled from "coil-comb-coil" triblock glycopolymers: preparation and recognition with Concanavalin A». *Soft Matter*. (2012) 8, 1634-1642.

(32) Lim D. W., Yeom Y. I., Park T. G. «Poly(DMAEMA-NVP)-b-PEG-galactose as Gene Delivery Vector for Hepatocytes». *Bioconjugate Chemistry.* (2000) 11, 688.

(33) Dong C. M. «Glyconanoparticles for Biomedical Applications». *Combinatorial Chemistry & High Throughput Screening.* (2011) 14, 3, 173–181.

(34) Bae Y., Kataoka K. «Intelligent polymeric micelles from functional poly (ethylene glycol)-poly(amino acid) block copolymers». *Adv. Drug Deliv. Rev.* (2009) 61, 768-784.

(35) Chen Y., Dong C. M. «pH-Sensitive supramolecular polypeptidebased micelles and reverse micelles mediated by hydrogen-bonding interactions or host-guest chemistry: characterization and in vitro controlled drug release». *J. Phys. Chem. B* (2010) 114, 7461-7468.

(36) Batrakova E. V., Kabanov A. V. «Pluronic block copolymers: Evolution of drug delivery concept from inert nanocarriers to biological response modifiers». *J. Control. Release.* (2008) 130, 98- 106.

(37) Caldas B. S., Lazarin-Bidóia D., Nakamura C. V., Halila S., Borsali R., Muniz E. C. «Drug Carrier Systems Made from Self-Assembled Glyco-Nanoparticles of Maltoheptaose-b-Polyisoprene Enhanced the Distribution and Activity of Curcumin against Cancer Cells». *Journal of Molecular Liquids*. (2020) 309, 113022.

(38) Zepon K. M., Otsuka I., Bouilhac C., Muniz E. C., Soldi V., Borsali R. «Glyco-Nanoparticles Made from Self-Assembly of Maltoheptaose-block-Poly(methyl methacrylate): Micelle, Reverse Micelle, and Encapsulation». *Biomacromolecules.* (2015) 16, 7, 2012–2024.

(39) Peyret A., Trant J. F., Bonduelle C. V., Ferji K., Jain N., Lecommandoux S., Gillies E. R. «Synthetic Glycopolypeptides: Synthesis and Self-Assembly of Poly(γ-Benzyl- l -Glutamate)-Glycosylated Dendron Hybrids». *Polymer Chemistry.* (2015) 6, 45, 7902–7912.

(40) Newman M. J., Actor J. K., Balusubramanian M., Jagannath C. «Use of nonionic block copolymers in vaccines and therapeutics». *Critical Reviews™ in Therapeutic Drug Carrier Systems*. (1998) 15, 2.

(41) Pachota M., Kłysik-Trzciańska K., Synowiec A., Yukioka S., Yusa S. I., Zając, M., ... Nowakowska M. «Highly effective and safe polymeric inhibitors of herpes simplex virus in vitro and in vivo». *ACS applied materials & interfaces*. (2019) 11, 30, 26745-26752.

(42) Förster S. «Amphiphilic block copolymers for templating applications». *Colloid Chemistry I*. (2003) 1-28.

(43) Rodríguez-Hernández J., Chécot F., Gnanou Y., Lecommandoux S. «Toward 'Smart' Nano-Objects by Self-Assembly of Block Copolymers in Solution». *Progress in Polymer Science.* (2005) 30, 7, 691–724.

(44) Israelachvili. J. N. «Intermolecular and surface forces». *Academic Press.* (1992)

(45) Fessi H., Devissaguet J., Puisieux F., Thies C. «Method of formation of colloidal nanoparticles». *French Patent*. (1988) 2, 988.

(46) Alexandridis P., Lindman B. «Amphiphilic block copolymers: self-assembly and applications». *Elsevier.* (2000)

(47) Li X., Liu H., Li J., Deng Z., Li L., Liu J., Yuan J., Gao P., Yang Y., Zhong S. «Micelles via Self-Assembly of Amphiphilic Beta-Cyclodextrin Block Copolymers as Drug Carrier for Cancer Therapy». *Colloids and Surfaces.* (2019) 183, 110425.

(48) Carrière M., Buzzetti P. H. M., Gorgy K., Mumtaz M., Travelet C., Borsali R., Cosnier S. «Functionalizable Glyconanoparticles for a Versatile Redox Platform». *Nanomaterials.* (2021) 11, 5, 1162.

(49) Giacomelli C., Schmidt V., Putaux J. L., Narumi A., Kakuchi T., Borsali R. «Aqueous self-assembly of polystyrene chains end-functionalized with β-cyclodextrin». *Biomacromolecules*. (2009) 10, 2, 449–453.

(50) Gross A. J., Chen X., Giroud F., Travelet C., Borsali R., Cosnier, S. «Redox-active glyconanoparticles as electron shuttles for mediated electron transfer with bilirubin oxidase in solution». *Journal of the American Chemical Society*. (2017) 139, 45, 16076-16079.

(51) Hammond J. L., Gross A. J., Giroud F., Travelet C., Borsali R., Cosnier S. «Solubilized Enzymatic Fuel Cell (SEFC) for quasi-continuous operation exploiting carbohydrate block copolymer glyconanoparticle mediators». *ACS Energy Letters*. (2018) 4, 1, 142-148.

(52) Gross, A. J., Haddad R., Travelet C., Reynaud E., Audebert P., Borsali R., Cosnier S. «Redox-Active Carbohydrate-Coated Nanoparticles: Self-Assembly of a Cyclodextrin-Polystyrene Glycopolymer with Tetrazine-Naphthalimide». *Langmuir.* (2016) 32, 45, 11939–11945.

(53) Liebig J. «Uber einige Stickstoff-Verbindungen». *Annalen der Pharmacie.* (1834) 10, 1, 1-47.

(54) Pauling L., Sturdivant J. H. «The Structure of Cyameluric Acid, Hydromelonic Acid and Related Substances». *Proc. Natl. Acad. Sci.* (1937) 23, 615–620.

(55) Li J., Tao L., Wang Y., Yao Y., Guo Q. «Heptazine-Based π-Conjugated Materials for Light-Emitting». *Frontiers in Chemistry.* (2021) 9, 482.

(56) Brachi M., Buzzetti P. H. M., Gorgy K., Shan D., Audebert P., le Goff A., Li H., Borsali R., Cosnier S. «Trialkoxyheptazine-Based Glyconanoparticles for Fluorescence in Aqueous

Solutions and on Surfaces via Controlled Binding in Space». *ACS Macro Letters.* (2022) 11, 1, 135–39.

(57) Li J., Nomura H., Miyazaki H., Adachi C. «Highly efficient exciplex organic light-emitting diodes incorporating a heptazine derivative as an electron acceptor». *Chem. Commun.* (2014) 50, 6174– 6176.

(58) Audebert P., Kroke E., Posern C., Lee S. «State of the Art in the Preparation and Properties of Molecular Monomeric s-Heptazines: Syntheses, Characteristics, and Functional Applications». *Chemical Reviews.* (2021) 121, 4, 2515–2544.

(59) Rabe E. J., Corp K. L., Huang X., Ehrmaier J., Flores R. G., Estes S. L., Sobolewski A. L., Domcke W., Schlenker C. W. «Barrierless Heptazine-Driven Excited State Proton-Coupled Electron Transfer: Implications for Controlling Photochemistry of Carbon Nitrides and Aza-Arenes». *J. Phys. Chem. C.* (2019) 123, 29580– 29588.

(60) Savateev A., Pronkin S., Epping J. D., Willinger M. G., Wolff C., Neher D., Antonietti M., Dontsova D. «Potassium Poly(heptazine imides) from Aminotetrazoles: Shifting Band Gaps of Carbon Nitride-like Materials for More Efficient Solar Hydrogen and Oxygen Evolution». *ChemCatChem*. (2017) 9, 167– 174.

(61) Dang Q. Q., Zhan Y. F., Wang X. M., Zhang X. M. «Heptazine-Based Porous Framework for Selective CO2 Sorption and Organocatalytic Performances». *ACS Applied Materials & Interfaces.* (2015) 7, 28452– 28458.

(62) Zeng Y., Liu X., Liu C., Wang L., Xia Y., Zhang S., Luo S. «Scalable One-step Production of Porous Oxygen-Doped G-C3n4 Nanorods with Effective Electron Separation for Excellent Visible-Light Photocatalytic Activity». *Applied Catalysis B: Environonmental.* (2018) 224, 1–9.

(63) Dai Y., Li C., Shen Y., Lim T., Xu J., Li Y., Niemantsverdriet H., Besenbacher F., Lock N., Su R. «Light-tuned Selective Photosynthesis of Azo- and Azoxy-Aromatics Using Graphitic C3N4». *Nature Communications.* (2018) 9, 60.

(64) Mir Sayed S., Deng L. L., Lin B. P., Yang H. «A room-temperature heptazine core discotic liquid crystal». *Liq. Cryst.* (2017) 44, 2175– 2183.

(65) Schwarzer A., Saplinova T., Kroke E. «Tri-s-triazines (s-heptazines)—from a "mystery molecule" to industrially relevant carbon nitride materials». *Coordination Chemistry Reviews.* (2013) 257, 13-14, 2032-2062.

(66) Le T., Galmiche L., Masson G., Allain C., Audebert P. «A Straightforward Synthesis of a New Family of Molecules: 2,5,8-Trialkoxyheptazines. Application to Photoredox Catalyzed Transformations». *Chemical Communications.* (2020) 56, 73, 10742–10745.

(67) Liu B. W., Zhou H., Zhou S. T., Yuan J. Y. «Macromolecules based on recognition between cyclodextrin and guest molecules: Synthesis, properties and functions». *European Polymer Journal*. (2015) 65, 63-81.

(68) Kakuta T., Takashima Y., Sano T., Nakamura T., Kobayashi Y., Yamaguchi H., Harada A. «Adhesion between Semihard Polymer Materials Containing Cyclodextrin and Adamantane Based on Host–Guest Interactions». *Macromolecules.* (2015) 48, 3, 732–738.

(69) Paolino M., Ennen F., Lamponi S., Cernescu M., Voit B., Cappelli A., Appelhans D., Komber H. «Cyclodextrin-Adamantane Host–Guest Interactions on the Surface of Biocompatible Adamantyl-Modified Glycodendrimers». *Macromolecules.* (2013) 46, 9, 3215–27.

(70) Haddad R., Holzinger M., Villalonga R., Neumann A., Roots J., Maaref A., Cosnier S. «Pyrene-Adamantane-β-Cyclodextrin: An Efficient Host–Guest System for the Biofunctionalization of SWCNT Electrodes». *Carbon.* (2011) 49, 7, 2571–2578.

(71) Itoh T. «Fluorescence and Phosphorescence from Higher Excited States of Organic Molecules». *Chemical Reviews*. (2012) 112, 8, 4541–68.

(72) Zheng M., Li Y., Wei Y., Chen L., Zhou X., Liu S. «Determining the Energy Gap between the S1 and T1 States of Thermally Activated Delayed Fluorescence Molecular Systems Using Transient Fluorescence Spectroscopy». *The Journal of Physical Chemistry Letters.* (2022) 13, 11, 2507-2515.

(73) Ehrmaier J., Rabe E. J., Pristash S. R., Corp K. L., Schlenker C. W., Sobolewski A. L., Domcke W. «Singlet–Triplet Inversion in Heptazine and in Polymeric Carbon Nitrides». *The Journal of Physical Chemistry A.* (2019) 123, 38, 8099–8108.

(74) Galmiche L., Allain C., Le T., Guillot R., Audebert P. «Renewing Accessible Heptazine Chemistry: 2,5,8-Tris(3,5-Diethyl-Pyrazolyl)-Heptazine, a New Highly Soluble Heptazine Derivative with Exchangeable Groups, and Examples of Newly Derived Heptazines and Their Physical Chemistry». *Chemical Science.* (2019) 10, 21, 5513–18.

(75) Zambon A., Mouesca J. M., Gheorghiu C., Bayle P. A., Pecaut J., Claeys-Bruno M., Gambarelli S., Dubois L. «s-Heptazine oligomers: promising structural models for graphitic carbon nitride». *Chemical Science.* (2016) 7, 945–950.

(76) Modena M. M., Rühle B., Burg T. P., Wuttke S. «Nanoparticle Characterization: What to Measure?» *Advanced Materials.* (2019) 31, 32, 1901556.

(77) Souza T. G. F., Ciminelli V. S. T., Mohallem N. D. S. «A Comparison of TEM and DLS Methods to Characterize Size Distribution of Ceramic Nanoparticles». *Journal of Physics: Conference Series.* (2016) 733, 012039.

(78) Malvern Panalytical. «Dynamic Light Scattering:An Introduction in 30 Minutes». http://www.malvernpanalytical.com

(79) Stetefeld J., McKenna S. A., Patel T. R. «Dynamic light scattering: a practical guide and applications in biomedical sciences». *Biophysical reviews*. (2016) 8, 4, 409-427.

(80) Souza T. G. F., Ciminelli V. S. T., Mohallem N. D. S. «A Comparison of TEM and DLS Methods to Characterize Size Distribution of Ceramic Nanoparticles». *Journal of Physics: Conference Series.* (2016) 733, 012039.

(81) Gammas S., Suzuki K., Sone C., Sakurai Y., Kataoka K., Okano T. «Thermo-responsive polymer nanoparticles with a core-shell micelle structure as site-specific drug carriers». *Journal of Controlled Release.* (1997) 48, 2–3, 157– 164.

(82) Abedi M., Cohan R. A., Ardestani M. S., Davami F. «Comparison of Polystyrene versus Cycloolefin Microplates in Absorbance Measurements in the UV/VIS Region of the Spectrum». *Journal of Shahrekord University of Medical Sciences.* (2019) 21, 3, 110–13.

(83) Holzinger M., Bouffier L., Villalonga R., Cosnier S. «Adamantane/β-cyclodextrin affinity biosensors based on single-walled carbon nanotubes». *Biosens. Bioelectron*. (2009) 24, 1128-1134.

(84) Waltman R. J., Bargon J. «Electrically Conducting Polymers: A Review of the Electropolymerization Reaction, of the Effects of Chemical Structure on Polymer Film Properties, and of Applications towards Technology». *Canadian Journal of Chemistry*. (1986) 64, 1, 76–95.

(85) Shirakawa H., Louis E. J., MacDiarmid A. G., Chiang C. K., Heeger A. J. «Synthesis of electrically conducting organic polymers: halogen derivatives of polyacetylene, $(CH)_x$». *J Chem Soc Chem Commun.* (1977) 16, 578-580.

(86) Quijada C. «Conductive polymers: Materials and applications». *Materials*. (2020) 13, 10, 2344.

(87) Deshpande P. P., Jadhav N. G., Gelling V. J., Sazou D. «Conducting polymers for corrosion protection: a review». *Journal of Coatings Technology and Research*. (2014) 11, 4, 473-494.

(88) Liu E. T., Mei S., Chen X. H., Yao C. J. «Conducting Polymers with Redox Active Pendant Groups: The Application Progress as Organic Electrode Materials for Rechargeable Batteries». *Journal of Materials Chemistry C*. (2022)

(89) Memon M. A., Bai W., Sun J., Imran M., Phulpoto S. N., Yan S., Huang Y., Geng, J. «Conjunction of conducting polymer nanostructures with macroporous structured graphene thin films for high-performance flexible supercapacitors». *ACS Appl. Mater. Interfaces.* (2016**)** 8, 11711–11719.

(90) Yoon H. «Current trends in sensors based on conducting polymer nanomaterials». *Nanomaterials.* (2013) 3, 524.

(91) Johansson E. M. J., Yang L., Gabrielsson E., Lohse P. W., Boschloo G., Sun L., Hagfeldt A. «Combining a small hole-conductor molecule for efficient dye regeneration and a hole-conducting polymer in a solid-state dye-sensitized solar cell». *J. Phys. Chem. C.* (2012**)** 116, 18070–18078.

(92) Kraft A., Grimsdale A. C., Holmes A. B. «Electroluminescent conjugated polymers-seeing polymers in a new light». *Angew. Chem. Int. Edit.* (1998) 37, 4, 402-428.

(93) Sadki S., Schottland P., Brodie N., Sabouraud G. «The Mechanisms of Pyrrole Electropolymerization». *Chemical Society Reviews.* (2000) 29, 5, 283–93.

(94) Kohlman R. S., Epstein A. J., Skotheim T. A., Elsenbaumer R. L., Reynolds J. R. «Handbook of conducting polymers». *Marcel Dekker, New York*. (1998) 85.

(95) Scrosati B. (Ed.). «Applications of electroactive polymers». *London: Chapman & Hall.* (1993) 75.

(96) Huang Y., Li H., Wang Z., Zhu M., Pei Z., Xue Q., Huang Y., Zhi C. «Nanostructured polypyrrole as a flexible electrode material of supercapacitor». *Nano Energy*. (2016) 22, 422-438.

(97) Zhou M., Heinze J. «Electropolymerization of Pyrrole and Electrochemical Study of Polypyrrole: 1. Evidence for Structural Diversity of Polypyrrole». *Electrochimica Acta.* (1999) 44, 11, 1733–48.

(98) Cosnier S., Deronzier A., Roland J. F. «Controlled-permeability of functionalized polypyrrole films by use of different electrolyte anion sizes in the electropolymerization step». *J. Electroanal. Chem.* (1991) 310, 71.

(99) Diaz A. F., Castillo J. I., Logan J. A., Lee W. Y. J. «Electrochemistry of conducting polypyrrole films». *Journal of Electroanal. Chem.* (1981) 129, 115.

(100) Audebert P., Bidan G. «Polyhalopyrroles: Electrochemical synthesis and some characteristics». *Journal of Electroanal. Chem.* (1985) 190, 1-2, 129-139.

(101) Laczkaa O., García-Aljaro C., del Campo F. J., Pascual F. X. M., Mas-Gordic J., Baldrich E. «Amperometric Detection of Enterobacteriaceae in River Water by Measuring β-Galactosidase Activity at Interdigitated Microelectrode Arrays». *Analytica Chimica Acta.* (2010) 677, 2, 156–61.

(102) Seymour I., O'Sullivan B., Lovera P., Rohan J. F., O'Riordan A. «Electrochemical Detection of Free-Chlorine in Water Samples Facilitated by in-Situ PH Control Using Interdigitated Microelectrodes». *Sensors and Actuators B: Chemical.* (2020) 325, 128774.

Chapter IV

β-cyclodextrin-based glyconanoparticles as electrode material for enzyme immobilization

Summary

1. Introduction

In the previous chapter, host-guest interactions between Ad and β-CDs of the GNPs derived from a PS-b-βCD copolymer allowed both the functionalization of the GNPs with a fluorescent compound, HTZ-Ad, and their immobilization on electrodes modified by N-substituted polypyrrole films. The previous findings have been applied for the construction of an amperometric enzymatic glucose biosensor. In particular, the immobilization of an Ad-modified GOx on the GNPs has been investigated as well as the role of the polypyrrole films as electrode modifiers for the biosensor performance. The results, already published [1], are here discussed.

1.1. Glucose oxidase as a protein model for the functionalization of GNPs

Glucose oxidase (GOx) has widespread applications in industry and biotechnology and it is one of the most studied enzyme since the development of the first EFC [2] and the first glucose biosensor [3]. It is produced by some fungi and insects, its main function in those organisms is antimicrobial activity against various pathogens via production of hydrogen peroxide, although it has also secondary functions such as decrease the environmental pH and degradation of lignin [4]. The most common used GOx is derived from the extracts of *Aspergillus niger sp.* (*An*). The crystallographic structure of *An*GOx has been determined and published [5], thus it is a well-characterized enzyme. It belongs to the family of oxidoreductase. It is a homodimer consisting of two identical subunits of 80 kDa and two non covalently-bound flavin adenine dinucleotide (FAD) cofactors, which are the redox centers involved in electron transfer, one for each subunit. The protein is highly glycosylated (16% to 25%) [6].

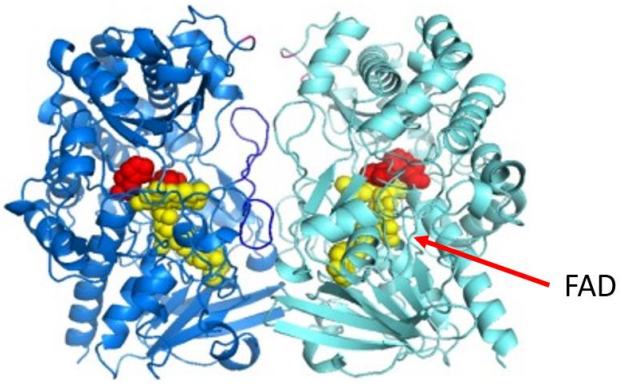

Fig. 1: Structure of glucose oxidase enzyme [1].

The enzyme catalyses the oxidation of β-D-glucose to D-gluconolactone and hydrogen peroxide. Both gluconic acid and hydrogen peroxide can cause inhibition of GOx if they accumulate excessively in the enzyme solution. The specificty of the enzyme towards glucose as well as the enzyme turnover reaction is very high. Indeed, GOx is characterized by a good stability. GOx requires an oxidant or electron acceptor to complete the enzymatic catalysis. Dissolved oxygen is the natural electron acceptor [7].

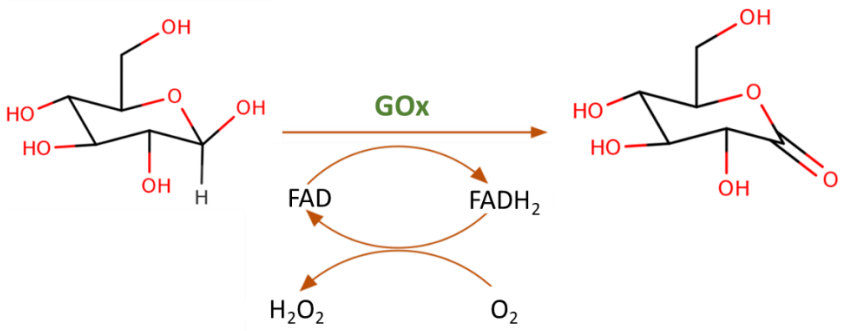

Fig. 2: conversion of β-D-glucose to D-gluconolactone by glucose oxidase.

Several glucose biosensors available in the market are based on immobilised GOx for medical [8] and food industry [9]. As already pointed out in the introduction chapter, amperometric glucose biosensors based on GOx can be divided into three generations according to their historical development and principle of operation [10]. In the first generation, the depletion of oxygen or the production of hydrogen peroxide (H_2O_2) are measured as indicators of glucose concentration upon its oxidation by GOx. The interference of other species in biologic fluids, such as ascorbic acid or uric acid, and the fluctuations of oxygen in the enzyme solution can be problematic. Different methods have been proposed to solve the issues of interference species such as the use of polymeric membranes for size exclusion [11, 12], the catalytic decomposition of the interference species [13], electrostatic repulsion [14] or the use of mediators [15]. In the second generation biosensors, mediators are used as electron shuttles between the reduced form of the enzyme and the electrode. The mediators thus replace oxygen as electron acceptor. These type of sensors operate at a lower potential, which prevent the oxidation of the interfering species, but they require strategies for the co-immobilization of the mediator to the electrode surface. In the third generation, the enzyme exchange electrons with the electrode by a DET mechanism. In this case, the enzyme needs to be electrically wired to the electrode using a series of "wired" relay centres or deglycosylated to shorten the distance between its prosthetic group and the electrode[16]. Given the difficulty in performing DET for

the GOx enzyme, due to the long distance of electron transfer between FAD and the periphery of the enzyme (13 to 18 Å) [17], the first biosensor generation and in particular those that are based on the detection of H_2O_2, remain the most simple and common [18].

1.2. Modification of glucose oxidase (GOx) by adamantanyl groups

The immobilization of biological macromolecules on electrodes is essential for the performances of the electrochemical sensing devices. In recent years, considerable attention has been focused on the development of novel reliable and stable methods of immobilization. The immobilization by affinity interactions is suitable for providing an anchoring point for enzymes avoiding the loss of their biocatalytic activity. The functionalization of the GNPs self-assembled from the PS-b-βCD copolymer via host-guest interactions with the Ad groups of an heptazine derivative has been shown to be effective. On this basis, the functionalization of the GNPs with Ad modified-GOx would be very interesting for the development of enzyme-based biosensor. Indeed, the formation of enzyme-coated GNPs would constitute an attractive route for the immobilization of the enzyme thanks to the useful properties of the GNPs such as their large surface area and biocompatibility.

GOx has been thus modified with Ad groups with the aim to investigate the interaction enzyme-GNPs at the electrode surface. The adamantan–modified GOx (GOx-Ad) was obtained according to the procedure described by Holzinger M. et al. [19]. For this, adamantylamine was reacted with 1-ethyl-3-(3-dimethylamino-propyl)carbodiimide hydrochloride (EDC) in a first step and then GOx was added and kept under stirring for 22 hours. Finally, the protein solution was purified by centrifugation. The final protein concentration obtained with this procedure was 0.5 mg mL^{-1}. The activity of GOx-Ad was measured to be 119 U mg^{-1} [19].

2. Elaboration of an amperometric glucose biosensor using GNPs for GOx immobilization

The description of the method of preparation and the characterization of the GNPs derived from the self-assembly of PS-b-βCD amphiphilic block copolymer has been already described in the previous chapter. In order to test the ability of the GNPs to bind the enzyme at the electrode surface, GNPs have been deposited on platinum (Pt) disk electrodes (5 mm

diameter) in a first step, followed by incubation with GOx-Ad solution. In particular, a volume of 50 µL of the suspension of GNPs was dropcasted on the surface of Pt electrodes and dried, following by extensive washing in water. Afterwards, the electrodes have been incubated with GOx-Ad (25 µL of 0.5 mg/ml enzyme solution) for 7 hours at 4 °C and then washed thoroughly with water. The activity of the enzyme has been evaluated indirectly by measuring the current originating from the electro-oxidation of the enzymatically produced H_2O_2 at + 0.7 V vs SCE in response to glucose concentration according to the following equation: $H_2O_2 \rightarrow O_2 + 2H^+ + 2e^-$. For this, the Pt modified electrodes have been immersed in stirred phosphate buffer pH 7 and the amperometric current at + 0.7 V vs SCE has been recorded upon subsequent glucose additions. The concept of the amperometric glucose biosensing electrode is schematized in *Fig. 3*.

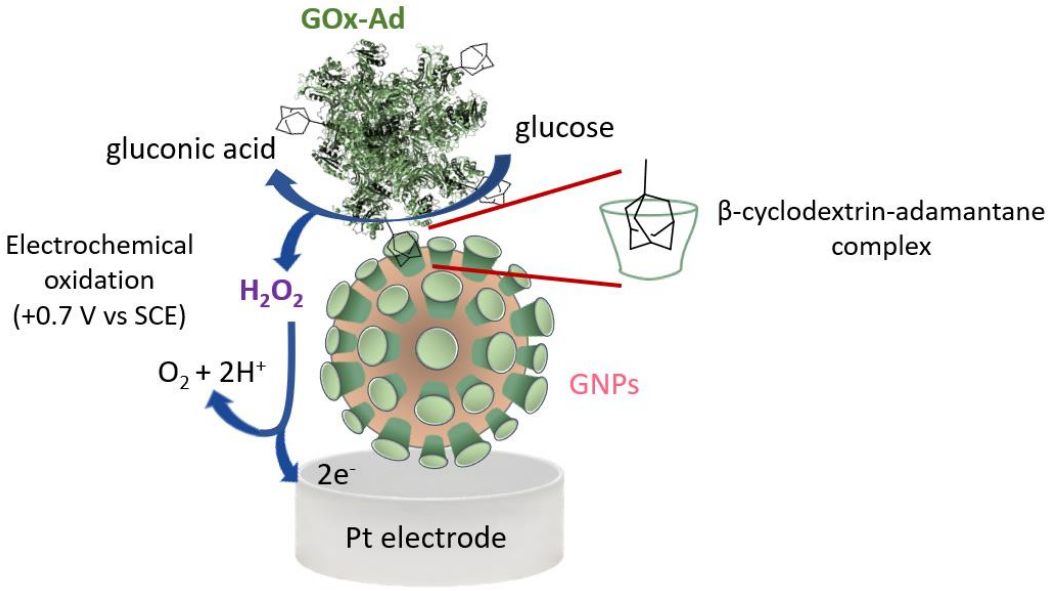

Fig. 3: a scheme of the amperometric detection of glucose of a bioelectrode fabricated by immobilization of the adamantane-labelled glucose oxidase (GOx-Ad) on GNPs at a Pt electrode.

Fig. 4 shows the plots of the amperometric response of three different configurations of electrodes as a function of glucose concentration. The resulting calibration curves follow a Michaelis–Menten kinetics: the current density (J) recorded at +0.7 V vs SCE increases quasi-linearly for low glucose concentrations and curved gradually for higher concentrations. The maximum catalytic current (J_{max}) corresponding to GOx-Ad incubated in the presence of GNPs, reaches 22 ± 5 µA cm^{-2} at saturated glucose concentration. Two control configurations made by incubation of the native GOx on GNPs, or by direct adsorption of the labelled GOx-Ad on the bare Pt surface, were also tested. It appears that the Jmax values are markedly

lower (3.36 μA cm^{-2} and 1.3 ± 0.1 μA cm^{-2} respectively) than that previously obtained by the association of GOx-Ad and GNPs.

These results are a proof of the importance of the GNPs for the immobilization of GOx-Ad. In particular, the affinity interactions between the Ad groups of the enzyme and the β-CDs exposed at the surface of the GNPs are specific and responsible for the increase in the amount of enzyme and the consequent improvement in the performance of the bioelectrode based on GOx-Ad/GNPs configuration. The non-specific interactions, such as those responsible for the adsorption of the enzyme onto the electrode, are on the contrary negligible.

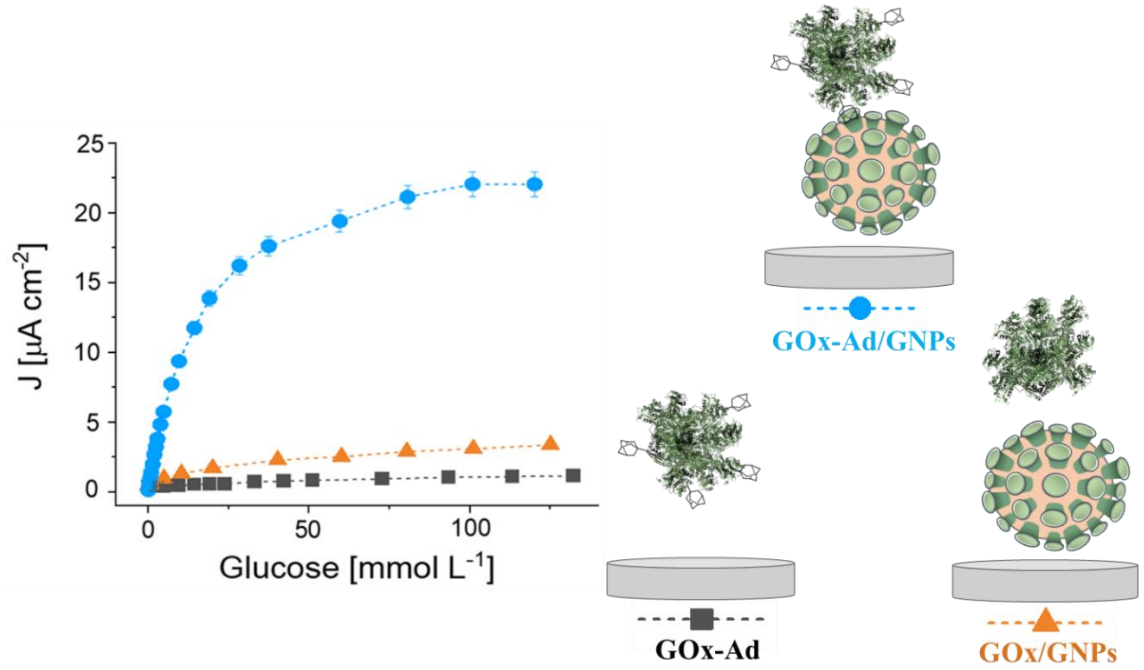

Fig. 4: calibration curves for glucose obtained at Pt electrode modified with GOx-Ad or with the non-labelled GOx with or without GNPs. Amperometric measurements are performed in stirred 0.1 mol L^{-1} phosphate buffer (pH 7, 25 °C).

The sensitivity of the GOx-Ad/GNPs biosensor was calculated to be 1.32 mA M^{-1} cm^{-2} while the apparent Michaelis–Menten constant (K_M^{app}), determined from the electrochemical Lineweaver-Burk form of the Michaelis-Menten analysis of the calibration curve, was 14 mmol L^{-1}. The K_M^{app} value reflects the kinetics of the immobilized enzyme and it is comparable to those obtained in the literature. In particular, it is lower than the value calculated in other works for the free enzyme (33 mmol L^{-1}) [20], although a bit higher than those obtained from enzyme monolayers anchored on biotinylated films (2–4 mM) [21]. This proves that the enzyme catalytic activity is not negatively affected by the formation of host-guest interactions.

3. Immobilization of the GNPs on poly-(pyrrole)-electrodes

3.1. Electrogenerated conducting polymers in the design of biosensors

Conducting polymers have been broadly used as transducers in electrochemical biosensors for biomolecule immobilization and signal amplification [21]. In particular, bioelectrodes formed by affinity interactions have the advantage to provide single binding sites for biomolecule immobilization without hindering the biorecognition sites and without altering excessively their biological activity. Furthermore, they provide means for the optimal orientation of the biomolecules. By electropolymerization, it is possible to create an ultra-thin, homogeneous, compact polymeric film in a controlled, localized and reproducible way, which is a really important characteristic nowadays for the development of miniaturized affinity sensors and biochips [21]. This technique, similar to photopatterning, screen-printing and spreading methods, allows the immobilization of the biomolecules with spatial resolution, as also demonstrated in the previous chapter. Another advantageous characteristic of the polymeric films is the flexibility of the monomer composition that provides a suitable microenvironment for hosting substituents of various nature (redox, photosensible, etc) allowing the modulation of the polymer properties [21]. Furthermore, polymeric films show good stability in air, organic and aqueous media. The formation of self-assembled monolayers (SAM) of thiols on gold surface, although suitable for biomolecule immobilization in a biocompatible environment that mimic the membrane bilayers, requires long procedures for cleaning the gold surfaces. Furthermore, the structure of the SAM is not defect free and their stability is not good for electrochemical experiments (for instance the electrochemical reduction can break the gold-sulfur bond). Another important point is the necessity of the post-functionalization of the terminal groups of the SAM for promoting specific interactions with the biomolecules, while the non specific adsorption of interfering species is very frequent [21]. Conductive polymers can be electrogenerated not only on gold but in a large variety of electrode materials. Apart from affinity interactions, conductive polymeric films can serve as immobilization platforms through various other strategies: adsorption by hydrophobic or electrostatic interactions, chemical grafting or photografting and the entrapment of the biomolecule inside the polymeric film during the electrochemical growth [22]. The latter method, compared to affinity interactions, does not require the chemical modification or the engineering of the biomolecules with affinity tags. However, it is not an ideal method for fabricating biosensing

surfaces due to the lack of orientation control of the biomolecule and the poor accessibility of analytes to biomolecules trapped in film [21].

Affinity sytems based on biotinylated conductive polymers are probably the most employed for biosensing applications for the development of immunosensors, protein sensors and DNA sensor chips [22]. These films are electrogenerated from functionalized biotin-pyrrole monomers and exploit the avidin-biotin interaction which is characterized by a strenght similar to that of covalent bonds. In these systems, a biotinylated biomolecule monolayer is generally linked to the biotinylated film via an intermediate layer of avidin. For instance, a biotinylated cholera toxin B subunit has been immobilized on biotinylated PPY film via avidin bridges, and the indirect detection of the toxin has been accomplished via a secondary antibody labeled by HRP [23]. Similarly, biotinylated monomers functionalized with dicarbazole groups have been used for the amperometric detection of chiral L- and D- norepinephrines [24]. As another example, the incorporation of lactose units on the biotin-PPY films allowed the fabrication of impedimetric protein sensors for the detection of Arachis hypogaea (peanut) agglutinin [25]. Thus, there is a vast range of possibilities in the choice of functional monomers that can be used. Some monomers have been synthezised by combining of biotin and pyrrole functions with redox or photoredox groups, such as tris bipyridyl ruthenium(II) complexes for the formation of a photosensitive transducing surface for detection of the cholera toxin [26]. In some cases, the bioreceptor itself can be modified with polymerizable groups. This principle has been applied especially for the electropolymerization of conductive films containing peptides used for the specific recognition of proteolytic enzymes and antibodies [21]. Recently, electrogenerated conducting polymers have been used for the formation of polymeric nanowires or nanoparticles with high conductivity using templates such as membranes or DNA structures, to guide their spatial polymerization. Composite materials, such as polypyrrole-silica colloidal or carbon nanotube-polypyrrole, have been formed to obtain novel interesting materials with hybrid characteristics that improve the immobilization of DNA and antibodies [21].

Affinity systems based on coordination of histidine tagged proteins with polymers functionalized by carboxylate or imidazole groups, that are able to form complexes with transition metals mimicking the chelation effect of iminodiacetic and nitrilotriacetic acid, have been used for biosensing and in particular for the immobilization of bacterial alkaline phosphatase [27]. In these systems, the transducing element can be regenerated by the

competitive binding of imidazole or EDTA. Some authors created a monolayer of histidine-tagged GOx on poly(pyrrole-NTA) films coordinated with copper ions. They showed that 5 cycles of enzyme detachment from the electrode surface by immersion in a imidazole solution followed by surface regeneration by immersion in Cu^{2+} and histidine-tagged enzyme solutions, did not produce a remarkable decrease in the the amperometric response [28]. The affinity interaction Ad/β-CDs, and specifically the one between a biotinylated GOx and a PPY-Ad film, has been used for the formation of an enzyme monolayer for the fabrication of an amperometric biosensor [19].

In the previous chapter, the interactions between the Ad groups of the electrogenerated PPY-Ad films and β-CDs of the GNPs led to the specific and spatially controlled immobilization of fluorescent functionalized HTZ-Ad GNPs on interdigitated electrodes. With the aim of improving the stability of the GOx-Ad biosensor reinforcing the immobilization of the GNPs at Pt electrodes, PPY films have been used as affinity layers for the anchoring of the GNPs via Ad/β-CDs affinity interactions. Different electrodes have been tested to determine the influence of the films on the biosensor performances.

3.2. Immobilization of the GNPs on a PPY-Ad homopolymer

A PPY-Ad film was thus formed from a 3 mM solution of the monomer, PY-Ad, in a solution of CH_3CN + 0.1 mol L^{-1} $LiClO_4$. Initially, the electro-oxidation of the monomer was carried out by selecting a wide potential window to verify the optimal conditions necessary for the electrochemical growth of the film and in particular, the value of the oxidation potential of the monomer at a Pt electrode. Fig. 5A shows a part of the first cyclic voltammogramm, presenting a sharp and broad oxidation peak that begins at +0.78 V vs Ag/Ag^+.

A potential slightly superior to this value is generally the most suitable for the electropolymerization reaction. If the potential is too low the electro-polymerization does not occur but if it is too high, the film is over-oxidized with formation of carbon oxide species, such as hydroxyls, carboxyls and keto-groups [19]. The over-oxidation affect negatively the growth of the film by destroying its electroactivity. The optimal growth of the polymer coating was verified also by cyclic voltammetry by performing 40 consecutive cycles between 0 and +0.79 V vs Ag/Ag^+ (*Fig. 5B*). The continuous growth of the redox system at $E_{1/2}$ = +0.27 V observed over this range, is the indication of the formation of a PPY-Ad film at the electrode.

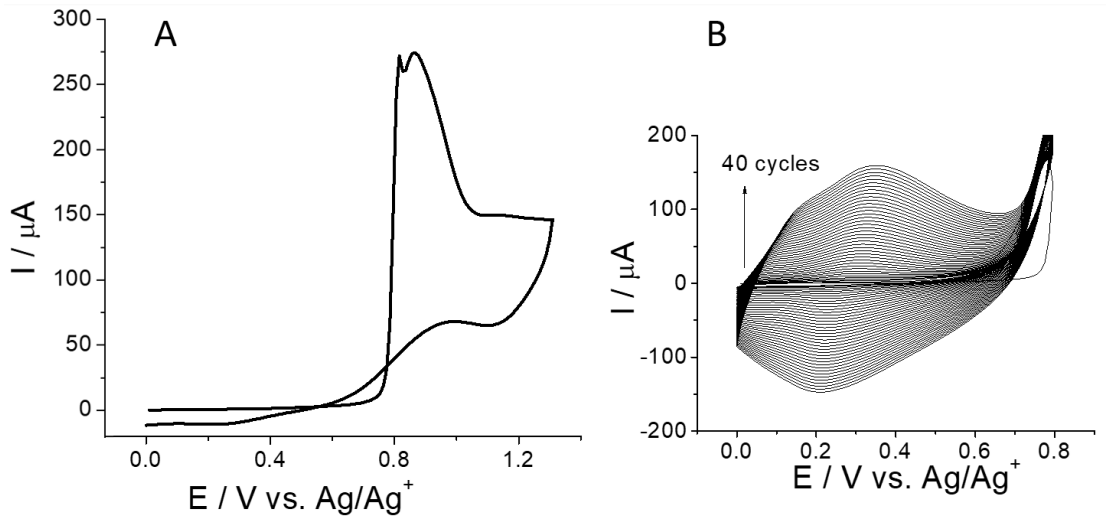

Fig. 5: A) oxidative electropolymerization of pyrrole-adamantane (3 mmol L^{-1}) with wide potential window and B) oxidative electropolymerization by 40 cycles between 0 V and +0.79 V vs Ag/Ag^+ recorded at Pt electrode (5 mm Ø) in CH_3CN + $LiClO_4$ 0.1 mol L^{-1}. Scan rate: 100 mV s^{-1}.

Taking into account the ideal conditions for the oxidative electropolymerization, a further investigation has been conducted on the film electrogeneration by controlled potential oxidation at +0.79 V vs Ag/Ag^+ to select the best electrolysis charge (1 mC cm^{-2}, 2.5 mC cm^{-2} or 5 mC cm^{-2}). The selection of a defined electropolymerization charge is intended to form reproducible ultra-thin films that do not affect the sensitivity of the biosensor. The selected charge will affect the final thickness of the polymer film. Ad groups are highly hydrophobic, the wettability and hydrophobicity of Ad-modified electrodes have been already proved in other works by contact-angle measurements [29]. In particular, when carbon nanotubes are modified with Ad groups, a consistent increase of the contact angle (from 38.5° to 68°) is observed compared to pristine nanotubes [29]. Hydrophobicity can impede the permeation of H_2O_2 through the polymeric deposit and thus hinder its diffusion to the surface of the underlying platinum electrode. The control of the polymer thickness is therefore an important parameter for the sensitivity towards H_2O_2.

After the electropolymerization from a 3 mM solution of the monomer in CH_3CN + $LiClO_4$ 0.1 mol L^{-1} with an electrolysis charge of 1 mC cm^{-2}, 2.5 mC cm^{-2} or 5 mC cm^{-2}, the electrodes were tested in monomer-free electrolytic solution to verify the presence of the polymer film. The electrodes showed the typical redox system of the poly(pyrrolic) matrix at

$E_{1/2}$ = +0.27 V and as expected, the intensity of the current values increases with the electropolymerization charge.

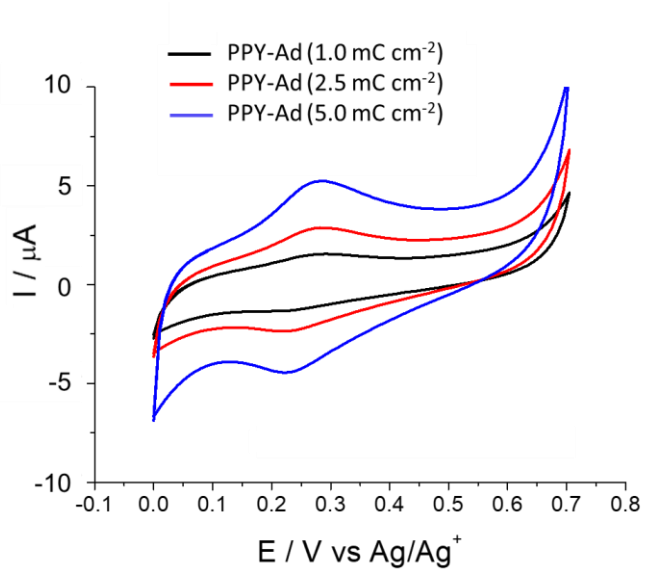

Fig. 6: voltamperograms recorded at Pt electrodes (5 mm diameter disk) after electropolymerization of pyrrole-adamantane (3 mmol L^{-1}) in CH_3CN + $LiClO_4$ 0.1 mol L^{-1} at +0.79 V vs Ag/Ag^+ with an electrolysis charge of 1 mC cm^{-2}, 2.5 mC cm^{-2} or 5 mC cm^{-2} and then transferred in CH_3CN + $LiClO_4$ 0.1 mol L^{-1} free of monomer.

Then, the sensitivity towards H_2O_2 of the three different electrodes was compared (*Fig. 7*). For this, the electrodes have been tested in phosphate buffer pH 7, the current density at + 0.7 V vs SCE has been recorded upon additions of increasing concentrations of H_2O_2. In all the cases, the variation of current density upon each addition was greatly lower compared to the bare Pt electrode. The electrode containing a PPY-Ad film generated by cyclic voltammetry showed an insulating behaviour and almost no variation in the current intensity was observed after each H_2O_2 addition. In *Fig. 7* are reported the plots of the current intensity versus H_2O_2 concentration. Even the thiniest film, the one formed with 1 mC cm^{-2}, resulted in a enormously reduced sensitivity compared to bare Pt electrodes. This indicates that PPY-Ad reduce the diffusion and the electro-oxidation of H_2O_2 at the electrode. As expected, the sensitivity of the electrodes decreased with the electropolymerization charge.

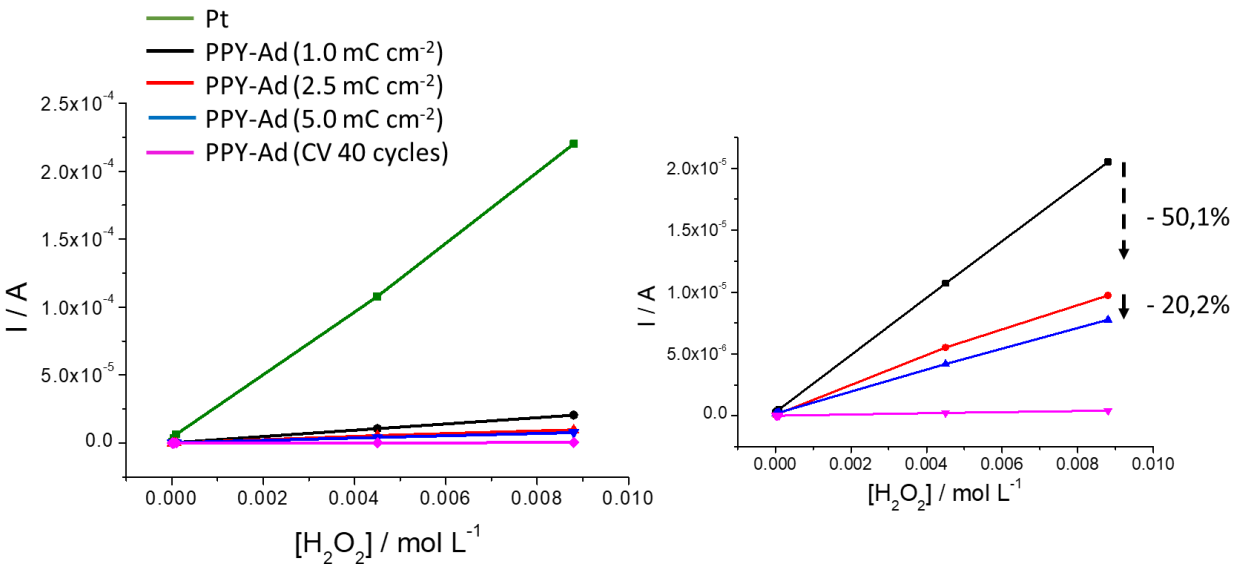

Fig. 7: plots of the current recorded in phosphate buffer pH 7 at +0.7 V vs SCE versus H_2O_2 concentration of different Pt electrodes covered by PPY-Ad films. The polymer films have been electrogenerated from a 3 mM solution of pyrrole-adamantane in CH_3CN + $LiClO_4$ 0.1 mol L^{-1} by controlled potential electrolysis at +0.79 V vs Ag/Ag^+ with different electrolysis charges or formed by 40 cycles between 0 and +0.79 V vs SCE.

The thickness of the resulting films was checked by optical microscope using ITO electrodes in the same experimental conditions (monomer concentration, electrolysis charges of 1, 2.5 or 5 mC cm^{-2}). The electrochemical characterization of PPY-Ad film on ITO electrodes has been already reported in the previous chapter. ITO electrodes, for their transparency and flat structure, are suitable for analysis under microscope. An analysis of the surface of the modified ITOs revelead the presence of film with a thickness between 1-2 µm when an electropolymerization charge of 2.5 mC cm^{-2} or 5 mC cm^{-2} was selected. On the other hand, it was not possible to determine the thickness of the PPY-Ad film formed with a charge of 1 mC cm^{-2} because it was too low and it appeared less homogeneous. For this reasons, 2.5 mC cm^{-2} has been selected as the best electrolysis charge for the electropolymerization of pyrrole-Ad. Indeed, the resulting PPY-Ad should be structurally more coherent to support the GNPs without decreasing excessively the sensitivity towards H_2O_2.

Thus for biosensor investigation, PPY-Ad films at Pt electrodes were electrogenerated by controlled potential electrolysis at +0.79 V vs Ag/Ag^+ up to 2.5 mC cm^{-2}. Then, the electrodes have been modified with GNPs and incubated with GOx-Ad using the same exact procedures described previously for bare electrodes. One configuration, fabricated omitting the

deposition step with GNPs, was used as control. The analytical performance of the biosensors for glucose detection was investigated by potentiostating the electrodes at +0.7 V vs SCE. The calibration curves are reported in *Fig. 8*.

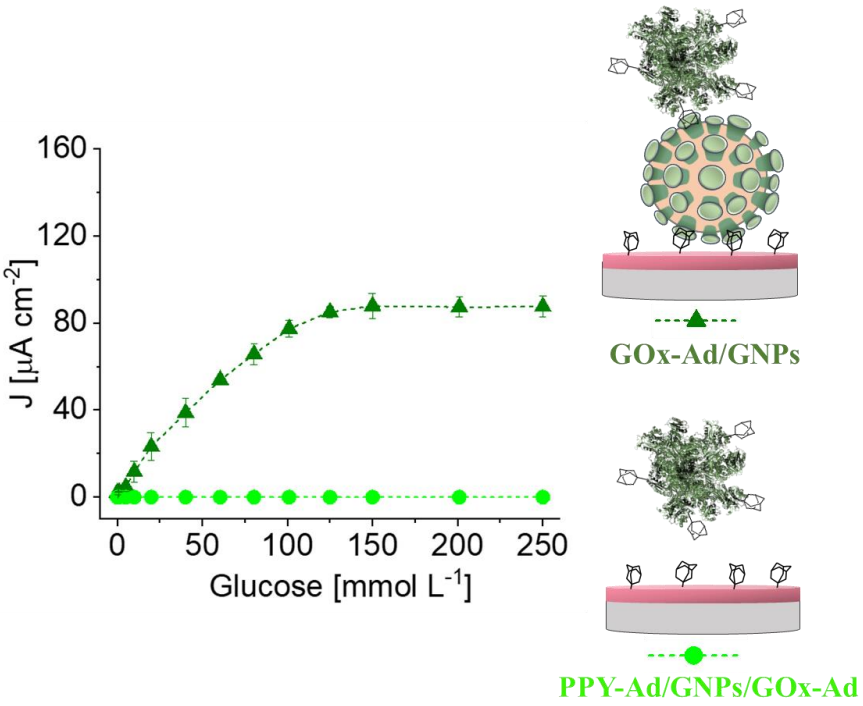

Fig. 8: calibration curves for glucose obtained at Pt electrodes modified with a PPY-Ad film and GOx-Ad with or without GNPs. Amperometric measurememnts are conducted in stirred 0.1 mol L^{-1} phosphate buffer (pH 7, 25 °C) at +0.7 V vs SCE.

The J_{max} extimated from the calibration curve for the PPY-Ad/GNPs/GOx-Ad configuration is 87 ± 6 µA cm^{-2}, almost four times higher than the one calculated before on the corresponding bare Pt electrode. Since the value of J_{max} is related to the amount of enzyme, this improvement indicates that the presence of the PPY-Ad film on the electrode indirectly increases the amount of the immobilized enzyme by reinforcing GNPs immobilization. This concept is further supported by the performance of the control, fabricated by incubating the same amount of GOx-Ad on the PPY-Ad-electrode in absence of the GNPs. In this case, the recorded J_{max} is considerably lower (0.5 ± 0.1 µA cm^{-2}). All interactions responsible for the improved catalytic current are once again very specific and determined by the formation of inclusion complexes between the β-CDs and Ad groups.

Importantly, the GNPs have a beneficial effect in improving J_{max} and therefore enzyme loading compared to similar systems in which an enzyme monolayer is attached at the

electrode surface by affinity interactions [19, 28]. For instance, Haddour N. et al. [28], developed a close-packed enzyme monolayer constituted by the successive coordination of Cu^{2+} ions and histidine-tagged GOx on a PPY film substituted by nitrilotriacetic acid (NTA). The J_{max} determined at glucose saturating conditions was 3.4 μA cm^{-2}. This value is very close to the one determined by immobilization of a monolayer of biotinylated GOX via avidin−biotin affinity interactions (3.7 μA cm^{-2}). The role of the GNPs, can be attributed to the spherical shape of the GNPs and their large surface-to-volume ratio that provides multiple binding sites for enzyme attachment compared to the monolayers, has been also highlighted in the work of Holzinger M. et al. [19]. In this case, when a GOx modified with β-CDs has been immobilized directly on PPY-Ad, the J_{max} was around 10 μA cm^{-2}. The addition of β-CDs-AuNPs as an intermediate layer betwen the polymer and the enzyme led to an improvement of the J_{max} up to 27.5 μA.

The K_M^{app} value for the PPY-Ad/GNPs/GOx-Ad biosensor increased from 14 mmol L^{-1} (on bare electrode) to 47 mmol L^{-1}, higher than those estimated for free enzymes [30]. The presence of the polymer also determined a decrease in the sensitivity, from 1.32 mA mol L^{-1} cm^{-2} of the previous experiment to 0.85 mA mol L^{-1} cm^{-2}. These variations can be attributed to the hydrophobic character of the PPY-Ad film that, although very thin, caused a limitation of the diffusion and oxidation of H_2O_2 at the electrode surface.

3.3. Immobilization of the GNPs on poly-(pyrrole) copolymers

In order to decrease the hydrophobicity of the polymer, a mixed film was electro-generated at Pt electrodes from a mixture of PY-Ad and a second component, pyrrole-lactobionamide (PY-Lac), in the concentration ratio of 1:3. This latter compound has hydroxylic functionalities and overall, a more hydrophilic character.

A similar biotinylated copolymer containing Lac groups, used by Ionescu et al. for the construction of an amperometric immunosensor for the detection of cholera B toxin [23], has already proved its utility in enhancing biosensor sensitivity due to its major hydrophilicity compared to the PPY-Ad or poly-phenolic films. In this case, the mass-transfer process through the homopolymer and the biotin-lactobionamide poly-(pyrrole) copolymer in aqueous solution was experimentally determined by rotating-disk electrode (RDE) voltammetry. The analysis of the plots of the reciprocal of the limiting current density versus the reciprocal of the square root of the rotation rate confirmed that the behaviour of the copolymer is similar to

that of bare electrodes (the intercept of the plot is in particular related to the polymer permeability) [23].

With the aim to determine the ideal conditions for the electropolymerization of a mixture of monomers, an electrochemical characterization has been carried out in CH_3CN + $LiClO_4$ 0.1 mol L^{-1}. During the electropolymerization process, the two monomers, PY-Ad and PY-Lac, are incorporated into the film resulting in a copolymer. The steps followed for the characterization are the same described previously. The electropolymerization has been conducted in a first step by cyclic voltammetry using a wide potential window. This first examination has allowed the selection of the ideal oxidation potential of the monomer (which is located slightly above the potential at which the broad oxidation wave of Fig. 9A begins, namely +0.74 V vs Ag/Ag^+). The redox system of the resulting copolymer film increased after each cycle upon repeated potential scanning between 0 and +0.74 V vs Ag/Ag^+ as in *Fig. 9B* highlighting the growth of the film under these conditions.

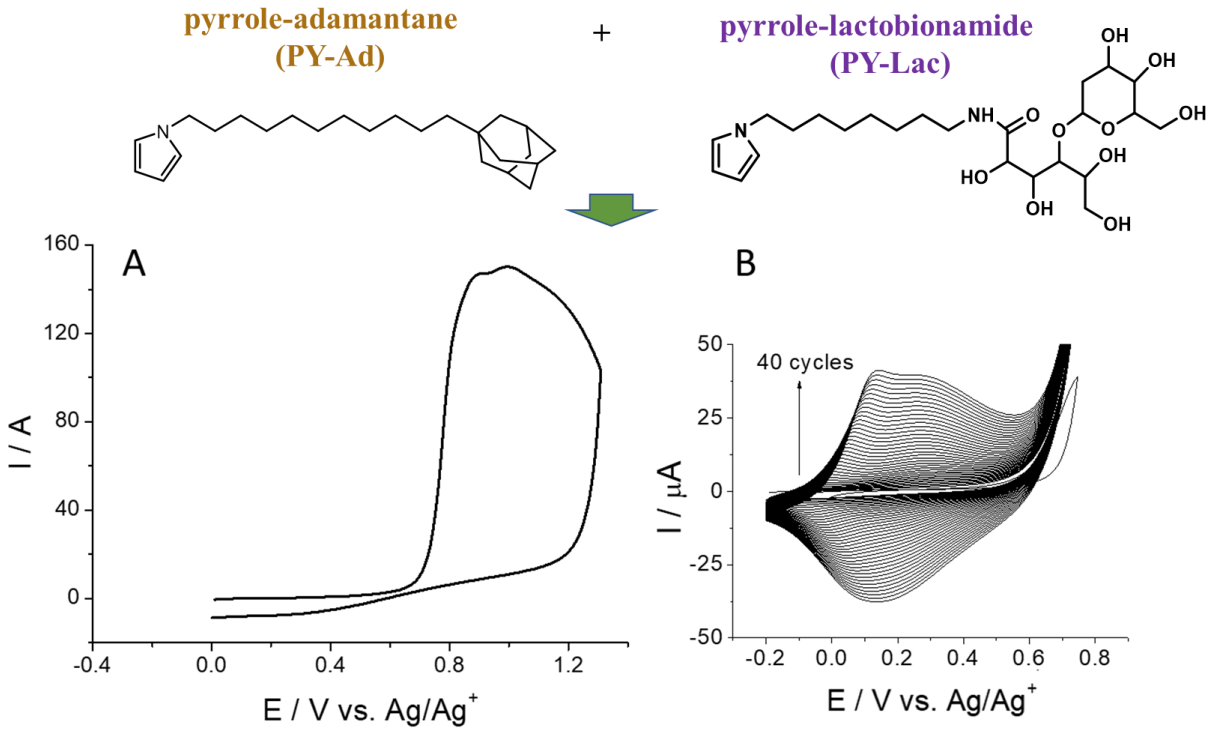

Fig. 9: oxidative electropolymerization of a mixture of pyrrole-adamantane and pyrrole-lactobionamide (1:3) by cyclic voltammetry by A) one cycle with wide potential window and B) 40 cycles between 0 V and +0.79 V vs Ag/Ag^+ recorded at Pt electrode (5 mm Ø) in CH_3CN + $LiClO_4$ 0.1 mol L^{-1}. Scan rate: 100 mV s^{-1}.

For the further investigation of the copolymer as support for the GNPs-based biosensor, a thin film was formed by chronoamperometry, similarly to the PPY-Ad polymer, by controlled potential electrolysis up to 2.5 mC cm^{-2} at +0.79 V vs Ag/Ag^+ at Pt electrodes. The electrodes have been then characterized in electrolytic solution free of monomer, showing a redox system at $E_{1/2}$ = + 0.26 V. The integration of the charge under the anodic peak of the cyclic voltammogram of the PPY-Ad and PY-Lac copolymer led to an electroactive surface coverage very similar to that observed for the pure PPY-Ad homopolymer (4.4 10^{-7} mol cm^{-2} vs 3.8 10^{-7} mol cm^{-2} respectively).

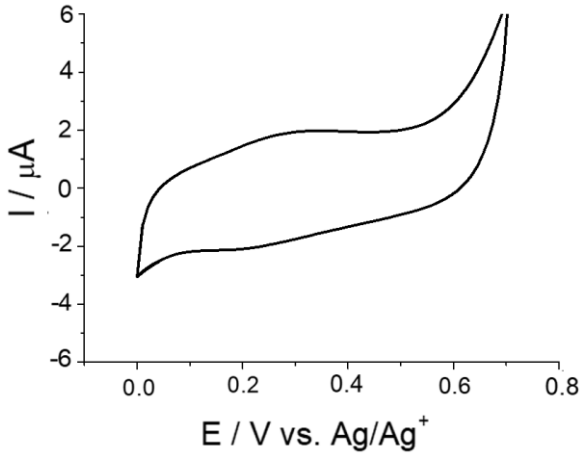

Fig. 10: voltamperogram of the copolymer made by electropolymerization of PY-Ad and PY-Lac recorded at a Pt electrode (5 mm diameter disk) in CH_3CN + $LiClO_4$ 0.1 mol L^{-1} at +0.79 V vs Ag/Ag^+ with an electrolysis charge of 2.5 mC cm^{-2} and then transferred in CH_3CN + $LiClO_4$ 0.1 mol L^{-1} free of monomer. Scan rate: 100 mV s^{-1}.

After the copolymer elaboration, the electrodes have been then modified with GNPs and GOx as already described and the performances of the bioelectrodes have been evaluated again. The results are reported in *Fig. 11*.

The calculated average value of the maximum current density is 144 ± 10 µA cm^{-2}, which is considerably higher than the value previously recorded with the PPY-Ad. This improvement is probably caused by the increase in the hydrophilicity of the copolymer induced by the Lac units incorporated into the film. The latter must cause a phenomenon of swelling of the polymer in the aqueous solution. The swelling of the film in turn increases the active surface of the GNPs able to interact with the enzyme. The K_M^{app} value decreases from 47 mmol L^{-1} in presence of the PPY-Ad polymer to 22 mmol L^{-1}, while the glucose sensitivity increases fourfold from 0.85 mA mol L^{-1} in presence of PPY-Ad to 3.3 mA mol L^{-1} cm^{-2} with the PPY-

Lac-PPY-Ad copolymer. The hydrophilic character of the film thus induces an improvement of the diffusion of H_2O_2 to the underlying electrode surface and consequently in its electro-oxidation. As observed previously with PPY-Ad, when the enzyme solution is incubated with the copolymer without the intermediate layer of GNPs, the electrochemical response of the electrode is very low with a J_{max} close to zero.

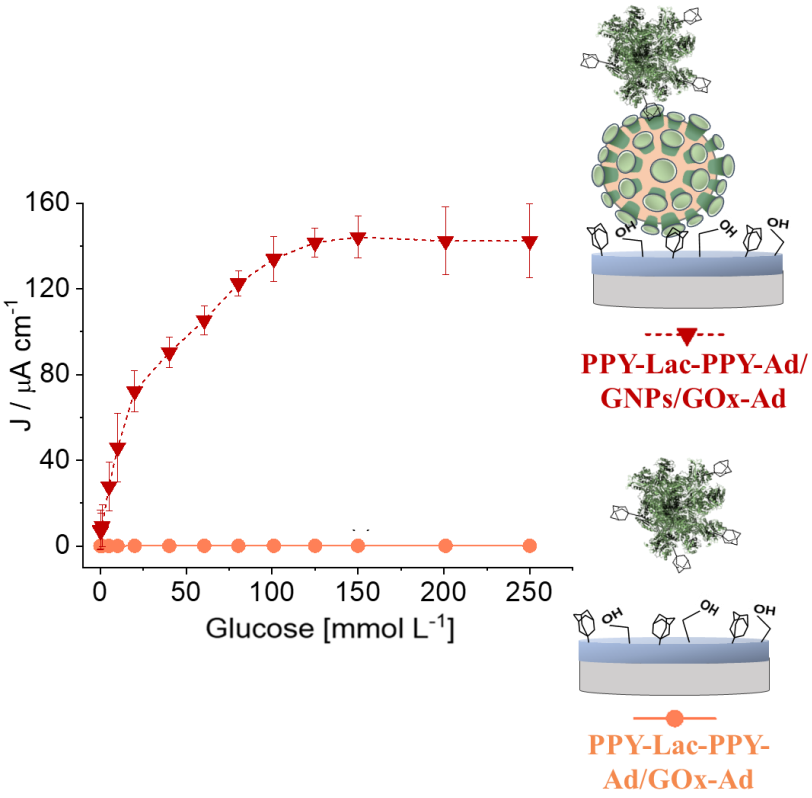

Fig. 11: calibration curves for glucose obtained at Pt electrodes modified with a PPY-Lac-PPY-Ad copolymer and GOx-Ad with or without GNPs. Amperometric measurememnts are conducted in stirred 0.1 mol L^{-1} phosphate buffer (pH 7, 25 °C) at +0.7 V vs SCE.

3.4. Fabrication of a multilayered biosensor

Given the encouraging results obtained on the functionalization of electrodes by several layers of GNPs and HTZ-Ad, the possibility of forming a multilayer composed alternately of GNPs and enzymes has been explored. For this purpose, the electrode modified by the PPY-Lac-PPY-Ad copolymer, was modified by two consecutive steps of deposition of GNPs and incubation with the GOx-Ad solution. Following this procedure, two theoretical layers of GNPs are formed on the copolymer, GOx-Ad acting as a bridge between GNPs. At this point, the performances of the bioelectrode have been evaluated and compared to those obtained in the previous experiment with a single layer of GNPs and GOx-Ad on the copolymer (*Fig. 12*).

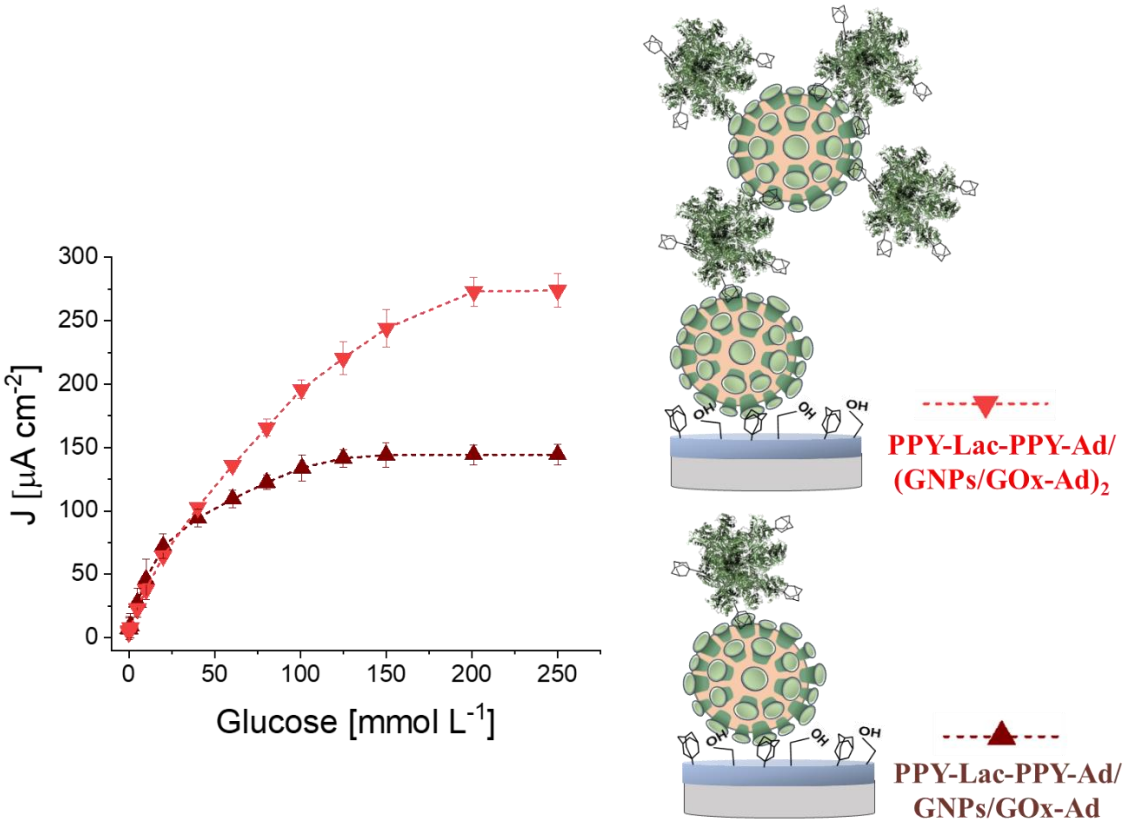

Fig. 12: calibration curves for glucose obtained at Pt electrodes modified with a PPY-Lac-PPY-Ad copolymer and GNPs and GOx-Ad to form one layer or two layers. Amperometric measurememnts are conducted in stirred 0.1 mol L^{-1} phosphate buffer (pH 7, 25 °C).

The biosensor shows a J_{max} of 274 µA cm^{-2}, almost twice the value observed for the electrode based on a single layer. This results suggests that the amount of enzyme is almost doubled. The sensitivity to glucose is slightly reduced (2.5 mA mol L^{-1} cm^{-2}). Another parameter that is considerably affected is the K_M^{app} which is increased to 61 mmol L^{-1} compared to 22 mmol L^{-1} for the single layer. The increase of the K_M^{app} is indicative of diffusional limitations, caused either by increased thickness of the catalyst layer or by the decreased permeability to substrates. In this case, the total increase of the thickness of the bioelectrode is certainly the cause of the increased K_M^{app}. The detection limit is good (68 µmol L^{-1}) and as expected, the linear range was extended.

SEM imaging was carried out on some ITO electrodes modified by the copolymer, GNPs and enzyme, to verify the morphology of the modified surfaces.

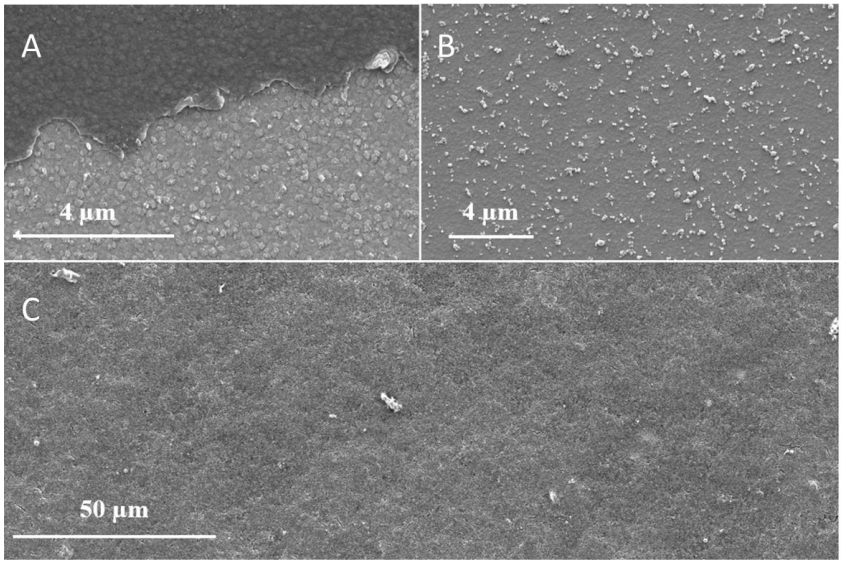

Fig. 13: SEM images of the PPY-Lac-PPY-Ad film A) before, B) after 30 min of incubation with GNPs, and C) after the formation of the GNP/GOx-Ad multilayer onto the copolymer.

The first image *Fig. 13A*, shows part of the electrode covered by a compact PPY-Lac-PPY-Ad copolymer (formed by chronoamperometry with an electrolysis charge of 2.5 mC cm^{-2}). On the surface of the electrode a little scratch was made on the film after the electropolymerization, in order to clearly show the contrast between the surface covered by the copolymer and the support. When an intact copolymer is incubated for 30 min with the GNPs suspension followed by rinsing in water, some GNPs remain stably attached on the film altough the surface is not completely covered with GNPs (*Fig. 13B)*. *Fig. 13C* is a SEM image of the top of the electrode after formation of a multilayer, constituted by two successive steps of GNPs deposition and incubation with GOx-Ad. In this case, is possible to observe a complete coverage of GNPs homogeneously distributed on the surface.

3.5. Overview on the bioelectrode performances

Fig. 14 shows the calibration curves relative to the different configurations of electrodes containing GNPs and presents a table summarizing the performance of each configuration. Overall, the presence of a polymer or copolymer film containing Ad groups is essential for improving the immobilization of the GNPs and consequently the amount of enzyme. The copolymer electrogenerated from the mixture of PY-Ad and PY-Lac gave the best configuration in terms of current density and sensitivity. The possibility of forming a multilayered structure augmenting enzyme loading has been demonstrated as well.

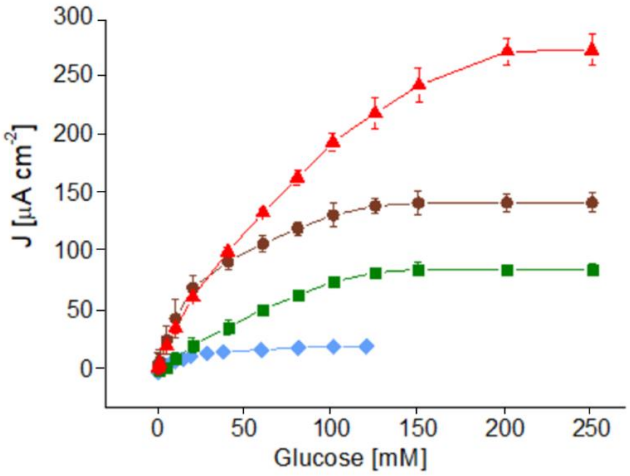

Type of electrode	GNPs/Gox-Ad	PPY-Ad/ GNPs/GOx-Ad	PPY-Lac-PPY-Ad/ GNPs/GOx-Ad 1 layer	PPY-Lac-PPY-Ad/ GNPs/GOx-Ad 2 layers
Detection limit [µmol L^{-1}]	80	44	84	68
Sensitivity [mA mol L^{-1} cm^{-2}]	1.32 ± 0.04	0.85 ± 0.05	3.3 ± 0.2	2.5 ± 0.2
Linear range [mmol L^{-1}]	0.08-2.89	0.04-60.5	0.084-72	0.068-100.6
J_{max} [µA cm^{-2}]	22 ± 5	87 ± 6	144 ± 10	272 ± 12
K_M^{app} [mmol L^{-1}]	14	47	22	61

Fig. 14: calibration curves for glucose obtained at different configurations of Pt electrodes (bare electrode, modified with a PPY-Ad polymer, with a PPY-Lac-PPY-Ad copolymer, followed by immobilization of GNPs and GOx-Ad to form one layer or two layers. Amperometric measurememnts are conducted in stirred 0.1 mol L^{-1} phosphate buffer (pH 7, 25 °C).

4. A qualitative QCM-D study of the GNPs binding on PPY-Ad films

Quartz crystal microbalance with dissipation monitoring (QCM-D) is an analytical technique that provides an in-situ real time analysis of the interactions occurring at surfaces that cause changes in mass per unit area [31]. The sensing surface is a circular piezoelectric quarz disc sandwiched between two metal electrodes that cause it to oscillate at a defined frequency by application of an appropriate alternating electric voltage. The frequency of oscillation is affected by small changes of the mass (the sensitivity is as small as a few ng/cm^2 [31]) caused by the adsorption, binding or detachment of molecules at the crystal surface. In the simplest case, when a rigid and homogeneous film is adsorbed on the quarz, the change in mass is linearly correlated with the change in the oscillation frequency by the Sauerbrey equation [32] (*Equation 1.*) where Δm is the adsorbed mass, Δf_n is the variation in resonance frequency measured at

the overtone number, *n*, and *C* is the mass sensitivity constant that depends on the property of the crystal used (it is equal to 17.7 ng cm^{-2} Hz^{-1} for a 5 MHz AT-cut quartz crystal).

$$\Delta m = \frac{\Delta f_n * C}{n} \qquad \textit{Equation 1.}$$

In a typical QCM-D experiment, both the frequency (Δf) and the dissipation (ΔD) changes need to be measured for the accurate determination of the mass change of a viscoelastic film. The dissipation change, that is related to the decay of the crystal's oscillation after a rapid excitation, takes into account the contribution of the hydration/solvation and the eventual entrapment of species within the adsorbed layer.

QCM-D has countless applications in various fields, it can be used to study all kind of surface chemistries (molecule-surface affinity interactions, protein-protein interactions, etc), the viscoelastic properties of the adsorbed layer, the build up of polymers and organic films, the effect on surfactants of various coatings, adsorption kinetics of polymers, polyelectrolytes, biomolecules, particles, cells [33]. QCM can be used for biosensing purposes as well [34].

QCM-D can be a complementary technique useful to study of the kinetics of GNPs attachment to a modified PPY-Ad surface, the importance of this immobilization and its stability. A preliminary analysis of the attachment efficiency of the GNPs on PPY-Ad has been thus carried out. Theoretically, the QCM-D instrument can be combined with an electrochemical module to directly study the growth and properties of a conductive polymeric film, such as PPY-Ad, while it is formed on the crystal quarz. In this case, due to technical limitations, the use of a specific electrochemical module was not feasible, and the analysis was thus focused on the interaction of the GNPs on PPY-Ad-modified crystals that were prepared separately using a common electrochemical three electrode set up (*Fig. 15B*).

The electropolymerization of pyrrole-Ad was conducted using a gold covered crystal quarz as working electrode (in particular the film was formed on the circular electrode area on the top side of the crystal, *Fig. 15*). In a first characterization, the oxidative electropolymerization of the PY-Ad monomer (3 mM solution in CH_3CN + 0.1 mol L^{-1} $LiClO_4$) was carried out by one cycle with a wide potential window as already described with other electrode materials. The ideal potential was calculated to be at + 0.86 V vs Ag/Ag^+. The growth of the film was also confirmed by performing successive cycles by repeated scanning of potential between 0 and + 0.86 V vs Ag/Ag^+. Afterwards, a thin PPY-Ad film was formed on the cleaned surface of the

crystal quarz by controlled potential oxidation at +0.86 V vs Ag/Ag^+ with a selected electrolysis charge of 5 mC cm^{-2}. In this condition, the resulting film appears to be homogeneous and not excessively thick (the excessive thickness reduce the sensitivity of the QCM measurements).

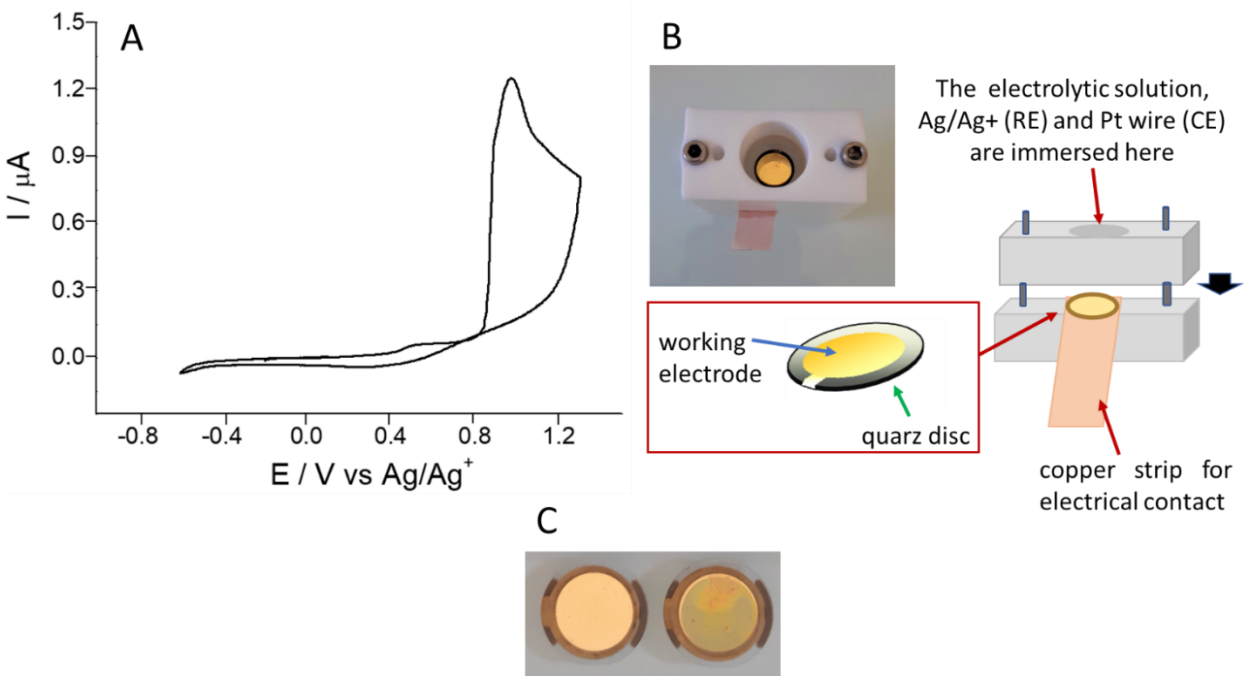

Fig. 15: A) oxidative electropolymerization of pyrrole-adamantane (3 mmol L^{-1}) by one cycle using a wide potential window on a gold quarz crystal. B) photo and scheme of the electrochemical cell set up used for the electropolymerization of the PPY-Ad on the quarz crystal. C) a photo of two quarz crystals before (left) and after (right) the formation of the PPY-Ad film.

The modified quarz discs have been then inserted in the QCM-D module in a temperature-controlled chamber (25 °C), the variation of the resonance frequency and dissipation over time at multiple overtones were recorded to detect the adsorption of GNPs. For this purpose, a peristaltic pump creates on the upper face of the sensor a controlled flow of an aqueous solution containing the GNPs. In a first step, a stable baseline with negligible variations of the Δf and ΔD was obtained by flowing only MilliQ water. When the suspension of the GNPs entered the system at 10 µL min^{-1}, a negative shift of the Δf and a concomitant positive shift of ΔD occurred, indicating the start of GNPs adsorption on the modified crystal surface. The injection of the GNPs continued for about 1 hour and during this time, the respective shifts continued to grow. Initially the shifts were more pronounced, while an almost steady-state value was reached after 1 hour. Afterwards, a washing step with MilliQ water was carried out

for 1 hour at 10 µL min^{-1} and then for a further hour at 20 µL min^{-1} to detach non-specifically adsorbed species.

The same procedure was repeated using a non-modified quarz crystal as a control to verify the Δf caused by non specific adsorption of the GNPs on the bare gold crystal in absence of PPY-Ad. In this case, the addition of the GNPs produced similar shifts of Δf and ΔD for all the overtones, although characterized by lower intensities compared to the previous experiment. The variation of the Δf of the third overtone of both experiments, after 1 hour of GNPs addition, are reported in *Fig. 16* a comparison. The third overtone is often used for calculations and data interpretation [50]. The values of Δf are already normalized with respect to the overtone number. As expected, the Δf was considerable lower (-4.1 Hz) for the control compared to the PPY-Ad-modifed crystal (-9.1 Hz). The experiments have been repeated twice with very little variation in the Δf and good reproducibility.

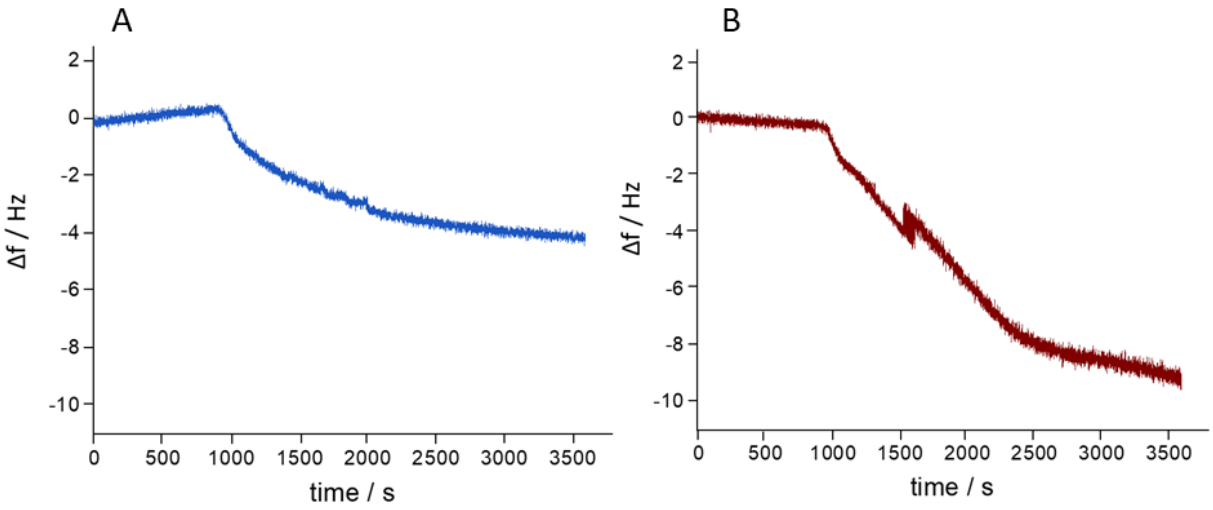

Fig. 15: frequency shifts of the third overtone as a function of time during GNPs deposition on A) a bare quarz crystal and B) a quarz crystal modified by a PPY-Ad.

SEM images of the surface of both quarz crystals were taken after the last washing step of the QCM-D experiments in order to check the integrity of the layer, the presence and coverage of the GNPs (*Fig. 16*).

Very few GNPs are adsorbed in the surface of the bare quarz crystal after the long rinsing in water, indicating that the non-specific adsorption of the GNPs on the quarz is minimal. In contrast, the quarz crystal modified with the electrogenerated PPY-Ad revealed the presence of GNPs still attached on the surface of the PPY-Ad film even after two hours of washing. SEM images thus support the QCM-D data.

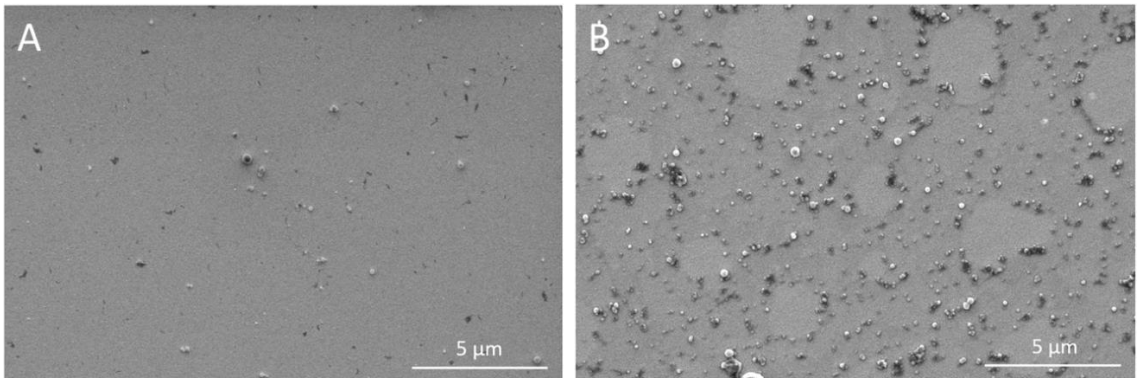

Fig. 16: frequency shifts of the third overtone as a function of time during GNPs deposition on A) a bare quarz crystal and B) a quarz crystal modified by a PPY-Ad.

The time used for GNPs injection during the QCM-D experiment was not sufficient to produce a complete coverage of the surface in the experimental conditions. Since the GNPs do not form a homogeneous rigid layer on the modified film, and the PPY-Ad is not rigid itself, *Equation 1.* is not directly applicable in this case. While the average size of the GNPs has been estimated by DLS and TEM imaging, the average mass of the GNPs has not been experimentally determined yet. For this reason without a high and nearly complete coverage of the surface, it was not possible to obtain a rigorous extrapolation of the amount of deposited GNPs. In future, further experiments are necessary for carrying out a semi-quantitative analysis and estimate the amount of GNPs necessary to obtain a close-packed monolayer (by treating the GNPs as spheres and dividing the area of the quarz crystal by the average size of the NPs). By using various modeling theories, it is possible to obtain information about the density of the modified layer, the mechanical properties and kinetics of the GNPs interactions. It would be interesting to track the amount and rate of encapsulation of biomolecules, for instance GOx-Ad, in the β-CDs of the GNPs adsorbed on the polymer films.

5. Conclusions

In this chapter, the possibility to use the GNPs as scaffold material for biomolecule immobilization at the electrode surface is explored. Host-guest interactions between Ad groups and β-CDs have been applied for the immobilization of an Ad-modified GOx enzyme for the fabrication of an amperometric biosensor for glucose detection.

The results show the importance of poly-(pyrrole) conductive films in improving GNPs attachment on the electrode by enhancing the accessible surface area for enzyme immobilization. Qualitative QCM-D experiments, combined with SEM imaging, confirmed the role of the polymers for GNPs immobilization. However, it should be noted that the homopolymer hinders the permeation of H_2O_2 at the electrode leading to a slight decrease in the biosensor sensitivity compared to bare electrode. The properties of the polymers can be tuned by the choice and concentration ratio of the monomeric constituents used during the electropolymerization. In particular, the hydrophilic character of the organic film was improved by electrogeneration of a copolymer bearing lactobionamide groups. At the same time, the copolymer maintained its anchoring abilities towards the GNPs via Ad groups of the PY-Ad monomer. The possibility to adjust the transport properties and chemical specificity of the polymer films makes them attractive materials for electrochemical sensing applications. The immobilization of GOx-Ad and GNPs on the copolymer gave the most efficient biosensor in terms of current density and sensitivity due to the increased permeation of H_2O_2 through the film and by promoting enzyme interaction with the GNPs.

In all cases, the presence of the GNPs was essential for the specific immobilization of GOx-Ad at the electrode while the non-specific interaction due to the direct adsorption of the enzyme on bare electrode, on polymer or copolymer, have little importance leading to biosensors with very poor performances. Given the high specific area and three-dimensional shape of the GNPs, the loading of the enzyme can be considerably improved compared to enzyme monolayers leading to higher current densities. Furthermore, the ability of the GNPs to act as bridges between the enzyme and the polymeric films, allowed the formation of a multilayered structure. The enzyme loading can be thus further improved by formations of consecutive layers of GNPs and modified enzyme. In the present work, a double layered biosensor with doubled current density was made. The limit of this type of approach for biosensing is the increase of the K_M with the increasing thickness of the final structure. Overall, the approach presented here based on the inclusion properties of the β-CDs of the GNPs used as bioelectrode material will be useful in future for the development of other types of biosensors, not only amperometric glucose biosensors, but even immunosensors or DNA sensors.

Bibliography

(1) Buzzetti P. H. M., Carrière M., Brachi M., Gorgy K., Mumtaz M., Borsali R., Cosnier S. «Organic β-cyclodextrin Nanoparticle: An Efficient Building Block Between Functionalized Poly (pyrrole) Electrodes and Enzymes». *Small*. (2022) 18, 10, 2105880.

(2) Yahiro A. T., Lee S. M., Kimble D. O. «Bioelectrochemistry: I. Enzyme utilizing bio-fuel cell studies». *Biochimica et Biophysica Acta (BBA) - Specialized Section on Biophysical Subjects.* (1964) 88, 375–383.

(3) Clark L. C., Lyons C. «Electrode Systems for Continuous Monitoring in Cardiovascular Surgery». *Annals of the New York Academy of Sciences.* (1962) 102, 29–45.

(4) Tsuge H., Natsuaki O., Ohashi K. «Purification, properties, and molecular features of glucose oxidase from Aspergillus niger». *The Journal of Biochemistry*. (1975) 78, 4, 835-843.

(5) Wohlfahrt G., Witt S., Hendle J., Schomburg D., Kalisz H. M., Hecht H. J. «1.8 and 1.9 Å resolution structures of the -Penicillium amagasakiense and Aspergillus niger glucose oxidases as a basis for modelling substrate complexes». *Acta Cryst D.* (1999) 55, 969–977.

(6) Prévoteau A., Courjean O., Mano N. «Deglycosylation of glucose oxidase to improve biosensors and biofuel cells». *Electrochemistry Communications.* (2010) 12, 213–215.

(7) Wong C. M., Wong K. H., Chen X. D. «Glucose oxidase: natural occurrence, function, properties and industrial applications». *Applied microbiology and biotechnology*. (2008) 78, 6, 927-938.

(8) Wilkins E., Atanasov P. «Glucose monitoring: state of the art and future possibilities». *Med Eng Phys.* (1996) 18, 273–288.

(9) Mello L. D., Kubota L. T. «Review of the use of biosensors as analytical tools in the food and drink industries». *Food Chem.* (2002) 77, 237–256.

(10) Newman J. D., Turner A. P. F. «Home blood glucose biosensors: a commercial perspective. *Biosens Bioelectron*». (2005) 20, 2435–2453.

(11) Sasso S. V., Pierce R. J., Walla R., Yacynych A. M. «Electropolymerized 1, 2-diaminobenzene as a means to prevent interferences and fouling and to stabilize immobilized enzyme in electrochemical biosensors». *Analytical Chemistry.* (1990) 62, 11, 1111-1117.

(12) Jung S. K., Wilson G. S. «Polymeric mercaptosilane-modified platinum electrodes for elimination of interferants in glucose biosensors». *Analytical chemistry.* (1996) 68, 4, 591-596.

(13) Yao T. «Amperometric determination of glucose in blood serum with a chemically modified enzyme membrane electrode in a continuous flow system». *Analytica chimica acta.* (1983) 153, 175-180.

(14) Szentirmay M. N., Martin C. R. «Ion-exchange selectivity of Nafion films on electrode surfaces». *Analytical chemistry.* (1984) 56, 11, 1898-1902.

(15) Wang J. «Electrochemical glucose biosensors». *Chemical reviews.* (2008) 108, 2, 814-825.

(16) Courjean O., Gao F., Mano N. «Deglycosylation of Glucose Oxidase for Direct and Efficient Glucose Electrooxidation on a Glassy Carbon Electrode». *Angewandte Chemie International Edition*. (2009) 48, 5897–5899.

(17) Hecht H. J., Schomburg D., Kalisz H., Schmid R. D. «The 3D structure of glucose oxidase from Aspergillus niger. Implications for the use of GOD as a biosensor enzyme». *Biosensors and Bioelectronics.* (1993) 8, 197–203

(18) Kajiya Y., Sugai H., Iwakura C., Yoneyama H. «Glucose sensitivity of polypyrrole films containing immobilized glucose oxidase and hydroquinonesulfonate ions». *Analytical chemistry.* (1991) 63, 1, 49-54.

(19) Holzinger M., Bouffier L., Villalonga R., Cosnier S. «Adamantane/β-cyclodextrin affinity biosensors based on single- walled carbon nanotubes». *Biosensors and Bioelectronics.* (2009) 24, 5, 1128-1134.

(20) Swoboda B. E., Massey V. «Purification and Properties of the Glucose Oxidase from Aspergillus niger». *Journal of Biological Chemistry.* (1965) 240, 5, 2209-2215.

(21) Cosnier S. «Affinity biosensors based on electropolymerized films». *Electroanalysis: An International Journal Devoted to Fundamental and Practical Aspects of Electroanalysis*. (2005) 17, 19, 1701-1715.

(22) Cosnier S. «Recent advances in biological sensors based on electrogenerated polymers: a review». *Analytical Letters*. (2007) 40, 7, 1260-1279.

(23) Ionescu R. E., Gondran C., Gheber L. A., Cosnier S., Marks R. S. «Construction of amperometric immunosensors based on the electrogeneration of a permeable biotinylated polypyrrole film». *Analytical chemistry*. (2004) 76, 22, 6808-6813.

(24) Cosnier S. «Biosensors based on electropolymerized films: New trends». *Anal. Bioanal. Chem.* (2003) 377, 507–520.

(25) Dubois M. P., Gondran C., Renaudet O., Dumy P., Driguez H., Fort S., Cosnier S. «Electrochemical detection of Arachis hypogaea (peanut) agglutinin binding to monovalent and clustered lactosyl motifs immobilized on a polypyrrole film». *J. Chem. Soc. Chem. Commun.* (2005) 4318–4320.

(26) Haddour N., Chauvin J., Gondran C., Cosnier S. «Photoelectrochemical immunosensor for label-free detection and quantification of anti-cholera toxin antibody». *J. Am. Chem. Soc.* (2006) 128, 9693–9698.

(27) Davis J., Glidle A., Cass A. E. G., Zhang J., Cooper J. M. «Spectroscopic evaluation of protein affinity binding at polymeric biosensors films». *J. Am. Chem. Soc.* (1999) 121, 4302–4303.

(28) Haddour N., Cosnier S., Gondran C. «Electrogeneration of a poly(pyrrole)-NTA chelator film for a reversible oriented immobilization of histidine-tagged proteins». *J. Am. Chem. Soc.* (2005) 127, 5752–5753.

(29) Haddad R., Holzinger M., Villalonga R., Neumann A., Roots J., Maaref A., Cosnier, S. «Pyrene-adamantane-β-cyclodextrin: An efficient host–guest system for the biofunctionalization of SWCNT electrodes». *Carbon.* (2011) 49, 7, 2571-2578.

(30) Ramanavičius A., Kaušaitė A., Ramanavičienė A. «Polypyrrole-coated glucose oxidase nanoparticles for biosensor design». *Sensors and Actuators B: Chemical*. (2005) 111, 532-539.

(31) Dixon M. C. «Quartz crystal microbalance with dissipation monitoring: enabling real-time characterization of biological materials and their interactions». *Journal of biomolecular techniques: JBT*. (2008) 19, 3, 151.

(32) Sauerbrey G. «Verwendung Von Schwingquarzen Zur Wiigung Dunner». *Schichten Und Zur Mikrowägung Z. Phys.* (1959) 155, 206– 222.

(33) Cheng C. I., Chang Y. P., Chu Y. H. «Biomolecular interactions and tools for their recognition: focus on the quartz crystal microbalance and its diverse surface chemistries and applications». *Chemical Society Reviews.* (2012) 41, 5, 1947-1971.

(34) Montagut Y., Garcia J., Jiménez Y., March C., Montoya Á., Arnau A. «QCM technology in biosensors». *Biosensors-Emerging Materials and Applications*. (2011) 153-178.

Conclusions and perspectives

Nanomaterials have unique properties such as high surface area, high adsorption capacity, high stability and high catalytic activity.All of these give an important contribution to the optimization of both biofuel cells and biosensors. Among the nanomaterials, carbon nanotubes, inorganic and organic nanoparticles, are the most employed and studied [1]. In this PhD project, novel functionalization strategies of nanomaterials have been investigated to tackle the challenges of biofuel cells and biosensors. The functionalization has the objective to promote biomolecule immobilization and loading on the electrode surface, improve the efficiency of the electron transfer increasing the power ouput of biofuel cells and the sensitivity of biosensors.

The thesis begins with an introduction chapter describing the peculiar characteristics and practical applications of enzymatic biofuel cells and biosensors, the principal enzyme immobilization strategies and a general overview on nanomaterials functionalization. The thesis is then essentially divided into two parts centered on the results obtained upon functionalization of two different types of nano-objects: multiwalled carbon nanotubes (MWCNTs) and organic carbohydrate derived glyconanoparticles (GNPs).

In the II chapter, the functionalization of MWCNTs with a thiol-yne reaction has been investigated. In general, “click” chemistry reactions have very appealing characteristics such as steoreospecificity, efficiency, simplicity, mild conditions [2]. The approach is modulable since virtually all range of compounds with appropriate functionalities can be “clicked”. These reactions have encountered a large success over the last years. Their importance in research has led the founders, Sharpless and Meldal, to win the Nobel Prize of Chemistry this year (2022). Among the “click” reactions, the copper-catalyzed azide–alkyne cycloaddition (CuAAC) reaction is surely the most used in various applications [3]. Nevertheless, the reaction requires a metal catalyst, and in case of enzyme immobilization, it requires the prior modification of the enzyme with an appropriate “clickable” group. Thiol-yne reaction, involving a thiol and an alkyne group, can be conducted instead without expensive metal catalysts and it makes bioconjugation more readily achievable since the aminoacid cysteine of proteins naturally contain a thiol group. Few reports are present in the literature about this reaction, in particular with respect to electrode modification and MWCNTs functionalization.

To investigate the feasibility of this reaction for the modification of MWCNTs, alkyne groups have been introduced on the sidewalls of MWCNTs by either covalent diazonium chemistry or non-covalent modification with pyrene.Thiol-modified redox compounds have been subsequently used to probe the effectiveness of the reaction by electrochemistry. Cyclic voltammetry was used to determine the amount and stability of the immobilized ferrocene probes. After a preliminary comparative investigation, the photoinduced thiol-yne reaction appeared to be the most efficient strategy to promote the immobilization of thiol-modified ferrocenes at the surface of the alkyne-modified MWCNTs. The data obtained by electrochemistry have been complemented by XPS analysis that confirmed the presence of iron species on the surface of the functionalized MWCNTs. The reaction has been subsequently applied to the immobilization of thiol-modified quinones, which are generally employed as redox mediators for promoting the electron transfer of glucose oxidizing enzymes. The immobilization of both thiol- ferrocene and quinones on nanotubes by the UV-catalyzed thiol-yne reaction enables the electrocatalytic oxidation of glucose by FAD-GDH enzyme with high efficiency.

Overall, the results show that this technique can be used as a functionalization strategy alternative to other “click” chemistry reactions. Finding novel immobilization strategies is important as each of them can respond to specific requirements and be suitable for specific applications. In this case, the reaction is operationally simple and it can lead to a high degree of functionalization since two consecutive thiols can be added to the alkyne. This feature is useful not only in synthetic and polymer chemistry for the generation of glycopolymers and hyperbranched structures, but for electrocatalytic applications as well to increase the amount of immobilized mediators, as demonstrated in the second chapter. The stable immobilization of the mediators is very important for enzymatic biofuel cell applications, especially for future implantable devices, to prevent power losses and reduce toxicity and inflammatory issues caused by the leaching of the mediator from the electrode surface. It is important as well for some types of enzymatic biosensors that require the co-immobilization of the mediators at the surface. Apart from mediators, this technique can be applied to the immobilization of other molecules, for instance compounds that mimick the enzyme substrates to promote enzyme immobilization and orientation by affinity interactions or molecular catalysts to perform similar electrocatalytic reactions

The possibility of using this functionalization strategy for the immobilization of bigger macromolecules such as enzymes, oligonucleotides, at the electrode still need to be assessed

properly. Ideally, a cysteine-containing enzyme, with natural occurring cysteines or engineered in order to display single cysteine residues in favourable sites, should be tested in future. Since the cysteine residue on proteins are usually very few, this technique can be useful to promote a specific orientation of the enzyme at the electrode. Furthermore, this approach is suitable for controlling the functionalization both in space and time, since the light can be conveniently switched “on” and “off”, controlled with optical fibers and by the use of appropriate photomasks that expose only determinate areas of a surface. This photolithographic approach can be thus envisaged for the creation of nanopatterned materials.

The second part of the thesis is centered on the functionalization of organic nanoparticles (NPs) derived from a process of self-assembly in aqueous solution from a polystyrene-block-β-cyclodextrin block copolymer. These NPs display β-CDs at the surface that are potentially able to form inclusion complexes with various compounds. In particular, the ability of the β-CDs to form host guest interactions with adamatane (Ad) of a fluorescent hetazine compound with three Ad groups (HTZ-Ad) has been investigated in the III chapter. The results clearly show the efficient functionalization of the GNPs with HTZ-Ad by their acquisition of fluorescent properties in aqueous solution and after their immobilization on surfaces. In general, the inclusion into β-CDs can be very useful to increase the solubility of some organic compounds, such as heptazine or hydrophobic mediators, promoting their catalytic applications in water. Conductive polymers, such as poly-(pyrrole)-adamantane films, can be conveniently electrogenerated on electrode surfaces to guide the immobilization of the GNPs at the electrode. This strategy allows the creation of spatially controlled functionalized regions of the electrodes via specific interactions.

The results have been then applied to the immobilization of a glucose oxidase (GOx) enzyme on GNPs fixed at the electrode via poly(pyrrole) polymeric films with the fabrication of amperometric glucose biosensors whose characteristics and performances are described in the IV chapter. The interactions based on the inclusion of specific enzyme tags in the β-CDs is advantageous because it generally do not perturb the thridimensional architecture of the enzyme and its catalytic activity. The creation of three-dimensional architectures based on GNPs on the electrode was advantageous for improving enzyme loading. Furthermore, β-CDs are very biocompatible. Multilayered structures can be also formed by this approach through interactions of tagged molecules with the GNPs of adiacent layers.

In general, the functionalization of the GNPs by host guest interactions is a very versatile method due to the vaste range of compounds that can be hosted in the β-CD cavity. The functionalization of the GNPs with redox compounds has been already proved by my colleagues for biofuel cell applications [4]. In future, the immobilization of other tagged enzymes, such as biotin, hystidine, pyrene, adamantane enzymes, on GNPs will be used for the design of novel enzymatic biofuel cells and biosensors. The GNPs will be used either in solution or upon their immobilization on electrodes via conductive polymeric films, in combination with redox mediators or redox modified GNPs. In the first case, a solubilized enzymatic biofuel cell will be created by confinement of the modified GNPs in permselective membranes. The positive effect of the inclusion of redox mediators in the GNPs shell for enzyme catalysis has been highlighted in previous works [5]. This improvement is attributed to the increased solubility of the mediator in water and to a redox hopping effect caused by the presence mediators in close proximity upon encapsulation in adiacent β-CDs on the GNPs. The concomitant immobilization of enzymes and mediators in the GNPs will likely allow a further improvement of the electron transfer by increasing the chances of interactions between enzyme and mediators, favoured by the rotation degree of the GNPs in solution. Preliminary experiments regarding the functionalization of both FAD-GDH and BOx enzymes with biotin for their further use in a biofuel cell set up have been already initiated.

Interestingly, GNPs with novel properties can be obtained by the choice of the hydrophobic and hydrophilic blocks of the amphiphilic block copolymers used in the self-assembly process. Hybrid GNPs, displaying different polar groups with different binding abilities, can be formed from a mixture of different amphiphilic block copolymers in different concentration ratio, as previously demonstrated by my colleagues [6]. For instance, β-CDs groups can be alterned with maltoheptahose groups. The latter can interact with nitriloacetic acid, which is able to form coordination complexes with histidine-tagged proteins via metal complexation. Thus, the formation of these hybrid polyvalent GNPs would allow the immobilization of different tagged-molecules, for instance two different enzymes to perform a multienzymatic reaction and increase the oxidation of the fuels and the power output of biofuel cells. Indeed, the density of the exposed polar groups can be optimized by formation of these hybrid GNPs allowing a better control over the immobilization of biomolecules. For instance, the reduction of the exposed β-CDs sites will prevent enzyme aggregation.

In future, GNPs self-assembled from an amphiphilic block copolymer constituted by a β-CD part linked with polycaprolactone instead of the polystyrene chain, will be prepared and

characterized. These GNPs will be totally biocompatible and biodegradable. Eventually, the addition of polymerizable motifs, such as pyrrole, in the copolymer structures, would be also worthy of investigation with the aim of reinforcing further the GNPs architectures and their long-term usability as electron materials for both biofuel cells and biosensors.

Overall, the methods and results discussed in this thesis, concerning the functionalization of MWCNTs by thiol-yne chemistry and GNPs via β-CDs host guest interactions, have been applied to the catalytic oxidation of glucose by immobilized oxydoreductases enzymes, FAD-GDH and GOx. The enzymatic oxidation of glucose is central for energy conversion and biosensors. Besides, these methods can be potentially extended to the immobilization of other classes of enzymes and other types of biomolecules, such as antibodies and aptamers, after opportune modification with thiol/alkyne groups or groups having an affinity with β-CDs. Thus, both these strategies have promising applications for the generation of spatially controlled electroactive materials and for the development of different types of biofuel cells and biosensors (immunosensors, aptasensors, etc.) and their full potential has yet to be realized.

Les nanomatériaux ont des propriétés uniques telles qu'une surface et unecapacité d'adsorption élevée qui participent à l'augmentation de la stabilité et de une activité catalytique. Tout cela apporte une contribution importante à l'optimisation des biopiles et des biocapteurs. Parmi les nanomatériaux, les nanotubes de carbone, nanoparticules inorganiques et organiques, sont les plus employés et étudiés [1]. Dans ce projet de thèse, de nouvelles stratégies de fonctionnalisation de nanomatériaux ont été étudiées pour proposer de nouveaux nanomatériaux hybrides pour les biopiles et les biocapteurs. La fonctionnalisation a pour objectif de favoriser l'immobilisation et la concentration des biomolécules sur la surface de l'électrode, d'améliorer l'efficacité du transfert d'électrons et augmenter la puissance des biopiles et la sensibilité des biocapteurs.

La thèse commence par un chapitre d'introduction décrivant les caractéristiques particulières et les applications pratiques des biopiles enzymatiques et des biocapteurs, les principales stratégies d'immobilisation des enzymes et un aperçu général sur la fonctionnalisation des nanomatériaux. La thèse est ensuite essentiellement divisée en deux parties centrées sur les résultats obtenus lors de la fonctionnalisation de deux types différents de nano-objets : les

nanotubes de carbone multiparois (MWCNTs) et les glyconanoparticules dérivées de glucides organiques (GNPs).

Dans le chapitre II, la fonctionnalisation des MWCNTs avec une réaction thiol-yne a été étudiée. Les réactions chimiques “click” ont des caractéristiques très attrayantes telles que la stéréospécificité, l'efficacité, la simplicité et leurs conditions de réaction douces [2]. L'approche est modulable puisque toute une librairiede composés avec des fonctionnalités appropriées peut être “cliquée”. Ces réactions ont rencontré un large succès ces dernières années. Leur importance dans la recherche a conduit les fondateurs, Sharpless et Meldal, à remporter le prix Nobel de chimie cette année (2022). Parmi les réactions “click”, la réaction de cycloaddition azide – alcyne catalysée par le cuivre (CuAAC) est sûrement la plus utilisée dans diverses applications [3]. Néanmoins, la réaction nécessite un catalyseur métallique, et en cas d'immobilisation enzymatique, elle nécessite la modification préalable de l'enzyme avec un groupe “cliquable” approprié. La réaction thiol-yne, impliquant un groupe thiol et un groupe alcyne, peut être menée à la place sans catalyseurs métalliques coûteux et rend la bioconjugaison plus facilement réalisable via la cystéine, acide aminée des protéines qui contient naturellement un groupe thiol. Peu d’études ont été menées dans la littérature dans la littérature sur cette réaction à la surface d’électrodes, en particulier en ce qui concerne la surface dede naomatériaux carbonés.

Pour étudier la faisabilité de cette réaction pour la modification des MWCNTs, des groupes alcynes ont été introduits sur les parois latérales des nanotubes soit par chimie covalente au diazonium, soit par modification non covalente avec des dérivés du pyrène.Des composés thiolés redox ont ensuite été utilisés pour sonder l'efficacité de la réaction par électrochimie. La voltammétrie cyclique a été utilisée pour déterminer la quantité et la stabilité des sondes à base de ferrocène immobilisées. Après une étude comparative préliminaire, la réaction thiol-yne photoinduite s'est révélée posséder la la meilleure efficacité pour favoriser l'immobilisation des ferrocènes thiolés à la surface des nanotubes modifiés par des alcynes. Les données obtenues par électrochimie ont été complétées par une analyse XPS qui a confirmé la présence d'espèces de fer à la surface des nanotubes fonctionnalisés. La réaction a ensuite été appliquée à l'immobilisation de quinones modifiées par un thiol. Ces composés organiques rédox sont généralement utilisées comme médiateurs redox pour favoriser le transfert d'électrons d'enzymes oxydant le glucose. L'immobilisation deferrocène et de quinones thiolés sur les nanotubes par la réaction thiol-yne catalysée par les UV a permis de

réaliser un transfert d’électrons indirect efficace et une oxydation électrocatalytique du glucose par l'enzyme FAD-déshydrogénase (FAD-GDH).

Globalement, les résultats montrent que cette technique peut être utilisée comme stratégie de fonctionnalisation alternative aux autres réactions de chimie “click”. Il est important de trouver de nouvelles stratégies d'immobilisation car chacune d'entre elles peut répondre à des besoins spécifiques et être adaptée à des applications spécifiques. Dans ce cas, la réaction est opérationnellement simple et elle peut conduire à un haut degré de fonctionnalisation puisque deux thiols consécutifs peuvent être ajoutés à l'alcyne. Cette caractéristique est utile non seulement dans la chimie synthétique et des polymères pour la génération de glycopolymères et de structures hyperramifiées, mais aussi pour les applications électrocatalytiques pour augmenter la quantité de médiateurs immobilisés, comme démontré dans le chapitre II. L'immobilisation stable des médiateurs est très importante pour les applications de biopiles enzymatiques, en particulier pour les futurs dispositifs implantables, afin d'éviter les pertes de puissance et de réduire la toxicité et les problèmes inflammatoires causés par la désorption du médiateur de la surface de l'électrode vers le milieu externe. Il est également important pour certains types de biocapteurs enzymatiques qui nécessitent la co-immobilisation des médiateurs à la surface. Outre les médiateurs, cette technique peut être appliquée à l'immobilisation d'autres molécules, par exemple des composés mimant les substrats enzymatiques pour favoriser l'immobilisation et l'orientation des enzymes par des interactions d'affinité ou l’immobilisation de catalyseurs moléculaires capables de réaliser le même type de réactions électrocatalytiques

La possibilité d'utiliser cette stratégie de fonctionnalisation pour l'immobilisation de macromolécules plus grosses telles que des enzymes, des oligonucléotides, à l'électrode doit encore être évaluée correctement. Idéalement, une enzyme contenant de la cystéine, avec des cystéines naturelles ou conçues pour afficher des résidus de cystéine uniques dans des sites favorables, devrait être testée à l'avenir. Étant donné que les les cystéines sur les protéines sont généralement très peu nombreux, cette technique peut être utile pour favoriser une orientation spécifique de l'enzyme au niveau de l'électrode. De plus, cette approche est adaptée pour contrôler la fonctionnalisation à la fois dans l'espace et dans le temps, puisque la lumière peut être facilement allumée et éteinte, contrôlée avec des fibres optiques et par l'utilisation de photomasques appropriés qui n'exposent que certaines zones d'une surface. Cette approche de photolithographie peut donc être envisagée pour la création de matériaux à nanomotifs.

La deuxième partie de la thèse est centrée sur la fonctionnalisation de nanoparticules organiques (NPs) issues d'un procédé d'auto-assemblage en solution aqueuse à partir d'un copolymère bloc polystyrène-bloc-β-cyclodextrine. Ces NPs présentent des β-CDs à la surface qui sont potentiellement capables de former des complexes d'inclusion avec divers composés. En particulier, la capacité des β-CDs à former des interactions hôtes hôtes avec l'adamatane (Ad) d'un composé hétazine fluorescent avec trois groupes Ad (HTZ-Ad) a été étudiée dans le chapitre III. Les résultats montrent clairement la fonctionnalisation efficace des GNPs avec HTZ-Ad par leur acquisition de propriétés fluorescentes en solution aqueuse et après leur immobilisation sur des surfaces. En général, l'inclusion dans les β-CDs peut être très utile pour augmenter la solubilité de certains composés organiques, tels que l'heptazine ou les médiateurs hydrophobes, favorisant leurs applications catalytiques dans l'eau. Des polymères conducteurs, tels que des films de poly-(pyrrole)-adamantane, peuvent être commodément électrogénérés sur des surfaces d'électrode pour guider l'immobilisation des GNPs au niveau de l'électrode. Cette stratégie permet la création de régions fonctionnalisées spatialement contrôlées des électrodes via des interactions spécifiques.

Les résultats ont ensuite été appliqués à l'immobilisation d'une enzyme glucose oxydase (GOx) sur des GNPs fixées à l'électrode via des films polymères poly (pyrrole) pour la fabrication de biocapteurs à glucose ampérométriques dont les caractéristiques et les performances sont décrites dans le chapitre IV. Les interactions basées sur l'inclusion d'étiquettes enzymatiques spécifiques dans les β-CDs sont avantageuses car elles ne perturbent généralement pas l'architecture tridimensionnelle de l'enzyme et son activité catalytique. La création d'architectures tridimensionnelles basées sur les GNPs sur l'électrode est avantageuse pour améliorer la concentration de surface en enzymes. De plus, les β-CDs sont biocompatibles. Des structures multicouches peuvent également être formées par cette approche par le biais d'interactions de molécules marquées avec les GNP de couches adjacentes.

En général, la fonctionnalisation des GNPs par les interactions hôte-invité est une méthode très polyvalente en raison de la vaste gamme de composés pouvant être hébergés dans la cavité β-CDs. La fonctionnalisation des GNPs avec des composés redox a déjà été démontrée au sein de l’équipe pour les applications en biopiles [4]. À l'avenir, l'immobilisation d'autres enzymes étiquetées par des groupements commela biotine, l'histidine, le pyrène ou l’adamantane, sur les GNPs seront utilisées pour la conception de nouvelles biopiles enzymatiques et biocapteurs. Les GNPs seront utilisés soit en solution, soit lors de leur

immobilisation sur des électrodes via des films polymères conducteurs, en combinaison avec des médiateurs redox ou des GNPs modifiés par des fonctions rédox. Dans le premier cas, une biopile enzymatique sera créée par confinement des GNPs modifiés dans des membranes permsélectives. L'effet positif de l'inclusion de médiateurs redox dans la coquille des GNPs pour la catalyse enzymatique a été mis en évidence dans des travaux antérieurs [5]. Cette amélioration est attribuée à l'augmentation de la solubilité du médiateur dans l'eau et à un effet de saut redox causé par la présence de médiateurs à proximitélors de l'encapsulation dans des β-CD adjacents sur les GNPs. L'immobilisation concomitante d'enzymes et de médiateurs dans les GNPs permettra une amélioration supplémentaire du transfert d'électrons en augmentant les chances d'interactions entre enzyme et médiateurs, favorisées par le degré de rotation des GNPs en solution. Des expériences préliminaires concernant la fonctionnalisation des enzymes FAD-GDH et BOx avec de la biotine pour leur utilisation ultérieure dans une installation de biopile ont déjà été lancées.

De manière intéressante, des GNPs aux propriétés nouvelles peuvent être obtenus par le choix des blocs hydrophobes et hydrophiles des copolymères à blocs amphiphiles utilisés dans le procédé d'auto-assemblage. Les GNPs hybrides, présentant différents groupes polaires avec différentes capacités de liaison, peuvent être formés à partir d'un mélange de différents copolymères blocs amphiphiles dans différents rapports de concentration [6]. Par exemple, les groupes β-CD peuvent être alternés avec des groupes maltoheptahose. Ce dernier peut interagir avec l'acide nitriloacétique, qui est capable de former des complexes de coordination avec des protéines marquées à l'histidine via une complexation métallique. Ainsi, la formation de ces GNP polyvalents hybrides permettrait l'immobilisation de différentes molécules marquées, par exemple deux enzymes différentes pour effectuer une réaction multienzymatique et multiélectronique et augmenter l'oxydation des combustibles et la puissance des biopiles. En effet, la densité des groupements polaires exposés peut être optimisée par la formation de ces GNPs hybrides permettant un meilleur contrôle de l'immobilisation des biomolécules. Par exemple, la réduction des sites β-CDs exposés empêchera l'agrégation enzymatique.

A l'avenir, des GNPs auto-assemblés à partir d'un copolymère bloc amphiphile constitué d'une partie β-CDs liée à la polycaprolactone à la place de la chaîne polystyrène, seront préparés et caractérisés. Ces GNPs seront totalement biocompatibles et biodégradables. À terme, l'ajout de motifs polymérisables, tels que le pyrrole, dans les structures de copolymères, mériterait également d'être étudié dans le but de renforcer davantage les architectures des GNPs et leur

utilisation à long terme en tant que matériaux électroniques pour les biopiles et les biocapteurs.

Globalement, les méthodes et résultats discutés dans cette thèse, concernant la fonctionnalisation des MWCNTs par la chimie thiol-yne et des GNPs via les interactions β-CDs hôte-invité, ont été appliqués à l'oxydation catalytique du glucose par les enzymes oxydoréductases immobilisées, FAD-GDH et GOx. L'oxydation enzymatique du glucose est centrale pour la conversion d'énergie et les biocapteurs. Par ailleurs, ces méthodes peuvent être potentiellement étendues à l'immobilisation d'autres classes d'enzymes et d'autres types de biomolécules, comme les anticorps et les aptamères, après modification opportune avec des groupements thiol/alcyne ou ayant une affinité avec les β-CDs. Ainsi, ces deux stratégies ont des applications prometteuses pour la génération de matériaux électroactifs spatialement contrôlés et pour le développement de différents types de biopiles et de biocapteurs (immunocapteurs, aptasensors, etc.) et leur plein potentiel n'a pas encore été réalisé.

References

(1) Holzinger M., Le Goff A., Cosnier S. «Nanomaterials for biosensing applications: a review». *Frontiers in chemistry*. (2014) 2, 63.

(2) Kolb H. C., Finn M. G., Sharpless, K. B. «Click chemistry: Diverse chemical function from a few good reactions». *Angew. Chem., Int. Ed.* (2001**)** 40, 11, 2004– 2021.

(3) Hein J. E., Fokin V. V. «Copper-catalyzed azide–alkyne cycloaddition (CuAAC) and beyond: new reactivity of copper (I) acetylides». *Chemical Society Reviews.* (2010) 39, 4, 1302-1315.

(4) Hammond J. L., Gross A. J., Giroud F., Travelet C., Borsali R., Cosnier S. «Solubilized Enzymatic Fuel Cell (SEFC) for quasi-continuous operation exploiting carbohydrate block copolymer glyconanoparticle mediators». *ACS Energy Letters*. (2018) 4, 1, 142-148.

(5) Gross A. J., Chen X., Giroud F., Travelet C., Borsali R., Cosnier, S. Redox-active glyconanoparticles as electron shuttles for mediated electron transfer with bilirubin oxidase in solution. *Journal of the American Chemical Society*. (2017) 139, 45, 16076-16079.

Experimental part

Summary

1. Materials

1.1. Solvents

All organic solvents used for synthesis and for electrochemistry (chloroform ($CHCl_3$), dichloromethane (CH_2Cl_2), acetonitrile (MeCN), acetone, ethyl acetate (AcOEt), dimethylformamide (DMF)) were reagent grade quality and were used as received from Sigma Aldrich. Tetrahydrofuran (THF), absolute ethanol were bought from Biosolve. N-methyl-2-pyrrolidone (NMP) was purchased from Acros Organics. Aqueous solutions used for the preparation of buffers for enzyme electrocatalysis were prepared using deionized water from purelab UHQ system (ELGA). Milli-Q water used for the preparation of GNPs suspensions was obtained by water purification to a resistivity of 18.2 MΩ cm using a Millipore Ultrapure system (MilliporeSigma, Burlington, MA, USA).

1.2. Reagents

All the reagents: sodium phosphate monobasic, sodium phosphate dibasic, terbutyl ammonium perchlorate (TBAP), lithium perchlorate ($LiClO_4$), potassium chloride (KCl), α-D-glucose, isopentyl nitrite, 2,2'-azino-bis(3-ethylbenzothiazoline-6-sulfonic acid) diammonium salt (ABTS), 1-methyl-2-pyrrolidinone (NMP), 4-ethynylaniline, ferrocene, 6-(ferrocenyl)hexanethiol (6-FcSH), 11-(ferrocenyl)undecanethiol (11-FcSH), tris(2-carboxyethyl)phosphine hydrochloride (TCEP), β-cyclodextrin (β-CD), 2,2-dimethoxy-2-phenylacetophenone (DMPA), 1,10-phenanthroline-5,6-dione, 8-mercaptooctanoic acid, tris-(diethylpyrazolyl)-heptazine (TDPH), 4-dimethylaminopyridine (DMAP), (adamantan-1-yl)-methanol, were purchased from Sigma-Aldrich and used as received. 1-ethynylpyrene was purchased from Alfa Aesar. Ferrocene methanethiol (FcSH), Adamantyl-11-pyrrolyl-1-undecyl carboxylic acid amide (pyrrole-adamantane) and 8-pyrrol-1-lactobionamide (pyrrole-lactobionamide) monomers were synthesized as described in the literature. The poly(ethylene glycol)-alginate-thiol (Alg-PEG-SH) has been obtained from École Polytechnique Fédérale de Lausanne. Commercial grade MWCNTs (9.5 nm diameter, purity > 95%) were purchased from Nanocyl and used as received without any purification step. MPL electrodes were purchased from PAXITECH (France).

1.3. Enzymes

Glucose Oxidase (from Aspergillus niger, lyophilized min 60% protein, 179 U mg^{-1}), FAD-dependent Glucose Dehydrogenase (from Pseudomonas sp., > 900 U mg^{-1} solid), Bilirubin

Oxidase (from Myrothecium verrucaria, 11.5 U mg^{-1} solid) were used as received from Sigma-Aldrich. Adamantane-tagged glucose oxidase was synthetized as previously reported in the literature.

2. Apparatus

2.1. Electrochemistry measurements

- Organic media

The electrochemical experiments performed in MeCN were carried out in a three-electrode electrochemical cell set up under dry argon atmosphere. A Pt wire was used as counter electrode while potentials given in organic media are referred to the $Ag/AgNO_3$ 10 mM in MeCN + TBAP (0.1 M) or $LiClO_4$ (0.1 M) reference electrode depending on the type of electrolyte used (TBAP (0.1 M) or $LiClO_4$ (0.1 M) respectively). The electrochemical experiments performed in DCM were carried out in a similar three-electrode electrochemical cell set up but using $Ag/AgNO_3$ 10 mM in DCM + TBAP (0.1 M) as reference electrode. DCM was dired before use by using molecular shieves of 3 Å. All electrochemical experiments were recorded on an Autolab PGSTAT100 potentiostat (Metrohm, The Netherlands) operated by Nova software.

- Aqueous media

The electrochemical characterizations of all electrodes in aqueous solutions were carried out in a three-electrode electrochemical cell using a Autolab PGSTAT100 potentiostat or a VMP3 Multi Potentiostat (Biologic, France) operated by EC-lab software. A platinum grid was used as the counter electrode and a saturated calomel electrode (SCE) served as reference electrode. All potentials given in this work are referred to the SCE reference electrode.

For both organic and aqueous media, electrochemical data fitting was performed using OriginPro9. All currents are normalized with the geometric surface of the electrodes.

2.2. Fluorescence emission and imaging

Fluorescence emission spectra of the HTZ-Ad-GNPs and GNPs suspensions (1:1000 dilution) were recorded at the excitation wavelength of 270 nm using a Perkin Elmer LS 55 Fluorescence Spectrometer operated by BioLight software.

Brighfield and fluorescence images of indium tin oxide (ITO) electrodes, gold interdigitated microelectrodes (IDE) were acquired with an Olympus BX61 microscope coupled with an Olympus DP30BW camera and CellP imaging software. For the fluorescence images, a 4′,6-diamidino-2-phenylindole (DAPI) filter (with $\lambda_{ex.}$ = 340 – 380 nm and $\lambda_{em.}$= 450 – 490 nm) was used and an exposure time of 5000 ms.

2.3. UV irradiation system

Samples were irradiated by a 200-500 W Mercury-Xenon arc lamp (Newport Corporation) connected by an optical cable with a core diameter of 1000 µm.

2.4. UV-vis spectroscopy, Raman spectroscopy and X-ray photoelectron spectroscopy (XPS)

UV-vis spectra were acquired using a Perkin Elmer UV-Lambda 650 spectrophotometer at room temperature with quartz cuvettes of 1 cm optical path length.

Raman spectra were recorded using a Renishaw inVia spectrometer. A laser at 633 nm and 3 mW power was used for used for acquisition of spectra from the sample surface.

XPS analysis was performed using a Thermoelectron ESCALAB 250 device (ICGM, France). The X-ray excitation was provided by a monochromatic Al-Kα (hυ=1486.6 eV) source. The analyzed area was ~0.15 mm^2. The background signal was removed using the Shirley [1] method. The surface atomic concentrations were determined from photoelectron peaks areas using the atomic sensitivity factors reported by Scofield [2]. Binding energies (BE) of all core levels were referred to the C=C of C1s carbon at 284.4 eV. XPS spectra were simulated using OriginPro 12.0.

2.5. Optical microscopy, scanning electron microscopy (SEM) and transmission electron microscopy (TEM)

Optical images and 3D and profile images were taken using a Keyence VK-X200 laser microscope.

SEM images were acquired using an ULTRA 55 FESEM based on the GEMENI FESEM column with beam booster with tungsten gun (Nanotechnology Systems Division, Carl Zeiss NTS GmbH, Germany). A drop of GNPs suspension was spread on a carbon substrate (0.5 mm diameter) and dried before imaging. TEM images were acquired at 200 kV using a

Phillips CM200 microscope equipped with a TEM-CAM 216 (TVIPS) camera and at 200 kV using a JEOL 2100 Plus microscope equipped with a RIO16 (GATAN) camera. A drop of GNPs suspension was deposited onto plasma treated carbon-coated copper-microgrid. 5 µL of 2 w/v % UranylLess (Delta Microscopies) lanthanide-based negative stain was applied for a few minutes and dried at room temperature.
Diagrams of the particle size distributions of GNPs, for both SEM and TEM images, have been determined by ImageJ software from multiple images and areas of the sample.

2.6. Dynamic light scattering (DLS)

DLS was used to evaluate the quantitative GNPs distribution using an ALV/CGS-8FS/N069 goniometer, consisting of a ALV/LSE-5004 multiple-τ digital corrector with an initial sampling time of 125 ns and 35 mW HeNe linearly polarized laser operating at a wavelength of 632.8 nm. 0.4 mL of GNPs suspension was diluted into 2mL MilliQ water and then transferred into quartz cells thermostated at 25 °C. Auto correlation functions C (q,t) were measured at scattering angles of 60^{o} -120^{o} and relaxation time distributions A(t) were determined using Contin analysis of the autocorrelation functions.

2.7. Quarz crystal microbalance with dissipation monitoring (QCM-D)

QCM-D measurements were performed using Q-Sense (Göteborg, Sweden) equipped with one laminar flow chamberand polished AT-cut piezoelectric quartz crystals (14 mm diameter) covered by a 100 nm thick gold layer (QSX 301-Q-Sense). F and D were measured at the fundamental resonance frequency (5 MHz) and at the third, fifth, seventh, ninth, eleventh, and thirteenth overtones (n = 3, 5, 7, 9, 11 and 13). Data analysis was performed using Q-Tools software.

2.8. Product analysis

NMR spectra were recorded on a Bruker AVANCE 400 operating at 400 MHz for ^{1}H.
ESI mass spectra were recorded with a Bruker APEX-Qe ESI FT-ICR mass spectrometer.

3.Procedures

3.1. Synthesis

3.1.1. Synthesis of 8-mercapto-N-(1,10-phenanthrolin-5-yl) octanamide (PLSH)

The synthesis of PLSH was adapted from the procedure reported by Elmes, Robert B.P. et al. [3]. 5-amino-1,10-phenanthroline (0.5 g, 2.56 mmol, 1 eq.) was dissolved in 100 ml distilled DCM before the solution was cooled to 0 °C. 8-mercaptooctanoic acid (0.56 g, 2.56 mmol, 1 eq.) and 1-Ethyl-3- (3-dimethylaminopropyl)carbodiimide (EDCI) (1.23 g, 6.4 mmol, 2.5 eq.) were added in the solution followed by 4- dimethylaminopyridine (DMAP) (0.31 g, 2.56 mmol, 1 eq.). The reaction mixture was stirred for 1 hour at 0 °C, then it was allowed to reach room temperature before being stirred for a further 24 hours. The solvent was removed under reduced pressure then, 50 ml of H_2O were added forming a white precipitate which was isolated by centrifugation. The resulting solid was redispersed 10 ml of MeCN and again centrifuged and collected by suction filtration and dried under vacuum to yield a beige/white solid. ^{1}H NMR (400 MHz, [D6]DMSO) δ(ppm) = 10.12 (s, 1H, - NH), 9.13 (dd, 1H, J=1.6, J=4.2), 9.04 (dd, 1H, J=1.7, J=4.2), 8.61 (dd, H, J=1.5, J=8.4), 8.44 (dd, 1H, J=1.7, J=8.2), 8.18 (s, 1H), 7.83 (dd, 1H, J=4.3, J=8.4), 7.74 (dd, 1H, J=4.3, J=8.1), 2.43 (t, 2H, J =7.2), 1.69 (t, 2H, J =6.5), 1.42 – 1.20 (br s, 6H).

Fig. 2: solvent evaporation during the synthesis of PLSH.

3.1.2. Synthesis of (4-ethylnyl)benzenediazonium tetrafluoroborate

The synthesis of (4-ethylnyl)benzenediazonium tetrafluoroborate was adapted from the procedure of Limoges et al. [4]. 1.9 mL of a cold solution of $NaNO_2$ (349 mg, 5,06 mM) in

milliQ water was added dropwise to 7.8 mL of a cold solution (over an ice bath) of 4-ethynylaniline (538 mg, 4.6 mM) in 1M of HCl. The mixture was left to react for 1 hour and then 1.25mL of a saturated $NaBF_4$ solution in milliQ water was added. Then, the mixture was filtered over a Bücher filtration system and then rinsed with 50 mL of cold ether 3 times. The crude product was re-dispersed in a small amount of acetonitrile, filtered and rinsed with cold ether several times. ESI-MS: shows the $[M+1]^+$ peak at 129.0 M/Z corresponding to the desired specie without BF_4^- anion.

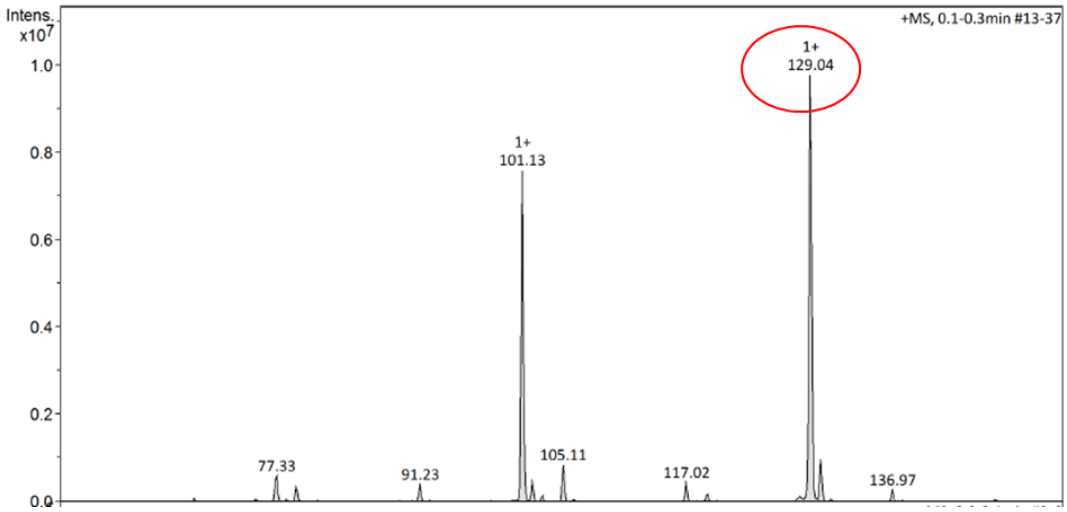

Fig. 1: ESI-MS spectrum of the synthetized (4-ethylnyl)benzenediazonium tetrafluoroborate.

3.1.3. Synthesis of 2,5,8-tris((adamantan-1-yl)methoxy)-heptazine (HTZ-Ad)

HTZ-Ad was prepared by Audebert P. et al. [5] by mixing an equimolar amount of tris-(diethylpyrazolyl)-heptazine (TDPH) and DMAP in a pressure tube (Aldrich, borosilicate glass) with a 3- fold excess of (adamantan-1-yl)-methanol in dichloromethane (about 5 mL g^{-1}). The sealed tube is then kept at 100°C for 3 h. The product was then purified by flash chromatography (AcOEt + EtOH gradient 0 to 10%).

3.1.4. Synthesis of polystyrene-block-β-cyclodextrin (PS-b-βCD) copolymer

The PS-b-βCD copolymer (MW: 4.5K for PS and 1.3 for βCD – the polydispersity is 1.1) was synthesized by Borsali R. et al. [6] by click reaction of azido-functionalized polystyrene (PS-N_3) with acetylene functionalized β-CD in DMF at 65°C, in the presence of copper nanopowder.

3.1.5. Synthesis of adamantane-tagged Glucose Oxidase (GOx-Ad)

The enzyme was synthetized by Holzinger M. [7] 1-adamantylamine (2.5 mg, 0.016 mmol) and 1-ethyl-3-(3-dimethylamino-propyl) carbodiimid hydrochloride (EDC) (3 mg, 0.016 mmol) were dispersed in 3 mL phosphate buffer (0.1 mol L^{-1}, pH 6.0) by sonication. Then GOx (1.6 mg) was added in this solution and kept for 22 h under stirring. The solution was then centrifuged in several steps using phosphate buffer (0.1 mol L^{-1}, pH 7) in an Amicon Ultra-15 Centrifugal Filter Unit-30 kDa to get a 0.5 mg mL^{-1} final concentration.

3.1.6. Synthesis of pyrrole derivatives

Adamantyl-11-pyrrolyl-1-undecyl carboxylic acid amide (PY-Ad) and 8-pyrrol-1-lactobionamide (PY-Lac) monomers were synthesized by Cosnier S. et al. [7,8]. PY-Ad was synthesized from pyrrole-carboxylic acid by formation of pyrrole succinimide (NHS) ester using standard Steglich reaction conditions. Then the pyrrole NHS (199.7 mg, 0.57 mmol, 1 eq.) ester was dissolved in 5 mL of DMF and 1-adamantylamine (86.1 mg, 1 eq.) and tetraethylamine (300 mg, an excess) were added. The reaction mixture was stirred for 3 days at 60 °C, dried and purified by column chromatography on silica gel (Et_2O–hexane (1/1)) to obtain the pure product. For the synthesis of PY-Lac, 8-pyrrol-1-aminooctane (0.500 g, 2.6 mmol) and lactobionic acid (26 mmol L^{-1}) were added in 100 mL methanol. Finally, the solution was stirred under reflux for 24 h and the solvent was evaporated under vacuum by freeze-drying.

3.2. Preparation of GNPs from PS-b-βCD copolymer

30 mg of PS-b-βCD was solubilized in 4 mL THF/H_2O solution (80:20) v/v% and stirred at 1000 rpm for 24 h. The solution was added in 160 mL of Milli-Q water under stirring (500 rpm) using a syringe pump at a speed of 10.2 mL h^{-1} and then stirred for a further 2 h at room temperature. Finally, THF was removed under reduced pressure at 36 °C and the final volume was adjusted to 160 mL to obtain a suspension of GNPs (concentration of PS-b-βCD: 0.187 mg L^{-1}).

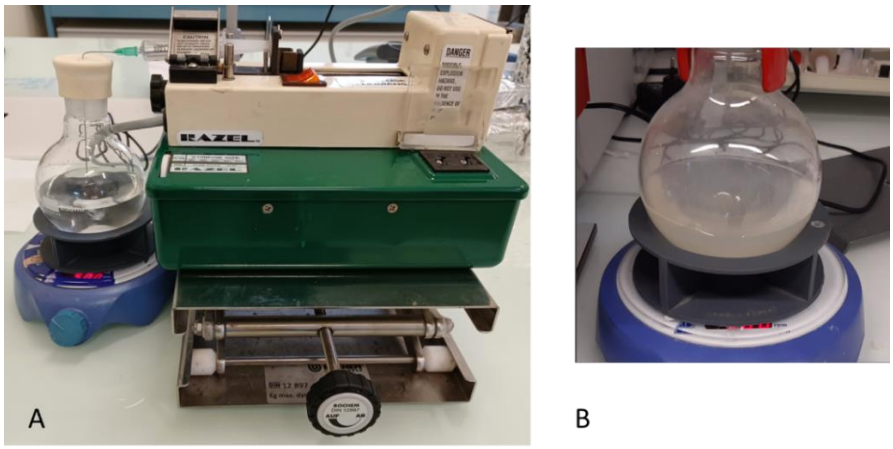

Fig. 3: A) addition of the copolymer solution in a large volume of water. B) GNPs suspension after the nanoprecipitation.

3.3. Functionalization of GNPs by HTZ-Ad

5 mL of GNPs suspension previously obtained from PS-b-βCD copolymer were added drop by drop in 1 mL of HTZ-Ad (3.2 mg mL^{-1}) solution in EtOH / Milli-Q water (70:30) v/v % under stirring (500 rpm). The resulting HTZ-Ad solution (0.66 mg mL^{-1}) was sonicated for 2 hours and stirred overnight (> 12 hours). Then, the solution was dialyzed against purified water at room temperature to remove ethanol (dialysis membrane cut-off = 3.5 – 5 kDa, 2 x 4 L of water, 500 rpm). After 24h HTZ-Ad was collected at the bottom of the bag as a white solid and discarded while 4 mL of supernatant containing the functionalized glyconanoparticles (HTZ-Ad-GNPs) were collected and conserved in fridge at 4 °C.

3.4. Electrodes preparation

3.4.1. Preparation of glassy carbon (GC) and platinum (Pt) electrodes

The surface of the GC electrodes (3 mm diameter) were polished with a 2 µm diamond paste purchased from Presi (France) and sonicated 5 min in water, acetone, and ethanol. Pt electrodes (diameter 5 mm) were thoroughly cleaned using 20 µm diamond paste, and rinsed several times successively with acetone, ethanol, and distilled water.

3.4.2. Preparation of multiwalled carbon nanotubes (MWCNTs) electrodes

MWCNTs dispersions in NMP were prepared initially by 2h sonication of 5 mg of CNTs in 1 mL of NMP until a homogenous black suspension was obtained. The suspension was

sonicated 30 min before use the following times. Then, 20 µL of the MWCNTs suspension were drop-casted on the cleaned GC electrode surface and NMP was completely removed under vacuum, leaving a dry 5 µm–thick MWCNT film on the GC electrode. The same procedure was used for the creation of the MWCNTs-MPL electrodes. In this case a PTFE adhesive of 1 cm X 1 cm with a cut out circular area of 6 mm diameter was attached on on side of a carbon fiber stripe (1 cm X 3 cm) and 20 µL of the MWCNTs suspension were drop-casted on the circular area followed by evaporation of NMP solvent until completely dry.

3.5. Electrodes functionalization

3.5.1. Functionalization of MWCNTs by (4-ethylnyl)benzenediazonium tetrafluoroborate

The electrochemical grafting of (4-ethylnyl)benzenediazonium tetrafluoroborate on GC and MWCNTs electrodes by repeated potential scans of a 2 mM solution of the diazoniums salt was performed in 0.1 M TBAP in CH_3CN from +0.5 V to −0.4 V vs. $Ag/AgNO_3$ for 2 scans. All solutions were deaerated for 20 min with argon before any electrochemical measurements.

For the chemical modification of MWCNTs by (4-ethylnyl)benzenediazonium tetrafluoroborate, the procedure already reported by Lalaoui et al. [9] was followed. 50 mg of MWCNTs were dispersed in 150 mL of DMF by sonication for 30 min. The dispersion was placed then under argon atmosphere and heated up to 80 °C. 0.9 g of 4-ethynylaniline and 1.1 mL of 8 mM isopentyl nitrite solution were added in the dispersion that was kept under stirring overnight under reflux at 80 °C (*Fig. 4*).

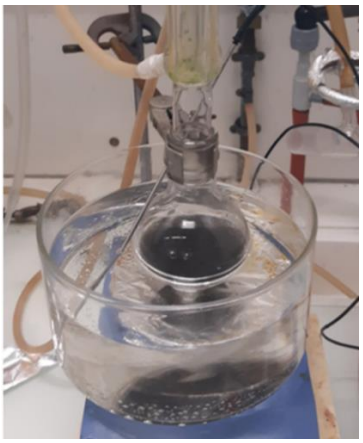

Fig. 4

The mixture was filtered through 0.45 μm PTFE membrane filters, washed several times with hot DMF and acetone. The modified MWCNTs were deposited on a circular area of 6 mm diameter delimited by PTFE adhesive on MPL electrodes.

3.5.2. Functionalization of MWCNTs and MPL electrodes by 1-Ethynylpyrene

20 μL of a 10 mM 1-ethynylpyrene solution in DMF was drop-casted onto pristine MWCNTs and MPL electrodes (in a circular area of 6 mm diameter delimited by PTFE) and dried completely under vacuum.

3.5.3. Functionalization of alkyne-modified MWCNTs electrodes by ferrocenyl-thiols

MWCNTs electrodes modified by AEBD and then 6-FcSH using TCEP as catalyst were immersed in a glass vial containing a 2 mM 6-FcSH + 2 mM TCEP solution in H_2O/methanol (3:7) v/v% for 3 hours. Then, the electrodes were thoroughly rinsed in methanol and water and subsequently dried. MWCNTs electrodes functionalized with 6-FcSH using β-CD as catalyst were immersed for 3 hours in a 2mM 6-FcSH + 2 mM β-CD solution in H_2O/DMF (1:1 v/v%), rinsed in DMF, water and dried. MWCNTs electrodes functionalized by UV irradiation were immersed in a glass vial containing 2 mM 6-FcSH + 0.4 mM DMPA solution in degassed $CHCl_3$ for 50 min under UV irradiation (240-400 nm, 200 W) then rinsed in $CHCl_3$ and dried. The same procedure was used also with other ferrocenyl thiols (using 2 mM of 11-FcSH and 2 mM FcSH). In all cases, the glass vials have been kept closed to avoid solvent evaporation during the reaction.

3.5.4. Functionalization of alkyne-modified MWCNTs electrodes by phenanthroline quinone-thiol (PLQ-SH)

MWCNTs electrodes were immersed in a glass vial containing 2 mM phenanthroline-thiol (PLSH) + 0.4 mM DMPA solution in degassed $CHCl_3$ for 50 min under UV irradiation (240-400 nm, 200 W) then rinsed in $CHCl_3$ and dried. The subsequent electro-oxidation of PLSH to form the phenanthroline quinone was carried out by repeated potential scans in phosphate buffer (pH 2, 7 or 12) from -0.4 V to +1.2 V vs SCE at 100 mV s^{-1} for 30 cycles.

3.5.5. Functionalization of alkyne-modified MWCNTs electrodes by alginates

20 µL of PEGylated-alginate-thiol (Alg-PEG-SH) in water (2% w/v) were mixed with 2 µL of DMPA (final concentration 0.4 mM) in DMF then, a 15 µL of the mixture was drop-casted onto the MWCNTs electrodes. The surface of the electrodes were irradiated by UV light for 30 minutes (240-400 nm, 200 W) and rinsed several times in water. Then, a drop of $CaCl_2$ 0.1 M was drop-casted on the electrode to cause geand rinsed again in water after 5 minutes.

3.5.6. Functionalization of electrodes by polypyrrolic films

PPY-Ad have been electrogenerated on gold ID and ITO electrodes, Pt electrodes, gold covered AT-cut piezoelectric quartz crystals, from a 3 mM adamantyl-11-pyrrolyl-1-undecyl carboxylic acid amide (PY-Ad) monomer in MeCN + $LiClO_4$ 0.1 M by repeated potential scanning or controlled potential oxidation at a fixed potential (see chapters III and IV for details). All potentials are referred to Ag/Ag^+ (0.01 M $AgNO_3$ + 0.1 M $LiClO_4$). The copolymer was formed from a solution of PY-Ad (0.75 mM) and pyrrole-lactobionamide (PY-Lac) (2.25 mM) in CH_3CN + 0.1 mol L^{-1} $LiClO_4$.

3.5.7. Functionalization of PPY-Ad-based IDE by GNPs

After the formation of PPY-Ad film on one side of the IDE, the IDEs have been immersed in eppendorfs containing 300 µL of the suspension of GNPs that were kept overnight under mild stirring and then washed thoroughly with water. Then different configurations of electrodes have been prepared:

- Electrode/PPY-Ad/GNPs/HTZ-Ad: the electrode was transferred in a 0.66 mg mL^{-1} HTZ-Ad solution in EtOH/ Milli-Q water (70:30) v/v % for 1 hour and then rinsed with ethanol and water.
- Electrode/PPY-Ad/GNPs/HTZ-Ad-GNPs: the electrode was transferred in a eppendorf containing 300 µL of the suspension of HTZ-Ad-GNPs kept under mild agitation overnight and then rinsed water.

3.5.8. Functionalization of Pt electrodes by GNPs

50 µL of GNPs (0.187 mg mL^{-1}) were deposited onto the poly-pyrrole electrogenerated film for incubation and dried at room temperature followed by extensive rinsing in water.

3.6. Enzyme bioelectrodes preparation and enzyme electrocatalysis

3.6.1. FAD-GDH bioelectrodes

40 µL of a 5 mg mL^{-1} solution of FAD-GDH in phosphate buffer (0.1 mol L^{-1}, pH 7) were deposited onto the surface of the ferrocenyl-thiols and phenanthroline-thiols modified electrodes and incubated for 3 hours at 4 °C. After rinsing in buffer, the electrodes were tested by performing one scan in argon deareated phosphate buffer (0.1 mol L^{-1}, pH 7) in absence of glucose and then by repeated potential scans from -0.4 V to +0.5 V vs. SCE after addition of 200 mM of glucose. The evaluation of the FADGDH/PLQSH-based biosensor by controlled potential oxidation at -0.2 V vs SCE upon successive glucose injections until saturation (200 mM) while stirring.

3.6.2. BOx bioelectrodes

After the immobilization of alginates on the MWCNTs electrodes, 40 µL of a 5 mg mL^{-1} BOx solution in Tris HCl (0.1 mol L^{-1}, pH 7) were drop-casted on the surface of MWCNTs electrodes that were kept for 2 hours at 4 °C. A drop of $CaCl_2$ 0.1 M was deposited on the top of the electrodes to start the gelation process. After 5 minutes, electrodes were rinsed in water. The catalytic activity of BOx was tested in Tris HCl (0.1 mol L^{-1}, pH 7) by performing one scan from -0.4 V to +0.5 V vs. SCE in argon deareated solution and then by performing another scan in oxygen saturated solution and finally by repeated potential scans after addition of 10 mM ABTS. Electrodes were stored at 4 °C and tested again after 72 hours in oxygen saturated Tris HCl (0.1 mol L^{-1}, pH 7) in presence of 10 mM ABTS. Experiments were performed while stirring at 150 rpm to avoid diffusion limitation.

3.6.3. GOx-Ad bioelectrodes

25 µL of 0.5 mg/ml GOx-Ad in phosphate buffer (0.1 mol L^{-1}, pH 7) solution were drop-casted on GNPs/PPY-Ad, GNPs/PPY-Ad-PPY-Lac or bare Pt electrodes and electrodes were incubated for 7 h at 4 °C and rinsed in phosphate buffer (0.1 mol L^{-1}, pH 7) for 5 min under weak stirring at room temperature. Enzyme catalysis was evaluated indirectly by 25 °C in 0.1 mol L^{-1} phosphate buffer (pH 7) by electro-oxidation of the enzymatically produced H_2O_2 by controlled potential oxidation at + 0.7 V vs SCE upon successive additions of glucose until saturation. Experiments were performed at room temperature with stirring at 500 rpm using OrigaMix magnetic stirrer to avoid diffusion limitation.

References

(1) Shirley D. A. «High-Resolution X-Ray Photoemission Spectrum of the Valence Bands of Gold». *Physical Review B.* (1972) 5, 12, 4709–4714.

(2) Scofield J. H. «Hartree-Slater Subshell Photoionization Cross-Sections at 1254 and 1487 EV». *Journal of Electron Spectroscopy and Related Phenomena*. (1976) 8, 2, 129–137.

(3) Elmes R. B. P., Orange K. N., Cloonan S. M., D. Williams C., Gunnlaugsson T. «Luminescent ruthenium (II) polypyridyl functionalized gold nanoparticles; their DNA binding abilities and application as cellular imaging agents». *Journal of the American Chemical Society*. (2011) 133, 40, 15862–15865.

(4) Evrard D., Lambert F., Policar C., Balland V., Limoges B. «Electrochemical Functionalization of Carbon Surfaces by Aromatic Azide or Alkyne Molecules: A Versatile Platform for Click Chemistry». *Chemistry – A European Journal*. (2008) 14, 3, 9286–9291.

(5) Le T., Galmiche L., Masson G., Allain C., Audebert P. A. «Straightforward Synthesis of a New Family of Molecules: 2,5,8-Trialkoxyheptazines. Application to Photoredox Catalyzed Transformations». *Chem. Commun.* (2020) 56, 73, 10742– 10745.

(6) Carrière M., Buzzetti P. H. M., Gorgy K., Mumtaz M., Travelet C., Borsali R., Cosnier S. «Functionalizable glyconanoparticles for a versatile redox platform». *Nanomaterials*. (2021) 11, 1162.

(7) Holzinger M., Bouffier L., Villalonga R., Cosnier S. «Adamantane/β-cyclodextrin affinity biosensors based on single-walled carbon nanotubes». *Biosensors and Bioelectronics.* (2009) 24, 5, 1128-1134.

(8) Cosnier S., Senillou A., Grätzel M., Comte P., Vlachopoulos N., Renault N. J., Martelet C. «A glucose biosensor based on enzyme entrapment within polypyrrole films electrodeposited on mesoporous titanium dioxide». *Journal of Electroanalytical Chemistry*. (1999) 469, 2, 176-181.

(9) Lalaoui N., de Poulpiquet A., Haddad R., Le Goff A., Holzinger M., Gounel S., Mermoux M. « A Membraneless Air-Breathing Hydrogen Biofuel Cell Based on Direct Wiring of Thermostable Enzymes on Carbon Nanotube Electrodes ». *Chemical Communications.* (2015) 51, 35, 7447-7450.

List of abbreviations

3PyHept : 2,5,8-tris(3,5-diethyl-pyrazol-1-yl)-heptazine

6-FcSH : 6-(ferrocenyl)hexanethiol

11-FcSH : 11-(ferrocenyl)undecanethiol

Ab : antibody

ABTS : 2,2-azino-bis-(3-éthylbenzothiazoline-6-acide sulphonique)

AcOEt : ethyl acetate

Ad : adamantane

ADH : alcohol dehydrogenase

AFC : alkaline fuel cell

Ag^{+}/Ag : reference electrode for organic solutions

AIDH : aldehyde dehydrogenase

Alg-PEG-SH : PEGylated-alginate-thiol

*An*GOx : glucose oxidase from *Aspergillus niger sp.*

AQS : anthraquinone sulfonate

ATR : attenuated total reflectance FT-IR spectroscopy

BCP : block glycopolymer

BFC : biofuel cell

BOx : bilirubine oxydase

BSA : bovin serum albumine

CD : cyclodextrine

CDH : cellobiose dehydrogenase

CGTase : cyclodextrin glucanotransferase

CMC : critical micelle concentration

CMT : critical micelle temperature

CNDs : carbon nanodots

CNT : carbon nanotube

COF : covalent organic framework

CuAAC : Cu(I)-catalyzed azide-alkyne cyclo-addition reaction

CV : cyclic voltammetry

CVD : chemical vapour deposition

Cyt Ox : cytochrome oxydase

DAPI : 4′,6-diamidino-2-phenylindole

DCM : dichloromethane

DET : direct electron transfer

DLC : discotic liquid crystal

DMF : dimethylformamide

DMSO : dimethyl sulfoxide

EDC : 1-ethyl-3-(3-dimethylaminopropyl)carbodiimide

EET : extracellular electron transport

EFC : enzymatic fuel cell

ELISA : enzyme linked immunosorbent assay

ESI-MS : electrospray ionisation mass spectrometry

EtOH : ethanol

FAD : flavine adenine dinucleotide

Fc : ferrocene

FcSH : ferrocenyl methanethiol

FDH : fructose dehydrogenase

FET : field effect transistor

FRET : Förster Fluorescence Resonance Energy Transfer

FTIR : Fourier-transform infrared spectroscopy

GC : glassy carbon

GDH : glucose dehydrogenase

GNP : glyconanoparticle

GOx : glucose oxydase

H_2ase : hydrogenase

HER : hydrogen evolution reaction

HOMO : highest occupied molecular orbital

HRP : horse radish peroxidase

HTZ-Ad : tris((adamantan-1-yl)-methoxy)-heptazine

ITO : indium tin oxide

j_{max} : maximum current density

K_a : affinity constant/association constant

K_M : Michaelis-Menten constant

K_M^{app} : apparent Michaelis-Menten constant

Lac : laccase

LDH : lactate dehydrogenase

LOD : limit of detection

LOx : lactate oxidase

LUMO : lowest unoccupied molecular orbital

MCFC : molten carbonate fuel cell

MeCN : acetonitrile

MET : mediated or indirect electron transfer

MFC : microbial fuel cell

MIP : molecularly imprinted polymer

MNP : magnetic nanoparticle

MOF : metal-organic framework

MPL: microporous layer

MWCNT : multiwalled carbon nanotube

NAD : nicotinamide adenine dinucleotide

NADP : nicotinamide adenine dinucleotide phosphate

NHS : N-hydroxysuccinimide

NMP : 1-methyl-2-pyrrolidinone

NMR : nuclear magnetic resonance

NP : nanoparticle

NTA : nitrilotriacetic acid

OCP : open circuit potential

OCV : open circuit voltage

OLED : organic light-emitting diode

ORR : oxygen reduction reaction

P_2ABTS : bis-pyrene-ABTS

PAC : pile à combustible

PAFC : phosphoric acid fuel cell

PAMAM : polyamidoamine

PDA : polydopamine

PEG : poly(ethylene glycol)

PEGDGE : poly(ethylene glycol) diglycidyl ether

PEMFC : polymer electrolyte membrane fuel cell

PFV : protein film voltammetry

PLQSH : 8-mercapto-N-(1,10-phenanthrolin-1,2-dione-5-yl) octanamide (phenanthroline-quinone thiol)

PLSH : 8-mercapto-N-(1,10-phenanthrolin-5-yl) octanamide (phenanthroline thiol)

PMAA : poly(methacrylic acid

PPO : polyphenol oxydase

PPY : polypyrrole

PQ : phenanthrene-quinone

PS-b-βCD : polystyrene-block-β-cyclodextrin

PS-b-MH : polystyrene-b-maltoheptaose

PS-N_3 : azido-functionalized polystyrene

PTFE : polytetrafluoroethylene

PSS : polystyrenesulfonate

PVP : polyvinylpyrrolidone

PY-Ad : adamantyl-11-pyrrolyl-1-undecyl carboxylic acid amide (pyrrole-adamantane)

PY-Lac : 8-pyrrol-1-lactobionamide (pyrrole-lactobionamide)

RDE : rotating-disk electrode

RGO : reduced graphene oxide

Ref. : reference

QCM-D : quartz crystal microbalance with dissipation monitoring

QD : quantum dot

SAM : self-assembly monolayer

SEFC : solubilized enzymatic fuel cell

SELEX : systematic evolution of ligands by exponential enrichment

SEM : scanning electron microscopy

SOFC : solide oxide fuel cell

STD : standard deviation

SWCNT : single-walled carbon nanotube

TBAP : tetrabutylammonium perchlorate

TBFP : tetrabutylammonium hexafluorophosphate

TCEP : tris(2-carboxyethyl)phosphine

TDPH : tris-(diethylpyrazolyl)-heptazine

TEM : trasmission electron microscopy

THF : tetrahydrofuran

UV-vis : UV-visible spectroscopy

V_{max} : maximal reaction rate

XPS : X-ray photoelectron spectroscopy

Publications

M. Brachi, P. H. M. Buzzetti, K. Gorgy, P. Audebert, A. le Goff, R. Borsali, S. Cosnier. «Trialkoxyheptazine-Based Glyconanoparticles for Fluorescence in Aqueous Solutions and on Surfaces via Controlled Binding in Space». *ACS Macro Lett*. (2022) 11, 135−139.

Buzzetti P. H. M., Carrière M., Brachi M., Gorgy K., Mumtaz M., Borsali R., Cosnier S. «Organic β-cyclodextrin nanoparticle: an efficient building block between functionalized polypyrrole electrodes and enzymes». *Small.* (2022) 18, 2105880.

Presentations

- Oral communications

Les enjeux de la chimie durable (invited speaker), «β-cyclodextrin-based glyconanoparticles for biosensing and energy conversion». Lyon, France, September 2022.

Journées d'Électrochimie, «Functionalization of β-cyclodextrin decored glyconanoparticles for enzymatic electrocatalysis and biosensing» Mons, Belgium, July 2022.

XXVII International symposium on Bioelectrochemistry and Bioenergetics, «Functionalized carbon nanotubes and glyconanoparticles for glucose oxidation in enzymatic biofuel cells and biosensors». Antwerp, Belgium, April 2022.

Online meeting of Groupe Français de Bioélectrochimie, «Trialkoxyheptazine-Based Glyconanoparticles for Fluorescence in Aqueous Solutions and on Surfaces via Controlled Binding in Space». March 2022.

- Poster presentations

16th European Biologic Inorganic Chemistry, «Functionalization of carbon nanotubes by thiol-yne chemistry for enzyme electrocatalysis». Grenoble, France, July 2022.

Journée de Printemps de la section régionale Rhône-Alpes de la Société Chimique de France (winner of the best poster award), «β-cyclodextrin-based glyconanoparticles functionalized via host-guest interactions for fluorescence and biosensing applications». Chambéry, France, June 2022.

Acknowledgements

My PhD has come to an end, but I will keep the memory of the years spent in the BioCEN team in my mind for the years to come. For sure it has been one of the most meaningful experience in my life both professionally and personally. Although things have not always be smooth for me and some times have been challenging, it has been a wonderful and rewarding adventure overall.

This thesis work has been carried out at the Département de Chimie Moléculaire, Université Grenoble Alpes, within the Bioélectrochimie pour les capteurs, l'énergie et les nanomatériaux (BioCEN) team led by Dr. Serge Cosnier. I have felt as part of the team since my first visit to the laboratory during the Erasmus program when I was a Master student.

There are so many people I would like to thank.

I am truly grateful first and foremost to my supervisors: Dr. Alan Le Goff and Dr. Serge Cosnier for believing in me, giving me the opportunity to undertake this doctorate and for their constant support and encouragement that has made this dissertation possible. Under their guidance I have gained a lot of experience and I built up my confidence. They always had my best interest at heart. I am very glad for the relationship we have established in the course of these years based on trust, respect. They were inspiring to me and I greatly appreciate them for their human qualities. I am particularly thankful to them for giving me the chance to continue my PhD journey after all the funding issues that have arisen, I know how difficult and stressful this has been even for them. Additionaly, they provided me access to some of the most recognised international conferences in the field.

My deep gratitude also goes to Dr. Fabien Giroud for the immense help and time he provided me during research activities and for his endless advices and honest feedback. Although, he was not my official supervisor, he acted as a mentor. I have always considered him a benchmark and a friend and I know I could always count on him for any concern.

A big thank must go to Dr. Paulo Buzzetti as I have worked closely with him during these years, he contributed data for the part of the thesis related to glyconanoparticles. The results I have presented about this part are the product of our joint efforts. Confronting and discussing ideas with him has undoubtedly strengthened my critical abilities.

All of them gave me valuable insights, their input and optimism have helped to keep me on track and dragged me to the finish line.

I am thankful for the useful suggestions and time that Dr. Karine Gorgy has gave up for me. She is very caring, she shared her knowledge about nanoparticles with me multiple times and she provided feedback when I presented an oral communication.

Yannig Nedellec is very kind, he is a reference point for all the students as well. I wish to thank him especially for his assistance on Raman spectroscopy. Arielle le Pellec is equally very sweet and always prompt to help for any question on lab equipment and chemical products.

I would like to thank Regine Rozand and Véronique Gineste for the administrative support and their assistance concerning arrangements for my participation at conferences and for being patient with my french difficulties.

I would like to express sincere thanks to the students and postdoc colleagues of the BioCEN team that I have met over these years, for our chats, laughs and cups of tea along the way. They are too numerous to mention here, but they all provided a sense of community and our company and friendship added a lot to my life.

Many thanks also to Dr. Michael Holzinger, Dr. Chantal Gondran and Dr. Andrew Gross. All members of BioCEN team have been kind, dynamic and sunny people. I think they all contributed to create a stimulating and enjoyable environment and I will never forget their smile.

I am very grateful for the collaboration I have done with the CERMAV team led by Dr. Redouane Borsali, for their relevant knowledge on glyconanoparticles, the block copolymers synthesis as well as SEM, TEM imaging and DLS analyses. During my visits to their laboratory, they were very welcoming and willing to offer any help they could.

I would like to extend my gratitude to other members of Nanobio, and especially Dr. Liliane Guerente and Hugues Bonnet of the I2BM team, that allowed me to use QCM-D equipment and supported me during the analyses.

I would like to thank the members of my jury that have accepted to take their time and effort to read and review this dissertation.

Finally, I would like to express my gratitude to my family, my parents and sister, who are so supportive in whatever I do in my life. I hope I made them proud.